PCA001

Effect of Bradykinin on Renal Hemodynamics of Anesthetized Wister Rats

Ahmad Ahmeda[1]

[1]Ajman University, College of Medicine, Ajman, United Arab Emirates

Background:

Bradykinin (BK) is an endogenously produced active peptide that causes vasodilation. However, its effect on the renal microvasculature is not well described when introduced as an exogenous compound. This study evaluated the effects of BK on renal cortical and medullary blood perfusion and investigated whether the effect of BK is similar when given locally into the renal medulla or systematically with the intravenous route (IV).

Materials and Methods:

Four groups (n=7) of male Wistar rats (250-300 g) were anaesthetised with an I.P injection of 1 ml chloralose/urethane, 16.5/250 mg/ml. The right femoral vein was cannulated for infusion of saline (154mM NaCl), BK (50µg/kg/min) at 3ml/h and supplemental doses of anaesthetic. The right femoral artery was cannulated to measure blood pressure (BP). The left kidney was exposed via a flank incision, and a small cannula was inserted 4.5mm into the kidney for intramedullary (i.m) infusion of saline or BK at 0.6-1.0 ml/h. Two Laser-Doppler microprobes (each 0.5 mm diameter) were inserted 1.5 and 4.0 mm into the kidney to measure cortical and medullary blood perfusion, respectively (100 perfusion units (PU) = 1 V). After 90 min, baseline measurements were taken, and then either vehicle or BK were infused i.m or IV for 60 min. At the end of the experiments, the animals were killed with an anaesthetic overdose. Data ± SEM were subjected to the Student's t-test, and significance was taken at $P<0.05$.

Results:

The baseline levels of BP were 95±8 mmHg, Heart Rates (HR) were 335±10 BPM, CP was 138±7 PU, and MP was 57±5 PU. Administration of bradykinin i.m significantly increased MP and CP (18 ± 6% and 33 ± 9%, respectively, $P<0.05$.). BK had no effect on BP and HR when given locally. IV Infusion of BK resulted in a significant increase in CP (23 ± 6%, $P<0.05$.) and a decrease in MAP (15 ± 6%, $P<0.05$.), but had no effect on MP and HR.

Conclusion:

BK, when given locally, dilates renal blood vessels, mediating an increase in CP and MP. When given systematically, the effect of bradykinin was less on the renal microvasculature and had no impact on the MP. These data indicate that the BK has a more significant effect on the medullary microvasculature when given locally. Further research is suggested to understand the action of BK on renal microvasculature and the involvement of the free radicals such as superoxide anion and nitric oxide.

PCA002

The effects of NS1643 on two disease causing hERG channel variants

Majid Khamis Al Salmani[1]

[1]*Department of Physiology, College of Medicine, Sultan Qaboos University, Muscat, Oman*

The human ether-a-go-go gene (hERG) encodes a voltage-dependent K^+ ion channel (KCNH2) largely responsible for the rapid component of the delayed rectifier currents in the heart. Loss of function mutations in hERG cause type-2 long QT syndrome (LQTS-2) and predispose affected individuals to cardiac arrhythmias. Several classes of hERG channel variants have been described, including variants that affect channel gating, conductance and/or expression. T1019PfsX38- and Q1070X-hERG are LQTS-2 causing variants reported in Oman and Saudi Arabia (Bhuiyan et al. 2008; Al Senaidi et al. 2014). When expressed as cDNA in heterologous expression systems, these variants exhibited functional ion channels on the cell surface (Bhuiyan et al. 2008; Al Salmani et al. 2022).. However, T1019PfsX38-hERG displayed characteristics of defective channel gating (Al Salmani et al. 2022). In this study we try to test the responsiveness of T1019PfsX38- and Q1070X-hERG channels to the hERG channel activator N,N'-Bis[2-hydroxy-5-(trifluoromethyl)phenyl]urea (NS1643). We expressed wild-type and the mutant channel variants in HEK293 cells and studied their electrophysiology using the whole-cell patch clamp technique. We used paired and non-paired Student's t-test where appropriate to assess the statistical significance of difference, n is the number of cells. A 400 ms ventricular action potential (VAP) clamp revealed that T1019PfsX38- ($p = 0.04$) but not Q1070X-hERG ($p = 0.774$) exhibits reduced potassium currents at the repolarisation phase of the action potential (AP) (75-95 % of the AP duration) when compared with WT-hERG ($I_{(integral)}$:.WT = 2.63 ± 0.29 pA.s/pF (n = 6), T1019PfsX38 = 1.43 ± 0.42 pA.s/pF (n=4), Q1070X = 2.94 ± 1.23 pA.s/pF (n = 4)). The application of NS1643 (10 µM) to the bath solution increased these $I_{(integral)}$ values by 53%, 80.3% and 78% in cells expressing WT- ($p = 0.031$, n=6), T1019PfsX38- ($p = 0.001$, n = 4) and Q1070X-hERG ($p = 0.036$, n = 4), respectively. To understand these effects further, we measured the voltage and time dependences of channel activation in response to NS1643. NS1643 shifted the half-maximum voltage (V_{mid}) of activation to more negative values ($p < 0.01$) compared to control but did not increase the maximal current amplitudes (control V_{mid}: WT =2.90 ± 3.25 mV (n = 5), T1019PfsX38 = 6.96 ± 4.94 mV (n = 3), Q1070X = 10.40 ± 2.40 mV (n = 5); NS1643 V_{mid}: WT = -16.70 ± 3.60 mV (n = 5), T1019PfsX38 = -13.57 ± 4.37 mV (n = 3), Q1070X = -15.38 ± 3.69 mV (n = 5)). In addition, NS1643 accelerated the activation process of the three variants at multiple test potentials ($p < 0.05$, n = 4 – 9). Moreover, NS1643 stabilised the open configuration of the channel and slowed the deactivation process when measured at -40 mV. When applied to untransfected HEK293 cells, NS1643 (10 µM) inhibited endogenous currents that display fast activation and fast inactivation kinetics at potentials ≥ 0 mV ($p < 0.01$, n = 5). Overall, NS1643 enhances the activities of WT-, T1019PfsX38- and Q1070X-hERG channels but its therapeutic potential require testing for undesired side effects.

Al Salmani MK, Tavakoli R, Zaman W, Al Harrasi A (2022) Multiple mechanisms underlie reduced potassium conductance in the p.T1019PfsX38 variant of hERG. Physiol Rep 10:e15341. https://doi.org/10.14814/PHY2.15341 Al Senaidi KS, Wang G, Zhang L, et al (2014) Long QT syndrome, cardiovascular anomaly and findings in ECG-guided genetic testing. IJC Hear Vessel 4:122–128. https://doi.org/10.1016/j.ijchv.2014.06.001 Bhuiyan ZA, Momenah TS, Gong Q, et al (2008) Recurrent intrauterine fetal loss due to near absence of HERG: Clinical and functional

characterization of a homozygous nonsense HERG Q1070X mutation. Hear Rhythm 5:553–561. https://doi.org/10.1016/J.HRTHM.2008.01.020

PCA003

Effect of Sodium Fluoride on Lipid Profile in Male Wistar rats

Olusola Ayegboyin[4], Abayomi Ige[3], Elsie Adewoye[2]

[1]University of Ibadan,, Ibadan, Nigeria, [2]University of Ibadan, Ibadan, Nigeria, [3]University of Ibadan, Ibadan, Nigeria, [4]University of Ibadan, Ibadan, Nigeria

This study investigated the effect of sodium fluoride (NaF) on lipid profile in the serum and aorta of male Wistar rats. Sodium fluoride has garnered increased attention due to its potential detrimental effects on human health. Excessive ingestion and accumulation of sodium fluoride from sources like water, toothpaste, and pesticides can trigger dyslipidemia in rats. These heightened disturbances in the lipid profile, pose a significant risk and may predispose individuals to severe vascular and cardiovascular-related diseases, which are the leading causes of global mortality. The study involved ten male Wistar rats weighing 150-180 grams. The rats were divided into two groups (n=5) Group I (Control), received distilled water, and Group 2 received an oral dose of 10 mg/kg of sodium fluoride daily for 21 days. Lipid profiles [Total Cholesterol (TC), Triglycerides (TG), High-Density Lipoprotein Cholesterol (HDL-C), Low-Density Lipoprotein Cholesterol (LDL-C), Very Low-Density Lipoprotein Cholesterol (VLDL-C)] were determined in the serum of male Wistar rats using UV/VIS spectrophotometer. Ethical consideration was obtained for this work from the University of Ibadan Animal Care and use research ethical committee. Data analysis was conducted using descriptive statistics and a student t-test with a significance level set at $\alpha=0.05$. Total cholesterol (116.10±7.84 vs 82.37±2.27 mg/dL), triglyceride (161.90±4.06 vs 105.80±4.26 mg/dL), VLDL-C (32.38±0.81 vs 21.16±2.85 mg/dL), and LDL-C (46.37±4.17 vs 25.82±2.40 mg/dL) levels significantly increased ($p<0.05$), while HDL-C (20.57±0.86 vs 40.80±6.44 mg/dL) level reduced significantly ($p<0.05$) in NaF compared with control. There was moderate congestion of the lumen in the aortic vessel in NaF, which was absent in control. These findings suggest that sodium fluoride exposure causes dyslipidemia. Hypertension and dyslipidemia are major risk factors for cardiovascular disease, responsible for global morbidity and mortality. Given these results, continuous fluoride exposure in populations residing in regions with endemic fluoride levels should be a matter of significant concern given the potential health risks associated with sodium fluoride exposure, emphasizing the need for vigilance in affected regions.

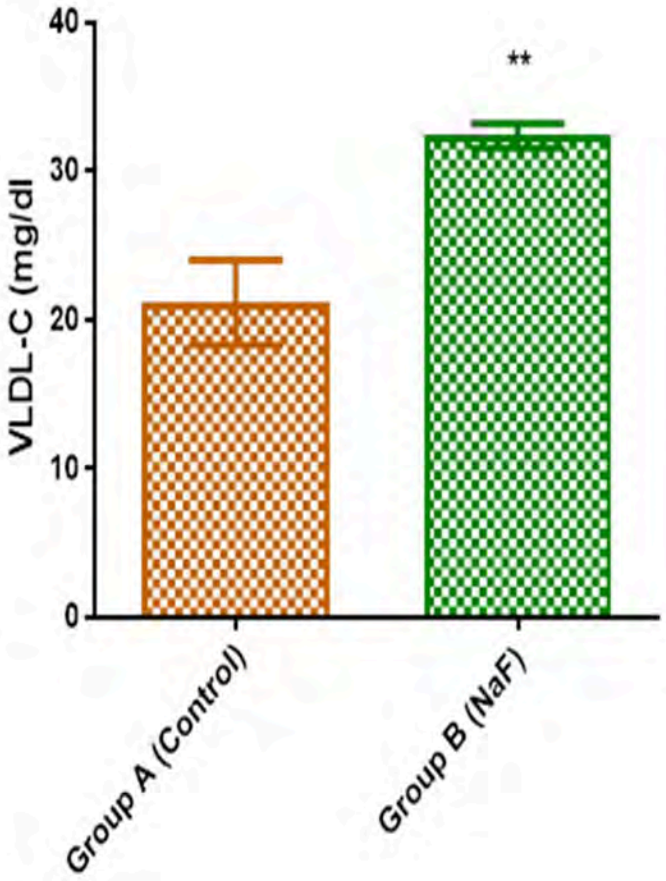

Figure 5. Sodium Fluoride (10mg/kg) effect on very low-density lipoprotein-cholesterol. Values are expressed as Mean ± SEM. (N=5) (**P<0.01)

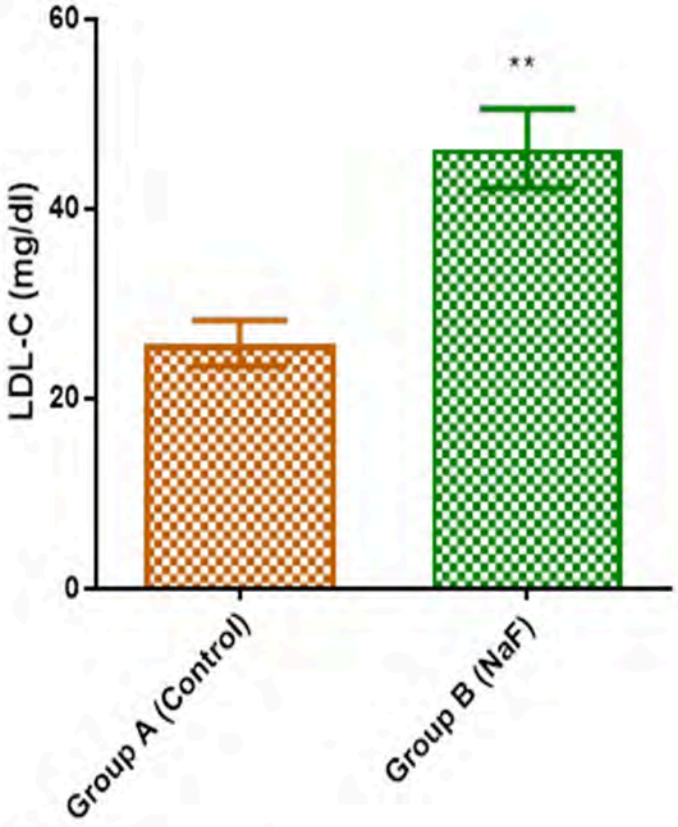

Figure 4. Sodium Fluoride (10mg/kg) effect on low-density lipoprotein cholesterol. Values are expressed as Mean ± SEM. (N=5) (**P<0.01)

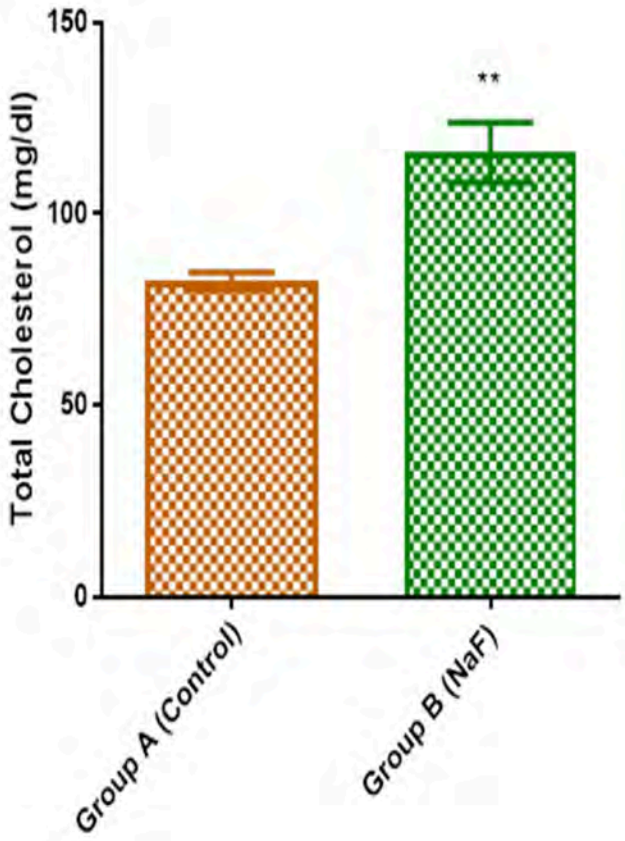

Figure 1. Sodium Fluoride (10mg/kg) effect on Total Cholesterol. Values are expressed as Mean ± SEM. (N=5) ($^{**}P<0.01$)

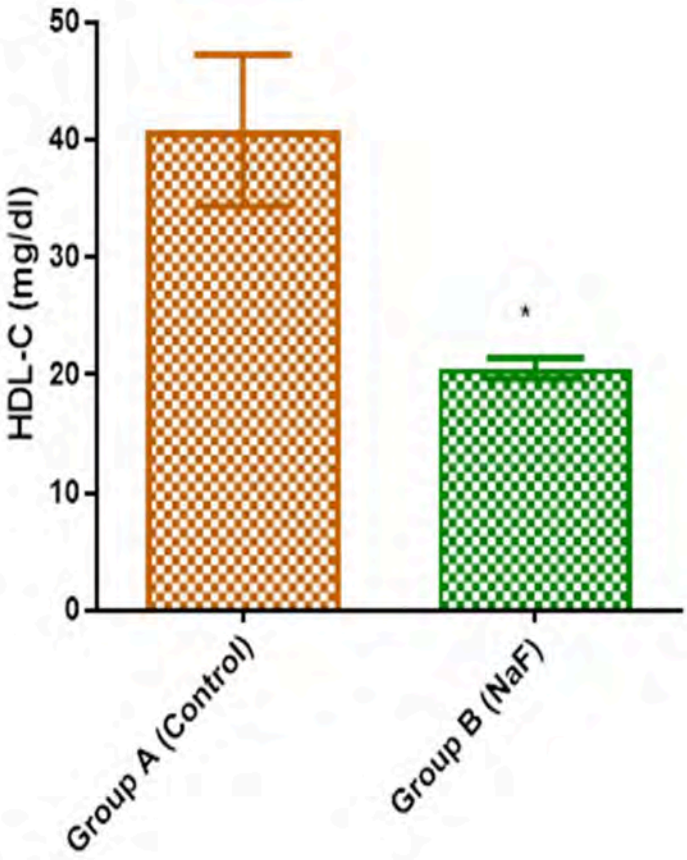

Figure 3. Sodium Fluoride (10mg/kg) effect on high-density lipoprotein cholesterol. Values are expressed as Mean ± SEM. (N=5) (* $P<0.05$)

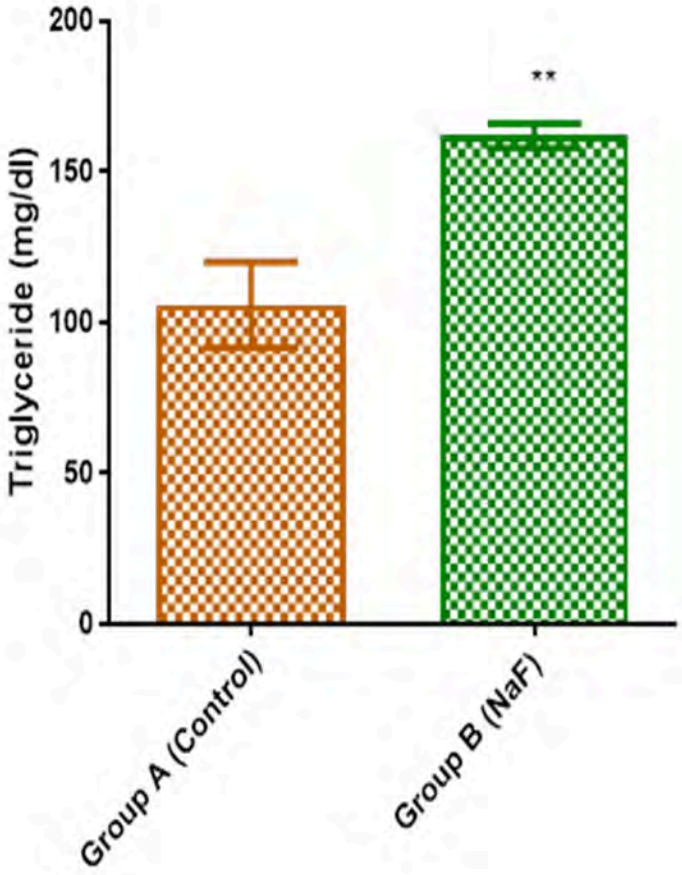

Figure 2. Sodium Fluoride (10mg/kg) effect on Triglyceride. Values are expressed as Mean ± SEM. (N=5) (**P<0.01)

PCA004

Improving Maturity of iPSC-derived Cardiomyocyte Models for Cardiac Disease, Cardiotoxicity and Drug Screening

Steven Broadbent[1], Jamie Bhagwan[1], George Buchanan[1], Ashley Barnes[1]

[1]Axol Bioscience Ltd., Edinburgh, United Kingdom

Despite decades of effort, there is a pressing need for better *in vitro* cardiac and cardiotoxicity models. Cardiovascular diseases (CVD) remain the leading global cause of death and cardiotoxicity is responsible for a third of all pre-clinical pharmaceutical regulatory failures. While traditional models (*ex vivo* and *in vivo* animal models, primary human tissue and immortalised cell lines) have provided valuable insights, there remains a translational gap between the "bench and bedside" due to issues with human-relevance, alongside well-characterized challenges with availability, throughput and cost.

Researchers have therefore been turning to human iPSC-derived cardiomyocytes for their potential to provide a limitless source of consistent, human-relevant cardiac cells. By taking donor cells, reprogramming them to an iPSC state and then differentiating them into cardiomyocytes, researchers can mimic human physiology in a scalable format, using these cells to power advanced *in vitro* cardiac disease and cardiotoxicity models.

However, standard differentiation protocols can lead to less mature cardiomyocyte phenotypes, impairing functional performance and therefore the utility of human iPSC-based models. Key measures of immature phenotype include the following six parameters; their sarcomere alignment, cardiac maturity marker expression, lower levels of spontaneous beating, longer Field Potential Duration (FPD), slower Conduction Velocity (CV) and a switch from glycolysis to fatty acid metabolism.

Axol Bioscience, in collaboration with partner organizations, have developed a new metabolic maturation media to enhance the maturity of human iPSC-derived cardiomyocytes, enabling better models for cardiac research, disease and cardiotoxicity.

This new metabolic maturation media has been validated on two healthy control-derived ventricular cardiomyocyte lines: a newborn male line (ax2508) and a middle-aged female line (ax5858). This media drives more mature cardiac morphology as measured by ICC, with improved sarcomere alignment and increased expression of the key cardiac maturity markers Troponin T and Connexin-43 by DIV8. Transcriptomics analysis demonstrates improvement in the expression of cardiac maturity markers including PLN, SCN1B, KCNJ2, KCNJ3 and KCNQ1, with a Log2fold change from 2.6 to 3.8 for KCNJ2 and corresponding decreases in the expression of immaturity markers including HCN2. Functionally, the maturation media drives more mature electrical activity measured via cardiac electrophysiology, with a reduction in beat rate from 44 ± 1 bpm to 23 ± 2 bpm, increases in CV from 0.40 ± 0.04 mm/ms to 0.70 ± 0.04 mm/ms and a shortening of FPD from 491 ± 55 ms to 312 ± 14 ms (all n=7-8, $p<0.05$-0.0001, unpaired t-test with Welch's correction) by DIV14. The maturation media also incorporates a factor which selects against cells utilising glycolysis in favour of cells utilising fatty acid metabolism causing the die-back of any remaining

immature cardiomyocytes as detected by microscopy and confluence measurements. These improvements represent a more mature cardiomyocyte phenotype across the six parameters described previously.

With these improvements, human iPSC-derived cardiomyocytes can be produced with enhanced structural and functional maturity to power advanced *in vitro* models of cardiac disease and cardiotoxicity. This addresses a key challenge to the wider adoption of iPSC-derived cardiomyocytes for cardiac research, drug testing and cardiotoxicity.

PCA005

The acute effect of maximal sprint exercise on cerebrovascular reactivity in healthy young adults

Philip Buys[1], Emma Curtin[1], Conor Brady[1], Cillian Rooney[1], Ahmed Alshahrabally[1], Paul McConkey[1], Shane Donohoe[1], Hoda Darwish[1], Shane Spring[1], Gustav Hagon[1], Cara Gallagher[1], Aidan Mahon[1], Norita Gildea[1], Mikel Egana[1], Max Weston[1]

[1]Department of Physiology, School of Medicine, Trinity College Dublin, Dublin, Ireland

Background and Purpose Exercise training is known to have positive effects on cerebrovascular health, and in particular there is a growing interest surrounding high-intensity exercise and cerebrovascular function. Cerebrovascular reactivity (CVR) is one measure of cerebrovascular function, and refers to the ability of the cerebral blood vessels to dilate and constrict in response to acute changes in the partial pressure of arterial CO_2. However, little is known about the acute effect of sprint exercise on CVR. Therefore, the purpose of this study was to investigate the acute effect of maximal sprint exercise on CVR in healthy young adults.

Methods Twenty-one healthy adults (mean ± SD age, height and weight: 22.7 ± 3.1 years, 173.4 ± 8.4 cm and 70.3 ± 10.1 kg, respectively, 13 males, 8 females) volunteered to participate in this study. Participants visited the laboratory for one experimental visit, having refrained from caffeine, alcohol and vigorous physical activity for 24 hours, and arrived at the laboratory >2 hours postprandial. CVR of the middle cerebral artery to hypocapnia was determined through one minute of voluntary hyperventilation, performed at 25 breaths.min^{-1}. Middle cerebral artery blood velocity (MCAv) was measured using transcranial Doppler ultrasonography, and the partial pressure of end-tidal carbon dioxide ($P_{ET}CO_2$) was measured breath-by-breath using a gas analyser. Participants completed the CVR protocol at baseline, and 30 minutes following a maximal, 30 second Wingate test completed on a cycle ergometer. CVR was quantified as both the absolute (cm.s^{-1}) and relative (%) change in MCAv from baseline per 1 mmHg change in $P_{ET}CO_2$, taken from the final 10 s of hyperventilation. The effect of the Wingate test on MCAv, $P_{ET}CO_2$ and CVR was explored using paired samples t-tests.

Results Baseline MCAv was significantly lower following the Wingate test (60.8 ± 11.0 *vs* 66.2 ± 11.5 cm.s^{-1}, P<0.01), as was baseline $P_{ET}CO_2$ (32.4 ± 4.3 *vs* 36.8 ± 4.2 mmHg, P<0.01). During the hyperventilation protocol, both MCAv and $P_{ET}CO_2$ fell by a significantly smaller magnitude following the Wingate test, compared to baseline (20.6 ± 8.9 *vs* 26.0 ± 9.7 cm.s^{-1} and 12.3 ± 5.1 *vs* 14.5 ± 5.7 mmHg, respectively, P<0.01). However, CVR remained unaltered following the Wingate test, when expressed in both absolute (1.7 ± 0.4 *vs* 1.9 ± 0.4 cm.s^{-1}.mmHg^{-1}, P=0.16) and relative (2.9 ± 0.6 *vs* 2.8 ± 0.6 %.mmHg^{-1}, P=0.70) terms.

Conclusion These findings indicate that both resting MCAv and $P_{ET}CO_2$ are not fully recovered 30 minutes following maximal sprint exercise in healthy young adults. However, despite these marked changes in baseline values, the reactivity of MCAv to hypocapnia remained unaltered 30 minutes following a Wingate test. Future research investigating the time-course of CVR responses following sprint exercise is warranted to further our understanding of high-intensity exercise on cerebrovascular function.

PCA006

Skin vasoconstriction during negative pressure is not mediated exclusively by the myogenic response, but also by the venoarteriolar reflex

Nigel A. Callender[1,2,3], Samuel J. Oliver[4], Lars Øivind Høiseth[5], Jamie H. MacDonald[4], Justin S. Lawley[7,8], Jonny Hisdal[1,2]

[1]Faculty of Medicine, University of Oslo, Oslo, Norway, [2]Department of Vascular Surgery, Oslo University Hospital, Oslo, Norway, [3]Otivio AS, Oslo, Norway, [4]Institute for Applied Human Physiology, Bangor University, Bangor, United Kingdom, [5]Department of Anaesthesiology, Oslo University Hospital, Oslo, Norway, [6]Faculty of Medicine, University of Oslo, Oslo, Norway, [7]Department of Sports Science, University of Innsbruck, Innsbruck, Austria, [8]Institute of Mountain Emergency Medicine, EURAC Research, Bolzano, Italy

The non-baroreceptor mediated reduction in limb blood flow during local negative pressure has been attributed to the myogenic response (Lott *et al*., 2002). However, local negative pressure influences vascular transmural pressure, which is the stimulus underlying both the myogenic response and the venoarteriolar reflex (VAR). Venoarteriolar reflex and myogenic response mechanisms can be differentially manipulated using either venous congestion, which engages only the VAR but reduces regional perfusion pressure, or limb dependency, which engages both the VAR and myogenic response while preserving perfusion pressure (Okazaki *et al*., 2005). Although there may be some neural mediation of the myogenic response (Scotland *et al*., 2004), the VAR is entirely axon dependent, therefore topical anaesthetic block combined with the experimental manipulations described previously can separate the relative contributions of the two responses (Okazaki *et al*., 2005). By combining these experimental manipulations, we aimed to investigate whether the VAR contributes to vasoconstriction during negative pressure and if so, what proportion it may account for.

Following ethical approval and provision of informed consent, 25 healthy participants were recruited (14 males, 11 females; age: 32±8 y; height: 1.75±0.09 m; weight: 70.8±13.6 kg). First (n=17), we investigated the change in skin blood flux (Laser doppler fluxometry; Periflux 4001; Perimed, Järfälla, Sweden) during -40 mmHg negative pressure (180-sec), in a region of anaesthetised skin upon one lower leg (EMLA cream; Aspen pharma, Dublin, Ireland). The contralateral leg underwent the same interventions without anaesthetic block. Among a subset of participants (n=11), using methods based on Okazaki *et al*. (2005), the responses in skin blood flux following venous congestion (40 mmHg thigh cuff) were compared to limb dependency (45cm below horizontal), and negative pressure (-40 mmHg). The difference between the reduction in skin flux under control and blocked conditions was calculated and assumed to represent the VAR alone during venous congestion (DeltaC), and a combination of the VAR and myogenic response during limb dependency (DeltaD) or negative pressure (DeltaNP). Thereafter, assuming similar transmural stresses during each manipulation, the relative contribution of the VAR during limb dependency was estimated as [DeltaC/DD] x 100, and during negative pressure as [DeltaC/DNP] x 100. Data were analysed using repeated measures ANOVA, or Wilcoxon signed rank tests (mean ± SD or median [IQR]; p<0.05).

Topical anaesthetic block attenuated the reduction in skin blood flux during negative pressure (control: -53 [16], blocked: -6 [38]%, p<0.001; Figure 1). Negative pressure and limb dependency

elicited similar reductions in skin blood flux (Figure 2). Results comparing the proportions of differences between skin sites (Figure 3) and between the interventions suggest the VAR is responsible for ~57% of the local vasoconstriction observed during negative pressure or limb dependency, with the remaining ~43% contributed by myogenic mechanisms.

These data suggest that the VAR *does* contribute to reduced skin blood flux during negative pressure, accounting for over half of local vasoconstriction. Negative pressure and limb dependency elicited comparable vasoconstriction, indicating that without baroreceptor-mediated input, local vascular responses are similar whether transmural stress is induced by gravity or external negative pressure.

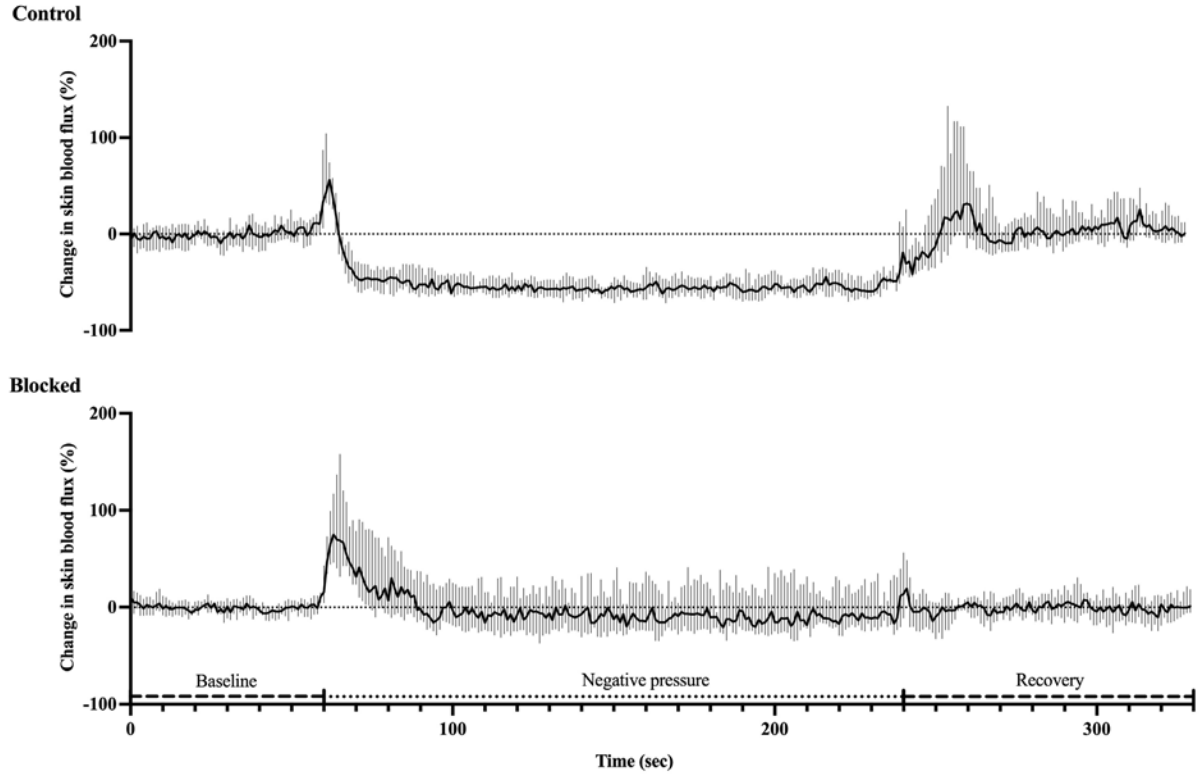

Figure 1: Time course of the changes to skin blood flux during sustained negative pressure (-40 mmHg)

Data (n=17) represent the **median [IQR]** percent change in skin blood flux per-second relative to the 60-sec baseline period, in control (upper panel) and blocked skin (lower panel).

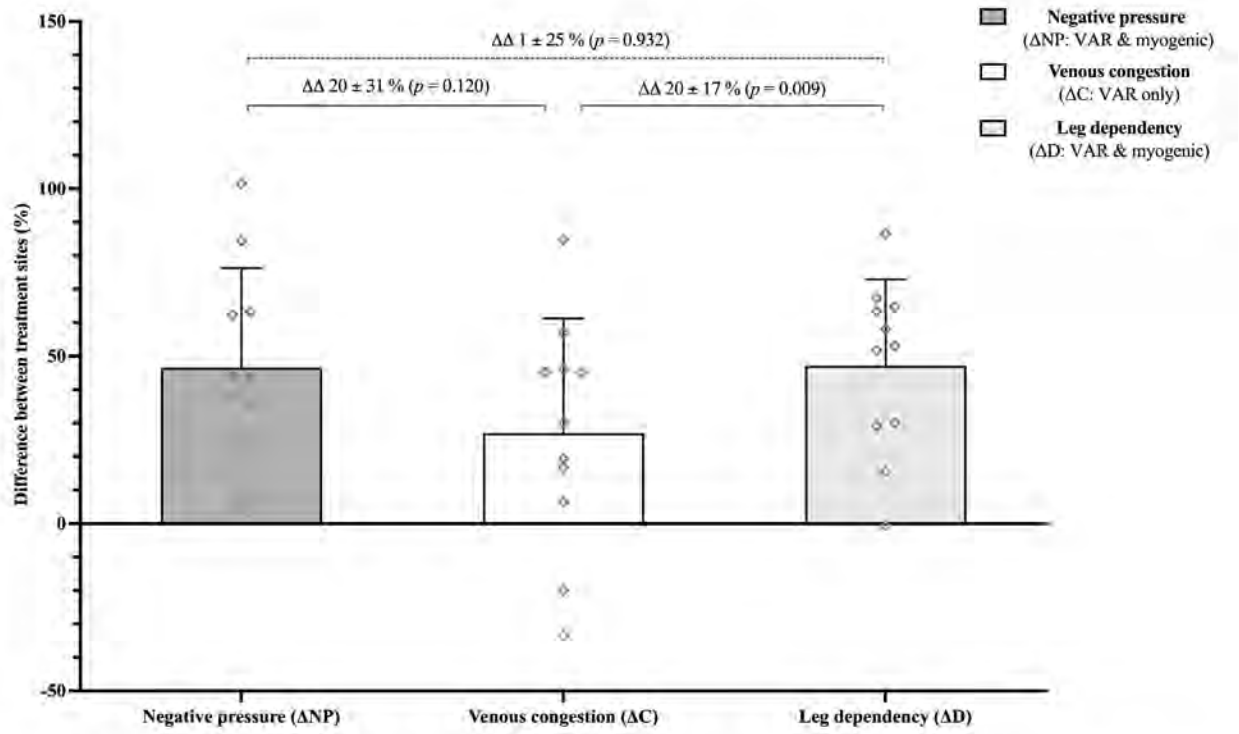

Figure 3: Differences in skin blood flux responses between treatment conditions during negative pressure (-40 mmHg), venous congestion (40 mmHg) and leg dependency (45 cm).

Data (n = 11) represent the **mean ± SD** difference between the percentage reductions in control and blocked skin found in Figure 2. Individual participants are indicated as diamonds. ΔΔ indicates between-intervention differences. P-values relate to comparisons between interventions using one-way repeated measures ANOVA and *post hoc* pairwise t-tests with Holm-Bonferroni correction.

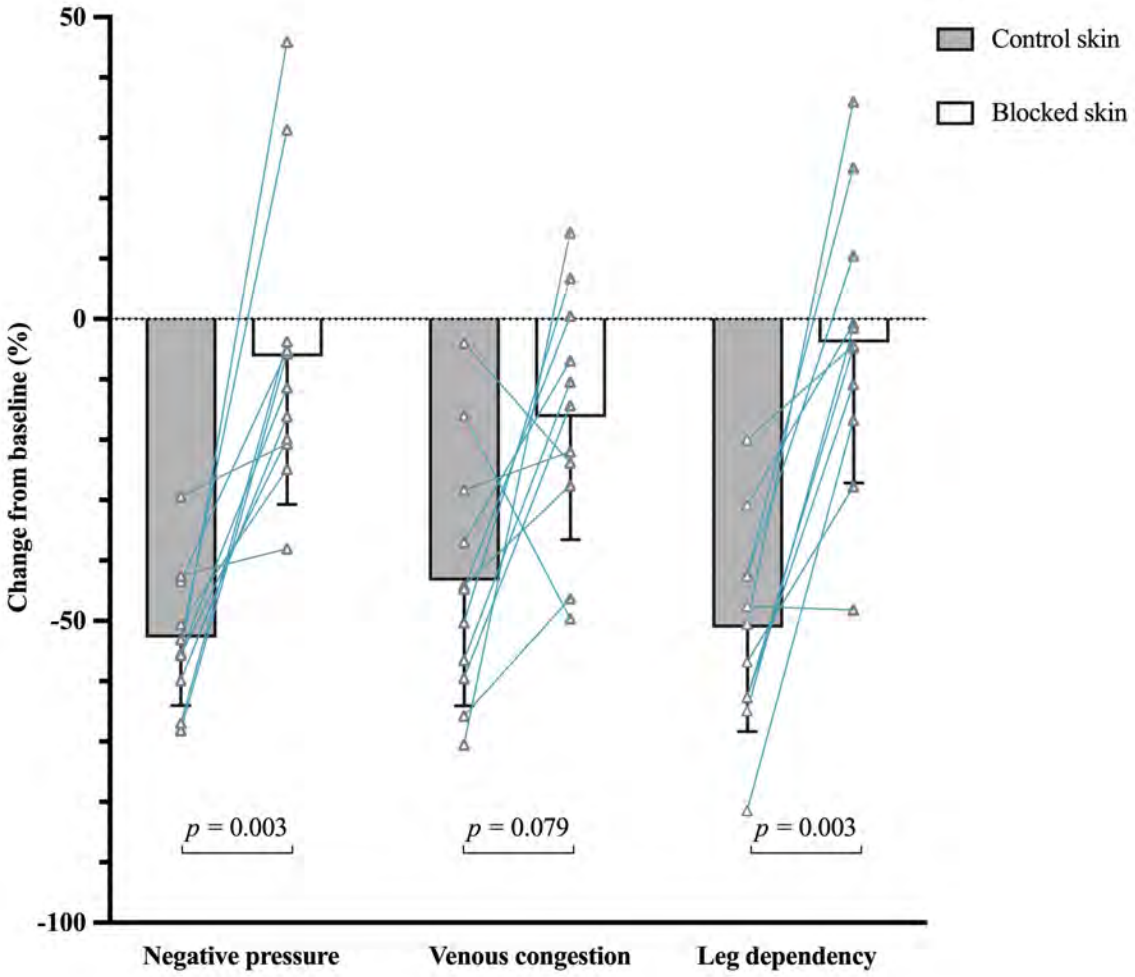

Figure 2: Changes in skin blood flux during negative pressure (-40 mmHg), venous congestion (40 mmHg) and leg dependency (45 cm).

Data ($n = 11$) represent the **mean ± SD** percentage reduction in skin blood flux relative to baseline during the final 60-sec of each intervention, in control (grey bars) and blocked skin (white bars). Individual participants indicated by triangles. *P*-values relate to comparisons between conditions using two-way repeated measures ANOVA and *post hoc* pairwise *t*-tests with Holm-Bonferroni correction.

Lott ME, Herr MD, Sinoway LI. Effects of transmural pressure on brachial artery mean blood velocity dynamics in humans. J Appl Physiol (1985). 2002 Dec;93(6):2137-46. doi: 10.1152/japplphysiol.00443.2002. Okazaki K, Fu Q, Martini ER, Shook R, Conner C, Zhang R, Crandall CG, Levine BD. Vasoconstriction during venous congestion: effects of venoarteriolar response, myogenic reflexes, and hemodynamics of changing perfusion pressure. Am J Physiol Regul Integr Comp Physiol. 2005 Nov;289(5):R1354-9. doi: 10.1152/ajpregu.00804.2004. Scotland RS, Chauhan S, Davis C, De Felipe C, Hunt S, Kabir J, Kotsonis P, Oh U, Ahluwalia A. Vanilloid receptor TRPV1, sensory C-fibers, and vascular autoregulation: a novel mechanism involved in

myogenic constriction. Circ Res. 2004 Nov 12;95(10):1027-34. doi: 10.1161/01.RES.0000148633.93110.24

PCA007

The effects of sex and fitness on cerebrovascular reactivity and cerebral autoregulation in healthy young adults

Emma Curtin[1], Max Weston[1], Philip Buys[1], Thayumaan Bissoonauth[1], Hassan Al-Shammary[1], Olamide Ojelabi[1], Ahmed Osman[1], Jason Li[1], Tihara Wickramasinghe[1], Ying Lim[1], Zhi Ching[1], Muireann Carey[1], Enda Rooney[1], Mikel Egana[1], Norita Gildea[1]

[1]Department of Physiology, School of Medicine, Trinity College Dublin, Dublin, Ireland

Background and Purpose Sex and fitness have been suggested to influence cerebrovascular function across the lifespan, but the effects of sex and fitness in healthy young adults remains debated. The purpose of this study was to investigate the effects of sex, cardiorespiratory fitness and anaerobic capacity on cerebrovascular reactivity (CVR) and dynamic cerebral autoregulation (dCA) in healthy young adults.

Methods 13 males (mean ± SD age, height and weight: 23.1±2.5 years, 178.0±5.3 cm and 73.7±9.4 kg, respectively) and 11 females (22.1±2.1 years, 165.2±6.5 cm and 61.6±9.5 kg) volunteered to take part in this study. Participants visited the laboratory on two occasions. During the first visit, participants completed a ramp incremental and verification test to determine maximal oxygen uptake ($\dot{V}O_{2max}$). In the second visit, dCA was assessed using a single sit-to-stand manoeuvre, and CVR to hypocapnia was determined during 60 seconds of voluntary hyperventilation. Middle cerebral artery blood velocity (MCAv) was measured via transcranial Doppler ultrasound, mean arterial pressure (MAP) via finger plethysmography and breath-by-breath end-tidal carbon dioxide ($P_{ET}CO_2$) through a gas analyser. dCA was quantified as the percentage fall in MCAv relative to the percentage fall in MAP upon standing (Δ%MCAv/Δ%MAP). CVR was calculated as both the absolute ($cm.s^{-1}$) and relative (%) change in MCAv from baseline per 1 mmHg change in $P_{ET}CO_2$, taken from the final 10 seconds of hyperventilation. Participants then completed a maximal, 30 second Wingate test on a cycle ergometer. Peak power output (PPO) and mean power output (MPO) from the Wingate test were recorded and expressed relative to body weight ($.kg^{-1}$). Independent samples t-tests explored differences in MCAv, dCA and CVR responses between males and females, and Pearson's correlation explored relationships between $\dot{V}O_{2max}$ and Wingate performance with dCA and CVR responses.

Results Males had a significantly greater $\dot{V}O_{2max}$ (49.5±8.0 *vs* 39.1±8.5 $ml.kg^{-1}.min^{-1}$, P=0.01), PPO (12.6±2.7 *vs* 9.5±2.0 $W.kg^{-1}$, P<0.01) and MPO (8.1±1.0 *vs* 6.3±1.1 $W.kg^{-1}$, P<0.01), compared to females. There were no significant differences between males and females in resting MCAv (62.5±10.9 *vs* 70.4±9.7 $cm.s^{-1}$, respectively, P=0.08), dCA (0.9±0.7 *vs* 0.8±0.4, P=0.76), absolute CVR (1.8± 0.3 *vs* 2.1± 0.5 $cm.s^{-1}.mmHg^{-1}$, P=0.08) nor relative CVR (2.8±0.5 *vs* 3.0± 0.8%$.mmHg^{-1}$, P=0.53). $\dot{V}O_{2max}$ was not significantly correlated with dCA, relative CVR or absolute CVR across the whole sample (r=-0.12 to 0.34, P≥0.12), in males (r=-0.19 to 0.50, P≥0.10) or in females (r=0.07 to 0.33, P≥0.32). MPO was also not significantly associated with dCA or CVR across the whole sample (r=-0.16 to 0.07, P≥0.45), in males (r=-0.16 to 0.25, P≥0.41) or in females (r=-0.27 to 0.35, P≥0.30).

Conclusion These findings indicate that, in healthy young adults, dCA and CVR are not different in males and females. Furthermore, cardiorespiratory fitness and anaerobic capacity were not associated with dCA or CVR in healthy young adults.

PCA008

Chronic Exposure to Global Pollutant Phenanthrene is Cardiotoxic in Mice

Ellie England[1], Holly Shiels[1], Alicia D'Souza[2]

[1]Division of Cardiovascular Sciences, Faculty of Biology, Medicine and Health, The University of Manchester, Manchester, United Kingdom, [2]National Heart and Lung Institute, Imperial College London, London, United Kingdom

Phenanthrene (Phe) is a polyaromatic hydrocarbon found predominantly in fossil fuel and petroleum-based pollution. Previous research has shown that acute exposure to high concentrations of Phe is pro-arrhythmic in mice. To determine the arrhythmic potential of chronic low-level exposure to Phe 16 5-week-old mice and 16 20-month-old mice were fed 6ug/kg Phe daily for 10 weeks. Repeat ECG and echocardiography measurements were collected during the exposure period. All animal work was carried out in accordance with the UK animals (scientific procedures) act 1986. Following the 10-week exposure hearts were subjected to an ex-vivo arrhythmia challenge and tissue was collected for gas-chromatography mass-spectrometry and histological analysis. Preliminary analysis has revealed an increased susceptibility to arrhythmia in aged mice. 63% of aged mice exposed to Phe showed spontaneous arrhythmic activity ex vivo versus none of the control or young mice (n=8, t test- $p<0.05$). Phe exposure significantly increased arrhythmia induction following pacing, from 17% to 75% (n=8, t test- $p<0.05$). This difference was not present when hearts were treated with isoprenaline before pacing, suggesting bradycardia as an underlying mechanism for Phe induced arrhythmia.

S. Yaar, et al. Global air pollutant phenanthrene and arrhythmic outcomes in a mouse model Environmental Health Perspectives, 131 (11) (2023), Article 117002: https://www.ncbi.nlm.nih.gov/pmc/articles/PMC10619431/

PCA009

Mechanistically complex effects of variant calmodulin on ryanodine receptor 2 in CPVT

Aisha Gendra[1], Ewan D. Fowler[3], Nordine Helassa[4], N Lowri Thomas[1]

[1]School of Pharmacy and Pharmaceutical Sciences, Cardiff University, Cardiff, United Kingdom, [2]School of Pharmacy & Pharmaceutical Sciences, Cardiff University, Cardiff, United Kingdom, [3]School of Biosciences, Cardiff University, Cardiff, United Kingdom, [4]Faculty of Health and Life Sciences, University of Liverpool, Liverpool, United Kingdom

The cardiac ryanodine receptor (RyR2) is a Ca^{2+} channel located on the sarcoplasmic reticulum of cardiomyocytes. In regulating Ca^{2+} release, it maintains both electrical and contractile function, and in these tasks its normal function is modulated by the Ca^{2+}-binding accessory protein calmodulin (CaM)[1,2]. Several CaM mutations have been linked to cardiac arrhythmias, such as Catecholaminergic Polymorphic Ventricular Tachycardia (CPVT), but their arrhythmogenic mechanisms are not fully resolved. This research investigates the effects of two arrhythmia-linked CaM mutations (D132E and Q136P) on RyR2 function (either directly, or by virtue of CaM's regulation of its associated kinase: CaMKII) and how this might lead to aberrant Ca^{2+} signalling[3].

RyR2 and CaM were recombinantly co-expressed in HEK293 cells and live-cell confocal Ca^{2+} imaging was used to assess recursive Ca^{2+} release dynamics. The effect of wild type (WT) CaM co-expression on RyR2 is inhibitory - decreasing the duration of Ca^{2+} release events (thereby affecting the frequency of release). Co-expression of D132E and Q136P CaM was shown to reverse this phenomenon by increasing the duration of Ca^{2+} release events (WT 9.79±0.54 vs D132E 12.62±0.52 vs Q136P 13.20±1.02 seconds (mean±SEM), $p<0.05$, one-way ANOVA test, n=11, 19 and 10 field of view containing approximately 15 cells each, for WT, D132E and Q136P CaM respectively). This finding suggests a decrease in direct regulation of RyR2 by these mutant CaMs. Additionally, in line with HEK293 data, D132E CaM significantly reduced the endoplasmic reticulum Ca^{2+} store load in HEK293 cells compared to WT CaM ($\Delta F/F_0$= WT 0.47, 95% CI [0.42, 0.55] vs D132E 0.24, [0.22, 0.28], $p<0.05$, Kruskal-Wallis test, n=150 cells for each construct, values are shown as median, 95% CI [lower confidence limit, upper confidence limit]), as determined by the addition of 10mM caffeine. It is, therefore, likely that D132E variant CaM is causing Ca^{2+} leakage from the channel which results in smaller Ca^{2+} stores.

Line-scans were used to detect Ca^{2+} sparks in permebilised C57BL/6 mouse ventricular myocytes in the presence of WT or mutant CaMs. D132E variant CaM was shown to significantly increase spark duration (WT 51.25, 95% CI [45, 57.5] vs D132E 58.75, 95% CI [52.5, 67.5] ms) and time to peak (WT 10, 95% CI [8, 11] vs D132E 12, 95% CI [10, 13.5] ms) in cardiac myocytes compared to WT CaM ($p<0.05$, Kruskal-Wallis test, n=39 and 37 cells isolated from 3 mice for WT and D132E CaM respectively, values are shown as median, 95% CI [lower confidence limit, upper confidence limit]).

The time course of CaMKII autophosphorylation showed significantly reduced autophosphorylation in the presence of Q136P CaM compared to WT ($p<0.05$ at each timepoint, one sample Wilcoxon signed rank test, n=5). Western analysis also revealed that Q136P CaM significantly reduced RyR2 phosphorylation at the S2814 CaMKII phosphorylation site compared to WT CaM ($p<0.05$, one

sample Wilcoxon signed rank test, *n*=6). These results show that D132E and Q136P exert their dysfunction in different ways, suggesting that calmodulinopathy in CPVT is likely mechanistically complex.

(1) W. Peng et al., “Structural basis for the gating mechanism of the type 2 ryanodine receptor RyR2,” Science, vol. 354, no. 6310, Oct. 2016, doi: 10.1126/SCIENCE.AAH5324. (2) A. B. Sorensen, M. T. Søndergaard, and M. T. Overgaard, “Calmodulin in a Heartbeat,” FEBS Journal, vol. 280, no. 21, pp. 5511–5532, Nov. 2013, doi: 10.1111/FEBS.12337. (3) N. Makita et al., “Novel calmodulin mutations associated with congenital arrhythmia susceptibility,” Circulation: Cardiovascular Genetics, vol. 7, no. 4, pp. 466–474, Aug. 2014, doi: 10.1161/CIRCGENETICS.113.000459/-/DC1.

PCA010

Long-term impact of high-intensity interval-training on cardiac structure and function after COVID-19: an investigator-blinded randomised controlled trial

Iben Elmerdahl Rasmussen[1,2], Mathilde Løk[2], Cody Garett Durrer[1], Anna Agnes Lytzen[1], Frederik Foged[1], Vera Graungaard Schelde[1], Josephine Bjørn Budde[1], Rasmus Syberg Rasmussen[1], Emma Fredskild Høvighoff[1], Villads Rasmussen[1], Mark Lyngbæk[1], Simon Jønck[1], Rikke Krogh-Madsen[1,3], Birgitte Lindegaard[1,4], Peter Godsk Jørgensen[5], Lars Køber[5], Niels Vejlstrup[5], Bente Klarlund Pedersen[1], Mathias Ried-Larsen[1,6], Morten Asp Vonsild Lund[2,5], Ronan M.G. Berg[1,2,7,8], Regitse Højgaard Christensen[1,9]

[1]Centre for Physical Activity Research, University Hospital Copenhagen – Rigshospitalet, Copenhagen, Denmark, [2]Department of Biomedical Sciences, Faculty of Health and Medical Sciences, University of Copenhagen, Copenhagen, Denmark, [3]Department of Infectious Diseases, University Hospital Copenhagen –Hvidovre Hospital, Hvidovre, Denmark, [4]Department of Pulmonary Medicine and Infectious Diseases – North Zealand Hospital, Hillerød, Denmark, [5]Department of Cardiology, University Hospital Copenhagen – Rigshospitalet, Copenhagen, Denmark, [6]Research Unit for Exercise Epidemiology, Department of Sports Science and Clinical Biomechanics, University of Southern Denmark, Odense, Denmark, [7]Department of Clinical Physiology and Nuclear Medicine, Rigshospitalet, University Hospital Copenhagen – Rigshospitalet, Copenhagen, Denmark, [8]Neurovascular Research Laboratory, Faculty of Life Sciences and Education, University of South Wales, Pontypridd, United Kingdom, [9]University Hospital Copenhagen – Herlev Hospital, Herlev, Denmark

Introduction: Following the acute phase of SARS-CoV-2 infection, ,ore than a quarter of individuals suffer from persistent exercise intolerance. In a recent study, we observed that a supervised 12w high-intensity interval training (HIIT) scheme resulted in a ~4 g/m^2 increase in left ventricular mass (LVM) with a corresponding improvement of functional limitations immediately after the intervention. However, there was no effect on pulmonary diffusing capacity or other lung function metrics [14]. Yet, it is unknown whether these changes persist at the long-term. We aim to investigate whether HIIT has long-term effects on cardiopulmonary function in individuals previously hospitalised for COVID-19.

Methods: We enrolled 28 patients (57 ± 11 years; 64% male) previously hospitalised for COVID-19 for this investigator-blinded randomized study with a 12-week (3 sessions/week) supervised HIIT intervention (4x4 HIIT scheme). Outcomes were assessed as the between-group change from baseline to 12mo follow-up. The primary outcome was change in LVM in grams measured by cMRI. The secondary outcomes were between-group change in pulmonary diffusing capacity for carbon monoxide corrected for haemoglobin ($D_{L,COc}$), $V\dot{O}_2$peak, a well as the post-COVID-19 function scale (PCFS) and King's Brief Interstitial Lung Disease (KBLID) questionnaire scores. A constrained baseline longitudinal data analysis was used to compare cardiopulmonary changes within and between groups. The study was approved by The Research Ethics Committee of the Capital Region of Denmark (H-20033733 with amendment 75068). The study conformed with the Declaration of Helsinki, and all participants provided oral and written informed consent prior to participation.

Results: Of the 28 patients invited from the main study, 23 consented to participate in the 12mo follow-up, which was completed on average 12.4±0.6mo after enrollment in the study. Ultimately, 28 participants were included in the final analysis at 12mo (HIIT: n=14, control: n=14). LVM was maintained between 3mo and 12mo follow-up in the HIIT group, whereas it decreased in the control group with a between-group difference of 9.7 [1.7; 17.6] g (p=0.018). LVEDV and LVESV showed a similar pattern, but without a significant between-group difference (Figure 1). $D_{L,COc}$%pred, FEV_1%pred, FVC%pred, TLC%pred and increased similarly in both groups, while RV%pred only increased in the control group.

Conclusion: In individuals previously hospitalised for COVID-19, a 12w supervised HIIT scheme leads to a persistently increased LVM reflecting physiological hypertrophy at 12mo follow-up.

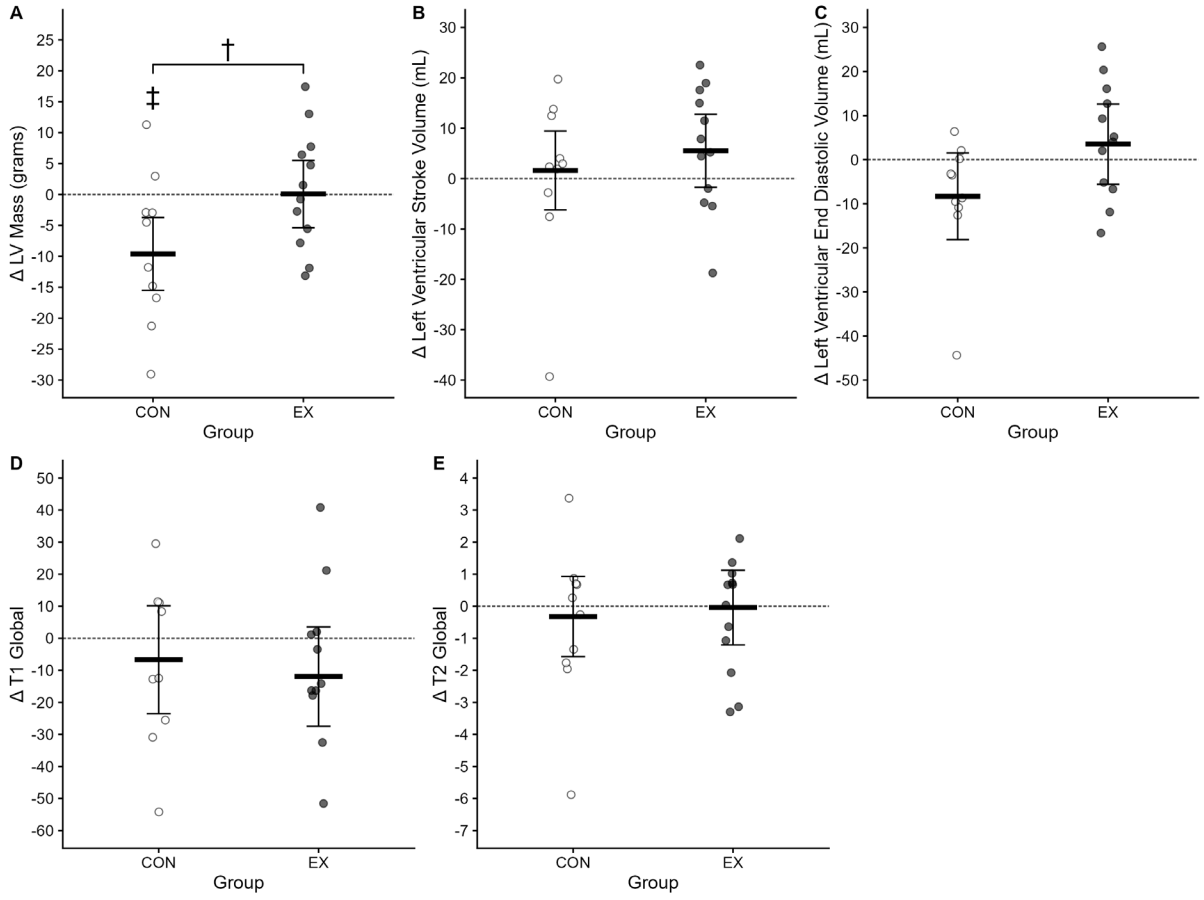

Rasmussen, I. E., Løk, M., Durrer, C. G., Foged, F., Schelde, V. G., Budde, J. B., Rasmussen, R. S., Høvighoff, E. F., Rasmussen, V., Lyngbæk, M., Jønck, S., Krogh-Madsen, R., Lindegaard, B., Jørgensen, P. G., Køber, L., Vejlstrup, N., Pedersen, B. K., Ried-Larsen, M., Lund, M. A. V., … Berg, R. M. G. (2023). Impact of high-intensity interval training on cardiac structure and function after

COVID-19: an investigator-blinded randomized controlled trial. Journal of Applied Physiology, 135(2), 421–435. https://doi.org/10.1152/JAPPLPHYSIOL.00078.2023

PCA011

Investigation of RyR2 Arg1051 arrhythmia and cardiomyopathy-linked mutations: functional effects at the single channel, population and whole cell level.

Tessa Harris[1], Lowri Thomas[1]

[1]School of Pharmacy and Pharmaceutical Sciences, Cardiff University, Cardiff, United Kingdom

The human cardiac ryanodine receptor (hRyR2) is a Ca^{2+} ion channel found on the sarcoplasmic reticulum of cardiomyocytes that plays a central role in excitation-contraction coupling. This channel is tightly regulated to prevent dysfunction, though mutation of hRyR2 is associated with arrhythmia and cardiomyopathy. Inter-channel clustering of hRyR2 is proposed to regulate its function[1], preventing uncontrolled Ca^{2+} release and possibly promoting concerted gating[2]. This research aims to functionally characterise arrhythmia / cardiomyopathy-linked mutations (R1051P, R1051C, and R1051H) found in the P1 domain – a region likely involved in inter-channel clustering[3] - to determine whether any Ca^{2+} release dysfunction is influenced by functional changes at the clustering level.

HEK293 cells recombinantly expressing either wild-type (WT) or mutant hRyR2 were loaded with Calbryte 520 AM Ca^{2+} sensitive dye and imaged using confocal microscopy to assess whole cell Ca^{2+} release. Ca^{2+} release from populations of human recombinant RyR2 channels incorporated into droplet interface bilayers (DIBs)[4] was analysed optically (with Cal590) using total internal reflection fluorescence microscopy (TIRF). Purified hRyR2 was incorporated into artificial bilayers for single channel recording and analysis of gating mechanisms[5].

Spontaneous whole cell Ca^{2+} release from R1051-mutants was significantly different from WT hRYR2 ($p<0.05$, one-way ANOVA with Tukey post-hoc tests) and displayed longer duration of oscillations (WT = 17.7±0.18, R1051P = 21.4±0.51, R1051C = 21.3±0.34, R1051H = 20.5±0.30, seconds), and lower amplitude (WT = 1.15±0.2, R1051P = 0.88±0.03, R1051C = 0.76±0.02, R1051H = 0.71±0.02, $\Delta F/F_0$) (n = number of cells, WT n=645, R1051P n=204, R1051C n=357, R1051H n=447, results expressed as mean±SEM), indicating Ca^{2+} release dysfunction. Populations of R1051P hRyR2 exhibited additional Ca^{2+} flux behaviours not observed for the WT indicative of rapid switching between stable periods of low and high Ca^{2+} flux (n=42-63 channel populations). Preliminary analysis estimating cluster size did not indicate any difference in cluster size between R1051P and WT hRyR2, although results suggested these behaviours manifested more frequently in larger populations. Single channel experiments showed comparable open probabilities (P_o) for mutant and WT channels (n=3-4 channels), although mathematical modelling of higher P_o traces indicated R1051P visited longer open states more frequently (WT τ = 36.5ms, amp = 54%, R1051P τ = 60.4ms. amp = 68%) with fewer flicker closings than WT hRyR2.

This research demonstrates that mutation of R1051 affects hRyR2 function at multiple organisational levels. Effects at the single channel level seem of minor impact, with dysfunction becoming more pronounced and distinct from the WT in populations of channels, suggesting that the mutational effect largely manifests at the cluster level. This has downstream effects on global Ca^{2+} release dynamics that may act as a substrate for arrhythmia. Future work aims to better quantify cluster size and correlate this to Ca^{2+} release behaviour from populations, and

consideration of hRyR2 distribution within clusters will be important in consolidating the mechanism of dysfunction.

1. Baddeley D et al. (2009). Proc Natl Acad Sci USA 106, 22275-22280. 2. Marx SO et al. (2001). Circ Res 88, 1151-1158. 3. Cabra V et al. (2016). Biophys Journal 110 12, 2651-2662. 4. Leptihn S et al. (2013). Nature Protocols 8, 1048-1057. 5. Mukherjee S et al. (2012). JGP 140(2), 139–158.

PCA012

Developing p21-activated kinase 1 (PAK1) activators to treat hypertrophic cardiomyopathy (HCM)

YU HE[2], James. S. H. Bae[1], Ming Lei[3]

[1]Department of Pharmacology, University of Oxford, Oxford, United Kingdom, [2]Department of Pharmacology, University of Oxford, Oxford, United Kingdom, [3]Department of Pharmacology, University of Oxford, Oxford, United Kingdom

Research rationale: Despite significant progress in comprehending the genetic and metabolic underpinnings of cardiomyocyte dysfunction, there is still a pressing need for targeted treatments to address hypertrophy and progressive remodelling (e.g., fibrosis), seen in HCM [1]. PAK1, a regulator of ion channels and myofilaments in cardiomyocytes, has shown promise in curbing pathological hypertrophy [2]. Our hypothesis centres on the potential therapeutic benefits of pharmacologically activating PAK1 in managing hypertrophy and adverse remodelling in HCM.

Methods: Molecular docking and high-throughput kinase assays using RapidFire-mass spectrometry were employed for virtual and physical screening to develop PAK1 activators. The effect of these activators on cellular hypertrophy was assessed using hypertrophic neonatal rat cardiomyocytes (n=200-300) induced by isoprenaline (ISO, 40 μM). Subsequently, the small molecule PAK1 activator JB2020A was evaluated in a well-characterized transgenic mouse model expressing the hypertrophic cardiomyopathy-causing mutation $Actc1^{E99K}$, known for its rapid disease progression [3]. A six-week oral treatment regime (10 mg/kg/day of JB2020A, Vehicle, and WT, N=5 in each group) was initiated at 4 weeks of age. The therapeutic efficacy of these pharmacological interventions and the endpoints were assessed using echocardiography, histology including Sirius red staining and H&E staining, and biomarker assessment using western blot. Data were analysed as mean ± SEM, ****$p < 0.0001$, ***$p < 0.001$, **$p < 0.01$, *$p < 0.05$, ns, not significantly different according to one-way ANOVA with Tukey's posthoc test.

Results: We have identified potent and effective small molecule PAK1 activators that significantly increased PAK1 activity by 3 to 5-fold, with an EC_{50} range between 0.5 and 2.5 μM. Through the evaluation of PAK1 activators on cellular hypertrophy, JB2020A not only prevented ISO-induced hypertrophy but also reversed pre-existing cellular hypertrophy induced by ISO 24 hours earlier. Moreover, after 6 weeks of JB2020A treatment, we observed a significant reduction in cardiomyocyte hypertrophy and cardiac fibrosis, accompanied by preserved cardiac function in $Actc1^{E99K}$ HCM mice compared to vehicle treatment. These cardio-protective effects were associated with increases in phosphorylated PAK1 observed after activator treatment. Furthermore, JB2020A treatment resulted in a reduction in pro-apoptotic CHOP expression and an upregulation of protective endoplasmic reticulum (ER) response molecules (such as ATF4 and Xbp1), suggesting an amelioration of ER stress in HCM.

Conclusions: Collectively, these findings underscore the therapeutic potential of small molecule PAK1 activators as a novel approach for addressing hypertrophy and progressive remodelling in HCM.

1Watkins, Hugh, et al. "Inherited cardiomyopathies." New England Journal of Medicine 364.17 (2011): 1643-1656. 2. Wang, Yanwen, et al. "The p21-activated kinase 1 (Pak1) signalling pathway in cardiac disease: from mechanistic study to therapeutic exploration." British journal of pharmacology 175.8 (2018): 1362-1374. 3. Song, Weihua, et al. "Molecular mechanism of the E99K mutation in cardiac actin (ACTC Gene) that causes apical hypertrophy in man and mouse." Journal of Biological Chemistry 286.31 (2011): 27582-27593.

PCA013

Evaluation of the skin microcirculation response by wavelet analysis: the impact of the cone of influence

Lana Kralj[1], Helena Lenasi[1]

[1]Institute of Physiology, Faculty of Medicine, Ljubljana, Slovenia, [2]Institute of Physiology, Faculty of Medicine, Ljubljana, Slovenia

Introduction

Wavelet analysis (WA) is a perspective method for performing spectral analysis of laser Doppler (LD) microcirculatory signals. WA decomposes LD signals into wavelet spectra consisting of six frequency intervals related to physiological influences (endothelial nitric oxide (NO)-independent, endothelial NO-dependent, neurogenic, myogenic, respiratory, and cardiac) that modulate the microcirculatory response and range from 0.005-2 Hz [1].

As WA is applied to finite length signals, the analysis results inevitably suffer from edge effects that lead to distortions of the spectral amplitude. The cone of influence (COI), defined as the e-folding time for the autocorrelation of wavelet transform at each scale, delineates the regions of the wavelet spectrum where such edge effects become important [2,3]. Since the cone of influence reduces the available data, these regions can affect the relevance of the results provided [4]. However, the extent to which performing WA by considering the values outside the COI affects the analysis results has not yet been fully investigated.

Aims

We aimed to determine whether accounting for COI leads to significant differences in the results obtained by WA. We observed two typical patterns of LD signal: a stationary signal represented by the baseline LD signal and a complex transient signal represented by the post-occlusive phase of transient arterial occlusion.

Method

Following ethical approval by the National Ethics Committee of the Republic of Slovenia (no. 87/06/13), eighteen healthy young volunteers were recruited.

LD signals were acquired at the volar forearm during a five-minute baseline recording, a transient three-minute occlusion of the brachial artery, and a recovery phase lasting an additional five minutes.

WA was performed on the signals acquired during the baseline and recovery phases. The time-averaged wavelet spectra were constructed in two ways: with and without the data affected by edge effects (i.e. without and with COI correction).

To compare the contribution of different physiological mechanisms to the regulation of microcirculatory responses during these phases, the relative power (RP = median power of each frequency interval / median power of the total spectrum) was determined for each frequency interval of the corresponding phase.

A non-parametric Wilcoxon signed-rank test was used to compare the differences between the RP of the spectral components obtained without and with COI correction, respectively. The results are presented as group medians and the interquartile range.

Results

No statistically significant differences were found between the RPs of the baseline phase determined without and with COI correction. Statistically significant differences were observed in the RPs of the frequency bands associated with endothelial NO-independent (9.72 [6.76-11.76] without vs. 2.47 [1.27-4.44] with correction, $p<0.001$), endothelial NO-dependent (4.33 [2.58-7.61] without vs. 1.15 [0.76-2.47] with correction, $p<0.001$), neurogenic (1.89 [1.25-2.62] without vs. 1.12 [0.81-1.19] with correction, $p<0.05$), myogenic (0.84 [0.51-0.93] without vs. 1.06 [0.97-1.41] with correction, $p<0.001$), respiratory (0.33 [0.22-0.42] without vs. 0.51 [0.44-0.77] with correction, $p<0.001$) and cardiac (0.25 [0.16-0.59] without vs. 0.54 [0.31-0.95] with correction, $p<0.001$) influence.

Conclusion

Our results suggest that it may be crucial to adjust WA results for COI correction in case of transient LD signals, especially for low-frequency endothelial intervals that are questionable to evaluate in practice.

[1] Kralj, L., & Lenasi, H. (2023). Wavelet analysis of laser Doppler microcirculatory signals: Current applications and limitations. Frontiers in Physiology, 13. https://doi.org/10.3389/fphys.2022.1076445 [2] Chen, X., Gupta, R. S., & Gupta, L. (2023). Exploiting the Cone of Influence for Improving the Performance of Wavelet Transform-Based Models for ERP/EEG Classification. Brain Sciences, 13(1). https://doi.org/10.3390/brainsci13010021 [3] Torrence, C., & Compo, G. P. (1998.). A Practical Guide to Wavelet Analysis. Bulletin of the American Meteorological Society, 79 (1). https://doi.org/10.1175/1520-0477(1998)0792.0.CO;2 [4] Reynès, C., Vinet, A., Maltinti, O., & Knapp, Y. (2020). Minimizing the duration of laser Doppler flowmetry recordings while maintaining wavelet analysis quality: A methodological study. Microvascular Research, 131. https://doi.org/10.1016/j.mvr.2020.104034

PCA014

Does exercise training and estradiol affect wound healing in microvascular smooth muscle cells of post-menopausal women?

Sophie Møller[1]

[1]*University of Copenhagen, Copenhagen, Denmark*

Introduction: Menopause is linked to decreased vascular function and increased cardiovascular risk (1). Although exercise is cardioprotective, improving vascular health, post-menopausal women have shown a blunted response due to lower estrogen levels (2). Research has solely focused on endothelial cells, neglecting the role of smooth muscle cells (SMCs) in vascular function. While literature on the direct effects of estrogen on SMCs are conflicting, what is clear is the existence of estrogen receptors on SMCs (3). Additionally, estrogen appears to inhibit SMC proliferation (4,5).

Objective: This study investigated if exercise training and/or estradiol treatment improved wound healing in microvascular SMCs from early and late post-menopausal women.

Methods: The study was approved by the ethics committee of Copenhagen (H-20037633) and conducted according to the Declaration of Helsinki. All participants were informed about the procedures and potential risks, both orally and in writing, with written informed consent obtained before enrollment.

Early (1-5 years) and late (≥10 years) post-menopausal women not on hormone replacement therapy participated. Microvascular SMCs were isolated from muscle biopsies of both early (n=7) and late (n=7) post-menopausal women, before and after an 8-week exercise regimen (aerobic interval training 3 times/week). Wound healing was assessed by scratching cultured SMCs and measuring wound closure at set time points (t=0, 4, and 24 post-wound infliction). An additional group were pre-incubated with 3.67 µM estradiol for 2 days prior to the wound healing assay.

Results: Basal wound healing was similar across groups. Estradiol pre-incubation had no independent effect. Exercise training improved wound healing profiles in both early and late post-menopausal groups. This improvement was significant in the late post-menopausal group with estradiol pre-treatment ($P = 0.034$).

Conclusion: Preliminary data suggests exercise training improves the wound healing profile of SMCs, potentially indicating improved cellular health. This effect might be amplified when combined with estrogen therapy in late post-menopause.

References: (1) Nyberg M, Egelund J, Mandrup CM, Nielsen MB, Mogensen AS, Stallknecht BM, Bangsbo J & Hellsten Y (2016). Early postmenopausal phase is associated with reduced prostacyclin-induced vasodilation that is reversed by exercise training. The Copenhagen Women Study. Hypertens 68, 1011-20. (2) Nyberg M, Egelund J, Mandrup CM, Anderson CB, Hansen KMBE, Hergel IMF, Valbak-Andersen N, Frikke-Schmidt R, Stallknecht B, Bangsbo J & Hellsten Y (2017). Leg vascular and skeletal muscle mitochondrial adaptations to aerobic high-intensity exercise training are enhanced in early postmenopausal phase. J Physiol 595, 2696-83. (3) Karas RH,

Patterson BL & Mendelsohn ME (1994). Human vascular smooth muscle cells contact functional estrogen receptor. Circ 89, 1943-50. (4) Li QY, Chen L, Zhu QH, Zhang M, Wang YP & Wang WM (2011). Involvement of estrogen receptor-β in ferrorol inhibition of rat thoracic aorta vascular smooth muscle cell proliferation. Acta Pharmacol Sinica 32, 433-40. (5) Ortmann J, Veit M, Zingg S, Di Santo S, Traupe T, Yang Z, Völzmann J, Dubey RK, Christen S & Baumgartner I (2011). Estrogen receptor-α but not -β or GPER inhibits high glucose-induced human VSMC proliferation: Potential role of ROS and ERK. J Clin Endocrinol Metab 96, 220-8.

PCA015

The Role of Sortillin-Related VPS10P Containing Receptor, SorCS2 in Endothelial and Smooth Muscle Cell Function.

Rashika Sivakumar, Elizaveta Melnikova, Christian Stæhr, Vladimir Matchkov

undefined

Introduction. Sortillin-related VPS10P containing receptor (SorCS2) is expressed in neurons and other tissues during development where it mediates trafficking of target proteins between cell membrane and intracellular compartments. It has also been suggested that SorCS2 modulates signal transduction (Malik et al., 2020; Salasova et al., 2022). Moreover, SorCS2 is upregulated in the vascular wall under pathological conditions, e.g., atherosclerosis (Amadio et al., 2017). The aim of this study was to elucidate the contribution of endothelial and smooth muscle SorCS2 to the vascular function.

Method. We compared mesenteric small arteries (MSA) from endothelium- and smooth-muscle-specific knockouts (KO) for SorCS2 with matching controls in isometric myograph. For the endothelium-specific KO study, mice of two genotypes were used as controls: mice with floxed SorCS2 gene but without any Cre-recombinase expression, and mice with Cre-recombinase expression without any SorCS2-floxed gene. The endothelium-specific SorCS2 KO was constitutive KO with Cre expression controlled by Tie2 promoter. For this knockout, the mice were grouped into homozygote and heterozygote sub-groups, respectively. Cre expression was controlled by estrogen receptor type 2 under smooth-muscle-myosin-heavy-chain promoter and the smooth-muscle-specific knockout was induced by tamoxifen treatment. Vascular compliance, inner arterial diameters, noradrenaline-induced contraction, acetylcholine-induced relaxation, and relaxation to NO donor, sodium nitroprusside were compared between KOs and matching wild types.

Results. The MSA from endothelial-specific SorCS2 homozygote KO mice (n= 5-6) showed reduced compliance and reduced contractility to noradrenaline in comparison with the matching controls (n = 3-6). Furthermore, the MSA from endothelial-specific SorCS2 homozygote KO (n=5-6) demonstrated an increased sensitivity to acetylcholine-induced relaxation, which seemed to be NO-dependent. The MSA from smooth-muscle-specific SorCS2 KO (n = 3) had no changes in both acetylcholine- and sodium-nitroprusside-induced relaxations but showed decreased noradrenaline-induced contraction and compliance in comparison with the control arteries.

Conclusion. Our findings from the cell-specific vascular KO models indicate that SorCS2 contributes to endothelial- and smooth muscle-cell functions in murine mesenteric arteries.

References: Amadio, P., Colombo, G. I., Tarantino, E., Gianellini, S., Ieraci, A., Brioschi, M., Banfi, C., Werba, J. P., Parolari, A., Lee, F. S., Tremoli, E., & Barbieri, S. S. (2017). BDNFVal66met polymorphism: a potential bridge between depression and thrombosis. Eur Heart J, 38(18), 1426-1435. https://doi.org/10.1093/eurheartj/ehv655 Malik, A. R., Lips, J., Gorniak-Walas, M., Broekaart, D. W. M., Asaro, A., Kuffner, M. T. C., Hoffmann, C. J., Kikhia, M., Dopatka, M., Boehm-Sturm, P., Mueller, S., Dirnagl, U., Aronica, E., Harms, C., & Willnow, T. E. (2020). SorCS2 facilitates release of endostatin from astrocytes and controls post-stroke angiogenesis. Glia, 68(6), 1304-1316. https://doi.org/10.1002/glia.23778 Salasova, A., Monti, G., Andersen, O. M., & Nykjaer, A. (2022). Finding memo: versatile interactions of the VPS10p-Domain receptors in Alzheimer's disease. Mol Neurodegener, 17(1), 74. https://doi.org/10.1186/s13024-022-00576-2

PCA016

Effects of maternal obesity on cardiac metabolism and mitochondrial respiratory function in young adult mice born to obese dams.

Benjamin Thackray[1], Denise Fernandez-Twinn[2], Alice Knapton[1], Susan Ozanne[2], Andrew Murray[1]

[1]Department of Physiology, Development and Neuroscience, University of Cambridge, Cambridge, United Kingdom, [2]Wellcome-MRC Institute of Metabolic Science, University of Cambridge, Cambridge, United Kingdom

Introduction: In a well-established model of murine diet-induced maternal obesity, offspring of obese dams show age-dependent and sex-specific cardiac hypertrophy and contractile dysfunction. While alterations in energy metabolism and myocardial substrate preference are associated with pathophysiological changes in cardiac function, programmed changes in offspring cardiac metabolism in response to maternal obesity remain incompletely defined. Recent studies have highlighted altered metabolic gene expression in the hearts of offspring of obese pregnancy, both in late fetal life and adulthood, however the impact on mitochondrial respiratory function in the developing and adult heart is unclear.

Objective: To evaluate myocardial mitochondrial respiratory capacity and metabolic substrate preference in young adult offspring born to obese dams in a well-established murine model of diet-induced maternal obesity.

Methods: Animal work received ethical approval from the University of Cambridge Animal Welfare and Ethical Review Board and was performed in accordance with UK Home Office guidelines under the Animals (Scientific Procedures) Act 1986. Cardiac tissue was collected from 8 week old C57BL/6J mice of both sexes born to dams fed either a control or obesogenic diet for 10 weeks prior to mating and throughout gestation and lactation, with all offspring subsequently weaned onto control diet. Mitochondrial electron transfer system (ETS) capacity was assessed using a protocol optimised for frozen samples. Respiratory complex subunit levels were measured by immunoblotting, and gene expression by RT-qPCR. Data was analysed by two-way ANOVA for sex and maternal diet, with Tukey *post-hoc* testing where $p(\text{Interaction}) < 0.05$ ($n = 8$).

Results: In the hearts of 8 week old offspring of obese pregnancy, myocardial mitochondrial complex I-supported respiration (relative to maximal ETS capacity) was greater than in the offspring of dams fed a control diet (control: 0.37 ±0.038 vs. obese: 0.41 ±0.065, $p(\text{Diet}) = 0.041$). This change in complex I-supported respiration was accompanied by an increase in NDUFA9 subunit protein levels which did not reach statistical significance (control: 0.31 ±0.002 vs. obese: 0.35 ±0.002, $p(\text{Diet}) = 0.063$). In the hearts of the offspring of obese dams, there was differential expression of genes encoding fatty acid oxidation associated proteins by maternal diet. *Hadh*

expression was 1.4-fold higher in the offspring of obese pregnancy compared with controls (p(Diet) = 0.0096). Expression of *Cpt1b* and *Ucp3* were altered by maternal diet in a sex-specific manner, being lower in the hearts of female offspring of obese pregnancy, compared with female offspring of control pregnancy. These findings suggest sex-specific alterations in myocardial fatty acid oxidation as a result of maternal diet.

Conclusions and further work: The hearts of young adult offspring of obese dams are characterised by metabolic alterations including changes in mitochondrial respiration and fatty acid oxidation (in a sex-specific manner). Further work is underway to profile mitochondrial respiration and substrate metabolism in the cardiac tissue of neonatal offspring of obesogenic diet- and control-fed dams, in order to understand the time course of metabolic alterations in relation to cardiac development.

PCA017

Spatiotemporal electrical excitations during spontaneous contraction in isolated uterine tissues of pregnant guinea pig

Wing Chiu Tong[1], Michael Taggart[1]

[1]Biosciences Institute, Newcastle University, Newcastle upon Tyne, United Kingdom, [2]Biosciences Institute, Newcastle University, Newcastle upon Tyne, United Kingdom

Regulation of the contractile activities of uterine smooth muscle underpins the fundamental physiological processes of parturition. It is accepted that contractions in uterine smooth muscle cells are determined by episodic, spontaneous electrical potentials. However, the mechanisms that spread the electrical excitations and thus contractions throughout the uterus are still in debate [1]. Optical mapping techniques enable the visualisation and quantification of the spatiotemporal spread of electrical excitations with high spatial and temporal resolutions, and at the same time, also allow simultaneous observations of both electrical activities and the corresponding contractions. We, therefore, have undertaken optical mapping experiments to examine the spatiotemporal characteristics of excitation propagation in isolated uterine tissues from pregnant guinea pigs at term.

Optical imaging was performed according to well-established methods described for the heart [2] with some modifications. Uterine tissues marked with position markers were mounted and stretched to its in vivo dimensions then superfused in Krebs (with 95% O_2 and 5% CO_2) at 37°C. After a period of stabilization, the tissues were stained with the voltage-sensing fluorescent dye di-4-ANEPPS. Fluorescence was excited by light-emitting diodes at 470 nm, and two ranges of emission signals (515 to 565 nm and >590 nm) were projected onto the same image frame and collected simultaneously by a highspeed camera at 250 Hz. A viewing area of 2 cm x 4 cm of uterine tissue was projected onto half of the image frame of 64x128 pixels, resulting in spatial resolutions of 312.5 x 312.5 μm^2. Uterine movements were separated from the electrical excitation signals by taking the ratio of the two emission signals [3]. The electrical excitation signals were then subjected to spatial and temporal filtering to reduce noise. Excitation wavefronts and conduction velocity vectors were computed using a modified method based on fitting a polynomial surface at each pixel along the wavefronts [4].

All isolated uterine tissues contracted spontaneously. The underlying electrical activities often originated from all around the edges of the tissue. The propagations consisted of mostly repetitive plane waves with occasional re-entrants that rotated around portions of contracted tissues. Multiple initiations might coexist and these excitations would collide, merge or dissipate, complicating the organisation. However, we never observed chaotic excitation patterns such as those of ventricular fibrillation in the heart. The average conduction velocity of 354 excitations is 4.29+/-1.56 cm/s (mean+/-SD). However, instantaneous speeds of the wavefronts can reach >52 cm/s momentarily, especially when multiple waves merged. The uterine contractions of the whole

tissue area did not require complete synchronised excitations, and it can be sustained by excitations originated from multiple directions. Further investigations would advance our understanding of the physiological processes of uterine electrical excitation at tissue and organ levels of organisation.

[1] Young RC. (2016). Reproduction 152, R51-R61. [2] Matiukas A et al. (2007). Heart Rhythm 4, 1441-1451. [3] Holcomb MR et al. (2009). Exp Biol Med 234, 1355-1373. [4] Tong WC & Taggart MJ. (2018). Proc Physiol Soc 41, PCB038.

PCA018

Liraglutide reduced the dark period core body temperature and curtailed cardiac sympathetic activity during the restraint stress.

Marian Turcani[1], Elham Ghadhanfar[1]

[1]*Department of Physiology, Faculty of Medicine, Kuwait University, Kuwait, Kuwait*

Glucagon-like peptide 1 (GLP-1) receptor agonists are proposed as a treatment option in patients with heart failure. However, the recommendation remains controversial because several clinical trials did not effectively improve cardiovascular outcomes in heart failure patients (1). One of the problems not settled is the concern about the positive chronotropic and sympathomimetic effect of GLP-1 receptor agonists (2).

We experimented to discover the potentially hazardous effects of chronic treatment with long-acting GLP-1 receptor agonist liraglutide on the hemodynamics and autonomic nervous system (ANS).

During general anesthesia (120 $mg.kg^{-1}$ ketamine & 6 $mg.kg^{-1}$ xylazine i.p.), we implanted 10-month-old male Sprague-Dawley rats (n = 14, randomly assigned to the control or treated groups, n = 7) with telemetric transmitters (HD-S11, Data Sciences, USA). Implants allowed simultaneous monitoring of aortic pressure, ECG, core body temperature, and locomotor activity. After baseline 24-hour (12 h light-dark cycles, dark started at 7.00 a.m.) recording of telemetric signals, we used pharmacological tests and 30-minute restraints to estimate ANS activity (3, 4). We applied (i.p.) liraglutide daily, gradually increasing the dose. We started with 0.1 mg/kg of liraglutide for 18 days, continued with 0.3 mg/kg for 55 days, and 1mg/kg for 59 days. We injected (i.p.) saline to control rats. Telemetric signals were recorded weekly for 24 hours. We performed pharmacological and restraint stress ANS tests one month after injecting liraglutide 0.3 $mg.kg^{-1}$ or 1 $mg.kg^{-1}$. In addition, we calculated time and frequency domain indices of cardiovascular variability (3, 4). Data were analyzed with the multivariate (Wilks) repeated measure ANOVA. The post hoc Tukey HSD test was used if the interaction between the main effects (treatment & time) was significant.

While body weight remained steady in control rats (645 (SD 80) g), liraglutide-treated rats lost 17 % ($p < 0.001$) of their body weight at the end of the experiment. We found no significant change in mean arterial pressure, but liraglutide accelerated the heart rate by 10% ($p < 0.001$) during the light period, increasing it from 278 (SD 10) bpm to 305 (SD 14) bpm. We recorded a significant ($p < 0.001$) reduction in the core body temperature (-0.4 (SD 0.2)°C) associated with liraglutide treatment during the dark period. No pharmacological tests or any heart rate variability or systolic pressure variability indices pointed to possible alterations in autonomic regulation of the hemodynamics. However, during the restraint stress test, liraglutide-treated rats showed a significantly ($p = 0.013$) lower elevation of mean arterial pressure by 30% and longer pre-ejection time by 28% ($p = 0.011$) than control rats.

In conclusion, chronic treatment with liraglutide did not affect the mean arterial pressure but accelerated heart rate during the light period. Surprisingly, we found signs of the sympatholytic

effect of liraglutide, i.e., reducing the core body temperature during the dark period and prolonging pre-ejection time during the restraint stress.

Reference 1: Merza N, et al. (2023). Curr Probl Cardiol 48, 101602 Reference 2: Heuvelman VD, et al. (2020). Cardiovasc Res 116, 916-930 Reference 3: Ghadhanfar E, et al. (2014). PloS One 9, e 108909 Reference 4: Turcani M & Ghadhanfar E. (2019). Sci Rep 9, 2586

PCA019

Vascular pulsatility in the ageing brain and confounding effects of isoflurane and ketamine/xylazine.

Mia Viuf Skøtt[1], Eugenio Gutiérrez[1], Vladimir Matchkov[1], Leif Østergaard[1], Dmitry Postnov[1]

[1]Aarhus University, Aarhus, Denmark

Increased vascular stiffness and, consequently, pulsatility increase the risk of developing Alzheimer's disease and several cardiovascular diseases, but the exact pathways are still a mystery. Most of our knowledge on the *in-vivo* effects of increased stiffness comes from the large vessels, while capillaries are expected to play the most significant role in cognitive decline. Using Laser Speckle Contrast Imaging (LSCI), we investigated how the microvascular pulsatility changes with age in wild-type mice (C57BL/6) and how it is affected by two of the most commonly used anaesthesias: isoflurane and ketamine/xylazine (k/x).

Twelve mice aged 18 (n=5), 43 (n=3), and 65 (n=4) weeks, respectively, were imaged at 5 separate time points, 4 weeks apart. To access the cortical microvessels, we used LSCI in awake-restrained mice with a chronic cranial window over the left middle cerebral artery (MCA) and its branches. Without changing the field of view, the animals were also imaged under isoflurane anaesthesia followed by k/x anaesthesia. After finishing *in-vivo* experiments, the MCA was isolated and mounted on a wire myograph and tone was recorded to assess the physiological changes of ageing in the vasculature.

The blood flow and pulsatility index in veins, arteries and parenchyma did not change with age and remained constant throughout the experiment. The pulse-associated relative diameter dilation remained constant in veins, but in arteries, it began to increase after 65 weeks of age, from 0.0986 arb. unit at 65 weeks to 0.1580 a.u. at 81 weeks (60.2 %, p= 0.0521). These results are supported by the myograph results, indicating an age-related increase in compliance of the MCA.
Both anaesthesia caused significant changes to the pulsatility of blood flow velocity in arteries ($p=8.5*10^{-10}$ under isoflurane and $p=1.4*10^{-11}$ under k/x using a paired t-test) veins ($9.4*10^{-9}$ under isoflurane and $1.3*10^{12}$ under k/x using a paired t-test) and parenchyma ($9.2*10^{-9}$ under isoflurane and $5.5*10^{-12}$ under k/x using a paired t-test). However, because isoflurane causes a strong vasodilation, the pulse-associated diameter change did not change in arteries (p=0.69, paired t-test) but did in veins ($5.4*10^{-7}$, paired t-test). But k/x caused a significant response in both arteries ($p=1.1*10^{-7}$, paired t-test) and veins ($1.8*10^{-8}$, paired t-test). These results clearly show that while more time-consuming, awake imaging is better when assessing physiological changes in the vasculature and blood flow.

All experimental protocols were approved by the Danish National Animals Experiments Inspectorate and conducted according to their guidelines.

PCA020

Dynamic cerebral autoregulation is unchanged following maximal sprint exercise in healthy young adults

Max Weston[1], Philip Buys[1], Emma Curtin[1], Delphine Guichard[1], Ellen Harbison[1], Alberto Croce[1], Evan Ng[1], Carlo Delle Monache[1], Alberto Maero[1], Gabriel Tan Tan[1], Tobias Khoo[1], Abhinav Sreekanth[1], Norita Gildea[1], Mikel Egana[1]

[1]*Department of Physiology, School of Medicine, Trinity College Dublin, Dublin, Ireland*

Background and Purpose Maximal sprint exercise is known to exert marked and dynamic changes in cerebral blood flow and blood pressure both during and following exercise. However, the effect of maximal sprint exercise on cerebral autoregulation has not been investigated, which forms an important area of investigation given the growing interest surrounding high-intensity exercise and cerebrovascular function. Therefore, the purpose of this study was to investigate the acute effect of maximal sprint exercise on dynamic cerebral autoregulation (dCA) in healthy young adults.

Methods Twenty-one healthy adults (mean ± SD age, height and weight: 22.7 ± 3.1 years, 173.4 ± 8.4 cm and 70.3 ± 10.1 kg, respectively, 13 males, 8 females) volunteered to participate in this study, which involved a single experimental visit. Participants visited the laboratory >2 hours postprandial, having refrained from caffeine, alcohol and vigorous physical activity for 24 hours prior to the visit. dCA was determined using a single sit-to-stand manoeuvre. Following >10 min of seated baseline, participants rapidly (< 3 seconds) stood up and remained standing for 3 minutes. Middle cerebral artery blood velocity (MCAv) was measured using transcranial Doppler ultrasonography, and beat-to-beat blood pressure was measured using finger plethysmography. Participants then completed a maximal, 30 second Wingate test on a cycle ergometer, before repeating the dCA assessment after 25 minutes of seated recovery. Baseline measurements were taken as the last 60 seconds of seated measurements, and the nadir in both MCAv and mean arterial pressure (MAP) were identified as the minimum value during the initial 20 seconds following standing. The fall in MCAv and MAP were expressed in both absolute and relative terms, and dCA was quantified as the percentage fall in MCAv relative to the percentage fall in MAP upon standing (Δ%MCAv/Δ%MAP). Paired samples t-tests explored the effect of the Wingate test on MCAv, MAP and dCA responses.

Results Baseline MCAv was significantly lower following the Wingate test (59.4 ± 10.4 *vs* 65.5 ± 11.3 $cm.s^{-1}$, P<0.01), whilst baseline MAP was unaltered (81.2 ± 10.3 *vs* 78.7 ± 11.1 mmHg, P=0.44). Upon standing, the fall in MAP was significantly greater following the Wingate test, expressed in both absolute (23.9 ± 6.4 *vs* 18.4 ± 8.5 mmHg, P=0.01) and relative (29.8 ± 8.3 *vs* 23.7 ± 11.1%, P=0.01) terms. The relative fall in MCAv from baseline during the sit-to-stand manoeuvre was significantly greater following the Wingate test (23.7 ± 6.2 *vs* 18.2 ± 8.1%, P=0.02), but not in absolute terms (14.1 ± 4.6 *vs* 12.0 ± 5.5 $cm.s^{-1}$, P=0.16). When expressed relative to each other, dCA was unaltered following exercise (0.9 ± 0.3 *vs* 0.9 ± 0.6, P=0.75).

Conclusion These findings indicate that maximal sprint exercise significantly impacts the MCAv and MAP responses during a single sit-to-stand manoeuvre. Specifically, the standing-induced fall

in both MAP and MCAv are augmented 25 minutes following sprint exercise. Despite this, dynamic cerebral autoregulation remained unaltered in healthy young adults following a Wingate test.

PCA021

Mitochondria-IP3Rs coupling is a key regulator of vascular tone in smooth muscle cells

Xun Zhang[1], Matthew Lee[1], Charlotte Buckley[1], Calum Wilson[1], John McCarron[1]

[1]University of Strathclyde, Glasgow, United Kingdom, [2]University of Strathclyde, Glasgow, United Kingdom

The contractility of vascular smooth muscle cells (VSMCs) in resistance arteries is the major contributor of vascular tone and blood pressure. In VSMCs, increase of intracellular Ca^{2+} level directly generates the force to contract arteries. A major source of intracellular Ca^{2+} is entry through voltage dependent Ca^{2+} channels (VDCCs) on plasma membrane. While mitochondria are now recognised as key regulators of intracellular Ca^{2+} homeostasis by modulating internal Ca^{2+} store in several cell types including smooth muscle cells and endothelial cells, their role in modulating Ca^{2+} signalling generated by VDCC in intact VSMCs is still under studied. Given the potential interaction between mitochondria and VDCCs in VSMCs, we hypothesize that mitochondria can directly regulate Ca^{2+} release from sarcoplasmic reticulum in VSMCs, hence regulate Ca^{2+} signalling and vascular tone generated mediated by VDCCs.

The interplay between mitochondria and VDCCs was investigated by imaging and analysing intracellular Ca^{2+} signals in smooth muscle cells in intact arteries from rat mesentery (n = 5). Summarized data were analyzed and presented as mean ± SD of n biological replicates. When the data extracted from same preparations under different treatment, data were analyzed by using paired t-test.

Depolarization of the plasma membrane potential, by high potassium (30 mM) physiological saline solution, triggered Ca^{2+} entry through VDCCs and a sustained increase in intracellular Ca2+ on which repetitive Ca^{2+} oscillations occurred. All Ca2+ signals were abolished by removal of external Ca^{2+} and by dihydropyridine inhibitors of VDCCs. Significantly, the repetitive Ca^{2+} oscillations, but not the sustained Ca^{2+} signals, were blocked by the IP_3 receptor inhibitor 2-APB and SERCA inhibitor cyclopiazonic acid. Neither the repetitive Ca^{2+} oscillations or the sustained Ca^{2+} signals were altered by the ryanodine receptor inhibitors ryanodine and dantrolene (paired t-test). These results suggest that Ca^{2+} entry via VDCC triggers Ca^{2+}-induced Ca^{2+} release via IP_3 receptors in intact mesenteric arteries.

Depolarization of the mitochondrial membrane potential (ψm, indicated by a membrane sensitive dye, TMRE), by the uncoupler CCCP (1 μM), but not ATP deprivation with the ATP synthesis blocker oligomycin (1 μM), inhibited VDCCs evoked IP_3 mediated Ca^{2+} oscillations but not the sustained Ca^{2+} signals. Furthermore, in intact arteries, depolarization of ψm directly suppressed inositol triphosphate receptors (IP_3Rs) mediated Ca^{2+} release from the internal Ca^{2+} store evoked by photolysis of caged IP_3. These results suggest that mitochondria regulate Ca^{2+} release via IP_3Rs triggered by voltage dependent Ca^{2+} entry. In return, Ca^{2+} entry via VDCCs did not alter ψm. In addition, depolarization of ψm supressed sustained vasocontraction that was mediated by voltage dependent Ca^{2+} entry.

Together, these results suggest that mitochondria regulate Ca^{2+}-induced Ca^{2+} release at IP_3 receptors triggered by Ca^{2+} entry via VDCCs but do not directly regulate VDCCs activity.

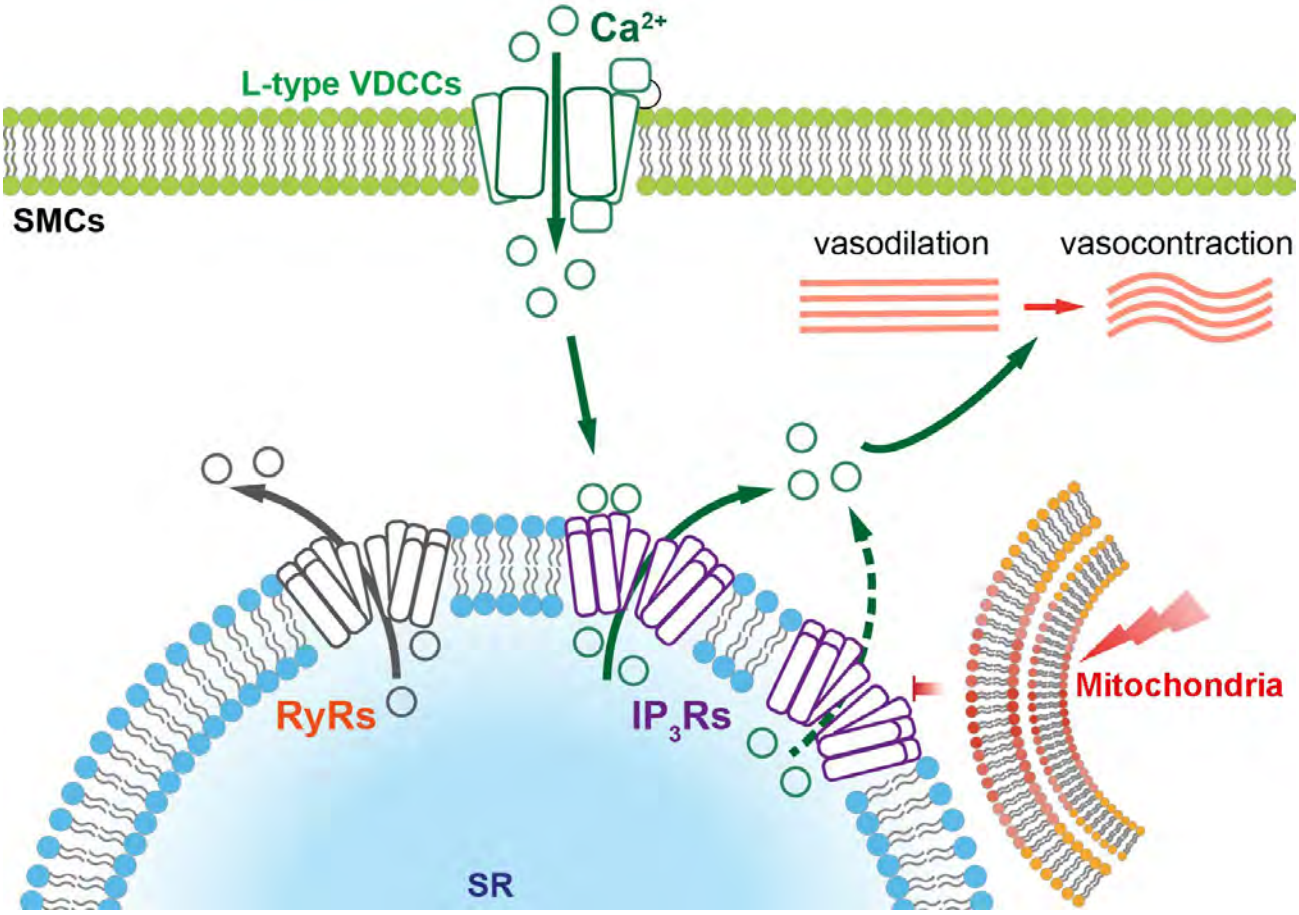

Chalmers, S., and McCarron, J.G. (2008). The mitochondrial membrane potential and Ca2+ oscillations in smooth muscle. Journal of Cell Science 121: 75–85. Poburko, D., Liao, C.-H., Breemen, C. van, and Demaurex, N. (2009). Mitochondrial Regulation of Sarcoplasmic Reticulum Ca2+ Content in Vascular Smooth Muscle Cells. Circulation Research 104: 104–112. Wilson, C., Lee, M.D., Heathcote, H.R., Zhang, X., Buckley, C., Girkin, J.M., et al. (2019). Mitochondrial ATP production provides long-range control of endothelial inositol trisphosphate–evoked calcium signaling. Journal of Biological Chemistry 294: 737–758.

PCA022

Development of a digital escape room to raise awareness of the effects of climate change on human health

André Justin Carpio[1], Catriona Jane Cunningham[1], Silvia Mazzotta[2]

[1]School of Medicine, Medical Sciences & Nutrition, University of Aberdeen, Aberdeen, United Kingdom, [2]School of Pharmacy & Life Sciences, Robert Gordon University, Aberdeen, United Kingdom

Climate change presents an increasing threat to human life and health. The World Health Organisation has predicted that malnutrition, malaria, diarrhoea and heat stress alone will cause around 250,000 additional deaths annually between 2030 and 2050. However, the health impacts of climate change are currently sparsely taught in medical curricula. The aim of this study was therefore to develop a digital escape room to raise awareness of the effects of climate change on human health.

The escape room was hosted on a WordPress website and H5P (HTML5 Package) was used to create interactive puzzles including a crossword and jigsaw. Solving each puzzle, revealed a code to “unlock” the door. Additionally, a countdown timer set to 40 mins was coded in to simulate the physical escape room experience. During summer 2023, all current medical students were invited to play the digital escape room via email. Anonymous pre- and post-activity questionnaires were used to explore existing knowledge and interest levels in the effects of climate change on health. A second iteration of the escape room with a standalone questionnaire was ran as a face-to-face activity during induction week for incoming year 1 medical students.

Both current (n=23) and new medical students (n=66) reported an increase in self-assessed knowledge of the effects of climate change on human health after participating in the activity. The majority agreed escape rooms could effectively teach new content (91.3%, 78.8%) and should be used in medical education (91.3%, 91%). Over 80% of year 1 medical students agreed the escape room was an excellent icebreaker activity.

In conclusion, this digital escape room was an engaging and enjoyable method of teaching medical students about the impact of climate change on health.

PCA024

A review of palliative and end-of-life care physiology education in Scottish paramedic undergraduate courses

Ross MacInnes[1], Laura Ginesi[2], Derek Scott[1]

[1]University of Aberdeen, UK, Aberdeen, United Kingdom, [2]University of East Anglia, Norwich, United Kingdom

Introduction: Paramedics are being increasingly dispatched to community palliative and end-of-life care (EoLC) patients (Kirk et al., 2017). Despite this, paramedics consistently report a lack of confidence in treating these patient populations (Blackmore, 2022). Sufficient education in these areas has been identified as a key enabler to the provision of adequate care for these patients by paramedics (Pentaris & Mehmet, 2019). Scotland has recently moved to a degree-based training programme for paramedics, and it has yet to be assessed whether or not paramedics qualifying in Scotland are being educated adequately in the physiology underpinning palliative and EoLC topics. We have previously reported that paramedic curriculum guidance had more reference to these topics than that for many other healthcare professions (Scott et al., 2023).

Aims: To review and analyse palliative and EoLC physiology education within the five Scottish undergraduate paramedic degrees and compare it to the recommendations made by the relevant educational guidance.

Methods: Information gathered from publicly accessible online curriculum documents and data collected by contacting course representatives from each university was screened for information regarding the following: (1) Content delivered in modules relating to palliative and EoLC; (2) Teaching techniques used to deliver palliative ad EoLC teaching content; (3) Number of hours dedicated to the delivery of palliative and EoLC material. A thematic analysis was carried out on the data collected regarding course content to gain a comprehensive summary of the educational framework in Scotland. This was compared to the educational recommendations identified.

Results: When compared to the educational guidance, 5 of the identified recommendations were met by ≥2 universities, 3 were only met by 1 university each, and 1 recommendation did not appear to be met by any of the courses studied. Teaching techniques used included lectures, tutorials/workshops, seminars, simulations and self-directed study. The mean teaching time dedicated to this content was 12.9±8.47 hours.

Conclusion: Scottish undergraduate paramedic courses largely met the education guidance for palliative and EoLC physiology teaching, however there is scope for implementing further interactive teaching sessions focussing on these topics to address the gaps in the existing framework and further develop student confidence in these areas of practice. This work has led to the design of a potential high-fidelity simulation session in an attempt to address these issues. We hope to deliver such simulations in the near future to continue this work.

Blackmore TA (2022). What is the role of paramedics in palliative and end of life care? Palliative Medicine 36(3), 402–404 https://doi.org/10.1177/02692163211073263 Kirk A, Crompton PP,

Knighting K, Kirton J, & Jack B (2017). Paramedics and their role in end-of-life care: perceptions and confidence. Journal of Paramedic Practice 9(2), 71–79 Pentaris P & Mehmet N (2019). Attitudes and perceptions of paramedics about end-of-life care: a literature review. Journal of Paramedic Practice 11(5), 206–215. https://doi.org/10.12968/jpar.2019.11.5.206 Scott D, Anderson J, Ginesi L & Naczk S (2023) Education about the physiology of death and dying in the training of healthcare practitioners - do we need to do more? Proc Physiol Soc 54, C23

PCA025

Comparison of Biomedical Science students' perceptions of online versus paper-based examinations

Mirza Subhan[1], Elizabeth Winters[2], William Mitchell[1], Kris Jeremy[1]

[1]School of Biomedical Sciences, Faculty of Health, University of Plymouth,, Plymouth, United Kingdom, [2]School of Biomedical Sciences, Faculty of Health, University of Plymouth,, Plymouth, United Kingdom

Online examinations are becoming increasingly incorporated into higher education. However, Biomedical Science students' perspectives on exam format preferences remains unexplored. This study aims to investigate exam format preferences and attitudes of these students. A secondary aim was to also determine any differences between responses regarding age, gender, and programme.

146 participants were sampled across six different programmes. The study was approved by the University of Plymouth Science and Engineering Human Ethics Committee. Questionnaire participants were asked to give their consent as a preliminary question and to confirm they were over the age of 18.

A self-reported survey of 31 questions on online exam perceptions was utilised and composed of six dimensions: affective factors, validity, practicality, reliability, security, and pedagogy. Median scores using a Likert scale measured student attitudes around online exams. Additionally, categorical questions examined attitudes around open-book online exams (OBOEs), closed-book online exams (CBOEs), and paper-based exams (PBEs). Qualitative analysis was conducted via the use of open-ended questions and a focus group on five participants. The results were statistically analysed in SPSS Version 25. Internal validation using Cronbach alpha test results were reported for each dimension. Descriptive statistics were used to report student demographics, examination preference, and responses to questions. A Mann-Whitney U test was used to assess differences in dimension perception with regard to gender and student programme. Multiple linear regression was conducted to look for associations between age and dimensions. $p < 0.05$ was considered as significant.

The findings revealed that 57.5% of students preferred OBOEs while only 19.9% preferred PBEs. OBOEs were perceived as more favourable in all six dimensions and superior in terms of reducing stress, ensuring fairness, allowing demonstration of understanding, and retaining information. Gender had no statistically significant influence on perception. However, programme showed significant difference in to dimensions. Qualitative data supported the main statistical analysis and identified a trade-off between the ability to retain information with PBEs, despite the stress and better demonstration of understanding with OBOEs.

Overall, OBOEs were viewed positively and were well accepted by most participants. Institutions wishing to implement online exams should consider the perceived benefits they have over traditional exams. These findings contribute to the understanding of students' perceptions of exam formats, which can inform their design and application in higher education. Further research

should explore the perceptions of other disciplines and identify ways to address any challenges associated with online exams.

PCA026

From Movie Theatre to Lecture Theatre: Using Films to Engage Students in Expanded Physiological Cases

Grace Hogan[1], Christopher Torrens[1]

[1]*Royal College of Surgeons in Ireland, Dublin, Ireland*

Introduction

It is widely appreciated that a considerable understanding of physiology is fundamental to medical practice and a solid factual knowledge is essential for developing clinical skills (Finnerty *et al*., 2010). However, time allocated to early years basic science teaching only ever decreases (Weston, 2018). This reduction limits sufficient exploration or application of concepts in the traditional manner. Fictional characters and events have been used by others to engage students in the application of concepts they have been taught (Berg & Polvsing, 2016; Scott *et al*., 2022), and we have utilised films during an elective module to encourage students to think about physiology in the extremes.

Methods

The medical programme at RCSI offers a student choice week in the middle of term, consisting of four taught sessions (Mon-Thu) and an assessment (Fri). We ran an optional Extreme Physiology course, with each of the four days being dedicated to one topic. The four topics were temperature (hypo/hyperthermia), pressure (altitude/depth), space and physiology in the intensive care unit. On the four didactic days, students were given presentations on content with examples linked to films and readily available clips. For the assessment, groups of students had to select a film depicting a relevant extreme situation and discuss the physiological challenges faced by the characters.

Results

All student groups chose highly appropriate scenes to discuss with no duplications. This gave a range of examples portraying situations relating to hypo- and hyperthermia, altitude, depth and/or microgravity . The students were able to discuss key physiological challenges faced by the characters and, in places, were able to critique the accuracy of the depiction portrayed. Feedback from the anonymised centralised student survey had students rating the session as very good (67%) or good (33%). There were also strongly positive comments in the free text sections, all of which indicated that the course had deepened their understanding of physiology.

Conclusions

Student engagement and discussion was good in the sessions and the positive feedback suggests that they found the content and delivery useful. In choosing appropriate scenes and then discussing them, the students were able to demonstrate their problem solving capacity by conducting a thought experiment on the physiological processes triggered by environmental change. As such, we think these fictional scenarios can be used to facilitate students thinking more deeply about physiology.

Berg RMG & Polvsing RR (2016). Advances in Physiological Education 40, 234-236 Finnerty EP et al. (2010). Academic Medicine 85, 349–355. Scott DA et al. (2022). Acta Physiologica 236 (s725), 263-264 Weston WW (2018). Canadian Medical Education Journal 9, e109-e114

PCA028

Mineralocorticoid receptor activation induced by hypoxia modulates hepatocyte lipid and glucose metabolism, implicating a role in liver cirrhosis progression.

Mohammad Mohabbulla Mohib[1], Sindy Rabe[1], Alexander Nolze[1], Alexander Zipprich[2], Michael Gekle[1], Barbara Schreier[1]

[1]Julius Bernstein Institute of Physiology, Medical School, Martin Luther University of Halle-Wittenberg, Halle, Germany, [2]Clinic for Internal Medicine IV, Universitätsklinikum Jena, Jena, Germany

Introduction:

The mineralocorticoid receptor (MR) is a pivotal regulator of water and electrolyte balance and has been implicated in various physiological processes, including blood pressure regulation and renal function. However, aberrant MR activation has been associated with detrimental effects such as promoting fibrosis in the cardiovascular system. Recent studies have indicated a potential role of MR activation in the progression of liver cirrhosis, particularly under conditions of hypoxia commonly observed in cirrhotic livers. Nevertheless, the precise impact of non-physiological MR activation in hepatocytes remains poorly understood.

Objective:

This study aimed to elucidate the consequences of hypoxia-induced MR activation in hepatocytes.

Methods:

We conducted RNA sequencing analysis on rat livers from control animals, cirrhotic animals, and those treated with eplerenone, an MR antagonist (N= 5 animals per group). Animal experiments complied with German law (Tierschutzgesetz, 42502-2-1123 MLU, Landesverwaltungsamt Sachsen-Anhalt), directive 2010/63/EU, and ethical guidelines (ARRIVE guidelines and NIH standards). With respect to the results of the Gene ontology (GO)term enrichment analysis from rat livers, we investigated the impact of MR activation on metabolic processes in HepG2 cells . To induce non-physiological MR activation, we exposed the cells to hypoxia, using an oxygen concentration of 0.2% for at least 24h. mRNA and protein levels of key metabolic genes was determined using quantitative RT-PCR and Western blotting. Glucose consumption, lactate production, and lipid accumulation were assessed as well with or without eplerenone treatment. The data are presented as mean ± standard error of the mean (SEM) % of control. Statistical significance was determined using a two-tailed t-test, with a significance threshold set at $p < 0.05$. Each experiment was conducted with N = 5-10 replicates, and there were n = 15-24 petri dishes per group.

Results:

GO term enrichment analysis revealed that in a rat model for liver cirrhosis (CCl4 treatment) eplerenone, an MR antagonist, reverses the downregulation of genes annotated to the GOterm

"Monocarboxylic acid metabolic process". We already demonstrated that under hypoxic conditions that the MR-induced transcriptional activity shifts to other response elements on the DNA (Schreier, 2018). Therefore, we incubated HepG2 cells with or whithout hypoxia in the presence of eplerenone. We have demonstrated that hypoxia reduced the mRNA levels of PPARα (46.3 ± 8.4%), PDK4 (11,4 ± 3.3%), AMACR (39.2 ± 6.6%), ABCC2 (67.4 ± 10.5%), and Lipin 1(49.1 ± 15.8 %; as well as the protein. This downregulation can be partially attenuated by eplerenone treatment for PPARα (73.7 ± 12.7 %), PDK4 (66.3 ± 17.9 %), and ABCC2 (99.3 ±12. 2 %), suggesting a mineralocorticoid receptor (MR)-dependent mechanism. Hypoxia augments glucose uptake (282,7± 33.2%), and lactate production (202,7± 11.8%) in HepG2 cells. This effect was partially reversed upon eplerenone administration (glucose: 169,2± 10.2% and lactate: 153,5± 10.2; $p<0.05$, two-tailed t-test) respectively. Additionally, hypoxia-associated lipid accumulation (257,9 ± 26,7%) in hepatocytes is partially mitigated by MR blocker(120.3 ± 9,8%,).

Conclusion

Our findings suggest role of MR in dysregulating glucose and lipid metabolism in hepatocytes, potentially contributing to liver cirrhosis development. Therefore, MR antagonism may hold therapeutic promise in the management of liver cirrhosis.

Schreier B, Wolf A, Hammer S, Pohl S, Mildenberger S, Rabe S, Gekle M, Zipprich A. The selective mineralocorticoid receptor antagonist eplerenone prevents decompensation of the liver in cirrhosis. Br J Pharmacol. 2018 Jul;175(14):2956-2967. doi: 10.1111/bph.14341. Epub 2018 Jun 7. PMID: 29682743; PMCID: PMC6016674.

PCA030

Regular practice of 12 weeks of Yoga Therapy attenuates worsening of lipid profile in Early Indian Postmenopausal Women

Praveena Sinha[1], Asha Gandhi[2], Sunita Mondal[3], Anju Jain[4], Ratna Biswas[5]

[1]Assistant Professor, Department of Physiology, Amrita School of Medicine, Faridabad, India, [2]Ex-Director Professor & HOD, Department of Physiology, Lady Hardinge Medical College, New Delhi, India, [3]Director Professor & HOD, Department of Physiology, Lady Hardinge Medical College, New Delhi, India, [4]Ex- Director Professor & HOD, Department of Biochemistry, Lady Hardinge Medical College, New Delhi, India, [5]Director Professor, Department of Obstetrics and Gynaecology, Lady Hardinge Medical College, New Delhi, India

Introduction: Postmenopause is an estrogen deficient state associated with increased incidence of deranged lipid profile, an important marker for cardiovascular diseases. CVD in projected to be the cause of 45% of deaths in Indian postmenopausal women by 2020. Yoga has been described as having beneficial effect on lipid profile in many studies and populations.

Aims: The aim of our research was to study the effect of 3-month long Yoga practice on lipid profile in early postmenopausal women within five years of their menopause.

Methods and Material : A prospective interventional study of 67 women within five years of menopause between 45 and 60 years of age attending the menopause clinic of a tertiary care hospital fulfilling inclusion and exclusion criteria and consenting were enrolled for study. Institutional Ethical Clearance (IEC- Lady Hardinge Medical College & SKH, New Delhi) was sought and obtained before conducting the study. The group was divided into two groups on the basis of their willingness to join the Yoga intervention - Group 1(n=37)- Postmenopausal patients receiving routine management along with Yogic intervention and Group 2(n=30)- Postmenopausal patients receiving routine gynaecological management.Yoga group participants received intervention of Integrated Yoga module comprising asanas, pranayama, savasana, and OM chanting for a period of 12 weeks under a trained Yoga teacher from Department of Yoga, Naturopathy and Lifestyle Intervention, Department of AYUSH, Ministry of Health and Family Welfare, India in addition to routine gynaecological management. Lipid profile of 37 cases (Yoga group) and 30 controls (non-Yoga group) was measured pre and postintervention. Statistical Analysis was done by GraphPad Prism Version 5 software. Values are a mean and standard error of mean. Mean and standard error of mean (Mean± SEM) of all the variables for both groups were calculated according to accepted statistical methods. Intergroup comparison was for parametric data was done using Unpaired 't' test to compare the different parameters in Group 1and Group 2. Intergroup comparison for non-parametric data was done using Mann-Whitney U test. Intragroup comparison within Group 1and Group 2 for normally distributed data was done using Paired 't' test. Intragroup comparison within Group 1 and Group 2 for non-parametric data was done using Wilcoxon matched pair test. Statistical significance was set up at $P < 0.05$.

Result: A definite decrease was observed in S. Total Cholesterol (mg/dl) [189.3±6.03(post) vs 188.5±5.72 (pre)], S.Triglycerides (mg/dl) [(129.0±7.51(post) vs 122.3±8.77(pre)], T.VLDL (mg/dl) [(25.8±1.50 (post) vs 24.46±1.75(pre)] in the Yoga Group post intervention but it failed to achieve

statistical significance. In the Non-Yoga Group, S. Total Cholesterol (mg/dl) [(187.6±6.36 (post) vs 196.4±5.58 (pre)], T.LDL(mg/dl) [(113.8±4.82 (post) vs 121.2±4.69 (pre)] worsened after 3 months while S.Triglycerides (mg/dl) [(153.2±14.93 (post) vs 152.8±10.66 (pre)] and T.VLDL (mg/dl) (30.65±2.98 (post) vs 30.56±2.13 (pre)] remained relatively unchanged. S.HDL(mg/dl) remained predominantly unchanged in both groups.

Conclusion: Three-month long Yoga practice attenuated worsening of lipid profile in early postmenopausal women and has the potential to prevent early onset of atherosclerosis and consequent cardiovascular diseases in our population if instated early in menopause.

1. Lopez AD, Murray CCJL. The global burden of disease, 1990–2020. Nat Med. 1998 Nov;4(11):1241–3. 2. Mehra P, Anand A, Nagarathna R, Kaur N, Malik N, Singh A, Pannu V, Avti P, Patil S, Nagendra HR. Role of Mind-Body Intervention on Lipid Profile: A Cross-sectional Study. Int J Yoga. 2021 May-Aug;14(2):168-172. 3. Nagarathna, R., Usharani, M.R., Rao, A.R. et al. Efficacy of yoga based life style modification program on medication score and lipid profile in type 2 diabetes—a randomized control study. Int J Diabetes Dev Ctries 32 (2012);122–130. 4. Ghazvineh D, Daneshvar M, Basirat V, Daneshzad E. The Effect of Yoga on the Lipid Profile: A Systematic Review and Meta-Analysis of Randomized Clinical Trials. Front Nutr. 2022 Jul 14;9:942702. 5. Innes KE, Selfe TK, Vishnu A. Mind-body therapies for menopausal symptoms: a systematic review. Maturitas. 2010 Jun;66(2):135–49.

PCA031

Are the effects of increased dietary potassium on blood pressure salt dependent?

Adrienne Assmus[1], Louise Nyrup Odgaard[1], Vladimir Matchkov[1], Robert Fenton[1]

[1]Department of Biomedicine, Aarhus University, Aarhus, Denmark

Hypertension is a primary risk factor for cardiovascular disease and a major driver of disability and premature death. High dietary sodium (Na^+) intake contributes to high blood pressure (BP), but evidence is mounting that dietary potassium (K^+), typically low in the western diet, also modulates BP. In some studies, greater K^+ intake lowers BP (1), an effect partially explained by a higher plasma K^+ being associated to lower activity of the sodium chloride cotransporter NCC in the distal convoluted tubule of the kidney (2). However, other studies do not always see a beneficial effect of greater K^+ intake on BP (3). The aim of this study is to investigate the mechanisms and potential of increasing dietary K^+ intake to lower BP, the effects of combining it with higher salt intake and the limitations of such an approach.

Methods: Initially, two cohorts of male mice were fed diets containing 0.74% NaCl and increasing percentages of K^+ (0.75% K^+, 1%, 1.25%, 1.5%, 1.75%, 2%, 2.5% and 5%) each for 5 sequential days. Cohort 1 had BP recorded using telemetry for 24 h on the last day of each diet. Cohort 2 had blood and 24 h urine collected at the same time points for assessment of renal function and electrolyte balance. In another cohort, mice were switched directly from a 0.75% K^+ to a 2% K^+ diet. Mice were then fed either a high salt diet (4% NaCl) combined with a 0.75% or 2% K^+ intake for 15 days.

Results: Incremental increases in K^+ intake led to a linear (R^2=0.98) increase in 24 h urinary K^+ excretion, which plateaued at 2.5% K^+ (0.35±0.05 to 1.19± 0.28 mmol/24h, mean ±SD). Natriuresis was not significantly different across the diets, with the exception of the 5% K^+ diet where Na^+ excretion was 33.8±10.6% lower (p=0.014). 24 h urine volume was significantly increased for all dietary K^+ intakes > 1.75% K^+. Systolic BP (SBP, active period) for all dietary K^+ intakes was not significantly different to control (n=7 *vs*. n=5), with the exception of the 5% K^+ where SBP increased by 7.16±1.72mmHg (p=0.014). Plasma K^+ was not significantly different across the diets relative to 0.75%K^+, until an intake of 2.5% K^+, after which plasma K^+ was significantly higher. A direct switch from a 0.75% to 2% K^+ diet on normal Na^+ intake led to an increase in SBP of 5.10±2.5mmHg after 5 days (active period, p=0.027). This increase in SBP was not apparent in mice concomitantly receiving a high Na^+ diet.

Conclusion: This study shows that progressively increasing K^+ intake on a normal salt diet leads to increased urinary K^+ excretion, but no changes in plasma K^+ or BP, until K^+ intake exceeds 2.5% K^+. However, a direct jump to a higher dietary K^+ intake increases BP on normal salt intake, but this effect is attenuated during high salt intake. The molecular mechanisms underlying these responses are under investigation.

(1) Mente, A. et al., N Engl J Med 371, 601- 611 (2014) (2) Poulsen, S et al., J Physiol 597, 4451-4464 (2019) (3) Chaudhary, P. & Wainford, R. D., J Hum Hypertens 35, 577-587 (2021)

PCA032

A novel urine pH-ammonium acid/base-score and progression of chronic kidney disease

Peder Berg[1], Samuel Levi Svendsen[1], Amalie Quist Rousing[1], Rasmus Kirkeskov Carlsen[2], Dinah Khatir[2], Danny Jensen[2], Nikita Misella Hansen[3], Louise Salomo[3], Henrik Birn[2], Niels Henrik Buus[2], Jens Leipziger[1], Mads Vaarby Sørensen[1]

[1]Department of Biomedicine, Aarhus University, Aarhus, Denmark, [2]Department of Renal Medicine, Aarhus University Hospital, Aarhus, Denmark, [3]Department of Nephrology, Copenhagen University Hospital, Copenhagen, Copenhagen, Denmark

Introduction: Acidosis is associated with exacerbated loss of kidney function in chronic kidney disease (CKD). Currently, acid/base status is assessed by plasma measures, although organ-damaging covert acidosis, subclinical acidosis, may be present before reflected in plasma. Low urine NH_4^+ excretion associates with poor renal outcomes in CKD and has been proposed as a marker for subclinical acidosis. However, a low NH_4^+ excretion could result from either a low capacity or a low demand for acid excretion. We hypothesized that a urine acid/base-score reflecting both the demand and capacity for acid excretion would better predict CKD progression.

Methods: 24-hour urine collections were included from three clinical studies of patients with CKD stage 3 and 4: A development cohort (n=82), a variation cohort (n=59), and a validation cohort (n=73). A urine acid/base-score was derived and calculated from urinary pH and [NH_4^+]. Subclinical acidosis was defined as an acid/base-score below the lower limit of the 95% prediction interval of healthy controls. Main outcomes were percentage change in measured GFR after 18 months and CKD progression (defined as ≥50% decline in eGFR, initiation of long-term dialysis or kidney transplantation) during up to 10 years of follow-up. To assess percentage change in measured GFR as a function of acid/base-score and subclinical acidosis status, log-transformed measured GFR values was analyzed as outcome variable using a mixed-effects models for repeated measures. Models included visit (baseline vs. 18 months follow-up), acid/base-score or subclinical acidosis and visit-by-acid/base-score or subclinical acidosis interaction as fixed effects. The risk for CKD progression as a function of acid/base-score and subclinical acidosis status was assessed by cox proportional hazards models. All estimates were assessed with and without adjustment for important clinical risk factors for GFR decline and CKD progression (sex, age, baseline GFR, proteinuria, systolic blood pressure, and plasma bicarbonate).

Results: Subclinical acidosis was prevalent (development cohort: n=51/82, 62%, validation cohort: n=47/73, 65%). Subclinical acidosis was associated with an 18% (95% CI: 2-32) larger percentage decrease of measured GFR after 18 months. During a median follow-up of 6 years, subclinical acidosis was associated with a markedly higher risk for CKD progression. Adjusted hazard ratios were 5.1 (95% CI 1.1-23.3) in the development cohort and 11 in the validation cohort (95% CI: 2.9-42.4). The adjusted hazard ratio in the pooled cohorts was 5.7 (95% CI: 2.3 to 14.4) for patients with subclinical acidosis. Kaplan-Meier plots for event-free survival stratified for acid/base-score tertile and subclinical acidosis are shown in figure 1. The acid/base-score had a higher predictive value for CKD progression than NH_4^+ excretion alone (C-score of 0.73 vs. 0.55, difference: 0.18, 95% CI: 0.05 to 0.30).

Conclusion: Subclinical acidosis, defined by a new urine acid/base-score, is associated with a higher risk of CKD progression in patients with CKD stage 3 and 4.

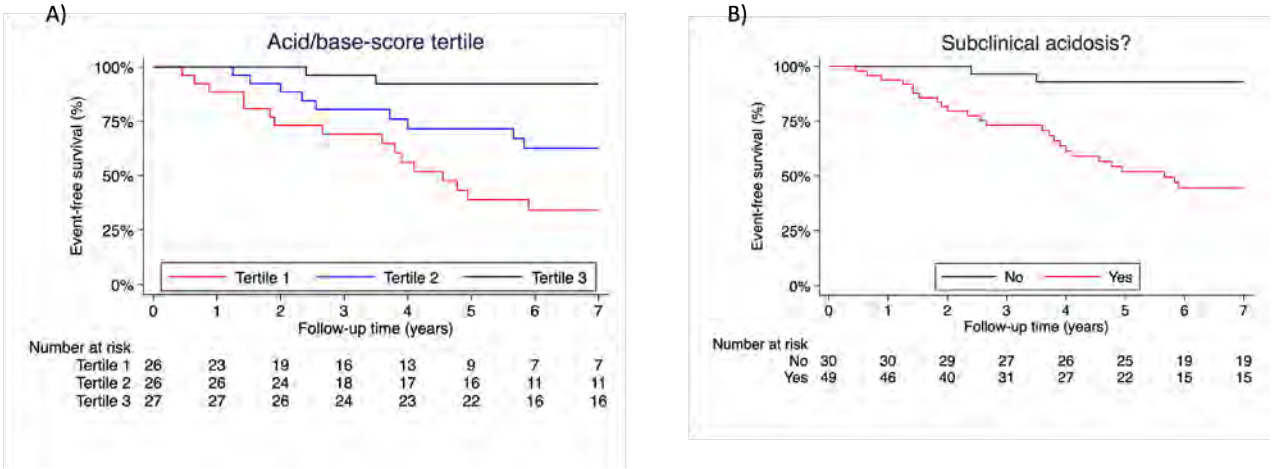

PCA033

Electrophysiological studies of TRPV4-mediated transepithelial electrolyte flux in relation to potassium channels involved in cerebrospinal fluid production

Cameryn Davis[1], Verayna Newland[1], Bonnie Blazer-Yost[1]

[1]*Indiana University Indianapolis, Indianapolis, United States*

Introduction: Hydrocephalus is a neurological disorder characterized by accumulation of cerebrospinal fluid (CSF) within the brain caused by an overproduction of CSF, blockage of flow, or decreased reabsorption. The CSF accumulation causes pathologies including ventriculomegaly, increased intracranial pressure, and cell damage. CSF is secreted by the choroid plexus, a fenestrated capillary network surrounded by an epithelial monolayer in the ventricles. This epithelium is composed of polarized choroid plexus epithelial cells (CPe) in which ion channels are located on either the apical (CSF-facing) or basolateral (blood-facing) membrane. The production and amount of CSF is regulated by a complex interaction between these channels including transient receptor potential vanilloid 4 (TRPV4), calcium-activated potassium channel (KCa3.1), K^+-Cl^- cotransporter (KCC) and the sodium, potassium 2 chloride channel (NKCC1). TRPV4 is an osmo-, shear-, temperature- and pressure-sensitive nonselective cation channel. TRPV4 activation causes an influx of Ca^{2+} and Na^+ which can secondarily activate KCa3.1. TRPV4 activation also involves the Ste20/SPS1-related proline-alanine-rich kinase (SPAK) pathway which inhibits KCC and regulates NKCC1. Altering the extracellular K^+ concentration within physiological parameters also has the potential to affect transport via electrochemical gradients.

Aim: Our goal was to identify a relationship between activation of TRPV4 and potassium channels within the CPe. Identifying the regulation of these channels, will provide further understanding of CSF production in normal and pathophysiological states and provide a basis for identifying potential targets for future drug development for a variety of diseases including hydrocephalus.

Methods: The human choroid plexus papilloma (HIBCPP) cell line was cultured in media supplemented with 10% fetal bovine serum, 1% penicillin and streptomycin, 5 ng/L insulin, and sodium bicarbonate. Cells were seeded onto permeable supports until they formed a monolayer with resistances <400 ohm.cm^2. Ussing-chamber electrophysiology was used to measure net ion flux and changes in cellular permeability. The relationship between ion channels were investigated using treatments including increasing extracellular K^+ to 10 mM, 50μM (Dihydroindenyl)oxy alkanoic acid (DIOA, KCC inhibitor), and 5 μM TRAM-34 (Triarylmethane-34, KCa3.1 inhibitor). Compounds were added to either the apical, basolateral, or bilateral sides to determine polarity. After a short (10 min) drug pre-treatment, 15 nM GSK1016790A (TRPV4 agonist) was added to the cells thereby stimulating a complex ion and fluid transepithelial flux. Each treatment had a minimum of six trials. Statistical significance was determined using a paired multiple T-test.

Results: When KCa3.1 was inhibited on the apical side, both a decrease in net transepithelial ion flux and membrane permeability occurred. Inhibition on the basolateral side resulted in an increased membrane permeability, while inhibition on both sides led to decreased transepithelial ion flux. When KCC was inhibited on the basolateral side, a decrease in both transepithelial ion flux and membrane permeability was observed while inhibition on both sides only showed a decrease

in transepithelial ion flux. Increasing the concentration of extracellular K^+ showed no significant change.

Conclusion: Our results show that there is a relationship between TRPV4 and the potassium channels KCC and KCa3.1, but no significant relationship with physiologically relevant changes in extracellular K^+.

PCA034

Identifying a binding site for voltage-independent CFTR blockade by GlyH-101

Tzyh-Chang Hwang[1], Zhiwei Ma[2], Shiting Ho[1]

[1]National Yang Ming Chiao Tung University, Taipei, Taiwan, Province of China, [2]University of Missouri, Columbia, United States

Cystic Fibrosis Transmembrane conductance Regulator (CFTR) is a chloride channel with characteristic structural similarities to ABC Transporters. Recent cryo-EM studies (Zhang et al., 2018) have revealed a large internal vestibule in the ion permeation pathway of activated CFTR proteins (i.e., phosphorylated, ATP-bound state). We and others lately identified a binding site at the external end of this vestibule for $CFTR_{inh}$-172 (Young et al., 2024; Gao et al., 2024), a known voltage-independent CFTR inhibitor. These cryo-EM data also suggest that the binding of $CFTR_{inh}$-172 induces conformational changes in CFTR's two transmembrane segments TM8 and TM12 to obstruct the external end of the pore. Interestingly, our patch-clamp electrophysiological studies show that GlyH-101, another membrane-permeant CFTR blocker, not only blocks CFTR from the external side of the membrane in a voltage-dependent manner (zd = 0.37 ± 0.02; Kd(0) = 3.2 ± 0.8 uM, n = 3) as reported previously (Muanprasat et al., 2004) but also inhibits CFTR currents from the cytoplasmic end with little voltage dependence, suggesting the presence of two distinct binding sites for GlyH-101. Despite structural differences between $CFTR_{inh}$-172 and GlyH-101, they are similar in size and polarized charge. We thus hypothesize that GlyH-101 and $CFTR_{inh}$-172 may share the same binding pocket—or at least their binding sites may overlap with each other. Indeed, molecular docking shows that GlyH-101 can be accommodated in the same area where $CFTR_{inh}$-172 binds. A poorly membrane-permeant GlyH-101 analog (GlyH-101-1) was synthesized by adding a hydrophilic polyethylene glycol tail to the C6 position of the naphthalene ring in GlyH-101. External GlyH-101-1 blocks whole-cell CFTR current in a voltage-dependent manner (zd = 0.30 ± 0.01, Kd(0) = 134 ± 18 uM, n = 5); however, when applied to the cytoplasmic side of an excised inside-out membrane patch, it blocks CFTR in a voltage-independent manner (zd = 0.04 ± 0.001, Kd(0) = 45 ± 17 uM, n = 4). Single-channel data suggest two steps of inhibition: a binding step leading to a short-lived blocked state and a stabler blocked state likely reflecting binding-induced conformational changes. Examining the effects of mutations at the residues involved in the binding of $CFTR_{inh}$-172 on the GlyH-101 blockade is underway to further test our hypothesis.

Zhang et al., (2018). Molecular structure of the ATP-bound, phosphorylated human CFTR. Proc. Natl. Acad. Sci. USA, 115 (50) :12757-12762. Young et al., (2024). Structural basis for CFTR inhibition by CFTRinh-172. Proc. Natl. Acad. Sci. USA, 121(10): e2316675121. Gao et al., (2024). Allosteric inhibition of CFTR gating by CFTRinh-172 binding in the pore. Submitted. Muanprasat et al., (2004). Discovery of glycine hydrazide pore-occluding CFTR inhibitors: mechanism, structure-activity analysis, and in vivo efficacy. J. Gen. Physiol. 124(2):125-137.

PCA035

Investigation of human UT-B urea transporter regulation in various cell lines

Lauren McKeever[1], Kate Duffy[1], Gavin Stewart[1]

[1]School of Biology and Environmental Science, University College Dublin, Dublin, Ireland

Facilitative UT-B urea transporters play a pivotal role in maintaining urea homeostasis by regulating levels of urea in various tissues of the human body. However, the precise regulatory mechanisms governing UT-B expression and activity in different tissues remain to be elucidated. Dysregulation of UT-B transporters has also been implicated in numerous pathological conditions including renal disorders, metabolic diseases, and certain cancers, underscoring the significance of understanding their regulatory mechanisms. This current study therefore compared the levels of both UT-B RNA and UT-B protein in various human cell lines - namely PC-3 (prostate adenocarcinoma), PWR-1E (prostatic epithelia), HT-29 (colorectal adenocarcinoma), and RT-4 (urinary bladder epithelia) - to investigate the regulatory mechanisms governing human UT-B expression. Initially endpoint RT-PCR experiments revealed detectable levels of UT-B RNA in PC-3, HT-29, and RT-4 cells. However, despite the presence of RNA, western blotting experiments detected no significant UT-B protein abundance in either the PC-3 or HT-29 cell lines (All NS, N = 3-4, unpaired T-test). In contrast to these findings, our analysis demonstrated a high UT-B protein abundance level in RT-4 cells and a moderate protein abundance level in the PWR-1E cell line (N = 4), with a 30-35 kDa UT-B1 signal/protein. Experiments were then carried out to assess if urea treatment could regulate UT-B abundance in the PWR-1E cell line, however, no significant changes were observed with either 24 or 48 hour exposure to 5mM urea (NS, N = 4, unpaired T-test). This disparity between the cell lines emphasises potential differences in cellular pathways governing protein synthesis and confirmed variances between UT-B1 protein abundance in ‘normal’ and cancerous prostate. Elucidating the intricate mechanisms governing UT-B abundance and its functional implications within prostate cells holds promise for advancing our understanding of prostate physiology and pathology.

KEYWORDS
Urea; UT-B transporter; protein

PCA036

Pathophysiological mechanisms of afatinib-induced epithelial barrier disruption in human colonoid models

Chatchai Muanprasat[2], Saravut Satitsri[1], Nichakorn Worakajit[1]

[1]Faculty of Medicine, Ramathibodi Hospital, Mahidol University, Bangkok, Thailand, [2]Faculty of Medicine Ramathibodi Hospital, Mahidol University, Bangkok, Thailand

As a severe adverse effects of afatinib, a tyrosine kinase inhibitor (TKI), diarrheas lead to mortality and morbidity in cancer patients. This study was designed to investigate the effect of afatinib on intestinal epithelial barrier integrity using a human colonoid model. Afatinib at 0.5 μM significantly decreased the transepithelial electrical resistance (TEER) in human colonoids (Mean± S.D.= 100 ± 12.2% vs 32 ± 5.4%; *p*-value = 0.0003, n =5, one-way ANOVA followed by Tukey test). Delocalization of zonular occluding-1 (ZO-1) and a decrease in mRNA and protein expression of claudin-4 and ZO-1 were observed in the afatinib-treated human colonoids (n =5). Nuclear translocation of nuclear factor kappa B (NF-κB) and mRNA expression of tumor necrosis factor (TNF)-alpha and inducible nitric oxide synthase (iNOS) were also found after afatinib treatment (n =5). Importantly, mRNA and protein expression of myosin light chain (MLC) kinase (MLCK) and MLC phosphorylation, a known inducer of intestinal epithelial barrier disruption, were observed (n =5). Treatment with iNOS inhibitor or MLCK inhibitor suppressed the effect of afatinib on TEER (Mean± S.D. = 22 ± 1.2 % vs 36 ± 3.5 % relative to non-treated group, *p*-value = 0.004, *n* = 5, one-way ANOVA followed by Tukey test). Collectively, our results indicate that afatinib induces intestinal epithelial barrier dysfunction via NF-κB-iNOS-MLCK-dependent mechanisms. These findings provide insight into pathophysiology of afatinib-induced diarrheas.

PCA037

A Reporter System to Study Adipocyte-Derived Extracellular Vesicles in vivo

Didde Riisager Hansen[1]

[1]*Institute of Molecular Medicine, Odense, Denmark*

Introduction
Adipocytes secrete extracellular vesicles (EVs), but how they affect whole-body metabolism remains unexplored. This is due to technical limitations of tracking and isolating adipocyte-derived EVs *in vivo*[1]. To address this, we have developed two Cre-dependent EV reporter mouse models: 1) The EGFP-EV reporter that labels EVs by CD9 fused to enhanced green fluorescent protein (EGFP), and 2) The NanoLuc-EV reporter labeling EVs by CD63 fused to Nanoluciferase (NanoLuc) and hemagglutinin (HA). We hypothesized that viral delivery of adiponectin-driven Cre to CD9-EGFP mice induces adipocyte-specific expression of EGFP. We also hypothesized that viral delivery of CD63-NanoLuc-HA to adiponectin-Cre mice induces adipocyte-specific expression of NanoLuc, creating a more sensitive reporter system.

Methods
To obtain our EGFP-EV reporter, we designed an adeno-associated viral (AAV) vector with adiponectin-driven Cre. CD9-EGFP mice (*Mus musculus)* were intraperitoneally injected with varying doses of AAV9 ($5*10^{10}$, $5*10^{11}$, and $1*10^{12}$ viral genomes) to determine the optimal dose for efficient AAV delivery.
To obtain our NanoLuc-EV reporter, we designed an AAV vector harboring a CD63-NanoLuc-HA construct. As a control, we included a vector with an IgK signal peptide-NanoLuc-HA construct. Both vectors were packed in AAV9 capsid, and adiponectin-Cre mice (*Mus musculus)* were given a dose of $5*10^{11}$ viral genomes by intraperitoneal injection.
After two weeks, mice were humanly sacrificed by terminal anesthesia (10 mg/kg xylazine, 50 mg/kg ketamine).
Organs such as adipose tissues and liver, and plasma were harvested and evaluated for adipocyte-specific expression of CD9-EGFP or NanoLuc and HA by western blotting and luciferase assays.

Results
For the EGFP-EV reporter, CD9-EGFP was not detected in non-adipose tissues (n=20) or non-AAV-treated CD9-EGFP mice (n=4). CD9-EGFP expression in tissues was robust using a dose of least $5*10^{11}$ viral genomes and was detected in brown adipose tissue (BAT) (n=16) and in white adipose tissue (WAT), including inguinal WAT (n=16), epididymal WAT (n=18) and mesenteric WAT (n=7). Unfortunately, CD9-EGFP was not detected in plasma (n=15). For the NanoLuc-EV reporter, a dose of $5*10^{11}$ viral genomes was tested. The HA-tag was not detected by western blotting of tissue homogenates (n=1). NanoLuc activity was detected in plasma (n=1) and tissues (n=1), with highest levels in liver, mesenteric and epididymal WAT. For control AAV, the NanoLuc levels were higher across tissues compared to the NanoLuc-EV reporter, having the highest levels in epididymal WAT, BAT, and plasma (n=1).

Conclusion
To obtain a proper adipocyte-specific EV reporter mouse model, the reporter system needs to be

sensitive enough to track circulating EVs. Using NanoLuc as a reporter instead of EGFP seems crucial in this context. The control AAV, reflecting normal cellular release, serves well as a baseline for comparison. Intriguingly, the highest NanoLuc levels were observed in the liver of the NanoLuc-EV reporter. This raises questions about the interplay between adipose tissue and the liver, and whether hepatocytes take up adipocyte-derived EVs. In conclusion, our NanoLuc-EV reporter enables adipocyte-specific Cre-dependent EV labeling, providing a tool to study adipocyte-derived EVs *in vivo* to unveil their role in normal physiology and during metabolic disturbances.

1. Welsh JA et al. (2024). J Extracell Vesicles, 13(2), e12404.

PCA038

Ubiquitylation of K890 in the thiazide sensitive sodium chloride cotransporter NCC is important for potassium-induced degradation of NCC

Lena Rosenbaek[1], Eric Delpire[2], Olivier Staub[3], Robert Fenton[1]

[1]Department of Biomedicine, Aarhus University, Aarhus, Denmark, [2]Department of Anesthesiology, Vanderbilt University Medical Center, Nashville, United States, [3]Department of Biomedical Sciences, University of Lausanne, Lausanne, Switzerland

Background: Dietary potassium intake inversely associates with blood pressure, with low dietary potassium intake increasing blood pressure and a high dietary potassium intake often resulting in a lower blood pressure (1). NCC phosphorylation (pseudo-marker of activity) and abundance are lower during higher dietary potassium intake, with the lower total NCC levels linked to greater ubiquitin-dependent NCC degradation (2). We have previously found that ubiquitylation of K890 in mouse NCC is important for modulation of NCC function *in vitro* (3). The aim of this study was to investigate the role of K890 ubiquitylation in the potassium-induced reduction of NCC *in vivo*.

Methods: A novel mouse model with a K890R mutation in NCC was generated using CRISPR/Cas9 technology. Male and female K890R and wildtype (wt) mice were fed a control (2% KCl, 0.74% NaCl) or high potassium (10% KCl, 0.74% NaCl) diet for 4 days after which their blood pressure was measured using tail cuff plethysmography and their kidney function assessed by balance studies in metabolic cages. After euthanasia, kidneys were collected and levels of NCC were examined by western blotting. *Ex vivo* kidney tubule suspensions from K890R and wt mice were incubated in control (4.2 mM KCl) or high potassium (8.0 mM KCl) media for 24 h and levels of NCC examined by western blotting.

Results: No significant differences in systolic blood pressure were apparent in male or female K890R and wt mice fed control or high potassium diets (males n=5-16, females n=5-8). No significant differences were observed in plasma potassium, chloride, or sodium levels, nor their urinary excretion rates, between genotypes fed either diet. On control diet, no differences between genotypes were detected in NCC or phosphorylated NCC abundances. In both male and female wt and K890R mice, high dietary potassium intake decreased total and phosphorylated NCC levels. In male K890R mice, the decrease of total NCC was greater than in wt mice, whereas phosphorylated NCC levels did not decrease to the same extent in female K890R mice relative to wt mice. Incubation of tubule suspensions from male or female wt mice in high potassium media significantly decreased total and phosphorylated NCC abundances. Similar reductions in total NCC (male and female) and phosphorylated NCC (females) were not detected in tubules from K890R mice.

Conclusion: These preliminary data suggest that ubiquitylation of NCC at K890, particularly in females, plays a role in the potassium-induced degradation of NCC. Further studies are required to clarify the role of K890 NCC ubiquitylation in potassium balance or blood pressure, and whether compensatory mechanisms exist in the K890R mice.

1. Poulsen, S. B., and Fenton, R. A. (2019) K(+) and the renin-angiotensin-aldosterone system: new insights into their role in blood pressure control and hypertension treatment The Journal of physiology 597, 4451-4464 10.1113/JP276844 2. Kortenoeven, M. L. A., Esteva-Font, C., Dimke, H., Poulsen, S. B., Murali, S. K., andFenton, R. A. (2021) High dietary potassium causes ubiquitin-dependent degradation of the kidney sodium-chloride cotransporter The Journal of biological chemistry 297, 100915 10.1016/j.jbc.2021.100915 3. Rosenbaek, L. L., Rizzo, F., Wu, Q., Rojas-Vega, L., Gamba, G., MacAulay, N. et al. (2017) The thiazide sensitive sodium chloride co-transporter NCC is modulated by site-specific ubiquitylation Sci Rep 7, 12981 10.1038/s41598-017-12819-0

PCA039

A pilot study on the role of potassium ion channel TRESK, in maintaining joint homeostasis in aged mice.

Annalise Bains[1], Humaira Ahmed[1], Oludayo Adeyemi[1], Joycelyn Boateng[1], Melisa Ceritli[1], Egezona Hyseni[1], Oluferanmi Oni[1], Sadaf Ashraf[1]

[1]Medway School of Pharmacy, Universities of Kent and Greenwich, Chatham, United Kingdom

Background: Potassium ion channels are implicated in aged-associated osteoarthritis and joint pain. The two-pore-domain potassium ion channel, TRESK, regulates neuronal excitability and governs resting cellular membrane potential. However, little is known about the role of TRESK in maintaining knee joint homeostasis. In a rat model of cancer-induced bone pain, over expression of TRESK, attenuated the bone pain [1]. Osteoarthritis affects all joint tissues, including the cartilage and subchondral bone, leading to joint pain. Bone sclerosis and cartilage calcification are key histopathological features of osteoarthritis. Chondrocytes, the main cell type in the cartilage, undergo a phenotypic shift, increasing calcification of the cartilage. Peripheral nerves can regulate bone remodelling, accelerating subchondral bone sclerosis.

Purpose: The aim of this pilot study was to determine whether TRESK influences joint homeostasis in aged-mice through regulating cartilage and bone health.

Methods: Paraffin-embedded, knee joint sections of aged (2 years and 6 months approximately) TRESK knockout (n=4) and wild-type control (n=3) C57BL/6 male mice were sectioned at 5µm thickness and at least 4 sections per knee joint were analysed for histopathological changes, by observers blinded to the groups. Thickness of the subchondral bone was analysed on haematoxylin and eosin stained sections. Osterix is a transcriptional factor which is expressed by osteoblasts (bone forming cells). Osterix-immunohistochemistry was performed to assess whether chondrocytes were adopting osteoblast-like phenotype. Trabecular bone area within the subchondral bone region and osterix-positive chondrocytes in the cartilage were quantified using Image-J (Fiji) software. Univariate comparisons were made using student's T-test. A two- tailed $P < 0.05$ was taken to indicate statistical significance. Data is shown as mean ± standard deviation.

Ethical Considerations: All procedures complied with the UK Animals (Scientific Procedures) Act of 1986 and were performed under a UK Home Office Project Licence in accordance with the University of Kent Policy on the use of Animals in Scientific Research and the ARRIVE guidelines.

Results: Knee-joints of aged wildtype control mice showed osteoarthritis-like changes, these included cartilage damage and subchondral bone remodelling. Aged TRESK-knockout mice had thicker trabecular bone measured as percentage of trabecular bone within the subchondral bone region compared to wildtype control mice (knockout: 45% ± 4.5, wildtype: 37% ± 2.5, p=0.04). Increased percentage of osterix-positive chondrocytes were observed in the cartilage of TRESK-knockout (62% ± 2.5) compared to wildtype control (46% ± 8.9) mice, although this difference did not reach significance (p=0.08).

Conclusion: This proof-of-concept study highlights that TRESK is indeed an important ion channel that regulates joint homeostasis through maintaining cartilage and bone health. Loss of TRESK can exacerbate age-associated osteoarthritis-like changes observed in mice knee joints. Further studies are needed to elucidate its role in osteoarthritis and joint pain.

References: 1. Liu JP et al. Contribution of TRESK two-pore domain potassium channel to bone cancer-induced spontaneous pain and evoked cutaneous pain in rats (2021). Molecular Pain. 17:1-18

PCA041

Carotid and brachial artery changes after 12 weeks of upper-body rowing exercise in spinal cord-injured humans

Rasmus Kopp Hansen[1,3], Rasmus Bering[1], Afshin Samani[1], Ryan Godsk Larsen[1]

[1]ExerciseTech, Department of Health Science and Technology, Aalborg University, Aalborg, Denmark, [2]Department of Research and Development, University College of Northern Jutland., Aalborg, Denmark, [3]Respiratory and Critical Care Group, Department of Health Science and Technology, Aalborg, Denmark

Introduction: A spinal cord injury (SCI) results in deconditioning of the cardiovascular system, including changes in both vascular function and structure (1), leading to an elevated risk of cardiovascular diseases (2). While exercise training (arms-only) for persons with SCI has been shown to increase the diameter of the peripheral conduit artery feeding the active limb, little is known about the effects of arm exercise on central artery diameter and wall thickness. Our main hypothesis was that peripheral, but not central, conduit artery diameter would be increased following 12 weeks of upper-body rowing exercise (UBROW) in SCI individuals.

Methods: Seventeen male and female adults with chronic (>1 yr) motor-complete and incomplete SCI (level of injury: C4-L3) were randomized to control (CON, n=9) or exercise (UBROW, n=8). Participants in UBROW performed 12 weeks of 3 weekly sessions of 30-min moderate-to-vigorous-intensity rowing (arms-only) on an ergometer adapted to wheelchair users. In supine resting position, common carotid artery (CCA) and brachial artery (BA) lumen diameters (M-line to M-line) were determined using high-resolution ultrasound at baseline, after 6 weeks (6W), and after the intervention (12W). CCA wall thickness was measured by near and far-wall carotid intima-media thickness (CIMT). Recordings of resting arterial diameters and CIMT were analyzed off-line frame-by-frame using semi-automated edge-detecting and wall-tracking software. Intra-observer coefficient of variation for CIMT and CCA diameter analyses was 1.6% and 0.95%, respectively. Linear mixed-effects model was used to determine main effects of group and time, and their interaction, with Holm-Sidak Post hoc tests in case of significant interaction effects.

Results: For BA diameter, there was a group-by-time interaction (P=0.016). UBROW increased BA diameter from baseline (4.80±0.72mm) to 12W (5.08±0.91mm; P<0.01), with no changes at 6W (4.96±0.91mm), and no changes in CON.
For CCA diameter, there was no interaction (P=0.478) or main effects of time or group (P≥0.102). For CIMT near-wall, there was no interaction (P=0.72) or main effects of time or group (P≥0.43). UBROW vs. CON: Baseline (0.69 mm vs. 0.73 mm); 6-week (0.70 mm vs. 0.72 mm); and 12-week (0.71 mm vs. 0.71 mm). For CIMT far-wall, there was a main effect of group (P≥0.02) but no interaction (P=0.06). UBROW vs. CON: Baseline (0.56 mm vs. 0.65 mm); 6-week (0.59 mm vs. 0.61 mm); and 12-week (0.55 mm vs. 0.60 mm).

Conclusions: 12 weeks of arms-only rowing significantly increased peripheral conduit artery diameter (BA) but did not change central artery diameter (CCA) or wall thickness (CIMT) in individuals with SCI. These results demonstrate localized, but not systemic, arterial adaptations in response to 12 weeks of arm exercise. While structural enlargement of the BA seems likely, it is

possible that changes in sympathetic nervous system activity may have influenced BA resting diameter. Further research is needed to fully understand the underlying mechanism for the exercise-induced enlargement in peripheral arterial diameter and the possible influence of this adaptation on cardiovascular disease risk.

1) West CR et al. (2013). Spinal Cord 51, 10-19. 2) Cragg JJ et al. (2013). Neurology 81, 723-728.

PCA042

An investigation of the acute effects of dance on heart rate variability in patients with Parkinson's disease

Jaspreet Kaur[1], Sophia Hulbert[2], Ruth Way[3], Mirza Subhan[4]

[1]UCLan School of Medicine & Dentistry, Preston, United Kingdom, [2]School of Health Professions, Faculty of Health, University of Plymouth,, Plymouth, United Kingdom, [3]School of School of Art, Design and Architecture, Faculty of Arts, Humanities and Business, University of Plymouth, Plymouth, United Kingdom, [4]School of Biomedical Sciences, University of Plymouth, Plymouth, United Kingdom

Parkinson's is a neurodegenerative movement disorder that has no cure. The most common motor symptoms observed are postural instability, rigidity, and bradykinesia. The role of therapies is well documented, however, there is now substantial evidence to support the use of alternative therapies to alter the progression of Parkinson's. Dance has shown improvements in mobility and balance. There is limited research currently available that investigates cardiovascular autonomic dysfunction in people with Parkinson's (PwP), especially in a dance community setting. Therefore, HRV could be used as a non-invasive marker during dance to detect autonomic dysfunction in PwP in its early stages and assess any autonomic benefits of dance. The main aim of this study was to investigate the effects of dance on heart rate variability in patients with Parkinson's.

Ten PwP were recruited from a Parkinson's dance class, situated at Pavilion Dance Southwest, Bournemouth with written informed consent. The study was approved by the Faculty of Health Research Ethics and Integrity Committee and procedures were in accordance with the Declaration of Helsinki. Inclusion criteria was mild-moderate Parkinson's diagnosis for more than 6 months. Exclusion criteria was previous surgeries that could alter their physiological response to dance. The classes took place once weekly for 90 minutes and consisted of the following sections in chronological order: rest 1, teach 1, dance 1, teach 2, dance 2 and rest 2. The first half was danced sitting while the latter half was standing. Wireless physiological monitoring measurements including breathing rate (BR), skin temperature and heart rate variability (HRV) were taken before, during and after the dance classes using LabChart software. HRV was assessed using time domain (heart rate - HR, standard deviation of the RR interval – SDRR, SD1 and SD2) and frequency domain (low and high frequency - LF and HF). Data was also normalised by considering the heart rate [1], prefixed by n. The results were statistically analysed in SPSS by repeated measures ANOVA. $p < 0.05$ was considered as significant.

Analysing all six sections together showed skin temperature ($p=0.00001$), HR ($p=0.029$), SD1 ($p=0.025$), nSDRR ($p=0.028$), and BR ($p=0.001$) were significantly different across all sections. LH and HF showed no significant difference.

The main finding of our study was that significant changes in HR, SD1, nSDRR, BR and skin temperature of PwP occurred during all six sections. Furthermore, it was noted that HR and HRV frequency domain variables altered, albeit non-significantly, for both the sitting and standing sections, with similar patterns, demonstrating internal consistency throughout dance classes. Our data showed dance improved autonomic function. However further work examining the long-term effects of HRV in a community setting with diverse groups is needed to fully understand the potential benefits of Parkinson's dance.

References Sacha J (2014). Ann Noninvasive Electrocardiol 19, 207-16

PCA043

How is regular swimming affecting micro- and macro-vascular physiology in older adults? The ACELA-II study findings.

Alexandros Mitropoulos[1], Markos Klonizakis[1]

[1]*Lifestyle, Exercise and Nutrition Improvement (LENI) Research Group, Sheffield Hallam University, Sheffield, United Kingdom*

Background: Cardiovascular disease (CVD) remains the number one death cause in the Western world, affecting also severely the quality of life (QoL) of those affected. Older people are of particular interest, as cardiovascular (CV) ageing affects pathophysiological pathways, which are also implicated in CVD development. Water-based, aerobic exercise such as swimming, may delay CV ageing, and consequently prevent the development of CVD in older adults.

Nevertheless, current literature presents conflicting evidence with some studies showing no improvement in CV parameters, while others suggest a positive effect on the intima-media thickness of carotid arteries, hemodynamic and biochemical markers. ACELA-II aimed to assess the micro- and macro-vascular function in older adults randomised to either regular (e.g., 2-3 times/week) swimming or no intervention for an 8-week period.

Methods: This was a single-centre, pragmatic, two-arm randomized controlled trial conducted in Sheffield, UK. The study was approved by the Ethics Committee of the Faculty of Health and Wellbeing of Sheffield Hallam University (ER5320861). Participants were invited at Sheffield Hallam University for two visits (i.e., baseline and 8-week follow up). Following baseline assessments, participants were randomised to either swimming (n=20) or control (n=17) groups. Assessments consisted of anthropometrics and demographics, smoking and clinical history, as well as micro- and macro-vascular function tests assessed by flow mediated dilation (using ultrasound) and laser Doppler flowmetry (using thermal hyperaemia), respectively. The swimming group followed an 8-week (2-3 sessions/week), self-managed exercise intervention, carried out in local public pools.

Results: Participant characteristics did not present any differences between groups both at baseline (Table 1) and follow up assessments. Following the exercise intervention, the exercise group significantly improved the macrovascular function (9.8 ± 4.2%, $p<0.001$) compared to the control group (4.6 ± 2.5%) as shown in Figure 1. Statistically significant differences were also found between groups comparison for the microvascular function as presented in both raw and the percentages of cutaneous vascular conductance (Table 2).

Conclusions: Regular swimming seems to benefit both the macro- and micro-vascular function in older adults when compared to no exercise (i.e., sedentary lifestyle). Considering that certain vascular parameters did not show a statistically-significant difference, rather a tendency towards improvement for the swimming group, it may be recommended that a longer (i.e., ≥ 12 weeks) intervention may offer great vascular health benefits.

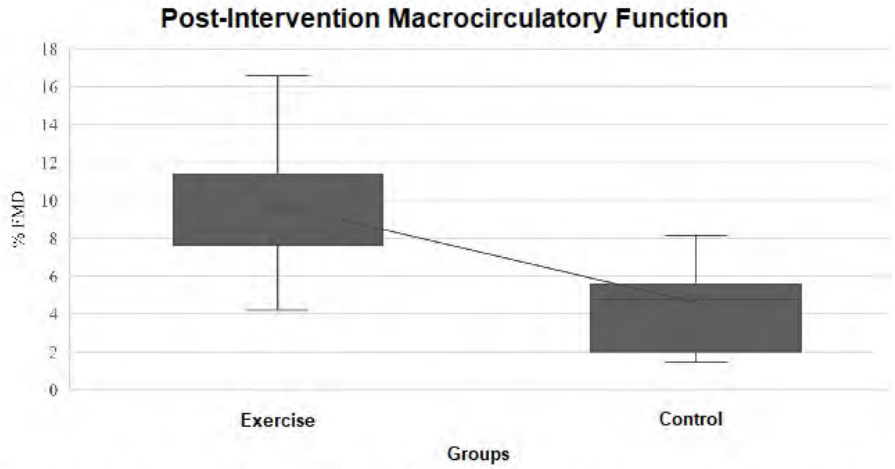

Figure 1. Comparison of brachial artery function post exercise intervention between the exercise and control groups.

Table 2. Between groups comparison of microvascular function pre- and post-intervention.

	Groups			
	Baseline		Follow up	
	Swimming	Control	Swimming	Control
CVC max (%)				
Baseline	8.73 ± 6.5	12.6 ± 9.1	10.7 ± 4.2*	7.9 ± 3.3
Initial peak	68.3 ± 8.7	74.1 ± 17.6	74.4 ± 18.1	66.6 ± 12.6
Plateau	87.3 ± 34.5	84.2 ± 21.0	85.3 ± 10.7	81.2 ± 10.1
RAW CVC (APU/mm Hg)				
Baseline	0.3 ± 0.2	0.4 ± 0.1	0.3 ± 0.1	0.2 ± 0.1
Initial peak	2.3 ± 0.8	2.3 ± 0.7	2.6 ± 0.8	2.2 ± 0.8
Plateau	2.7 ± 0.5	2.7 ± 1.1	3.1 ± 0.9	2.6 ± 1.1
Max	3.2 ± 1.0	3.1 ± 0.8	4.1 ± 0.9**	3.2 ± 1.1

Table 1. Subject characteristics at baseline assessments.

	Swimming (n=20)	Control (n=17)
Age (years)	61 ± 4	62 ± 5
Body mass (kg)	83 ± 15	75 ± 14
Body fat (%)	36.7 ± 9.0	36.2 ± 6.5
BMI (kg m^{-2})	27.7 ± 8.6	27.2 ± 4.2
Waist circumference (cm)	94 ± 15	92 ± 12
Hip circumference (cm)	109 ± 11	104 ± 9
WHR	0.9 ± 0.1	0.9 ± 0.1

Data is presented as means ± SD. BMI, body mass index; WHR, waist to hip ratio.

PCA044

Characterization of an inflammation-driven chronic kidney disease model using human precision-cut kidney slices

Camilla Merrild[1], Gitte Albinus Pedersen[1], Kristian Wiborg Antonsen[1], Sterre Bente Verwoerd[1], Mia Gebauer Madsen[2], Anna Krarup Keller[2], Holger Jon Møller[1], Lene Niemann Nejsum[1], Henricus Antonius Maria Mutsaers[1], Rikke Nørregaard[1]

[1]Department of Clinical Medicine, Aarhus University, Aarhus, Denmark, [2]Department of Urology, Aarhus University Hospital, Aarhus, Denmark

Introduction

Chronic Kidney Disease (CKD) represents a substantial global health burden, affecting approximately 10% of the adult population. A major contributor to CKD progression is low-grade inflammation, which promotes fibrosis, leading to gradual loss of kidney function. To date, a need remains for reliable and translational human models of inflammation-driven CKD to enhance our understanding of the mechanisms linking inflammation and fibrosis driving CKD pathogenesis.

Aim

Our objective was to establish a novel model of inflammation-driven CKD using human precision-cut kidney slices (PCKS).

Methods

Human PCKS were prepared from macroscopically healthy kidney tissue obtained from tumor nephrectomies. The PCKS were cultured for 24h or 48h with or without Tumor Necrosis Factor α (TNFα) or Lipopolysaccharide (LPS) stimulation. The inflammatory response in the slices was assessed via qPCR by studying the expression of four different pro-inflammatory genes (*TNF*, *IL1B*, *CCL2*, and *IL6*) and a 42-target cytokine membrane array. Furthermore, the presence of tissue resident macrophages and their activation potential, were investigated using immunofluorescent staining of the macrophage markers: CD68 and CD163, along with ELISA measurements of soluble CD163 (sCD163) – a macrophage activation marker.

Results

Stimulation of the PCKS with TNFα, a key pro-inflammatory mediator, led to a more than 2.5-fold increase in the gene expression of *TNF, IL1B, CCL2, and IL6* compared with the 24h and 48h control ($n=10$, $p<0.01$ shown by a Wilcoxon signed rank test). In addition, the cytokine membrane array revealed that 17 out of the 42 targets could be detected in the culture media from the slices. The levels of these cytokines and chemokines varied depending on the incubation time and presence of TNFα stimulation.

Moreover, using immunofluorescence we observed clear staining of CD68+ and CD163+ cells in the tissue, indicating the presence of tissue resident macrophages in the PCKS model. As a

measure for macrophage activation, we detected a 1.5-fold increase in the amount of sCD163 in the culture media after 24h of stimulation with LPS, known to mediate CD163 shedding and macrophage activation, compared to the 24h control ($n=4$, $p<0.05$ shown by a Mann-Whitney test). There was no significant change in sCD163 levels after TNFα stimulation.

Conclusion

In conclusion, this study presents a novel human model for investigating inflammation-driven CKD, paving the way for an improved understanding of the complex CKD pathophysiology. Furthermore, the PCKS model holds potential as a future platform for the screening of anti-inflammatory CKD therapeutics.

PCA046

Differences in Physiological Responses to submaximal graded exercise and its recovery in Adults With and Without Type 1 Diabetes

Ivana Potočnik[2], Eva Gabrovšek[1], Nejka Potočnik[2]

[1]Department of Physiotherapy, Faculty of Health Sciences, University of Ljubljana, Ljubljana, Slovenia, [2]Institute of Physiology, Medical Faculty, University of Ljubljana, Ljubljana, Slovenia

Introduction: Physical activity is an important part of the management of type 1 diabetes (T1D) and reduces the risk of associated complications. Many people with T1D exercise regularly. For safe exercise in T1D, in addition to glycemic control, it is important to recognise the differences in physiological response to exercise compared to healthy peers. **Aim:** We aimed to determine the changes in cardiovascular, respiratory and metabolic parameters in response to short-term submaximal exercise (SGSE) in recreational athletes with T1D compared to age- and sex-matched healthy controls. **Methods:** Eighteen recreational athletes, 9 per group, performed SGSE in the form of graded cycling on a cycloergometer until 85% of the maximal heart rate was reached, with 20 minutes recovery in a seated position. Cardiovascular (heart rate, mean arterial blood pressure (MAP)), respiratory (respiratory rate, ventilation) and metabolic (oxygen consumption, exhaled CO2 (VCO2)) parameters were measured non-invasively and averaged at three minutes before, one minute at the end and three minutes in recovery to SGSE. Cutaneous blood flow was measured using the laser Doppler method in the recovery phase after SGSE. Heart rate variability (HRV), heart rate recovery 30 and 60 seconds at the end of exercise, acral and forearm cutaneous vascular conductance (lnCVC), ventilatory equivalent for oxygen and carbon dioxide (VE/VCO2), respiratory quotient and the slope of oxygen uptake efficiency (OUES) were calculated. Normality was tested using the Shapiro-Wilk test. Data before, at peak power and after SGSE were compared for differences over time and between groups using a two-way ANOVA for repeated measures with Sidak adjustment for multiple comparisons. Independent samples t-test was used to determine differences between groups. **Results:** The expected temporal dynamics during exercise and its recovery were comparable in both groups for all measured parameters except MAP. The effect of exercise on MAP varied between groups: at peak exercise, MAP was significantly higher in the T1D group than in the control group (146.7±8.6mmHg in T1D; 129.8±11.2mmnHg in controls; p=0.002). There was a significant main effect of the group on VE/VCO2. At peak exercise and in the recovery, VE/VCO2 was significantly lower in T1D compared to control group (25.7±2.4 in T1D; 30.5±4.7 in controls; p=0.016 at peak exercise and 34.6±2.5 in T1D; 41±4.3 in controls; p=0.001 in the recovery phase). In addition, higher OUES (3833.8±1133.1 in T1D; 2761.0±576.4 in healthy subjects; p=0.0396) and lower forearm lnCVC (-2.4±0.4 in T1D; -1.1±1.2 in healthy subjects; p=0.009) were observed in T1D compared to controls. **Discussion and conclusion:** The response of recreational athletes with T1D to SGSE differed from healthy subjects primarily in MAP and ventilatory response, which may be attributed to the differences in baroreflex and chemoreflex described in T1D compared to healthy participants. Cutaneous forearm blood flow after exercise is decreased in T1D compared to control subjects, which confirms the previously described decreased ability to excrete heat in T1D and may be related to differences in autonomic nervous system activity on the vasculature in T1D. Further studies are needed to confirm these conclusions and possibly uncover the mechanisms underlying our findings.

PCA047

Toward Efficient Musculoskeletal Function Rehabilitation via the use of Artificial Intelligence: The MSC-AI Project at UoD

Francesco V. Ferraro[1], Oluwarotimi W. Samuel[2]

[1]School of Sports and Exercises Science, University of Derby, Derby, United Kingdom, [2]School of Computing, University of Derby, Derby, United Kingdom

Introduction Conventional methods for analysing MSK characteristics of healthy individuals and pathological patients are limited by their inaccuracies and confounding factors that preclude proper assessment and treatment strategies. However, the recent research progress in the field of Artificial intelligence (AI) has re-iterated possibilities in healthcare applications (Rajpurkar et al., 2022; Volpp & Mohta, 2016), particularly in the domain of musculoskeletal (MSK) rehabilitation. Based on the current state of literature, this study proposes an AI-based approach for analysing MSK characteristics to provide accurate and robust assessment outcomes that will inform adequate and real-time therapeutic intervention for common MSK conditions. **Aim** This initiative is aimed at addressing the critical need for evidence-based practices and improved treatment outcomes, which are currently lacking in Sports Therapy and Rehabilitation (STR)**. Ethical Considerations** While acknowledging ethical considerations raised by Kiani et al. (2020), the project will adhere to standardised protocols established by SPIRIT and CONSORT for rigorous evaluation of medical AI applications. The project would employ a collaborative effort between the University of Derby's AI research team and the STR clinics toward leveraging AI to enhance MSK assessment and treatment strategies. **Objectives** Additional expected contributions of the project include (a) the provision of an AI-powered platform that enables STR students to analyse various MSK conditions and make informed decisions, (b) the provisioning of real-world clinical datasets that can aid the advancement of research and development in the field of MSK analysis for researchers at the University and beyond. **Methods** The research team will initially create a database with anonymised pictures and no-personal information collected from the STR clinic; these will then be processed by AI, which will identify the MSK condition and provide the best treatments. The AI will be coded using objective-oriented program language. All code and user information are stored in server-secured databases, not in clouds (e.g., Github), to prevent data leaks. Additionally, to compare and test the validity of AI, the STR practitioner will complete a full parallel screening, and the results between AI and STR experts will be compared to report the level of agreement and accuracy of the results. **Conclusion** This proposed project has the potential to make significant contributions to the burgeoning field of AI-powered MSK rehabilitation. By developing a robust AI framework within the STR clinics, we can enhance the students' learning experience, promote evidence-based practices, and improve patient outcomes. This initiative aligns with our research commitment to cutting-edge projects and dedication to providing students with the skills and knowledge necessary to excel in a rapidly evolving healthcare landscape. The project (titled MSC-AI) has recently applied for funding, and the methodological approach will be discussed at the conference.

References Commins, J. (2010). Nurses say distractions cut bedside time by 25%. Health Leaders. Davenport, T., & Kalakota, R. (2019). The potential for artificial intelligence in healthcare. Future healthcare journal, 6(2), 94. Kiani, A., Uyumazturk, B., Rajpurkar, P., Wang, A., Gao, R., Jones, E., Yu, Y., Langlotz, C. P., Ball, R. L., & Montine, T. J. (2020). Impact of a deep learning assistant on the

histopathologic classification of liver cancer. NPJ digital medicine, 3(1), 23. Rajpurkar, P., Chen, E., Banerjee, O., & Topol, E. J. (2022). AI in health and medicine. Nature medicine, 28(1), 31-38. Volpp, K. G., & Mohta, N. S. (2016). Patient engagement survey: improved engagement leads to better outcomes, but better tools are needed. NEJM Catalyst, 2(3).

PCA048

The venoarteriolar reflex decreases skin flowmotion entropy

Henrique Silva[1,2,3], Carlota Rezendes[2]

[1]Research Institute for Medicines (iMed.ULisboa), Faculdade de Farmácia, Universidade de Lisboa, Av. Prof. Gama Pinto, 1649-003, Lisbon, Portugal, [2]Department of Pharmacy, Pharmacology and Health Technologies, Faculdade de Farmácia, Universidade de Lisboa, Av. Prof. Gama Pinto, 1649-003, Lisbon, Portugal, [3]Biophysics and Biomedical Engineering Institute (IBEB), Faculdade de Ciências, Universidade de Lisboa, Campo Grande, 1749-016, Lisbon, Portugal

The robustness of a given physiological effector can be assessed by exploring the complexity profile of the biological signals it generates. The complexity of a signal is typically assessed as "entropy", a general measure of disorganization. Higher complexity level reflects a higher robustness of the respective physiological effector, i.e., a higher adaptation capability to changing internal and external conditions. Recent publications have reported that physiological signals from subjects in pathological and prepathological states show lower entropy than in healthy subjects. On an experimental level, provocation maneuvers (e.g. postural changes, limb occlusion, drug administration, etc.) that challenge certain physiological effectors are also able to highlight their robustness, even in healthy subjects. Our objective was to assess the robustness of the physiological effectors of skin perfusion during a classic maneuver to evoke the venoarteriolar reflex (VAR). Fifteen healthy subjects (22.4 ± 5.2 y.o.) participated in this study after giving informed consent. After acclimatization, subjects performed a protocol to evoke VAR on the upper limb while sitting upright – 7 min resting with both arms at heart level (phase I), 5 min with one random arm (i.e., test limb) placed 40 cm below heart level (VAR, phase II) and 7 min recovery in the initial position (phase III). Skin blood flow was assessed in the index finger of both limbs with photoplethysmography (PPG). Raw PPG signals were then decomposed into their respective spectral components (cardiac, respiratory, myogenic, sympathetic, endothelial NO-dependent and endothelial NO-independent) with the wavelet transform. Finally, the complexity index of the raw PPG signal and of its components was calculated using the multiscale entropy analysis (MSE) algorithm. The Wilcoxon signed rank test was used to compare skin blood flow and complexity index between the different phases of the protocol ($p<0.05$). As expected, VAR induced a significant bilateral decrease in skin blood flow, more pronounced in the test limb. Similarly, during VAR the complexity index of the raw PPG signals and their components decreased significantly, again with higher magnitude in the test limb. These results suggest that a decrease in the competence of skin perfusion regulation effectors might be present during VAR, likely related to the magnitude of skin perfusion decrease.

Silva H, Ferreira HA, Rocha C, Monteiro Rodrigues L. Texture Analysis is a Useful Tool to Assess the Complexity Profile of Microcirculatory Blood Flow. Applied Sciences. 2020; 10(3):911. https://doi.org/10.3390/app10030911

PCA049

Assessing skin perfusion with USB digital microscopy – a pilot study

Henrique Silva[1,2,3], Carlota Rezendes[2]

[1]Research Institute for Medicines (iMed.ULisboa), Faculdade de Farmácia, Universidade de Lisboa, Av. Prof. Gama Pinto, 1649-003, Lisbon, Portugal, [2]Department of Pharmacy, Pharmacology and Health Technologies, Faculdade de Farmácia, Universidade de Lisboa, Av. Prof. Gama Pinto, 1649-003, Lisbon, Portugal, [3]Biophysics and Biomedical Engineering Institute (IBEB), Faculdade de Ciências, Universidade de Lisboa, Campo Grande, 1749-016, Lisbon, Portugal

Assessment of skin microcirculation can be noninvasively assessed with many different technologies, including laser Doppler flowmetry and imaging, photoplethysmography and capillaroscopy, among others. Capillaroscopy is an imaging technique employed for observation of skin microvasculature at nail cuticle level, particularly for the detection of the morphological abnormalities that accompany several diseases, including connective tissue diseases. In recent years several publications have demonstrated that universal serial bus (USB) digital microscopes provide high quality images with comparable diagnostic sensitivity to conventional devices at a lower cost. However, few studies have tested the usefulness of USB digital microscopes to assess skin perfusion in vivo. This pilot study aimed at assessing skin perfusion in healthy subjects during a classic upper limb occlusion maneuver to evoke reactive hyperemia using a USB digital microscope. Seven healthy subjects (21.2 ± 3.4 y.o.) participated in this study after giving informed consent. After acclimatization, subjects performed a standard suprasystolic limb occlusion (SLO) protocol in a random upper limb while sitting upright, as follows: 5 min resting with both arms at heart level (phase I), 3 min occlusion (200 mmHg, phase II) with a tourniquet cuff and 5 min recovery (phase III). The nailfold capillaries of the fourth finger were continuously visualized with a USB digital microscope throughout the protocol. Each video recording was decomposed into its individual frames and several regions of interest (ROI) were selected. For each ROI several image texture parameters were calculated (entropy, contrast, correlation, energy, homogeneity). Skin blood flow was quantified in the pulp of the second finger with photoplethysmography. These parameters were compared between the different phases of the protocol with the Wilcoxon test for related samples ($p<0.05$). As expected, skin blood flow decreased significantly during occlusion and increased significantly upon release of the cuff. Most texture parameters also changed significantly in both phases of the protocol, although with opposite trends and with different magnitudes. These results suggest that skin perfusion could be easily assessed with low-cost USB digital microscopes, although further studies are needed to compare its performance with other optical technologies.

Chanprapaph K, Fakprapai W, Limtong P and Suchonwanit P (2021) Nailfold Capillaroscopy With USB Digital Microscopy in Connective Tissue Diseases: A Comparative Study of 245 Patients and Healthy Controls. Front. Med. 8:683900. doi: 10.3389/fmed.2021.683900

PCA050

Evaluating the suitability of precision-cut tissue slices to study bile acid-induced nephrotoxicity

rianne van Dekken[1]

[1]*Aarhus University, Aarhus, Denmark*

Evaluating the suitability of precision-cut tissue slices to study bile acid-induced nephrotoxicity

Rianne van Dekken, Sandra M. Hansen, Rikke Nørregaard and Henricus A.M. Mutsaers

Department of Clinical Medicine, Aarhus University

Background: Chronic kidney disease (CKD) is characterized by progressive damage to the kidneys, leading to a gradual decline in kidney function over time. In 2017, 1.2 million deaths were caused by CKD, which is expected to rise to 2.2-4.0 million deaths by 2040. Currently, dialysis and kidney transplantation are the only treatment options for patients with end-stage renal disease, emphasizing the need for novel treatments. Recent studies suggest that elevated bile acid levels in the blood are a risk factor for CKD; however, the exact pathophysiological mechanism remains unclear. This study will evaluate the suitability of Precision-Cut Kidney Slices (PCKS) to study bile acid-induced nephrotoxicity. The PCKS model is a unique technique in the sense that each slice contains all cell types and components of the kidney in the original configuration, with intact cell-cell and cell-matrix interactions.

Methods: Using the Alabama R&D Tissue Slicer (formerly Krumdieck Tissue Slicer), mice PCKS (mPCKS) were prepared from kidneys harvested from C57BL/6 mice (n=5). Mice were anesthetized with 5% sevoflurane and sacrificed by cervical dislocation. mPCKS were cultured for 24H, 48H, and 72H. Afterwards, the gene expression of various bile acid receptors (FXR, PXR, VDR, CAR, TGR5, and S1PR2) was evaluated using RT-PCR. Gene levels were normalized and compared to the 0H control using one-way ANOVA.

Results: The results demonstrated that all tested bile acid receptors are expressed on gene level in mPCKS. The gene expression of FXR, PXR, VDR, and CAR significantly decreased more than 3,7-fold after 24H (P-value: <0.0011 for all receptors), after which expression levels remained stable up to 72H. The gene expression of TGR5 and S1PR2 significantly increased more than 5-fold after 24H, after which the expression levels increased consistently up to 72H (P-value: <0.0141). In addition, mPCKS remained viable during the whole incubation period, as illustrated by stable ATP levels.

Conclusion: These data indicate that the various components for bile acid signaling are present in mPCKS. Based on this we suggest that mPCKS can be used as a model for bile acid-induced nephrotoxicity.

PCA052

Unveiling the metabolic health landscape: a machine learning exploration of regional adiposity's influence on phenotypic variations among young adults

Shipra Das[1], Manjish Pal[2], Sanjay Kumar[3]

[1]Bharat Ratna Late Shri Atal Bihari Vajpayee Memorial Medical College, Rajnandgaon, India, [2]IIT kharagpur, Kharagpur, India, [3]Sikkim Manipal Institute of Medical Sciences, Gangtok, India

Introduction: Complex interface between adiposity and metabolic health heterogeneity has led to the detection of distinct phenotypes like metabolically healthy obese (MHO) and metabolically unhealthy normal weight (MUNW) individuals. Understanding the association between regional adiposity and metabolic disorder components of different young adult phenotypes is necessary to develop appropriate intervention strategy in early stage.

Aim and objectives: The present study aims to use advanced statistical methods including path analysis, random forest analysis, and support vector machine (SVM) to unwind the association of regional adiposity among MHO, metabolically unhealthy obese (MUO), and MUNW young adult population.

Methodology: On the basis of body mass index (BMI) and cardio-metabolic risk factor 400 young adults aged 18-25 years were categorized into metabolically healthy obese (MHO), metabolically unhealthy obese (MUO), and metabolically unhealthy normal weight (MUNW) groups. Regional adiposity was assessed by using predictive equations for Asian Indians (Goel K et al, 2008). Path analysis was used to explore direct and indirect effects of regional adiposity on metabolic health. Random forest analysis and SVM were employed to predict metabolic health status.

Results: Metabolically Healthy Obese (MHO): Path analysis shown that in the MHO group, Visceral adipose tissue (VAT) had a significant direct effect on metabolic health ($\beta = 0.34$, $p < 0.01$), while Subcutaneous adipose tissue (SAT) showed a weaker direct effect ($\beta = 0.17$, $p < 0.05$). Random forest analysis identified VAT (importance score = 0.41) as the most important predictor of metabolic health in this group, followed by SAT (importance score = 0.27). **Metabolically Unhealthy Obese (MUO)**: In the MUO group, both VAT and SAT had significant direct effects on metabolic health (VAT: $\beta = 0.38$, $p < 0.01$; SAT: $\beta = 0.29$, $p < 0.05$). Random forest analysis indicated that VAT (importance score = 0.43) was the most important predictor of metabolic health in this group, followed by SAT (importance score = 0.39). **Metabolically Unhealthy Normal Weight (MUNW):** Path analysis showed that in the MUNW group, VAT had a significant direct effect on metabolic health ($\beta = 0.21$, $p < 0.05$), while SAT show a very weaker direct effect ($\beta = 0.09$, $p < 0.05$). Random forest analysis identified VAT (importance score = 0.39) as the most important predictor of metabolic health in this group.

Conclusion: This research provides important insights into the association between regional adiposity and cardio-metabolic risk factors among young adults across different obesity phenotypes. The results emphasize the differential effects of VAT and SAT on metabolic health in each phenotype, highlighting the significance of personalized approach to obesity management and prevention.

Keywords: metabolically healthy obese (MHO), metabolically unhealthy normal weight (MUNW), metabolically unhealthy obese (MUO), Visceral adipose tissue (VAT), Subcutaneous adipose tissue (SAT).

PCA053

Correlation of serum levels of nitric oxide metabolites with body mass index and arterial stiffness in young individuals

VIDYA GANJI[1]

[1]ASSISTANT PROFESSOR, ALL INDIA INSTITUTE OF MEDICAL SCIENCES, BIBINAGAR, HYDERABAD, India

Introduction: Obesity is a multi-factorial disorder defined as abnormally high levels of body fat accumulation. It is a major emerging pandemic of this century which can be attributed to alterations in eating habits, lifestyle choices and rise in sedentary behaviour. The activation of pro-inflammatory signalling pathways linked to obesity can result in vascular endothelial dysfunction and changed levels of Nitric oxide(NO). Hyperlipidaemia may exacerbate arterial stiffness which is a precursor to atherosclerosis. In this study, we tried to evaluate the changes in levels of nitric oxide in obese individuals and its association with arterial stiffness.

Objectives: To identify the association of serum levels of Nitric oxide metabolites with Body Mass Index(BMI) in apparently healthy subjects.

2. To evaluate any correlation between serum nitric oxide metabolites, BMI and arterial stiffness in obese individuals.

Methodology: The study was conducted after obtaining Institutional Ethical committee(IEC) approval on 120 adults in the age group of 20 -40 yrs, non-smokers having sedentary working habits who are apparently healthy.The weight and height of all the study participants were measured according to standard protocols. Body mass index (BMI) was calculated as weight divided by square of height(h2). The subjects were divided into three groups depending on their BMI as follows: **Group I: BMI 18.5 to 22.9 (controls)(n=40), GROUP II: BMI 23 to 29.9 (overweight and pre-obese subjects) (n=40) and Group III: BMI 30 and above (obese subjects) (n=40)(Asian classification of BMI).** Fasting venous blood samples were collected and Serum NOx concentration were measured by the nitrite, nitrate assay kit which determines the levels of NO metabolites (total nitrite and nitrate) using GREISS reaction method and absorbance read at 540nm. Serum lipids and triglycerides were measured using enzymatic colorimetric method with glycerol phosphate oxidase and serum cholesterol levels were estimated using standard kits. **Arterial stiffness** of the participants was measured using an oscillometric non-invasive arteriography for cardiovascular risk assessment.

Result: The results showed a significant increase in systolic blood pressure ($p<0.001$) and no change in diastolic blood pressure and significant increase in pulse pressure($p<0.001$) with increase in visceral adiposity (Waist Circumference) more than BMI. Results of Pearson correlation indicated that there is a significant small negative relationship between BMI and Serum NO levels , (r =- 0.534, p < .001). There was significant increase in Brachial ankle Pulse Wave Velocity (Ba PWV) (p=0.001) and Carotid Femoral Pulse Wave Velocity (CF PWV) (p=0.01) in obese subjects when compared to controls.

Conclusion: Our study results showed that abdominal obesity more than overall obesity is more strongly associated with decreased serum NO levels and Increased arterial stiffness. In obese individuals, increased arterial stiffness as reflected by increased pulse wave velocity may contribute to predicting cardiovascular disease in both genders in addition to development of hypertension.

Figure 1. The various mechanisms causing increased arterials stiffness in obesity

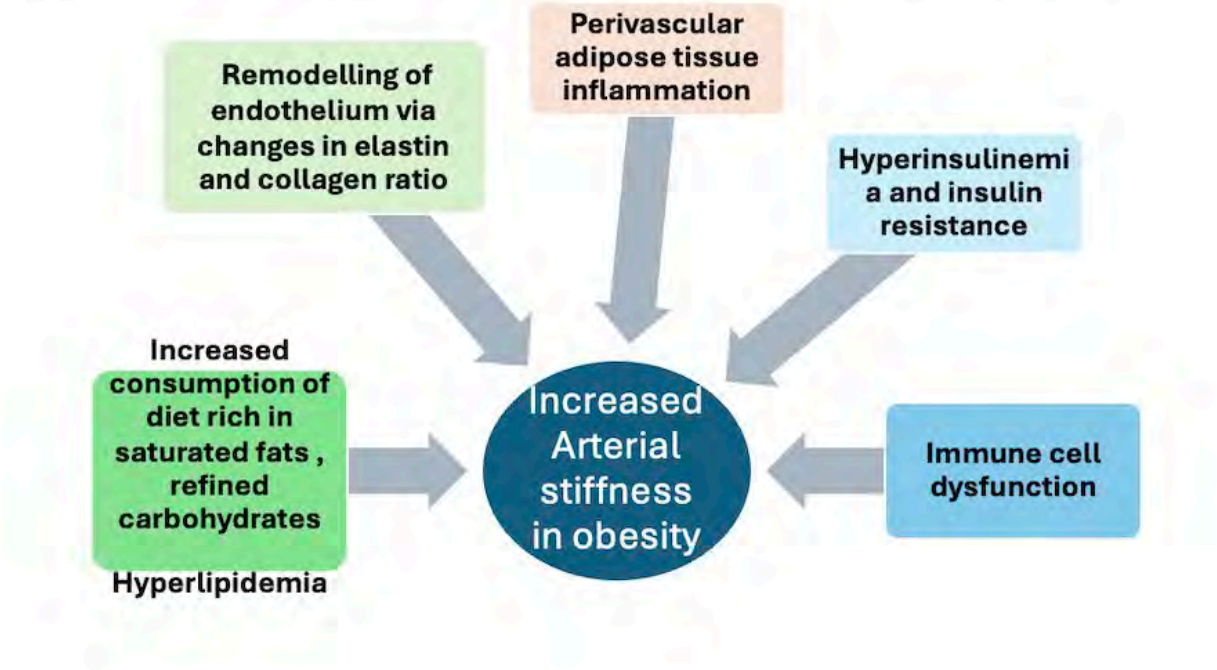

References: 1. NHMRC. Clinical practice guidelines for the management of overweight and obesity in adults. Treatment. Canberra, ACTNHMRC.2003,81-106. 2. Aroor AR, Jia G, Sowers JR. Cellular mechanisms underlying obesity-induced arterial stiffness. Am J Physiol Regul Integr Comp Physiol.2018;314(3):387-398. 3. Miranda K M, Espey MG, Wink DA. A rapid, simple spectrophotometric method for simultaneous detection of nitrate and nitrite. Nitric oxide. 2001;5(1):62-71. 4. Raddino R, Caretta G, Teli M, Bonadei I et al: Nitric oxide and cardiovascular risk factors: Heart Int:2007;3(1):18. 5. Ghasemi A, Zahediasl S, Azizi F. Elevated Nitic oxide metabolites are associated with obesity in women. Arch Iran Med. 2013; 16(9): 521-525. 6. Perreault M, Marette A. Targeted distribution of inducible nitric oxide synthase protects against obesity-linked insulin resistance in muscle. Nat Med.2001;7(10):1138-1143. 7. Dallaire P, Marette A. Obesity-linked insulin resistance. Is nitric oxide the missing link? Can J Diabetes.2004;28:59-66. 8. Gruber HJ, Mayer C, Mangge H, Fauler G et al. Obesity reduces the bioavailability of nitric oxide in juveniles: Int J Obesity: 2008;32(5),826-831. 9. Ahmed N, Adam SI, Nawi AM et al. Abdominal obesity indicators: Waist circumference or waist-to-hip ratio in Malaysian adult population. Int J Prev Med. 2016 Jun; 7:82. 10. Fisher E, Brzezinski RY, Ehrenwald M et al. Increase in Body mass

index and waist circumference predicts development of metabolic syndrome criteria in apparently healthy individuals with 2 and 5 yrs follow up. Int J Obes.2019;43(4):800-807.

PCA054

Intergenerational Impact of Parental Zinc Deficiency on Metabolic Outcomes in Drosophila melanogaster

Kasimu Ghandi Ibrahim[2], Kamaldeen Olalekan Sanusi[3,4], Murtala Bello Abubakar[4,5], Mustapha Umar Imam[4,6]

[1]Department of Human Physiology, Faculty of Health Sciences, Al-Hikmah University, P.M.B. 1601, Ilorin, Nigeria, Sokoto, Nigeria, [2]Department of Basic Medical and Dental Sciences, Faculty of Dentistry, Zarqa University, P.O. Box 2000, Zarqa 13110, Jordan, [3]Department of Human Physiology, Faculty of Health Sciences, Al-Hikmah University, P.M.B. 1601, Ilorin, Nigeria, [4]Centre for Advanced Medical Research and Training (CAMRET), Usmanu Danfodiyo University, P.M.B. 2254, Sokoto, Nigeria, [5]Department of Physiology, College of Medicine and Health Sciences, Sultan Qaboos University, Muscat, Oman, [6]Department of Medical Biochemistry, Faculty of Basic Medical Sciences, College of Health Sciences, Usmanu Danfodiyo University, P.M.B. 2254, Sokoto, Nigeria

Background

Gene-environment interactions play a crucial role in shaping the health of the offspring, with environmental factors like dietary zinc deficiency exerting significant impacts. Yet, the effect of parental zinc deficiency on the health of the offspring demands a holistic approach beyond solely examining maternal zinc status.

Aim

In this study, we investigated the physiological and molecular basis of both maternal and paternal zinc deficiency on offspring metabolic health, using the *Drosophila melanogaster* model.

Methods

Dietary zinc deficiency was induced in flies by incorporating TPEN (N, N, N', N'-tetrakis (2-pyridylmethyl) ethylenediamine) into their diet, starting from the egg stage through adulthood. Offspring were subsequently raised on standard diets. Following adulthood, parents and offspring were assessed for various parameters after seven days of exposure. Male and female flies (n = 10) were weighed and their locomotion was analysed. After being anaesthetized with ice, haemolymph was extracted and used to measure levels of glucose, trehalose, triglycerides, malondialdehyde, catalase activity, and total antioxidant capacity using commercially available kits. Finally, RNA was extracted, and quantitative real-time PCR (qPCR) was used to assess the mRNA expression of genes involved in zinc transport (*dZIP1*, *dZnT1*, *dZIP71B*, and *dZnT53*), glucose regulation (*DILP2* and *PEPCK*), antioxidant defence (*SOD1* and *CAT*), and inflammatory pathways (*UPD2* and *Eiger*). Data were analysed using two-way ANOVA followed by Bonferroni multiple comparison *post hoc* test and expressed as mean ± standard deviation.

Results

While parental flies exhibited significantly reduced ($p<0.05$) body weight, both male and female offspring showed increased body weight. Moreover, the offspring manifested disruptions in glucose metabolism, lipid homeostasis, and antioxidant enzyme activity. Gene expression analysis revealed significant ($p<0.05$) alterations in zinc transport genes, with elevated *dZIP1* mRNA levels in females and increased *dZnT1* mRNA levels in males. Both sexes displayed reduced *dZnT35C* mRNA fold change. Additionally, *DILP2* and the pro-inflammatory markers *Eiger* and *UPD2* mRNA were upregulated.

Conclusion

This study reveals the lasting consequences of paternal zinc deficiency, impacting offspring health and highlighting the need to consider both parents when studying intergenerational health effects. Understanding these mechanisms could lead to preventative strategies against zinc deficiency-related metabolic disorders.

Keywords: Zinc deficiency, intergenerational, *Drosophila melanogaster*, metabolism, zinc transport

Not applicable

PCA056

Wars1 knockdown in hepatocytes regulates whole-body glucose homeostasis

Francesca Pontanari[1]

[1]*EPFL, Lausanne, Switzerland*

INTRODUCTION:

Aminoacyl tRNA synthetases (ARSs) are central and indispensable enzymes facilitating protein synthesis by shuttling amino acids to tRNA molecules. The vital importance of ARSs is exemplified by the embryonic lethality resulting from their knockout *in vivo*. We aimed to identify the metabolite transported by SLC25A47, a unique mitochondrial carrier specific to hepatocytes. To achieve this goal, we implemented a commercially available hepatocyte-specific knockout mouse model of *Slc25a47*. Unexpectedly, the genomic recombination of the *Slc25a47* locus, in this mouse model, induces a knockdown of the cytosolic tryptophanyl tRNA synthetase (*Wars1*), found in the same locus (hereafter referred to as the *Slc25a47-Wars1* locus).

METHODS:

To delineate the effects associated with *Wars1*, we employed a co-injection protocol wherein *Slc25a47-Wars1*$^{lox/lox}$ mice were administered AAV8_*Cre* to induce gene locus recombination. Concomitantly, mice were injected with either *Slc25a47* or *Wars1* enabling us to segregate the phenotypic outcomes attributable to *Wars1*. The injected viruses were under the human alpha-1 anti-trypsin promoter, which made the expression hepatocyte-specific. C57BL/6J mice were fed either tryptophan-deficient, methionine-deficient, or amino acid-sufficient diets. Body weight was collected twice per week, and an oral glucose and an insulin tolerance test were performed. Significance was determined using Two-way ANOVA followed by Tukey's post-hoc correction, n=9 mice for the rescue experiment and n=10 mice for the special diet were tested. qPCR analysis of inflammation and fibrosis markers was performed on n=6 mice, and statistical significance was determined using One-way ANOVA followed by Tukey's post-hoc correction.

RESULTS:

The knockdown of *Wars1* in hepatocytes induced a hypermetabolic phenotype, reflected by reduced body weight, improved glucose tolerance, and insulin sensitivity. When we compared these phenotypes with tryptophan-deficient and methionine-deficient feeding, we found that *Wars1* knockdown in hepatocytes was sufficient to recapitulate the whole-body phenotypes of these amino acid-deprived diets. However, the better metabolic health came at a high cost for the liver, as inflammation and fibrosis were observed after *Wars1* knockdown.

CONCLUSIONS:

These findings underscore the significance of amino acid incorporation into protein, particularly within hepatocytes, in governing whole-body homeostasis. Further investigation is warranted to elucidate the central role of hepatocytes and amino acid metabolism in metabolic diseases.

PCA057

The safety and efficacy of free protein diet with ketoacid analogues in chronic kidney disease-affected diabetic rats

Ahmed Taha[1], Ahmed El-Sayed Nour El-Deen[1]

[1]Department of Basic Medical and Dental Sciences, Faculty of Dentistry, Zarqa University, Zarqa, Jordan

Background: Diabetic nephropathy (DN) is a common vascular complication of diabetes mellitus (DM) which needs weight control and caloric restriction, especially for protein. A protein-restricted diet with ketoacids reduces the intake of nitrogen while avoiding the harmful consequences of inadequate dietary protein intake.

Objective: This study examined the safety and effectiveness of a free-protein diet with ketoacid analogues (KAA) in diabetic rats with chronic kidney disease (CKD).

Material and methods: Adult male albino rats (n=60) were induced with diabetes mellitus using streptozotocin and grouped into six *vis*: (1) Control group rats received standard diet (2) Normal rats received low protein diet (3) Diabetic control rats received standard diet (4) Diabetic rats received low protein diet (5) Diabetic rats received α-keto amino acids with low protein diet (6) Diabetic rats received α-keto amino acids with free protein diet. The body weights of the rats were measured weekly, and the urine volume recorded for 24 hours. After 12 weeks of treatment, the rats were euthanized using halothane inhalation. Blood samples were collected via the carotid artery and used to assess blood glucose (mg/dl), insulin (pmol/L), urea (mg/dl), creatinine (mg/dl), total cholesterol (TC) (mg/dl), LDL (mg/dl), HDL (mg/dl), triglycerides (TG) (mg/dl), and albumin (mg/dl) levels were determined. Data were analyzed using a one-way analysis of variance followed by Tukey's *post hoc* test to compare between the groups.

Results: A significant decrease ($p<0.05$) in blood glucose, serum total cholesterol, LDL, triglycerides, serum urea and creatinine were observed, while insulin level, albumin, GFR, urine volume and HDL were significantly increased ($p>0.05$) in diabetic rats received α-keto amino acids with free protein diet, without significant changes in body weight.

Conclusion: A free-protein diet containing KAA improves renal function, lowers blood glucose levels, maintains body weight, and does not worsen nutritional status in CKD in diabetic rats over time.

Not applicable

PCA058

An investigation into the impact of functional mutations on the binding of leucine to Sestrin2 in the context of aging and age-related degenerative conditions using structural and molecular simulation approaches

Abbas Khan[1], Muhammad Ammar Zahid[1], Muhammad Shahab[2], Raed Al-Zoubi[3], Mohanad Shkoor[4], Tarek Benameur[5], Abdelali Agouni[1]

[1]Department of Pharmaceutical Sciences, College of Pharmacy, QU Health, Qatar University, Doha, Qatar, [2]Department of Chemistry, Beijing University of Chemical Technology (BUCT),, Beijing, China, [3]Surgical Research Section, Department of Surgery, Hamad Medical Corporation, Doha, Qatar, [4]Department of Chemistry, College of Arts and Science, Qatar University, Doha, Qatar, [5]College of Medicine, King Faisal University, PO Box 400, Al-Ahsa, Saudi Arabia

Leucine is the native known ligand of Sestrin2 (Sesn2) and its interaction with Sesn2 is particularly noteworthy, as it influences the activity of mTOR in aging and its associated pathologies. It is important to find out how leucine interacts with Sesn2 and how mutations in the binding pocket of leucine affect the binding of leucine. Therefore, this study was committed to investigating the impact of non-synonymous mutations by incorporating a broad spectrum of simulation techniques, from molecular dynamics to free energy calculations. Our study was designed to model the atomic-scale interactions between leucine and mutant forms of Sesn2 already described in the literature.

Due to the crucial role of hydrogen bonding in biological processes, we assessed hydrogen bonds in each trajectory over time. The wild-type displayed a higher average number of hydrogen bonds in comparison to the mutants, particularly evident in T374A, T386A, R390A, and E451Q mutants. Our results demonstrated that the interaction paradigm for the mutants has been altered thus showing a significant decline in the hydrogen bonding network. These mutations compromised dynamic stability by disrupting conformational flexibility, sampling time, and leucine-induced structural constraints, leading to variations in binding affinity and structural stability. The analysis of molecular dynamics-based flexibility highlighted an increased fluctuation in regions 217-339 and 371-380. These regions correspond to a linker and a loop that cover the leucine binding cavity. This cavity is critical for the "latch" mechanism in the N-terminal, which is essential for binding leucine. Specifically, mutations at three threonine residues that show a high degree of conservation, Thr374, Thr377, and Thr386, disrupted interaction with leucine, as these residues are critically located above the binding site. Mutations at these positions (T374A or T386A) lead to the disruption of the interaction with leucine. Further validation of reduced binding and modified internal motions caused by the mutants was obtained through binding free energy calculations, Principal Components Analysis (PCA), and Free Energy Landscape analysis (FEL). The MM/PBSA approach was used to calculate the total binding free energy for wild-type and mutants. The values obtained were as follows: -47.32±0.71 kcal/mol for the wild-type, -31.93±0.73 kcal/mol for T374A, -37.79±0.76 kcal/mol for Y375F, -35.67±0.82 kcal/mol for T386A, -38.13±0.85 kcal/mol for R390A, -35.44±0.84 kcal/mol for W444E, and -32.21±0.77 kcal/mol for E451Q mutants. Similar patterns were noted in the total binding free energy determined by the MM/GBSA approach. The significant drop in total binding free energy in mutants reinforces previous observations suggesting the functional impairment of Sesn2 caused by these mutations.

Through studying the complex molecular interactions between Sesn2 and leucine, as well as their mutations, and identifying specific areas where mutations significantly affect leucine binding. These findings will aid in identifying potential targets for drugs that can control the mTOR pathway. These therapeutic compounds may play a crucial role in treating metabolic diseases, cancer, and neurological disorders, thereby extending the health span, and improving the quality of life for the aging population.

PCA059

Exploring the light adaptation effect of photopic electroretinogram components with the use of long duration stimuli in healthy participants

Harry Arbuthnott[2,3], Charlie Bosshard[2,3], Isabelle Chow[4,5], Shaun Leo[3,6], Xiaofan Jiang[3,5], Omar Mahroo[2,3,4,5,6]

[1]college, Harpenden, United Kingdom, [2]Physiology, Development and Neuroscience, University of Cambridge, Cambridge, United Kingdom, [3]Institute of Ophthalmology, University College London, London, United Kingdom, [4]Department of Ophthalmology, St Thomas' Hospital, London, United Kingdom, [5]Section of Ophthalmology, King's College London, St Thomas' Hospital Campus, London, United Kingdom, [6]NIHR Biomedical Research Centre at Moorfields Eye Hospital and the UCL Institute of Ophthalmology, London, United Kingdom

Purpose

The electrical response of the human retina to light stimuli can be recorded non-invasively as the electroretinogram (ERG). The light adaptation effect (LAE) refers to the increase, over several minutes, in the amplitude of the ERG elicited in response to repeated flashes delivered superimposed on a light-adapting background, following a prior period of dark adaptation. Previous studies investigating the LAE measured the a-wave and b-wave elicited by brief flash stimuli. We used long duration stimuli to explore the LAE of the response to stimulus onset and offset.

Methods

Bilateral ERG recordings were made to 200ms flash stimuli over the course of light adaptation in 3 healthy adult male participants (6 eyes), aged 21, 21 and 32. Participants gave written informed consent, and the study had Research Ethics Committee approval and conformed to the tenets of the Declaration of Helsinki. Pupils were dilated pharmacologically and conductive fibre electrodes were placed in the lower conjunctival fornix. Participants were fully dark adapted for 20 minutes, and then exposed to a white rod-suppressing background (40 cd m^{-2}), and 50 white 200 ms flashes (250 cd m^{-2}) were delivered in quick succession. The train of flashes was repeated at 2-minute intervals for up to 20 minutes; responses to each series of 50 flashes were averaged. The amplitude and peak time of the response to stimulus onset (a-wave, b-wave) and offset (d-wave) were measured.

Results

In all participants, the a-wave, b-wave, and d-wave increased in amplitude during the course of light adaptation, reaching a plateau after 10-12 minutes following the onset of the background. The peak times were found to shorten during this period. A time point of 14 min following background onset was chosen for comparison: the amplitudes of all components were significantly larger ($p<0.013$) and peak times significantly shorter ($p<0.01$) compared with the corresponding values measured immediately following background onset (paired t test). The mean (SEM) proportional increases in amplitude were 43 (19)%, 38 (5.5)% and 73 (20)% for a-wave, b-wave and d-wave

respectively. Mean (SEM) advancements in peak time were 1.1 (0.2), 3.0 (0.6) and 2.8 (0.6) ms respectively.

Conclusions

We consistently found an increase in amplitude for all 3 components, indicating that the response to both stimulus onset and offset increases in amplitude over the course of light adaptation. Response kinetics also appear to become more rapid over this time period. The mechanisms underlying the LAE are still unknown, but our findings indicate that they apply to electrical activity elicited by both onset and offset of light stimuli.

PCA060

Measuring [O2] in mouse brain slices reveals changes in modelled oxygen consumption kinetics following changes in bath [O2]

Sam Atkinson[1]

[1]*University of Sussex, Brighton, United Kingdom*

The brain is disproportionately aerobic for its size, consuming 20% of inspired oxygen primarily to produce ATP via oxidative phosphorylation (1,2). However, this high oxygen demand leads to a vulnerability to hypoxia when oxygen supply drops below demand (3).
The structure of the hippocampal vascular network, alongside pericyte and endothelial function, results in reduced blood flow and neurovascular coupling compared to the neocortex, potentially underlying the particular vulnerability of this region to hypoxia (4). Hypoxia may occur in Alzheimer's disease (AD) development, as perturbed blood flow is observed prior to symptomatic AD (5) and a decline in hippocampal function is an early AD cognitive marker (6,7). To better understand the impact of mild hypoxia on hippocampal function we investigated how neuronal function and oxygen use was altered by a mild reduction in oxygen supply in mice in vivo and in mouse hippocampal brain slices.
Using haemoglobin spectrometry and laser doppler flowmetry to measure changes in blood oxygen saturation and blood flow, and 2-photon microscopy to measure neuronal calcium signals in Thy1/GCaMP6f mice, our preliminary data shows that mild acute hypoxia is associated with both increased oxygen consumption and frequency of calcium events.
We then tested whether we could recapitulate these findings in mouse hippocampal slices to provide a better model for studying underlying mechanisms.
Using a Unisense A/S oxygen microsensor, we measured depth profiles of [O2] through the pyramidal layer of the hippocampus of acute sagittal forebrain slices (300µm thickness, 32 slices from 7 mice (5 C57BLJ/6 2 Thy1xDsRed, 3 males, 4 females)), while varying bath [O2] gassing between 95% and 20%. Slice [O2] was largely hyperoxic at 95% O2, 5% CO2, approached normoxia at 58% O2, 5% CO2 and became hypoxic at 20% O2, 5% CO2, though surface [O2] in this condition was in the normoxic range (4,9).
We then compared these profiles to theoretical [O2] profiles generated by an oxygen diffusion and Michaelis-Menten consumption model, adapted from our previous work (10) . The kinetic parameters that best fit experimental data varied depending on bath [O2] (Median: 95%:Km: 1e-5mM, Vmax: 1.2mM/min; 58%:Km: 0.0025mM, Vmax: 4mM/min; 20%:Km: 7.5e-4mM, Vmax: 0.55mM/min), predicting highly variable rates of oxygen consumption.
Our data suggest a deviation in the O2-dependence of oxidative phosphorylation (which accounts for the bulk of oxygen consumption in the brain (1)) from simple Michaelis-Menten kinetics, which could contribute to increased oxygen consumption rates in hypoxic brain tissue . Previous work on isolated mitochondria and cytochrome c oxidase suggest that alterations in pH and cellular energy balance, such as likely occur during hypoxia, can cause such kinetic changes (11) .
Here we show that in vivo [O2] can be recapitulated in acute mouse brain slices, and that modelled oxygen consumption kinetics are altered as bath [O2] is changed.
In summary, our data show a counter-productive increase in hippocampal neuronal activity and oxygen use in mild hypoxia in vivo and altered O2 consumption kinetics across different [O2] in brain slices. Improving understanding of hypoxia as a potential early AD mechanism will help

enable clinical translation.

1. Silver I, Erecińska M. Oxygen and Ion Concentrations in Normoxic and Hypoxic Brain Cells. In: Hudetz AG, Bruley DF, editors. Oxygen Transport to Tissue XX [Internet]. Boston, MA: Springer US; 1998. p. 7–16. Available from: https://doi.org/10.1007/978-1-4615-4863-8_2 2. Erecińska M, Silver IA. Tissue oxygen tension and brain sensitivity to hypoxia. Respir Physiol. 2001 Nov 15;128(3):263–76. 3. Mukandala G, Tynan R, Lanigan S, O'Connor JJ. The Effects of Hypoxia and Inflammation on Synaptic Signaling in the CNS. Brain Sci. 2016 Feb 17;6(1). 4. Shaw K, Bell L, Boyd K, Grijseels DM, Clarke D, Bonnar O, et al. Neurovascular coupling and oxygenation are decreased in hippocampus compared to neocortex because of microvascular differences. Nat Commun. 20210527th ed. 2021 May 27;12(1):3190. 5. Badimon A, Torrente D, Norris EH. Vascular Dysfunction in Alzheimer's Disease: Alterations in the Plasma Contact and Fibrinolytic Systems. Int J Mol Sci. 2023 Apr 11;24(8). 6. Swinford CG, Risacher SL, Wu YC, Apostolova LG, Gao S, Bice PJ, et al. Altered cerebral blood flow in older adults with Alzheimer's disease: a systematic review. Brain Imaging Behav. 2023 Apr;17(2):223–56. 7. Rao YL, Ganaraja B, Murlimanju BV, Joy T, Krishnamurthy A, Agrawal A. Hippocampus and its involvement in Alzheimer's disease: a review. 3 Biotech. 2022 Feb;12(2):55. 8. Setti SE, Hunsberger HC, Reed MN. Alterations in Hippocampal Activity and Alzheimer's Disease. Transl Issues Psychol Sci. 2017 Dec;3(4):348–56. 9. Lyons DG, Parpaleix A, Roche M, Charpak S. Mapping oxygen concentration in the awake mouse brain. Kleinfeld D, editor. eLife. 2016 Feb;5:e12024. 10. Hall CN, Klein-Flügge MC, Howarth C, Attwell D. Oxidative phosphorylation, not glycolysis, powers presynaptic and postsynaptic mechanisms underlying brain information processing. J Neurosci. 2012 Jun 27;32(26):8940–51. 11. Wilson DF, Owen CS, Erecińska M. Quantitative dependence of mitochondrial oxidative phosphorylation on oxygen concentration: A mathematical model. Arch Biochem Biophys. 1979;195(2):494–504.

PCA061

Change of voltage-gated sodium channel repertoire in skeletal muscle of a MuSK myasthenia gravis mouse model

Olena Butenko[1]

[1]*Department of Human Genetics, Leiden University Medical Center, Leiden, Netherlands*

Muscle-specific kinase myasthenia gravis (MuSK MG) is an autoimmune neuromuscular disorder. It is caused by autoantibodies against MuSK, a key postsynaptic membrane molecule involved in acetylcholine receptor clustering at the neuromuscular junction (NMJ). MuSK MG patients have fluctuating, fatigable weakness. The disease severity can vary greatly between patients, in spite of comparable autoantibody levels. One explanation for inter-patient and inter-muscle variability in sensitivity might be variations in compensatory muscle responses. Previously, we developed a passive transfer mouse model for MuSK MG, using purified patient IgG4. In our *ex vivo* experiments we observed that nerve stimulation-evoked contraction of muscles from mild MuSK MG mice appeared partly insensitive to μ-Conotoxin-GIIIB. This blocker of $Na_V1.4$ voltage-gated sodium channels normally completely eliminates muscle contraction. We hypothesized that changes in Na_V channel expression profile, possibly compensatory expression of (μ-Conotoxin-GIIIB insensitive) $Na_V1.5$ cardiac-type channels, might lower the muscle fibre's firing threshold and improve neuromuscular synaptic transmission in mild MuSK MG.

We performed passive transfer in immuno-deficient NOD.CB17-Prkdcscid/J (Nod/scid) mice, using 'high'(n=12), 'intermediate' (n=3) and 'low' (n=12) dosing regiments of purified MuSK MG patient IgG4. Next, we assessed myasthenia levels, μ-Conotoxin-GIIIB resistance and firing thresholds. *Ex vivo* analysis of myasthenic NMJs was performed by evaluation of miniature endplate potentials and endplate potentials in the presence of μ-Conotoxin-GIIIB in diaphragm-nerve preparations. To detect changes in $Na_V1.4$ and $Na_V1.5$ channels expression profile we performed qPCR and immunostaining in muscle tissue. Data is presented as mean ± S.E.M., with n representing the number of animals per group. Statistical analysis was performed using multiple unpaired t-tests or one-way ANOVA with Tukey's post hoc tests. All procedures involving the use of laboratory animals were performed in accordance with Dutch law and Leiden University guidelines.

High- and intermediate-dosed mice showed severe, progressive myasthenia, not detected in low-dosed animals. However, during electrophysiological analysis of diaphragm NMJs we found equally reduced amplitudes and frequencies of miniature endplate-potentials (MEPPs), and equal reductions of endplate potentials (EPPs) amplitudes (all by~40-50%, as compared to the PBS-control), probably associated with direct exposure to MuSK MG patient IgG4 via the intraperitoneal injection route. Notably, the diaphragms from low-dosed mice (n=12) showed a much higher degree of μ-Conotoxin-GIIIB resistance according to the scale for contraction responses when compared with PBS mice (n=7) or high-dosed mice (n=12). However, *Scn5a*, the gene encoding $Na_V1.5$, was not upregulated in muscle tissue of these mice (PBS mice: n=4, low-dosed mice n=6, high-dosed mice n=6; $p > 0.05$). Furthermore, no reduction of firing thresholds or expression of histologically detectable $Na_V1.5$ channels was found (PBS mice: 8.61 ± 0.11 mV (n=4); low-dosed mice: 8.60 ± 0.28 mV (n=6); high-dosed mice 8.69 ± 0.22 mV (n=6)). Thus, we observed $Na_V1.4$-independent muscle contraction *ex vivo*, preferentially in mice experiencing subclinical MuSK MG,

which is unlikely associated with upregulation of $Na_V1.5$. It remains to be established which other Na_V channels or factors are responsible for the observed μ-Conotoxin-GIIIB insensitivity and if the change in Na_V repertoire is compensatory beneficial.

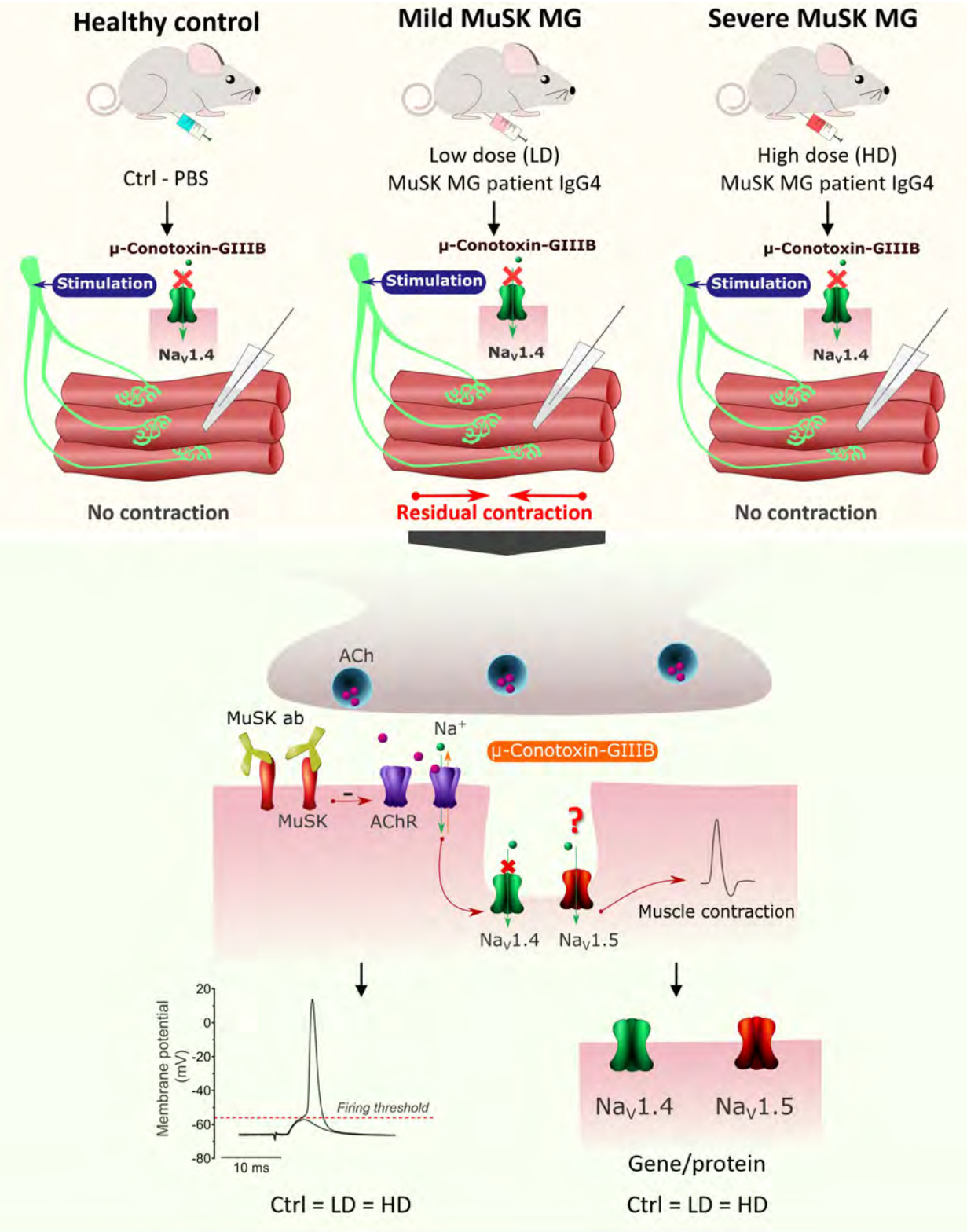

PCA062

Does cerebrospinal fluid flow along the basement membranes of brain capillaries? In a new in vitro model, oscillating lateral displacement of a porous medium increased flow by a factor of at least 3.6.

Jonathan Coles, Michael Hale[1]

[1]*School of Physical Sciences, The Open University, Walton Hall,, Milton Keynes, United Kingdom*

Cerebrospinal fluid (CSF) delivers molecules, such as vitamin E, to the vicinity of brain cells and may carry away others, such as amyloid-beta. CSF enters the brain parenchyma by flowing from the brain surface down peri-arteriolar spaces: its subsequent pathway is uncertain (see Hladky & Barrand, 2022). Protein marker molecules in CSF are observed to accumulate in the pericapillary basement membranes of brain capillaries (e.g., Rennels et al. 1985; Fig. 3C in Iliff et al. 2012) but it is improbable that a constant physiological pressure gradient could drive adequate CSF along a pericapillary pathway. Brain tissue moves at the cardiac frequency (Sloots et al., 2020) and accumulation of CSF marker in the pericapillary space is slower if blood pulsation is reduced (e.g., Rennels et al. 1985). We had previously tested the effect of a pulsating pressure gradient on flow through a medium mimicking a basement membrane in various configurations but observed at most only a small enhancement. We have now tested the effect of oscillating lateral movement on flow of 0.15 M NaCl through a vertical silicone tube (i.d. 1.0 mm, o.d. 2.0 mm) filled with a porous medium (a thread of wool, 30 mm long; Fig. 1). With a longitudinal pressure difference of 125 mm H_2O, moving the centre of the tube by 3.5 mm at 5 Hz increased flow by a mean factor of 3.62, SEM = 0.10, n = 5. When the pressure difference was increased to 225 mm H_2O, the enhancement was 1.87, SEM = 0.26, n = 5, which is significantly less (P = 0.0002). Menisci at air/liquid interfaces are susceptible to oscillating pressures, so we took care to avoid them.

We have found no previous report of the effect of experimental movement on flow through a porous medium, apart from that of McMaster & Parsons, 1938, on transport of Evans Blue in a rabbit ear.

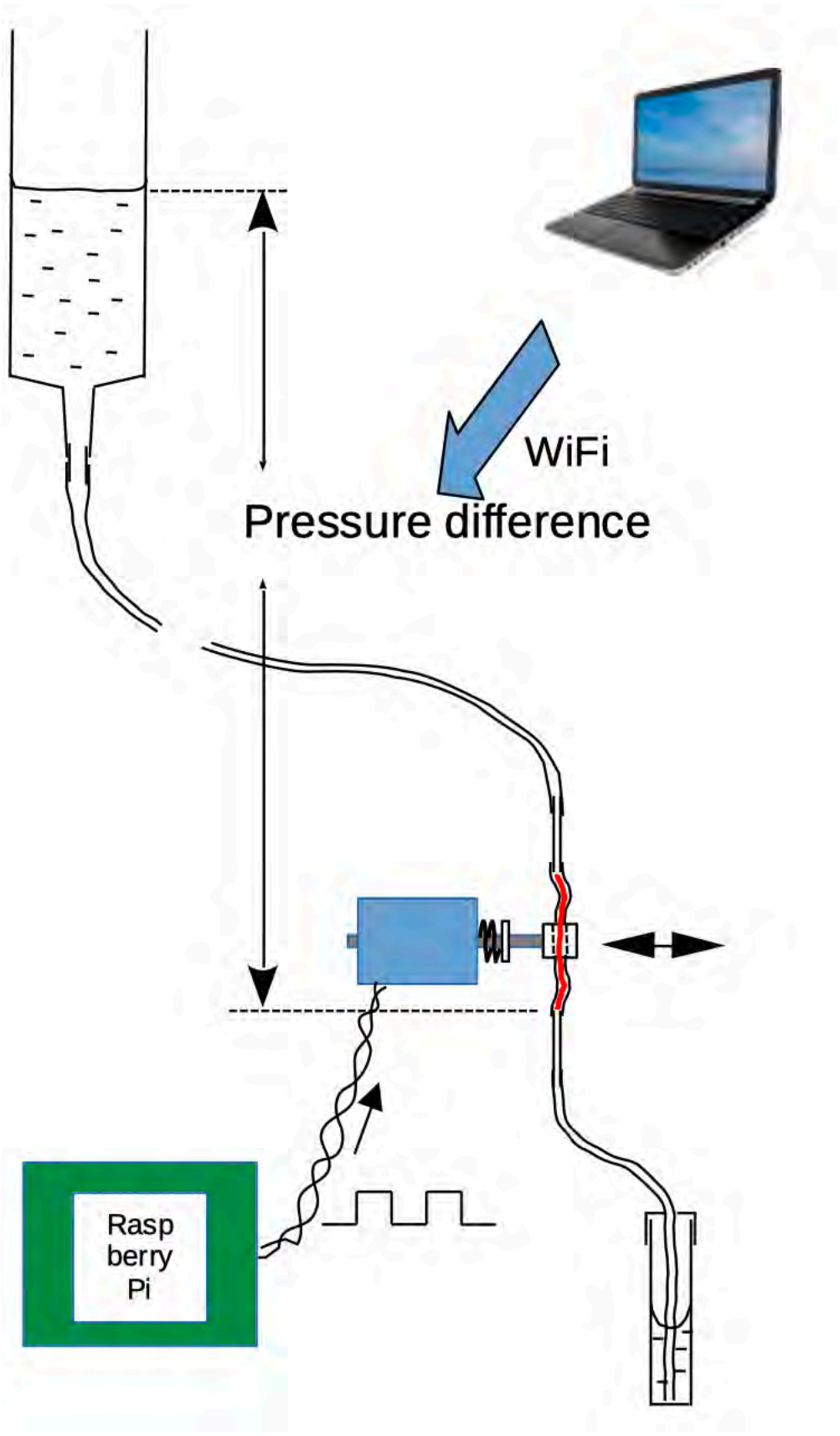
WiFi
Pressure difference
Rasp
berry
Pi

Hladky SB & Barrand MA (2022). Fluids Barriers CNS 19.9. Iliff JJ et al. (2012). Sci Transl Med 4,147ra111 McMaster PD & Parsons RJ (1938). J Exp Med 68, 377-400. Rennels ML et al. (1985). Brain Res 326, 47-63 Sloots JJ, Biessels G, Zwanenburg JM (2020). Neuroimage 210, 116581

PCA063

Comparison of Cx45 and Cx36 expression in retinal organoids and mice retinas

Hannah Kendall[2], Mingaile Jackson[2], Simon Rutter[2], Birthe Dorgau[3], Evelyne Sernagor[3], Majlinda Lako[3], Gerrit Hilgen[2,3]

[1]Applied Sciences, Faculty of Health and Life Sciences, Northumbria University, Newcastle-upon-Tyne, United Kingdom, [2]Applied Sciences, Faculty of Health and Life Sciences, Northumbria University, Newcastle upon Tyne, United Kingdom, [3]Biosciences Institute, Faculty of Medical Sciences, Newcastle University, Newcastle upon Tyne, United Kingdom

Gap junctions, direct cell-cell connections deemed crucial in facilitating the synchronisation and collection of electrical signals, are widely prevalent in the nervous system. In vertebrates, gap junctions are comprised of two adjacent hemichannels, which in turn, are made up of six connexins (Cx). During neural development, connexins and their gap junctions emerge before chemical synapse formation and are thought to be involved in establishing distinct neural circuits. Despite being the most abundant in mouse retinas, it is unclear to what extent Cx45 and Cx36 are involved in retinal circuit creation, or indeed, how much they contribute to this process in human induced pluripotent stem cell derived retinal organoids (ROs).

To assess whether developmental parallels can be found in both systems, we quantified the expression patterns of Cx45 and Cx36 in mice retina (postnatal day 8-16) (Hilgen *et al*, 2022) and ROs at varying differentiation stages (days 40, 90, 150 and 200, respectively). In order to do this, we developed a custom software enabling automatic analysis of multiple anatomical parameters (e.g. size, overlap and near-by location) of all channels within a confocal microscopy stack. Our results show that numerous soma-somatic Cx45 and Cx36 gap junctions exist in ROs, and, both connexins are localised on and near synaptic terminals in both tissues (shown by synaptophysin and vesicular glutamate transporter 1 staining). Expression levels of Cx45 and Cx36 in both plexiform layers of the mouse retina increased until eye opening, which then reduced slightly from this stage. Within ROs, expression patterns of Cx45 showed increasing densities at the latter stages of differentiation (number of analysed sections for d20 = 125, d45 = 67, d90 = 133, d>150 = 214), whereas Cx36 expression was less pronounced than in mice (number of analysed sections for d20 = 112, d45 = 21, d90 = 73, d>150 = 119)

Heterotypic Cx45/Cx36 gap junctions, which can be found in the rod pathway between ON cone bipolar cells and all amacrine cells, were similarly expressed in both mice and ROs. Within mice, the percentage of Cx45/Cx36 gap junctions was found to be higher before eye opening (number of analysed sections for P8 =54, P10 = 50, P12 =51, P16 = 66), whereas, in ROs, it steadily increased (number of analysed sections for d20 = 24, d45 = 54, d90 = 78, d>150 = 216). In addition to this, our multielectrode array recordings from ROs revealed gap-junction-coupled retinal ganglion cells (RGCs) which is consistent with our findings from both connexins between RGCs in mice (not yet quantified).

In conclusion, our data suggests that both mice and ROs have very comparable Cx45 and Cx36 expression patterns. In addition to this, we have shown for the first time, ROs have both heterotypic Cx45/Cx36 gap junctions, and functional gap junctions between RGCs. Together, these findings

imply that both connexins play a pivotal role during the development of both mouse retina and ROs.

Hilgen, G (2022) Connexin45 colocalization patterns in the plexiform layers of the developing mouse retina. Journal of Anatomy, 243 (2), 258-264. doi: 10.1111/joa.13651

PCA064

Tracking of tibialis anterior motor units reveals no detrimental effects of intramuscular needle electrode insertion .

Mollie O'Hanlon[1], Elisa Nédélec[2], Tom Inns[2], Caroline Sunderland[1], Angus Hunter[1], Mathew Piasecki[3], Jessica Piasecki[1]

[1]Sport Health and Performance Enhancement (SHAPE) Research Centre, Nottingham Trent university, Department of Sport Science., Nottingham, United Kingdom, [2]Sport Health and Performance Enhancement (SHAPE) Research Centre, Nottingham Trent university, Department of Sport Science., Nottingham, United Kingdom, [3]Centre of Metabolism, Ageing and Physiology (COMAP), University of Nottingham, Nottingham, United Kingdom

Introduction. Exploration of human motor unit (MU) characteristics in clinical and research settings is commonly applied using intramuscular electromyography (iEMG) [1]. This typically involves the insertion of a concentric needle electrode into the muscle during voluntary contractions, and although minimally invasive, may cause discomfort and/or intramuscular damage. Afferent feedback from the muscle as a direct cause of needle insertion may influence MU characteristics such as firing rate (FR) and recruitment [2], thereby influencing the parameters it is designed to investigate. However, this has not yet been fully explored. Methodological advances in non-invasive high-density (HD) EMG allow the direct tracking of MUs across successive contractions in humans, inclusive of simultaneous recording with intramuscular needles, and presents an opportunity to investigate the true effects of needle insertion.

Aim. The aim of this study was to track the function of individual MU characteristics across subsequent contractions, with and without intramuscular needle insertion.

Method. Following familiarisation, six individuals (females n = 3) performed two dorsiflexor trapezoid contractions at 25% of maximum force (3s ascent, 12s hold, 3s descent). HD-EMG was recorded from the tibialis anterior (TA) with a 64ch surface electrode, and signals were decomposed into individual MU potentials and their corresponding spike trains [3]. Prior to the second contraction, a 26-gauge iEMG needle electrode was inserted into the TA, and individual MUs from HD-EMG were tracked with and without needle insertion. Multi-level regression models were used to determine the effect of needle insertion on MUFR at recruitment, decruitment and during the sustained phase, MU recruitment threshold ratio (recruitment:derecuitment), and the coefficient of variation in force. Statistical significance was accepted at $p<0.05$.

Results. The mean number of recorded and tracked across MUs contractions was 27 ± 13. MUFR at recruitment was 11.33 Hz without the needle and did not differ with needle insertion (9.96 Hz, $p = 0.259$). During the steady phase at 25% MVC, MUFR was 15.40Hz without needle and did not differ significantly with needle insertion (13.02 Hz, $p = 0.175$). MUFR at de-recruitment was 7.90 Hz without the needle and did not change significantly with the needle inserted (7.24 Hz, $p = 0.198$). The recruitment ratio was not altered between the contraction types ($p = 0.627$). The coefficient of variation in force was not impaired with needle insertion ($p = .895$).

Conclusion. The current pilot data reveal minimal effects of intramuscular needle insertion on a range of TA MU characteristics at 25% of maximum force and highlight the applicability of combining EMG techniques. However, further exploration is required in a variety of muscle sizes and locations, at different contraction intensities to allow definitive conclusions to be determined.

1. Piasecki M, Garnés-Camarena O, Stashuk, DW. Near-fiber electromyography. Clinical Neurophysiology. 2021;132(5):1089-1104. [Accessed 10 April 2024]. Available from: https://doi.org/10.1016/j.clinph.2021.02.008 2. Cabral HV, Inglis JG, Cudicio A, Cogliati M, Orizio C, Yavuz U, Negro F. 2023. Muscle contractile properties directly influence shared synaptic inputs to spinal motor neurons. bioRxiv. 2023:2023-11. [Accessed 10 April 2024]. Available from: https://doi.org/10.1101/2023.11.30.569389 3. Guo Y, Jones EJ, Škarabot J, Inns TB, Phillips BE, Atherton PJ, Piasecki M. 2024. Common synaptic inputs and persistent inward currents of vastus lateralis motor units are reduced in older male adults. GeroScience. 2024:1-13. [Accessed 10 April 2024]. Available from: https://doi.org/10.1007/s11357-024-01063-w

PCA065

Muscle spindles, motor control and mitochondrial superabundance - what is the connection?

Maria Roxana[1], Amy Vincent[2], Robert W Banks[3], Guy S Bewick[4]

[1]Institute of Medical Sciences, University of Aberdeen, Aberdeen, United Kingdom, [2]Translational and Clinical Research Institute, Faculty of Medical Sciences, Newcastle University, Newcastle Upon Tyne, United Kingdom, [3]Department of Biosciences, Durham University, Durham, United Kingdom, [4]Institute of Medical Sciences, University of Aberdeen, Aberdeen, United Kingdom

Mitochondrial dysfunction represents the most prevalent inherited metabolic disorder, affecting 1 in 5,000 individuals. Sensory ataxia, a disruption in motor control, is frequently an early symptom of mitochondria dysfunction, leading to an increased risk of falling and associated injury and fears. Mutations causing mitochondrial dysfunction may arise within the mitochondrial genome or nuclear-encoded mitochondrial genes (1). Mitochondria occupy approximately 55% of the volume of sensory terminals in the mouse muscle spindle, making them extraordinarily abundant (2). To investigate their function within muscle spindle primary sensory terminals, we have examined the effects of drugs that interfere with different aspects of mitochondrial activity on the firing of the primary afferents in response to muscle stretching.

Trapezoidal stretch-hold-release extensions (+10% of resting muscle length) were administered every 20 minutes to isolated adult C57/Bl6 mouse soleus muscles *ex vivo*. Whole nerve responses were recorded, for control, drug and drug washout from the same preparation. We investigated the effects of NH_4Cl (0.5-50 mM), which neutralizes pH in intracellular compartments and regulates mitochondrial biogenesis (3), caffeine (0.1-10 mM), which releases Ca^{2+} from intracellular stores (4), and thapsigargin (0.1-1 μM), which also releases Ca^{2+} from intracellularly stores and, in mitochondria, induces the permeability transition (5).

NH_4Cl (50 mM) abolished stretch-evoked firing in all preparations (n = 5; $P < 0.05$, paired *t*-test) within 20 min, indicating great importance of pH in some functional aspect. Caffeine resulted in a substantial inhibition in firing (1 mM, 63.5 ± 9.5 %, $P < 0.05$; & 10 mM, 42.9 ± 18.8 %, $P < 0.05$; n = 11. All data expressed as mean ± SEM). Finally, thapsigargin (0.1, 0.5 & 1.0 μM) tended to produce a dose-dependent decrease (to 48.8 ± 12.5 % at 1 μM) in firing but did not reach significance (n = 7; $P = 0.09$). All effects were at least partially reversible on drug washout.

In summary, these findings suggest that mitochondrial function significantly influences the capacity of primary afferent mechanosensory terminals to respond to physiological stimuli.

References 1. Zhang Q et al.(2021). Front Hum Neurosci. 15, 639871. 2. Banks RW et al. (2023). Proc Physiol Soc. 54, PCA082 3. Genders AJ et al. (2021). Physiol Rep. 9 e14797. 4. Usachev YM & Thayer SA. (1999) J Physiol. 519, 115–130. 5. Korge P & Weiss JN. (1999) Eur J Biochem. 265, 273–280.

PCA066

Suppressed Triose-phosphate isomerase activity affects synaptic vesicle dynamics and reduces Drosophila life span

Ælfwin Stone[1], Joern. R Steinert[1]

[1]*University of Nottingham, Nottingham, United Kingdom*

Neurodegeneration has been extensively linked to aberrant production of redox active molecules, e.g. nitric oxide (NO). One target of NO-mediated post-translational modifications, specifically 3-Nitrotyrosination, is the glycolytic enzyme triose-phosphate isomerase (TPI) which catalyses the conversion of dihydroxyacetone phosphate and glyceraldehyde-3-phosphate. In parallel, reported mutations within the TPI protein render it inactive and are also associated with neurodegenerative human disease, such as in TPI deficiency which is caused by a point mutation in the TPI gene.

In this work *Drosophila melanogaster* expressing mutant TPI (wstd[1], M80T, and I170V point mutations) were used as disease models *vs* wild-type controls (w^{1118} and Canton.S), to identify impacts of aberrant TPI function on neuronal physiology at excitatory glutamatergic neuromuscular junctions (NMJ).

Two-electrode voltage-clamp recordings were taken from third instar larvae fillets. Confocal images of larval NMJs and adult brains, labelled with HRP/BRP, and caspase/anti-AGE, were taken on a Zeiss LSM 880 confocal microscope to characterise active zones (BRP), bouton morphology (HRP), apoptosis (caspase), and advanced glycation end-products (AGE). Western blots were run as standard, longevity assays assessed daily survival.

Data is expressed as mean±SEM (n=no. of muscles/flies). Student's t-test and Log-rank (Mantel-Cox test) were used for comparisons with $p<0.05$ being significant.

Longevity was seen to be reduced in TPI mutants, median lifespans of 40 and 42 days in wstd[1] and M80T *vs* 60 and 68 days in w^{1118} and Canton.S respectively ($p<0.005$, N=145,165,146,139).

M80T showed slightly increased evoked amplitudes and Wstd1 showed significantly increased evoked amplitudes compared to Canton.S (88.12nA and 99.07nA vs 69.8nA). I170V showed significantly reduced amplitudes compared to w1118 (72.2nA vs 108.6nA).

None of the TPI mutants showed altered amplitudes of spontaneous events; 0.6787nA, 0.9194nA, 1.235nA for wstd[1], M80T, and I170V, 0.8132nA and 0.8656 for w1118 and Canton. S respectively. For evoked and spontaneous events $n\geq9$, $N\geq3$, $p<0.05$.

Quantal content was seen to be reduced in I170V in comparison to w1118 (68.2 vs 183), M80T showed no significant difference and in wstd1 quantal content was seen to be increased in comparison to Canton.S (80.26, and 167.3 vs 83.93).

Synaptic depletion following 50Hz train stimulations varied between lines, amplitudes were suppressed to 67±4%, 47±6%, 52±8%, and 54±9% for w^{1118}, $wstd^{1}$, M80T, and I170V respectively (n=11,11,5,4 N=≥3 $p<0.0001$).

Wsdt1 and M80T lines show significantly reduced expression of TPI protein, however the I170V line does not show this reduction in comparison to controls. Preliminary confocal data suggests higher levels of AGE and apoptosis in $wstd^{1}$ cf w^{1118}. The data suggests that the TPI-mutant phenotype is in part due to altered synaptic vesicle dynamics, possibly associated with vesicle pool organisation or endo/exocytosis. Supressed TPI activity also enhances protein glycation and redox stress, possibly contributing to the observed phenotypes. Both of these possibilities offer potential therapeutic routes to manage or treat disease.

Gnerer J., Kreber R., & Ganetzky B. (2006). PNAS, 103(41), 14987–14993. Hrizo S., Fisher I., Long D., Hutton J., Liu Z., & Palladino M. (2013). 54, 289–296. Roland B., Amrich C., Kammerer C., Stuchul K., Larsen S., Rode S., Aslam A., Heroux A., Wetzel R., VanDemark A., & Palladino M. (2015). 1852(1), 61–69. Stone Æ., Cujic O., Rowlett A., Aderhold S., Savage E., Graham B., & Steinert J. (2023). Front. Synaptic Neurosci., 15.

PCB001

Role of sex hormones in modulating cardiovascular responses to fructose and high salt diet: insights from Dahl salt-sensitive rats.

Muhammad Asad Akhtar[1], Stian Ludvigsen[2], Costantino Mancusi[3], ANNE DRAGØY HAFSTAD[1], Eva Gerdts[4], KIRSTI YTREHUS[1]

[1]Cardiovascular Research Group, UiT-The Arctic University of Norway, Tromsø., Tromsø, Norway, [2]Cardiovascular Research Group, UiT-The Arctic University of Norwat, Tromsø, Norway, [3]Dept of Advanced Biomedical Science, University of Naples Frederico II, Naples, Italy, Naples, Italy, [4]Dept of Clinical Science, University of Berge, Bergen, Norway, Bergen, Norway

Background: The prevalence of hypertension is rising alongside obesity rates. High-fructose corn syrup and high sodium intake are linked to metabolic disorders, cardiovascular morbidity, hypertension, aortic stiffness, and diastolic dysfunction. The sex-specific responses to these dietary factors and the role of sex hormones in salt-sensitive hypertension and fructose-induced cardiovascular dysfunction remain unclear.

Aim: The study aims to examine the impact of a fructose-rich diet, with or without high salt, on blood pressure regulation, cardiac function, and molecular remodelling in Dahl salt-sensitive (DSS) rats. Additionally, we explored the influence of sex hormones by comparing male, females with intact ovaries and ovariectomized (OVX) Dahl salt sensitive (DSS) rats.

Methods: The study utilized 60 female and 30 male DSS rats, aged 10 weeks, where 15 females underwent OVX before the diet intervention. The diet intervention groups were given chow with 6% NaCl and 10% fructose in drinking water for 9 weeks: male-NaCl (DSSM-NaCl), female-NaCl (DSSF-NaCl), and female OVX-NaCl (DSS-OVX-NaCl). Control groups received regular chow with 10% fructose water: male (DSSM), female (DSSF), ovariectomized female (DSS-OVX). LV assessment was conducted using echocardiography at baseline and at endpoint, using a short axis view (SAX) and M-mode imaging. Rats were euthanized for LV biopsies, and gene expression was analyzed using RT-qPCR. Echocardiography and gene data were analyzed using two-way ANOVA multiple comparison test. For ovariectomy and echocardiography, we used gaseous anaesthesia with isoflurane, (4% induction and 1.8 % maintenance).

Results. Ovariectomized rats gained more weight than intact females, but echocardiography showed no significant LV functional differences. However, LV mass and wall thickness increased in ovariectomized groups, especially with salt treatment. Males differed significantly in LV functional and morphological parameters from females.

When analyzing genes related to heart function in LV tissue, we found that beta myosin heavy chain mRNA expression levels were significantly upregulated in both OVX female groups (DSS-OVX and DSS-OVX-NaCl) compared to the DSSF group. Atrial natriuretic factor mRNA expression was upregulated in the DSS-OVX, DSS-OVX-NaCl and DSS-M-NaCl group compared to the DSSF group. Notably, brain natriuretic peptide mRNA expression level was significantly higher only in DSS-OVX-NaCl group.

In terms of genes related to fibrosis and inflammation, monocyte chemoattractant protein-1 mRNA expression was slightly elevated in salt treated female groups. Additionally, TIMP metalloproteinase inhibitor 1 mRNA expression were upregulated in the DSS-OVX-NaCl and DSS-M-NaCl group as compared to DSSF group. Interestingly, transforming growth factor β2 mRNA expression was significantly higher in DSS-OVX, DSS-OVX-NaCL and DSSM-NaCl groups.

Furthermore, genes encoded by the mitochondrial genome, such as mitochondrially encoded cytochrome C oxidase I and cytochrome b (subunit of complex III) MT-CYB exhibited changes in expression across all salt-treated groups compared to intact females. Peroxisome proliferator activated receptor coactivator 1 beta mRNA expression was significantly higher only in DSS-OVX-NaCl group.

Conclusion. Ovariectomy in female DSS rats leads to gene expression and cardiac morphology changes, intensified by salt. Males exhibit distinct cardiac responses, indicating sex hormones' role in cardiovascular outcomes. The study underscores the complex relationship between diet, sex hormones, and cardiovascular health in hypertension.

PCB002

The truth of air pollution. Does woodsmoke induce cardiac hypertrophy?

Raghad Al-Dulaymi[1], Andrew Trafford[1], Katharine Dibb[1], Aristeidis Voliotis[1], Gordon Mcfiggans[1]

[1]University of Manchester, Manchester, United Kingdom, [2]University of Manchester, Manchester, United Kingdom

The Truth of Air Pollution. Does Woodsmoke Induce Cardiac Hypertrophy?

Authors: Raghad Al-Dulaymi, Prof. Andrew Trafford, Dr. Katharine Dibb, Dr. Aristeidis Voliotis, Prof. Gordon Mcfiggans

Background:

Air pollution from indoor and outdoor sources is a global health problem and is predicted to cause millions of deaths annually. Previous studies demonstrated that short- and long-term exposure to woodsmoke emissions was associated with an increased risk of respiratory diseases. However, the evidence on the association between air pollution from woodsmoke and cardiovascular diseases is not conclusive. Cardiac hypertrophy has been recognised as an independent risk factor for adverse cardiovascular outcomes such as heart failure and sudden cardiac death. Previous evidence suggested the role of tadalafil, a phosphodiesterase 5 (PDE5) inhibitor, in protecting against cardiac hypertrophy in various animal studies.

Objectives:

For this stage of the project, our objective was to measure the effect of woodsmoke particles on the surface area of neonatal rat ventricular myocytes (NRVM) cells to detect any signs of hypertrophy.

Methods:

All experiments and procedures were conducted in accordance with the University of Manchester guidelines for animal care under the Animal (Scientific Procedures) Act 1986 (ASPA). Ethical approval for the work was obtained from the University of Manchester Animal Welfare and Ethical Review Board. Samples of woodsmoke were collected from a modern wood-burner based at the University of Manchester. Woodsmoke was collected from 2 phases of combustion: flaming and smouldering. Emission particles were immersed in cell maintenance media before cell exposure. NRVM were harvested from 1-2 days old Wister rats (Charles River). The effect of pollutants on the cell surface area (hypertrophy) was measured using fluorescent microscopic techniques and software analysis.

Results

Our results showed an increase in cell surface area in response to increasing pollutant concentrations. Incubation of cells with pollutants (from either the flaming or smouldering phases)

and a cardioprotective agent (tadalafil 50nM) was associated with a significantly smaller surface area compared to incubation with pollutants alone ($P<0.0001$). Moreover, incubation of the cells with pollutants first then with a combination of pollutants and PDE5 inhibitor reversed the hypertrophy for both the flaming and smouldering phase groups.

Conclusions:

Our data showed that woodsmoke-derived pollutants induced cardiac hypertrophy in NRVM in a dose-dependent manner. The cardiac hypertrophy could be prevented and reversed by an antihypertrophic agent 'tadalafil'. The next phase of the project will be dedicated to exploring the mechanism by which woodsmoke pollutants induce cardiac hypertrophy.

PCB003

DNA damage accumulation causes dystrophin deficiency in heart muscle

Daniel Brayson[1], Ehsan Ataei Ataabadi[2], Keivan Golshiri[3], Anton Roks[4]

[1]School of Life Sciences, University of Westminster, London, United Kingdom, [2]Department of Internal Medicine, Erasmus Medical Center,, Rotterdam, Netherlands, [3]Department of Internal Medicine, Erasmus Medical Center, Rotterdam, Netherlands, [4]Department of Internal Medicine, Erasmus Medical Center, Rotterdam, Netherlands

Introduction: DNA damage accumulation is a classical hallmark of ageing often culminating in replicative senescence. In cells such as cardiac myocytes, which do not replicate, downstream mechanisms resulting in functional decline are less well understood. The stochastic model of DNA damage accumulation states that long genes are more susceptible to DNA damage induced lesions than shorter genes. Dystrophin is large structural protein encoded by one of the longest genes in the genome, DMD. Loss of function mutations result in profound skeletal and cardiac muscle disease and age-related reductions in protein have been observed. Therefore, we hypothesised that DNA damage would confer a loss of dystrophin in cardiac muscle.

Methods: In line with local regulations regarding the use of animals in research we dissected cardiac tissues from 3 male and 3 female 17-week old Ercc1Δ/- mice, a well-established model to investigate the pathophysiological effects of DNA damage in vivo. We used an antibody directed to the C-terminus of the dystrophin protein to perform Western blotting on these tissues and compared abundance with a panel of proteins from cardiac genes of short and medium lengths known to play an important role in cardiac physiology and health.

Results: We discovered that Ercc1Δ/- mouse hearts exhibited a substantial decline in protein abundance of the 427kDa isoform of dystrophin in both male and females when compared with wildtype littermate controls ($P<0.05$, Mann-Whitney U test). Modest reductions were also observed in proteins of cardiac genes, these however, were not found to be statistically significant.

Conclusion: Our preliminary investigation supports the hypothesis that dystrophin abundance is highly susceptible to DNA damage. Future research will seek to understand the precise DNA/RNA signatures leading to dystrophin deficiency, how these can be measured in humans and how important this mechanism is to functional outcomes in ageing.

PCB004

Disturbed cardiac circadian rhythm in diabetes: autonomic contributions

Connor J Leadley[2], Shivani Sethi[2], Roseanna A Smither[2], Grace W Belworthy[2], Colin H Brown[2], Regis R Lamberts[2], Carol T Bussey[2,3]

[1]Manaaki Manawa Centre for Heart Research, Department of Physiology, Faculty of Medical and Health Sciences, University of Auckland, Auckland, New Zealand, [2]Department of Physiology and HeartOtago, School of Biomedical Sciences, University of Otago, Dunedin, New Zealand, [3]Manaaki Manawa Centre for Heart Research, Department of Physiology, Faculty of Medical and Health Sciences, University of Auckland, Auckland, New Zealand

Introduction: The healthy heart displays a circadian rhythm in which heart rate and blood pressure decrease overnight. However, this rhythm is blunted, absent or even reversed in the diabetic heart, which is a crucial risk factor for the development of cardiovascular disease. The origin of the circadian rhythm in the heart and its dysregulation, has not yet been fully elucidated, but changes in autonomic neural control have been implicated.

Objective: Determine changes in circadian cardiac autonomic responsiveness in diabetes.

Methods: We investigated autonomic regulation in 20-week old male Zucker type 2 Diabetic Fatty rats (DM) and their non-diabetic littermates (ND) at two timepoints, the start of the inactive and the active period (Zeitgeber times 3 and 15, respectively). Autonomic responsiveness (noradrenaline 0.5µM, acetylcholine 1µM) was assessed in the Langendorff-perfused isolated heart preparation, following pentobarbital anaesthesia (80mg/kg i.p.) (2-way RM ANOVA). Sinoatrial node (SAN) and left ventricle were dissected from naïve ND and DM ZDF for assessment of protein expression via Western Blot (2-way ANOVA). Brains, post-fixed in paraformaldehyde (4%), were immunostained for quantification of activated sympathetic cells (c-fos and tyrosine-hydroxylase co-expression) (2-way ANOVA). Data are presented as mean±SEM.

Results: We observed diurnal variation in cardiac sympathetic responsiveness (noradrenaline; ΔDevP ND: ZT3 25.7±13.4, ZT15 32.6±11.9; DM: ZT3 6.3±10.1, ZT15 32.5±7.9 ΔmmHg, n=8-9, $p<0.05$). Conversely, lower parasympathetic responsiveness was associated with diabetes (acetylcholine; ΔHR ND: ZT3 -93.5±21.6, ZT15 -88.0±15.4; DM: ZT3 -66.4±11.5, ZT15 -72.3±13.5 Δbpm, n=4-10, $p<0.05$). While no significant difference in the expression of cardiac beta-adrenergic (β_1, β_2) or muscarinic (M_2) autonomic receptors was found, circadian rhythms were observed in the expression of calcium handling proteins (SERCA2a, PLB), which were higher during the active period (ZT15). CLOCK protein levels were also lower in the SAN in DM (ND: ZT3 0.5±0.1, ZT15 0.6±0.1; DM: ZT3 0.4±0.1, ZT15 0.3±0.02, n=5-6, $p<0.05$). Activation of sympathetic cells was higher in DM in the nucleus tractus solitarius ($p<0.001$), and significantly higher both in DM and during the active period (ZT15) in the rostral ventrolateral medulla ($p<0.001$).

Conclusions: Physiological circadian signalling was primarily associated with sympathetic regulation, while we uncover changes in parasympathetic responsiveness in diabetes that might signal an underestimated therapeutic target. Increased activation of sympathoregulatory brain

regions might contribute to sympathetic overactivation as well as disrupted circadian rhythms in diabetes.

PCB005

Systolic and diastolic shear stress and endothelial cell orientation and polarity in mouse common carotid artery

Nabil Nicolas[1], Clémence Caillaud[1], Alexandre de Tilly[3], Etienne Roux[1]

[1]Univ. Bordeaux, INSERM, Biologie des maladies cardiovasculaires, U1034, Pessac, France, [2]Univ. Bordeaux, INSERM, Biologie des maladies cardiovasculaires, U1034, Pessac, France, [3]Hemovis, Fontenay-sous-Bois, France

Blood flow produces fluid shear stress (SS), a frictional force parallel to the blood flow, on the endothelial cell (EC) layer of the lumen of the vessels. ECs themselves are sensitive to this SS in terms of directionality and intensity. The aim of this study was to determine the physiological SS value during the cardiac cycle and EC polarity and orientation from blood flow in healthy male and female mouse carotid artery. All procedures were done according to current national and European legislation, and agreed upon by the local ethical committee. Experiments were performed on 8 male and 8 female 8-week-old C5BL/6J mice. Measurements of maximum blood velocity and vessel diameter in diastole and systole of the right common carotid artery were performed in vivo by Doppler ultrasound imaging on isoflurane-anesthetized mice. Blood samples were then collected for determination of plasmatic and total blood viscosity and hematocrit, using a newly developed device [1]. After animal euthanasia, the right common carotid was dissected for confocal imaging after labeling the EC nucleus and Golgi apparatus. Diastolic and systolic SS values were calculated from maximal velocity, vessel diameter, and viscosity values applying a newly developed method assuming heterogeneous blood flow, i.e., a red cell central plug flow surrounded by a peripheral plasma sheath flow, initially evidenced by Fahraeus [2] (F-method), compared with the classical method considering total blood as a “Newtonian” homogenous fluid with constant viscosity (N-method) [3]. F- and N-methods differed in blood velocity profile (including hematocrit in the F-method) and viscosity values, plasmatic and total, respectively. EC orientation was defined as the angle of the nucleus-Golgi apparatus vector to the blood flow direction, classified as dromic [0;60°], antidromic [120°;180°], and lateral [60°;120°], and compared to random distribution. EC polarity was defined by the length of this vector and nucleus elongation (long/short axis ratio). Statistical comparisons were done using Mann-Whitney and Chi^2 tests when appropriate and considered significant for $P<0.05$. Total blood and plasmatic viscosity were 4±0.5 cP and 1.27 cP, respectively. Diastolic and systolic SS, calculated by F-method, were 6±2.5 Pa and 30±6.5 Pa, respectively. Diastolic and systolic SS, calculated by the N-method, were, respectively, 6% and 14% higher than by the F-method. Total blood and plasmatic viscosity were 4±0.5 cP and 1.27 cP, respectively (table 1). ECs were significantly oriented against blood flow but not polarized. No sex difference was identified, whatever the parameters. Our results showed that both methods, though based on different theoretical assumptions, were convergent in their SS calculated values. However, the F-method seems more accurate since it considers the hematocrit value whereas the N-method does not. The cardiac cycle is characterized by high rate and amplitude changes in WSS values and ECs are sensitive to the direction of the blood flow, without sex difference.

1. de Tilly A et al. (2023). Measurement system for a liquid (WO2023111614A1). Available at : https://patents.google.com/patent/WO2023111614A1/en?q=(tilly+jouenne)&oq=tilly+jouenne. 2. Fåhraeus R (1929). Physiological Reviews 9, 241–274. 3. Roux E et al. (2020). Front Physiol 11, 861.

PCB006

Associations between accelerometry and echocardiographic measurements in individuals with hypertrophic cardiomyopathy

Katie Cooper[2], Christopher Eggett[1,2], Peter Luke[1,2], Alasdair Blain[2], Nduka Okwose[1,2,3], Amy Fuller[1,2,3], Alaa Alyahya[1,2], Kristian Bailey[1], Guy MacGowan[1,4], Djordje Jakovljevic[1,2,3], Sarah Charman[1,2]

[1]Newcastle upon Tyne Hospitals NHS Foundation Trust, Newcastle Upon Tyne, United Kingdom, [2]Translational and Clinical Research Institute, Faculty of Medical Sciences, Newcastle University, Newcastle Upon Tyne, United Kingdom, [3]Faculty of Health and Life Sciences, Coventry University, and University Hospitals Coventry and Warwickshire NHS Trust, Coventry, United Kingdom, [4]Biosciences Institute, Newcastle University, Newcastle Upon Tyne, United Kingdom

Background: Physical activity is recommended to individuals with hypertrophic cardiomyopathy (HCM) as a management option to reduce disease burden. However, over 50% of individuals with HCM are not meeting the recommended physical activity guidelines. Beta-blockers (BB) are prescribed to individuals with HCM to aid symptom management, but the effects on physical activity are relatively unknown. The aim of this study was to investigate the associations between accelerometry and echocardiographic measurements in individuals with HCM. Data described as median unless otherwise stated.

Methods: Twenty-one individuals with HCM (males, n=15, age (mean±SD) 52±15 years old, body mass index (BMI) 29 (25-31) kg/m^2, prescribed BB, n=11, left atrial volume index (LAVI) 32 (30-35) mL/m^2 and stroke volume (SV) 55 (44-65) mL) had accelerometry and echocardiographic measurements recorded. Accelerometry categories were measured over 7 days using wrist-worn accelerometers (GENEActiv, ActivInsights Ltd., United Kingdom). Echocardiographic measures were taken in the rest-supine position and included LAVI and SV.

Results: In individuals with HCM, time spent in 1 to 5 minute bouts of light intensity physical activity was positively correlated with LAVI (r=0.55, p<0.01). However, time spent in 1 to 5 minute bouts of light physical activity was negatively correlated with SV (r=-0.50, p<0.05). A positive trend was found between time spent in 10 minute bouts of moderate to vigorous physical activity and SV (r=0.20, p=0.44). The same trends applied for those prescribed BB versus those who were not.

Conclusion: In individuals with HCM, our findings highlight that there are associations between light and moderate to vigorous physical activity and cardiac structure and function that requires further explorations.

PCB007

Hypoxia Inducible Factor Signalling Pathway in a Neuronal PC12 Cell-Line Deprived from Oxygen (1% O2) and Glucose

Rebecca Edwards[1]

[1]*Keele University, Newcastle-under-Lyme, United Kingdom*

Introduction: Vascular cognitive impairment (VCI) is the second most prevalent for of dementia and is associated with reduced cerebral blood flow. We know this causes hypoxia inducible factor (HIF) expression and harnessing this could represent a new therapeutic target for VCI. Prolyl-hydroxylase domains (PHD) increase HIF expression; DMOG and FG4592 are PHD inhibitors. We aim to characterise additional mechanisms of action.

Methods: Neuronal cell-line rat pheochromocytoma (PC12 cells) were cultured with D5H5B media at 37˚ C with 21% O_2 and 5% CO_2. DMOG, FG4592 (100uM) or 1% DMSO (vehicle) was added across four oxygenation conditions: 21% O_2, 21% O_2 and glucose deprivation (GD), 1% O_2, and 1% O_2 glucose deprivation (OGD) for a duration of 6 or 24-hours. Each experiment consisted of three biological and three technical replicates. 3-(4, 5-dimethylthiazolyl-2)-2,5-diphenyltetrazolium bromine (MTT) and lactate-dehydrogenase (LDH) assays were carried out to determine energy production and cytotoxicity. HIF-1α and HIF-2α protein levels were examined by Western immunoblotting while HIF-1α and PHD2 RNA expression was also analysed via q-PCR.

Results: Relative HIF1α RNA expression was increased following oxygen deprivation, and this was exacerbated with OGD at 6-hours but was not observed at 24-hours (Figure 1A). Interestingly, PHD2 RNA expression was only increased with OGD exposure at 6-hours, but the inverse was observed at 24-hours exposure (Figure 1B), though high variability was observed with the OGD group.

As expected, under typical oxygenation conditions at 24-hours HIF-1α protein expression was low, but it only slightly increased when oxygen was withdrawn. Expression levels increased dramatically during OGD and the same was true under vehicle conditions and with DMOG. However, there was an increase in expression when oxygen was withdrawn and FG4992 was provided (Figure 2A).

Decreased metabolic activity is presented across all OGD exposures when compared to 1% O_2, thus highlighting the role of glucose in cellular metabolism (Figure 3). Paired with LDH release to assess cytotoxicity, an increase in cytotoxicity is observed in GD exposed cells with FG4592 administration (Figure 4).

Conclusions: HIF signalling increases following OGD exposure due to PHD inactivation, thus limiting HIF degradation and increasing its abundance. With the inhibition of PHD by DMOG administration, we see a further increase in OGD HIF abundance, thus supporting the role of DMOG in HIF therapeutics. Regarding PHD2 expression at an RNA level, it is possible that a negative feedback-loop is in play by which increased HIF-1α expression causes a further increase in PHD2 expression to counteract this signalling alteration. The pathway by which DMSO causes increased HIF signalling remains unclear but poses useful insights for future research.

Deoxygenation causes PHD expression downregulation to therefore allow the activation of HIF, which aligns with these results. When paired with FG4592, we see further increase in HIF signalling as this increases the deregulatory effects of PHD inactivation to form a summative HIF abundance response. Further research is required to understand the precise mechanisms at play for the signalling pathways of DMOG and FG4592. Furthermore, western immunoblotting for HIF 6-hour exposures and PHD2 will be carried out and paired with q-PCR data for HIF-2α.

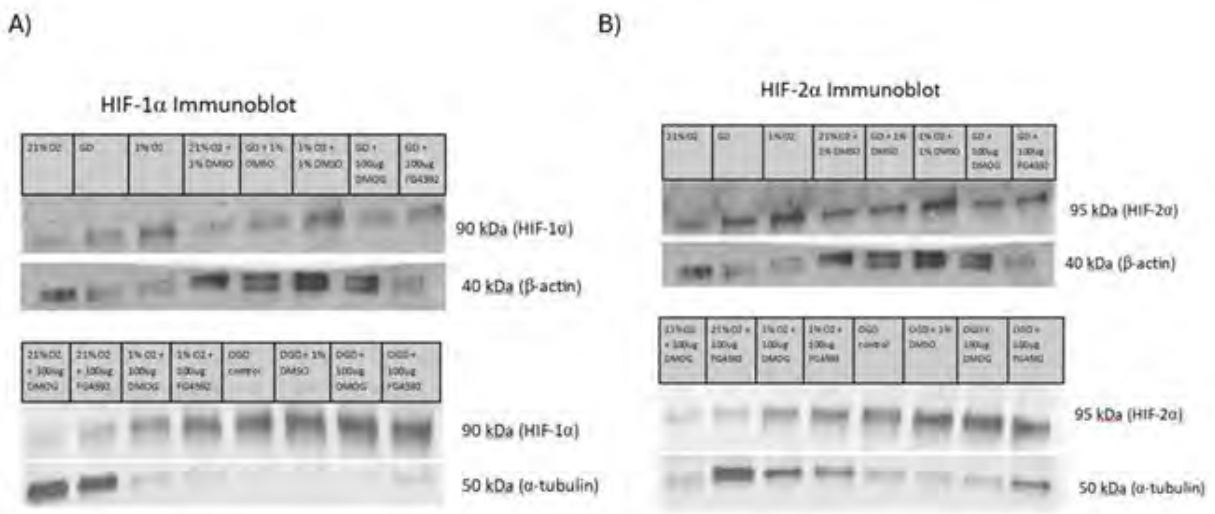

Figure 5: Western immunoblotting layout and raw data for HIF-1α and HIF-2α proteins.

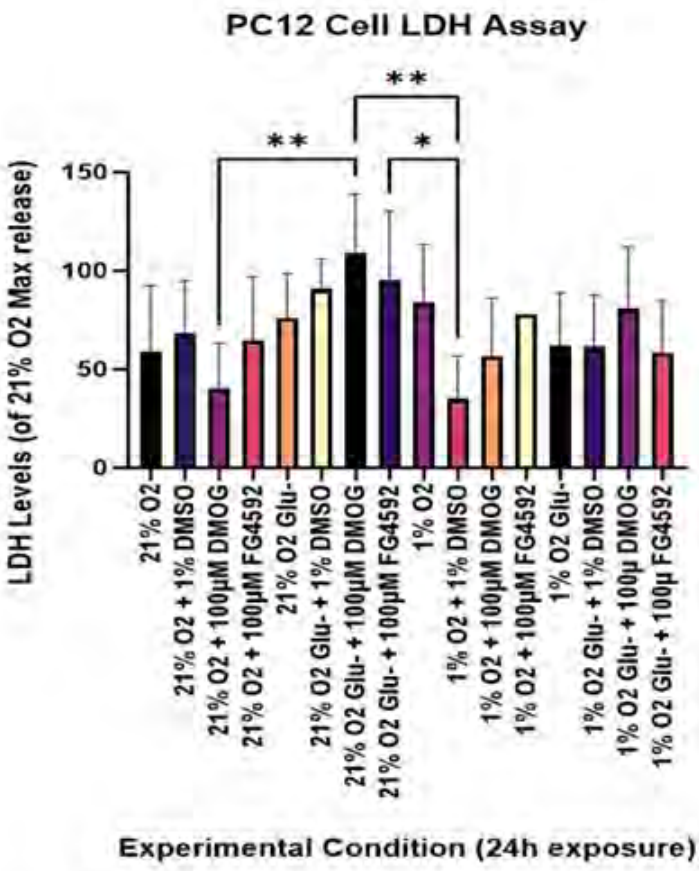

Figure 4: LDH Assay of PC12 cells across 4 oxygenation states and drug/vehicle exposures for 24 hours. Statistical analysis was conducted using a one-way ANOVA where * indicates $p<0.05$ and ** indicates $p<0.01$, lack of * suggests no significance.

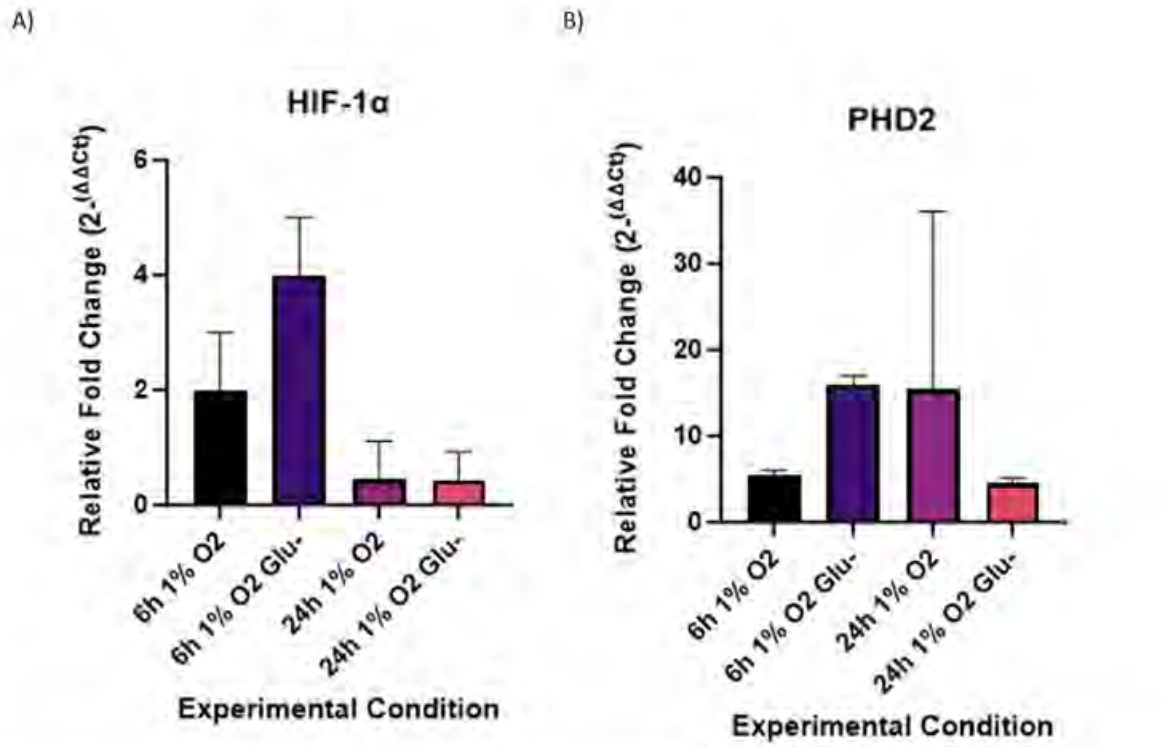

Figure 1: q-PCR analysis of HIF-1α (A) and PHD2 (B) following differential durations of oxygen deprivation and oxygen-glucose deprivation (n=3 each).

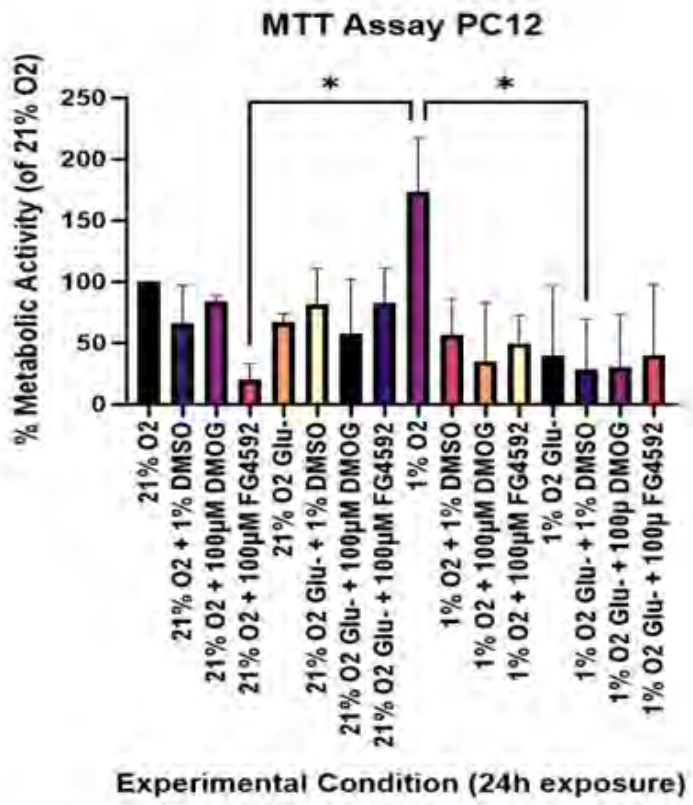

Figure 3: MTT Assay of PC12 cells across 4 oxygenation states and drug/vehicle exposures for 24 hours. Statistical analysis was conducted using a one-way ANOVA where * indicates $p<0.05$, lack of * suggests no significance.

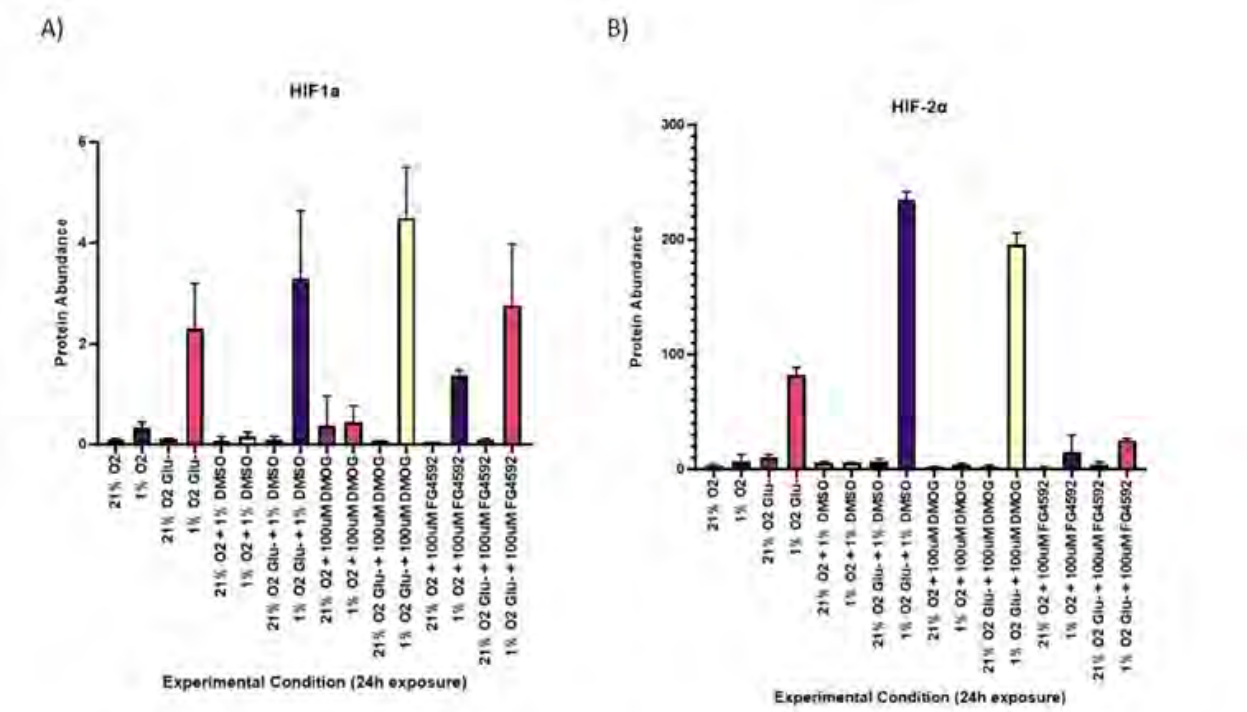

Figure 2: Western blot analysis of HIF-1α (A) and HIF-2α (B) following 24-hours of exposure with PHD inhibitors, DMOG, FG4592 or vehicle (n=3 each). Analysis was conducted on PC12 cells following 24 hour exposures.

1) Linton, A.E., Weekman, E.M. and Wilcock, D.M. (2021) 'Pathologic sequelae of vascular cognitive impairment and dementia sheds light on potential targets for intervention', Cerebral Circulation - Cognition and Behavior, 2 Available at: https://doi.org/10.1016/j.cccb.2021.100030. 2) Zhou, M., Hou, J., Li, Y., Mou, S., Wang, Z., Horch, R.E., Sun, J. and Yuan, Q. (2019) 'The pro-angiogenic role of hypoxia inducible factor stabilizer FG-4592 and its application in an in vivo tissue engineering chamber model', Scientific reports, 9(1), pp. 6035-5 Available at: https://doi.org/10.1038/s41598-019-41924-5.

PCB008

Hypoxia increases blood pressure variability and impairs arterial baroreflex sensitivity in middle-aged hypertensive men

Ojikutu Qudus[1], Jeann Sabino-Carvalho[2], Katherine Latham[1], Igor A Fernandes[1]

[1]Purdue University, West Lafayette, United States, [2]Emory University, Atlanta, United States

Introduction: Sleep apnea-induced acute hypoxia and arterial oxygen desaturation are common phenotypes in arterial hypertension. While the transient hypoxic insult alone does not consistently elevate blood pressure, it does trigger exaggerated increases in muscle sympathetic activity (MSNA) among hypertensive individuals. Elevated resting MSNA levels correlate with greater blood pressure variability (BPV), an index associated with an increased likelihood of target organ damage regardless of absolute blood pressure levels**. Hypothesis:** We hypothesized that transient hypoxic insults would provoke exaggerated increases in BPV among hypertensive individuals. Additionally, hypoxia is known to reset the arterial baroreflex operating point to higher pressures. We also theorize that exaggerated increases in BPV will be followed by reduced sensitivity of the spontaneous cardiac and sympathetic arms of the baroreflex. **Methods:** Eight 1-2 stage naive hypertensive (HT– 43 ± 12 yrs.) and normotensive (NT – 40 ± 11 yrs.) men were exposed to 5-minute bouts of (1) normoxia (21% O_2) and (2) isocapnic-hypoxia (10% O_2). Oxygen saturation (pulse oximetry), beat-to-beat BP (photoplethysmography), MSNA (Microneurography), and partial pressure of end-tidal carbon dioxide ($PETCO_2$) were monitored throughout the study. $PETCO_2$ clamp was performed through a rebreathing system. We calculated the standard deviation (SD), average real variability (ARV), and other indices of BPV. Spontaneous cardiac baroreflex was assessed via the sequence technique and cardiac autonomic modulation through time- and frequency-domain HR variability. The sensitivity (gain) of the sympathetic baroreflex was determined via weighted linear regression analysis between MSNA and diastolic BP. **Results:** Independent T-tests indicated that both experimental groups showed similar reductions in oxygen saturation in response to isocapnic-hypoxia (NT −25.7 ± 3.3 vs. HT −21.2 ± 4.0%, $p > 0.05$). There were no substantial changes in BP absolute levels and PETCO2 during isocapnic hypoxia. MSNA recordings revealed greater increases in sympathetic activation of hypertensive individuals (HT +12.7 ± 6.7 vs. NT +3.6 ± 1.6 bursts/min, $p = 0.012$). Isocapnic-hypoxia similarly increased BPV (HT SD: +4.7 ± 1.6 versus NT +7.6 ± 4.4 mmHg, $P = 0.006$; HT +2.9 ± 1.0 versus NT +4.7 ± 1.9 mmHg, $P = 0.001$; HT +3.3 ± 1.1 versus NT +5.4 ± 2.7 mmHg, $P = 0.002$, for systolic, diastolic and mean BP, respectively) in both hypertensive and normotensive individuals. Other traditional measures of variability showed similar results. Isocapnic-hypoxia provoked similar reductions in cardiac and sympathetic baroreflex gain in both groups. **Conclusion:** In summary, isocapnic hypoxia increases blood pressure variability and reduces both cardiac and sympathetic baroreflex sensitivity in normotensive and hypertensive men.

PCB009

The effects of fetal hypoxia on arrhythmia sensitivity in catecholaminergic polymorphic ventricular tachycardia mouse model

Zarin Tasnim Gias[1], Luigi Venetucci[1], Gina Galli[1]

[1]Division of Cardiovascular Sciences, School of Medical Sciences, University of Manchester, Manchester, M13 9NT, United Kingdom

INTRODUCTION: Catecholaminergic polymorphic ventricular tachycardia (CPVT) is an inherited arrhythmic condition defined by episodic syncope that occurs during intense emotion or exercise. CPVT is usually caused by mutations in the cardiac ryanodine receptor (RyR2) gene, and while some patients remain asymptomatic into adulthood, others develop the disease during childhood, which suggests environmental factors can influence disease progression. However, to our knowledge, no one has considered the role of the maternal environment in programming CPVT outcomes. Recent data from our laboratory suggests that ventricular arrhythmia sensitivity can be programmed during fetal development by exposure to hypoxia. Therefore, we hypothesised that fetal hypoxia increases disease severity in individuals with a CPVT mutation.

METHOD: RyR2-R2474S knock-in male mice were bred with wild-type C57BL/6NRj female mice. Pregnant mice were either subjected to normoxic (21% O_2, n = 10) or hypoxic (13% O_2, n = 5) conditions from gestational day (GD) 6-18. From this experimental design, four groups were established - (1) Wild Type Normoxia (WT-N), (2) RyR2 normoxia (RyR2-N), (3) Wild Type Hypoxia (WT-H) and (4) RyR2 Hypoxia (RyR2-H). Maternal weight, food and water intake were monitored during the incubations, as well as offspring litter size, sex split and body weight from birth to 16 weeks. Ventricular electrical mapping was used to investigate offspring arrhythmia sensitivity at 16 weeks using programmed electrical stimulation.

RESULT: There were no significant differences in maternal body weight, food intake or water intake between the normoxic and hypoxic offspring. Furthermore, no significant relationship was found between litter size, sex split, individual offspring body weight, and litter weight between the experimental groups. The initial data suggests that fetal hypoxia and CPVT mutation both increase the likelihood of arrhythmia under programmed electrical stimulation, but there was no significant interaction between these factors.

CONCLUSION: At this preliminary stage, we show that hypoxia had no significant effect on maternal and fetal parameters in either wild-type or CPVT mutants, suggesting no overt morphological effects of either treatment. The electrical mapping showed that arrhythmia sensitivity is increased by fetal hypoxia or CPVT mutation, but no interaction was observed between these factors. However, data should be interpreted cautiously because of a low sample size (n = 4-7 offspring). Therefore, future work will increase the sample size to fully ascertain whether exposure to fetal hypoxia can influence cardiovascular outcomes in CPVT mutants.

PCB011

Peripheral vascular adaptations to high-intensity interval training in patients with COPD

Jacob Peter Hartmann[1,2,3], Stine Nymand[1], Helene Louise Hartmeyer[1], Camilla Ryrsø[1,2], Milan Mohammad[1], Iben Rasmussen[1], Amalie Bach Andersen[1], Rie Skovly Thomsen[1], Jann Mortensen[3], Ronan Martin Griffin Berg[1,2,3,4], Ulrik Winning Iepsen[1,5]

[1]Centre for Physical Activity Research, Copenhagen University Hospital – Rigshospitalet, Copenhagen, Denmark, [2]Department of Biomedical Sciences, Faculty of Health and Medical Sciences, University of Copenhagen, Copenhagen, Denmark, [3]Department of Clinical Physiology and Nuclear Medicine, Copenhagen University Hospital – Rigshospitalet, Copenhagen, Denmark, [4]Neurovascular Research Laboratory, Faculty of Life Sciences and Education, University of South Wales, Pontypridd, United Kingdom, [5]Department of Anaesthesiology and Intensive Care, Copenhagen University Hospital, Hvidovre Hospital, Copenhagen, Denmark

Aim: Patients with chronic obstructive pulmonary disease (COPD) exhibit markedly diminished exercise capacity, particularly in advanced stages, hindering their ability to perform routine activities of daily living. Previous studies have shown that skeletal muscle convective and diffusive O_2 transport mechanisms play pivotal roles as peripheral determinants of exercise capacity in COPD (1, 2). This study aims to investigate whether a 12w high-intensity interval training (HIIT) intervention could reverse some of the peripheral alterations observed in patients with COPD when compared to healthy, matched controls.

Methods: Eight patients diagnosed with mild to severe COPD and eight healthy controls, untrained, matched for age, sex, and BMI, participated in this study. Baseline assessments were conducted, and the COPD patients followed by a 12-week HIIT intervention, which consisted of three weekly sessions, each comprising a 40-minute 4x4 HIIT protocol on a bicycle ergometer. Leg blood flow ($\dot{Q}_{leg}$) was assessed using Doppler ultrasound during submaximal single-leg knee-extensor exercise (KEE), with arterio-venous variables sampled across the leg. Reconstruction of the capillary oxyhaemoglobin dissociation curve was performed utilizing paired femoral arterial-venous O_2 tensions and saturations for the assessment of microvascular oxygenation, including skeletal muscle O_2 conductance ($D_{sm}O2$) and its correction for flow ($D_{sm}O_2/\dot{Q}_{leg}$) to differentiate convective from diffusive O_2 transport.

Results: The COPD and control group were similar in height, sex, and BMI, but the COPD group had more pack years (p=0.0001) as well as a lower FEV_1 (p=0.002) and diffusion capacity (p=0.008). While resting values were similar, COPD patients had a higher $D_{sm}O2/\dot{Q}_{leg}$, but a lower $\dot{Q}_{leg}$ during KEE **(Figure 1).** After the HIIT intervention in COPD patients, the $\dot{Q}_{leg}$ increase to KEE became more pronounced (428; 156 to 811 mL/min, p=0.01), but with similar O_2 extraction and arterio-venous difference levels compared to pre-intervention (p=0.43). This led to a significantly higher $D_{sm}O2$ to KEE compared to pre-intervention (0.65; 0.16 to1.12 (mmol/min)/kPa), p=0.01)), but with a similar change in $D_{sm}O2/\dot{Q}_{leg}$ (0.02; -0.18 to 0.13 (mM/kPa), p=0.7) **(Figure 1).**

Conclusion: The diminished convective O_2 transport response observed in working muscle of COPD patients can be enhanced by a 12-week HIIT intervention, so that it becomes similar to that of healthy untrained individuals without COPD. In contrast, the skeletal muscle diffusive O_2 transport response in working muscle appears to be unaffected by the intervention, indicating limited skeletal muscle microvascular adaptations in COPD.

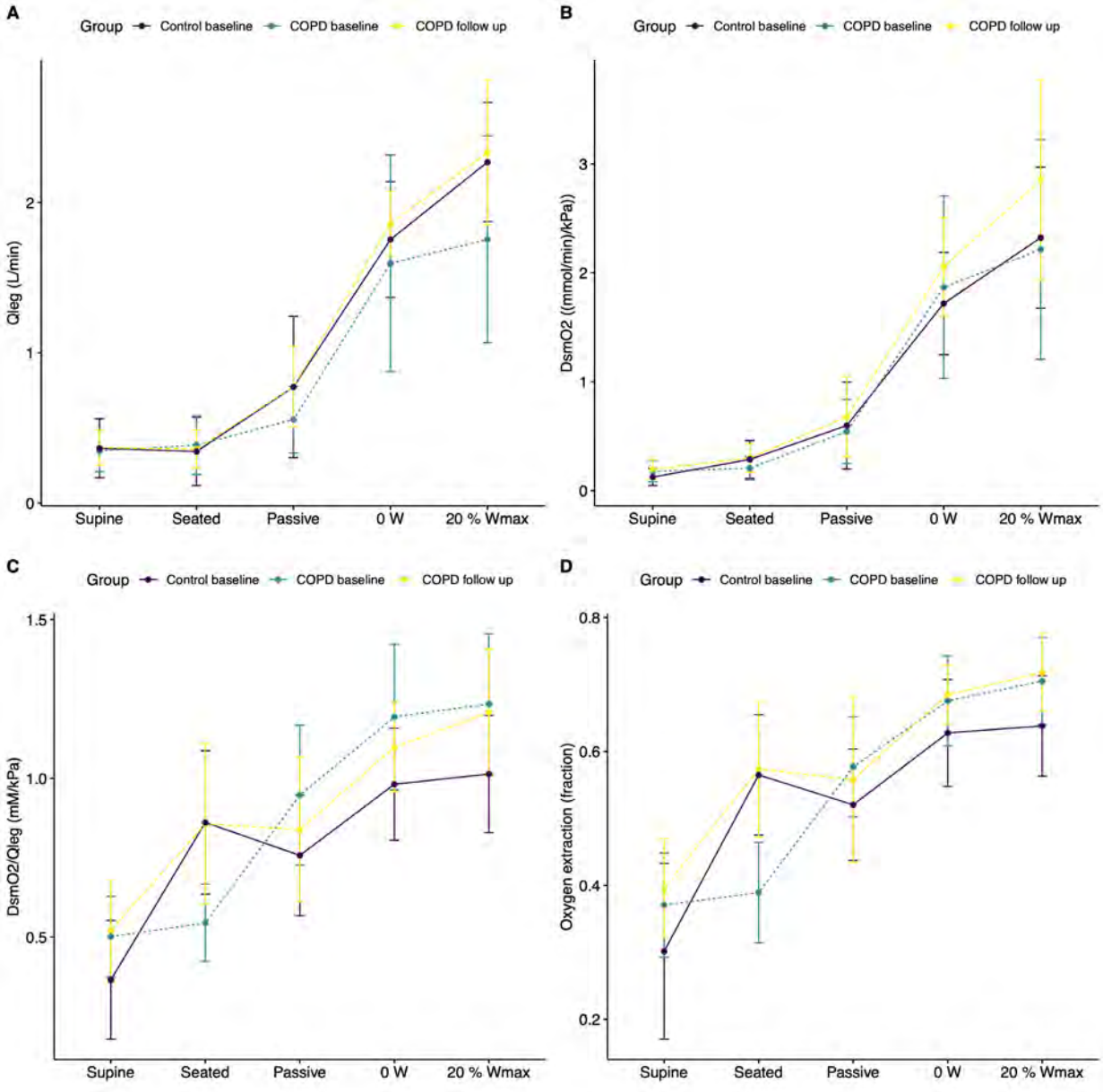

1. Hartmann JP, Dahl RH, Nymand S, Munch GW, Ryrsø CK, Pedersen BK, Thaning P, Mortensen SP, Berg RMG, Iepsen UW. Regulation of the microvasculature during small muscle mass exercise in chronic obstructive pulmonary disease vs. chronic heart failure. Front Physiol 13, 2022. doi: 10.3389/fphys.2022.979359. 2. Broxterman RM, Wagner PD, Richardson RS. Exercise training in COPD: Muscle O2 transport plasticity. European Respiratory Journal 58, 2021. doi: 10.1183/13993003.04146-2020.

PCB012

Circadian rhythms in the electrophysiology and pro-arrhythmic activity of pulmonary vein cardiomyocytes

Andrew F. James[1], Laura M.K. Pannell[1], Alexander Carpenter[1], Francisca Segers[2], Yi Zhe Koh[1], Stephen C. Harmer[1], Hugh D. Piggins[1], Jules C. Hancox[1]

[1]School of Physiology, Pharmacology & Neuroscience, University of Bristol, Bristol, BS8 1TD, United Kingdom, [2]Bristol Genomics Facility, School of Biological Sciences, University of Bristol, Bristol, BS8 1TQ, United Kingdom

Episodes of atrial fibrillation (AF) in patients are more prevalent at night, and cardiomyocytes in the pulmonary vein (PV) sleeves are a major source of ectopic activity driving AF. While it is known that circadian clocks within heart muscle cells contribute to the control of pacemaking and ventricular repolarisation, the mechanisms underlying the nighttime preponderance in AF are unknown. We aimed to address the hypothesis that circadian clocks exist within PV cardiomyocytes, controlling their electrophysiology and susceptibility to pro-arrhythmic activity. Animal procedures were approved by the University of Bristol Animal Welfare and Ethics Review Board and conducted in accordance with UK law. Male Wistar rats were maintained in a 24-hour cycle of 12-hr light/dark (lights-on at Zeitgeber time, ZT=0; lights-off, ZT12) and hearts were removed at ZT=0, 6, 12 or 18 hr under terminal general anaesthesia (140 mg/kg Na pentobarbital i.p.). RNA was extracted from left atrial (LA) appendage (LAA) and proximal PV at the LA/PV junction (3 rats per ZT) and RNA sequencing conducted. Reads were mapped to the rat genome, counts normalised and models in which ZT was or was not included as a factor compared (Likelihood Ratio Test, adjusted-$P<0.01$). Whole-cell current clamp recordings were made from cardiomyocytes isolated from the proximal PV (n=308) and the LAA (n=264) (N=74 rats). The effects of noradrenaline (NA, 1 μM) and acetylcholine (ACh, 1 μM) were examined. Data were plotted against the ZT of the time of recording and fitted to a sine wave to establish circadian rhythmicity ($P<0.05$, extra-sum-of-squares F-test). The effect of ≥24 hr constant dark in the period immediately before experiment was examined. Data are reported as mean ± standard error. The expression of 1368 genes varied significantly with ZT, including circadian clock components (e.g. *Bmal1*). PV cells were larger than LAA cells (73±1.6 pF vs 53±1.3 pF, $P<0.0001$) and had more depolarised resting membrane potential (-69±0.2 mV vs -72±0.1 mV, $P<0.0001$). Both cell types showed circadian variation in action potential duration at 90% repolarisation (APD_{90}) and frequency of pro-arrhythmic activity. Pro-arrhythmic activity was greatest in PV cells and the frequency was greater during the rest phase (ZT0-12) in both cell types. In contrast, the circadian rhythm in APD_{90} differed between cell type, with the longest APD_{90} recorded during the resting phase in PV cells (ZT12-24) but during the active phase in LAA cells. Pro-arrhythmic activity was increased by NA and decreased by ACh in both cell types, with the maximal effect of either neurotransmitter during the rest phase. Circadian variation in APD_{90} and proarrhythmic-activity has been demonstrated in isolated proximal PV and LAA cardiomyocytes, with differences in rhythm between the two cell types. RNA sequencing suggests the presence of peripheral clocks in LAA and PV cardiomyocytes. Understanding circadian rhythms in the pro-arrhythmic activity of PV cardiomyocytes is likely to be valuable in the development of future therapeutic options for AF.

PCB013

Doppler ultrasound-based leg blood flow assessments during single-leg knee-extensor exercise in patients with chronic obstructive pulmonary disease vs. healthy controls: a test-retest reliability study

Milan Mohammad[1,2,3], Jacob Hartmann[3,4], Amalie Andersen[4], Helene Hartmeyer[1], Ulrik Iepsen[1,5]

[1]Centre for Physical Activity Research, Copenhagen University Hospital – Rigshospitalet., Copenhagen, Denmark, [2]Department of Biomedical Sciences, Faculty of Health and Medical Sciences, University of Copenhagen., Copenhagen, Denmark, [3]Department of Clinical Physiology and Nuclear Medicine, Copenhagen University Hospital – Rigshospitalet., Copenhagen, Denmark, [4]Centre for Physical Activity Research, Copenhagen University Hospital – Rigshospitalet, Copenhagen, Denmark, Copenhagen, Denmark, [5]Department of Anaesthesiology and Intensive Care, Copenhagen University Hospital, Hvidovre Hospital, Copenhagen, Denmark

Introduction: Patients with chronic obstructive pulmonary disease (COPD) exhibit markedly diminished exercise capacity. Studies have shown that skeletal muscle leg blood flow ($\dot{Q}_{leg}$) plays an important role as a peripheral determinant of exercise capacity (1, 2). Doppler ultrasound may be used to assess $\dot{Q}_{leg}$ both at rest and during exercise. However, the reliability of this method remains unknown when applied to patients with chronic obstructive pulmonary disease (COPD).

Objectives: This study aimed to investigate the within-day and between-day reliability of Doppler ultrasound in quantifying $\dot{Q}_{leg}$ during single-leg knee-extensor exercise in COPD patients and compare these measurements with those obtained from healthy matched controls.

Methods: In this case-control study, 16 participants with COPD were matched based on sex and age with 16 healthy controls. All participants underwent measurement of $\dot{Q}_{leg}$ using Doppler ultrasound in a single-leg knee-extensor setup at various intensities on two separate visits (Figure 1). Influential factors on $\dot{Q}_{leg}$ were controlled for, and the ultrasound scans were consistently performed by the same sonographer. The study was approved by the Regional Ethical Committee of the Capital Region of Denmark (file no. H-23049997) and performed according to the most recent guidelines of the Declaration of Helsinki. All participants provided oral and written informed consent prior to enrolment. The study was registered on ClinicalTrials.gov (ID: NCT06135701).

Results: Results indicated a high within-day and acceptable to high between-day reliability for Doppler ultrasound measurements in both COPD patients and controls. Coefficient of variance ranged from 2.9 % to 10 % for within-day and 7.9 % to 20.4 % for between-day with small between-group differences in reliability estimates favouring the healthy control group. $\dot{Q}_{leg}$ was similar between group at rest, but significantly lower in COPD during single-leg knee-extensor exercise.

Conclusion: Doppler ultrasound is a reliable tool for evaluating $\dot{Q}_{leg}$ in both COPD patients and healthy individuals. Furthermore, the findings of this study offer novel insights into the peripheral circulatory constraints experienced by COPD patients during exercise, as evidenced by consistently diminished leg blood flow when compared to their healthy control.

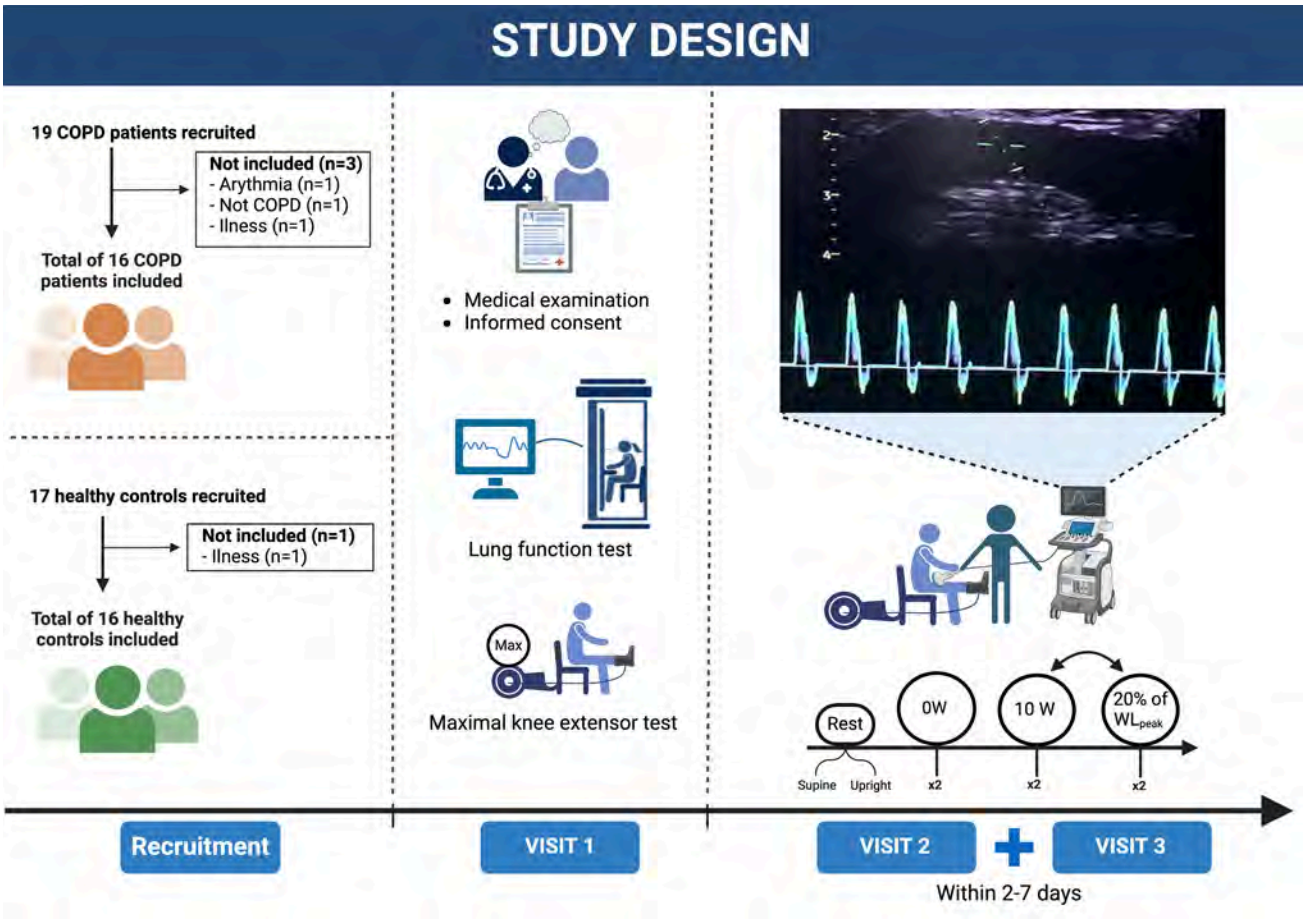

1. Hartmann JP, Dahl RH, Nymand S, Munch GW, Ryrsø CK, Pedersen BK, Thaning P, Mortensen SP, Berg RMG, Iepsen UW. Regulation of the microvasculature during small muscle mass exercise in chronic obstructive pulmonary disease vs. chronic heart failure. Front Physiol 13, 2022. doi: 10.3389/fphys.2022.979359. 2. Broxterman RM, Wagner PD, Richardson RS. Exercise training in COPD: Muscle O2 transport plasticity. European Respiratory Journal 58, 2021. doi: 10.1183/13993003.04146-2020.

PCB014

Impact of Air Pollution on the Cardiohepatic Transcriptome and Inflammation

Joseph Morris[1], Holly Shiels[1]

[1]*University of Manchester, Manchester, United Kingdom*

Air pollution is responsible for around 7 million deaths per year, with around half of these attributable to cardiovascular conditions. Pollution modelling in Greater Manchester identified a 1.4% increased incidence of ischaemic heart disease per 1 ug/m3 increase in PM2.5 concentration. Cardiotoxic polyaromatic hydrocarbons like phenanthrene are frequently found adsorbed to the surface of this inhalable fraction of PM. However, the source and impact of phenanthrene-induced inflammation on this cardiovascular dysfunction is unknown. Mice were exposed to environmentally relevant concentrations (3 ug/kg or 30 ug/kg) of phenanthrene by intraperitoneal injection every day for 6 weeks. Single nucleus RNA sequencing was carried out on liver samples of 12 (n=4) male mice to identify changes in expression of pro/anti-inflammatory genes. Thirteen distinct cell populations were identified via UMAP clustering, including a population subset seen only in mice exposed to the high dose of phenanthrene. In this subset, pro-inflammatory genes like LCN, Syt12, TERC, CYP4a31 and APCS were significantly overexpressed by scores of 51.2, 28.8, 17.0, 15.8 and 15.7 respectively. Further RNA velocity analysis in the high dose phenanthrene group suggests rapid differentiation of ‘neutral’ cell types into inflammatory subsets. Initial cytokine panel analysis identified dose-dependent increases in plasma and liver of potent Th2-related cytokines like IL-16 and IL-33, although not significant. Together, these findings demonstrate the range of effects phenanthrene has on the immune system, and subsequently, the cardiovascular system.

PCB015

Capillary dysfunction is associated with impaired neurovascular coupling after ischemic stroke

Christian Staehr[1,2], John T. Giblin[1], Eugenio Gutiérrez-Jiménez[3], Halvor Ø. Guldbrandsen[2], Shaun L. Sandow[4], David A. Boas[1], Vladimir V. Matchkov[2]

[1]Neurophotonics Center, Dept. Biomedical Engineering, Boston University, Boston, United States, [2]Dept. Biomedicine, Aarhus University, Aarhus, Denmark, [3]CFIN, Aarhus University, Aarhus, Denmark, [4]Biomedical Science, School of Health, University of the Sunshine Coast, Sippy Downs, Australia

Introduction: Neurovascular coupling, as the local hyperemic response to neuronal activity, is impaired in peri-ischemic brain regions after stroke, with the mechanism being poorly understood. The mechanism is important for the control of brain blood flow, and its dysfunction after stroke, where reduced neurovascular coupling may contribute to futile reperfusion, as poor neurological outcome despite successful recanalization. Understanding these mechanisms is therefore critical for the development of targeted therapy.

Objective: The study aimed to assess neurovascular responses and capillary perfusion in the peri-ischemic area before stroke and after ischemia reperfusion. It was hypothesized that impaired neurovascular coupling in the peri-ischemic area is associated with disrupted capillary microcirculation.

Methods: Mice implanted with chronic cranial windows were trained for awake head-fixation prior to experiments. One-hour occlusion of the anterior middle cerebral artery branch was induced using single vessel photothrombosis. Cerebral perfusion and neurovascular coupling were assessed by optical coherence tomography and laser speckle contrast imaging. Capillaries and pericytes were studied in perfusion-fixed tissue by labelling lectin and platelet-derived growth factor receptor β.

Results: Arterial occlusion induced on average 11 spreading depressions over one hour associated with substantially reduced blood flow in the peri-ischemic cortex. Approximately half of the capillaries in the peri-ischemic area were no longer perfused after reperfusion (45% [95% CI, 33%, 58%] and 53% [95% CI, 39%, 66%] reduction in number of perfused capillaries at 3- and 24-hour follow-up, respectively; $P < 0.0001$, $n = 6$), which was associated with a reduced diameter of capillaries surrounded by pericytes. The capillaries in the peri-ischemic cortex that remained perfused showed an increased prevalence of flow stalling (0.5% [95% CI, 0.2%, 0.7%] at baseline, 5.1% [95% CI, 3.2%, 6.5%] and 3.2% [95% CI, 1.1%, 5.3%] at 3- and 24-hour follow-up, respectively; $P < 0.001$, $n = 6$). Blood flow velocity in the capillaries that remained perfused was similar to baseline at the 3-hour follow-up but increased at the 24-hour follow-up compared with baseline (1.16 mm/sec [95% CI, 1.08, 1.24 mm/sec] at baseline, and 1.29 mm/sec [95% CI, 0.97, 1.63 mm/sec] and 1.62 mm/sec [95% CI, 1.44, 1.79 mm/sec] at 3- and 24-hour follow-up, respectively; $P < 0.05$ $n = 6$). Whisker stimulation led to reduced neurovascular coupling responses in the sensory cortex corresponding to the peri-ischemic region 3 and 24 hours after reperfusion compared with baseline (19.2% [95% CI, 16.3%, 22.5%] blood flow increase at baseline, 13.4%

[95% CI, 10.0%, 16.8%] at 3-hour follow-up, and 12% [95% CI, 9%, 15%] at 24-hour follow-up, $P < 0.001$, $n = 6$).

Conclusion. Arterial occlusion led to a reduced diameter of pericyte-surrounded capillaries in the peri-ischemic cortex associated with microcirculatory failure. This reduced capillary capacity may, at least in part, underlie impaired neurovascular coupling in peri-ischemic brain regions after reperfusion. Control and correction of capillary capacity may reduce the neurological dysfunction after stroke as a target for therapy.

Staehr, Christian et al. “Neurovascular Uncoupling Is Linked to Microcirculatory Dysfunction in Regions Outside the Ischemic Core Following Ischemic Stroke.” Journal of the American Heart Association vol. 12,11 (2023): e029527. doi:10.1161/JAHA.123.029527

PCB016

The Long-Term Impact of Vaping on Brachial Artery Blood Flow Responses to Exercise

Mared Tomkinson[1], Maddie Roscoe[1], Rhiannon Price-Wickenden[1], Cory Richards[2], Thomas Griffiths[2], Zoe Adams[2], Lydia Simpson[1], Rachel Lord[2], Ben Chant[1], Emma Hart[1]

[1]University of Bristol, Bristol, United Kingdom, [2]Cardiff Metropolitan University, Cardiff, United Kingdom

Electronic cigarette use (e-cigarettes) has surged in popularity over the last decade particularly among young adults. Despite perceptions of reduced harm compared to traditional tobacco cigarettes, studies suggests that e-cigarette use may have adverse impacts on cardiovascular health, comparable to those of tobacco smoking. Understanding the impact of vaping on brachial artery blood flow responses to exercise is crucial for evaluating its impact on endothelial function, a biomarker for cardiovascular disease. This study aims to investigate brachial artery blood flow and diameter responses to dynamic handgrip exercise (DHG) in a vaping group compared to a non-vaping control group. This study had ethical approval from the University of Bristol (17598) and conformed to the Declaration of Helsinki. Fourteen healthy, non-tobacco smokers were recruited. Six participants (4 males) were regular e-cigarette users (vaping group; defined as ≥5 days per week >6 months) and 8 (5 males) were non-users who have never used e-cigarettes or tobacco products (non-vaping control group). The vaping group were asked not to vape before attending the study visit. After a 2-min baseline, DHG was performed at 40% maximal voluntary contraction (MVC) for 4 minutes, at 20 contractions/minute, followed by a 2-min recovery period. Brachial artery blood flow and diameter were measured continuously using vascular ultrasound via a (12-Hz Doppler probe with an insonation angle of 60**°** over the brachial artery). Blood pressure (Finapres) and heart rate (3-lead ECG) were measured continuously throughout the protocol. Brachial artery diameter and mean blood flow were calculated via synchronised Doppler waveform envelope analysis, edge detection, and wall-tracking of high-resolution B-mode arterial ultrasound images. Absolute and change from baseline values were analysed over 30s increments. Brachial vascular conductance was calculated as flow (mL/min) / mean arterial pressure (mmHg). The change in brachial blood flow and conductance from rest to the final 30 seconds of handgrip exercise were compared using an unpaired t-test. Data are mean +/- SD. There were no differences in age (controls; 22 ± 1.5 years vs. vapers; 22 ± 1.4 years, P=0.4467) or body mass index (23.3±2.1 kg/m2 vs. 22.6±3.8 kg/m2, P=0.6284). There was no difference in the change in blood flow from rest to exercise between controls and vapers (Δ359±176 ml/min vs. 291±201 mL/min, P=0.2448). However, there was a large effect of vaping on brachial vascular conductance, where controls had a larger change from rest to exercise vs. vapers (Δ4.0±1.6 ml/min/mmHg vs 2.6±1.5 ml/min/mmHg, P=0.0544, Cohen's d (effect size)=0.90). Vaping potentially impacts vasodilator response to exercise but needs further research.

PCB017

The cardioselective beta1-adrenergic receptor antagonist, bisoprolol, inhibits isoprenaline-induced relaxation of human chorionic plate arteries

Teresa Tropea[1,2], Paul Brownbill[1,2], Anthony M. Heagerty[3], Jenny E. Myers[1,2]

[1]Maternal & Fetal Health Research Centre, University of Manchester, Manchester, United Kingdom, [2]St Mary's Hospital, Manchester University Hospital NHS Foundation Trust, Manchester, United Kingdom, [3]Division of Cardiovascular Sciences, University of Manchester, Manchester, United Kingdom

Introduction: The placenta is a low-resistance vascular organ that provides an efficient maternal-fetal exchange system for oxygen and nutrients. The cardioselective beta1-adrenergic receptor antagonist, bisoprolol, is commonly prescribed to women with pre-existing cardiac disease to improve maternal stroke volume and cardiac output during pregnancy. Clinical evidence of decreased umbilical blood flow velocity and increased rate of low-birth-weight babies in women exposed to bisoprolol [1] raises safety concerns. Although the placenta is devoid of innervation, we hypothesised that bisoprolol may alter placental perfusion via a direct effect on beta-adrenergic receptors in isolated human placental chorionic plate arteries (CPAs).

Methods: CPAs (<500µm diameter) were dissected from biopsies of uncomplicated term placentas (N=3-5). Using wire myography, concentration-dependent effects of the non-selective beta-adrenergic receptor agonist isoprenaline (10^{-9}-10^{-5}M) were tested on CPAs pre-incubated with bisoprolol (10^{-5}M and 10^{-4}M) and pre-constricted with an EC_{80} dose of U-46619. Sensitivity was evaluated as the molar concentration of isoprenaline causing 50% of the maximal effect (Emax) and expressed as logarithm.

Results: Isoprenaline caused significant relaxation of CPAs in a dose-dependent manner ($P<0.0001$. Figure 1A). The relaxant effect of isoprenaline was significantly reduced after pre-incubation with bisoprolol 10^{-5}M ($P<0.05$. Figure 1B) and was abolished by blockade with bisoprolol 10^{-4}M ($P<0.0001$. Figure 1B). Maximum relaxation to isoprenaline was significantly reduced by bisoprolol 10^{-4}M (Emax, $P<0.01$; 24.01 ± 6.09 vs 5.21 ± 6.94%. Figure 1C), whereas the sensitivity was not different between the two groups ($P=0.800$, -7.178 ± 0.56 vs -8.316 ± 1.53 $LogEC_{50}$; isoprenaline vs isoprenaline + bisoprolol 10^{-4}M).

Conclusions: These data show non-selective functional activation and inhibition of beta-adrenergic receptors on CPAs. The increased inhibitory effect of bisoprolol at supraphysiological concentration (10^{-4}M) tested on isoprenaline-induced relaxation may suggest potential off target beta1 blockade effects. Further study is needed to determine the functional role of beta-adrenergic receptors on the fetoplacental vasculature and to identify the relationship between actions mediated by maternal plasma levels of bisoprolol on CPAs and placental perfusion.

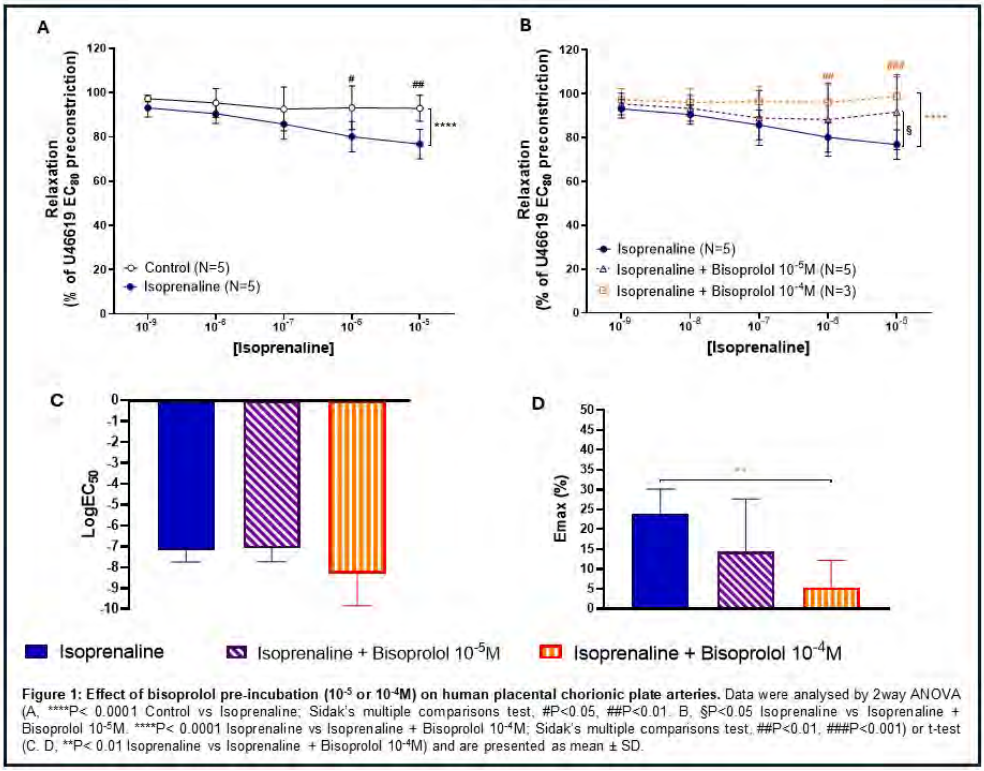

Figure 1: Effect of bisoprolol pre-incubation (10^{-5} or 10^{-4}M) on human placental chorionic plate arteries. Data were analysed by 2way ANOVA (A, ****P< 0.0001 Control vs Isoprenaline; Sidak's multiple comparisons test, #P<0.05, ##P<0.01. B, §P<0.05 Isoprenaline vs Isoprenaline + Bisoprolol 10^{-5}M, ****P< 0.0001 Isoprenaline vs Isoprenaline + Bisoprolol 10^{-4}M; Sidak's multiple comparisons test, ##P<0.01, ###P<0.001) or t-test (C. D, **P< 0.01 Isoprenaline vs Isoprenaline + Bisoprolol 10^{-4}M) and are presented as mean ± SD.

[1] Ormesher, L., et al., Prevalence of pre-eclampsia and adverse pregnancy outcomes in women with pre-existing cardiomyopathy: a multi-centre retrospective cohort study. Sci Rep, 2023. 13(1): p. 153.

PCB018

Sodium-Glucose Cotransporter-2 Inhibition Prevents Development of Left Ventricular Hypertrophy

Anna Vingborg[1], Vladimir Matchkov[1], Markus Rinschen[1,2,3,4], Tina Pedersen[1], Elina Kovalenko[1]

[1]Department of Biomedicine, Aarhus University, Aarhus, Denmark, [2]III Department of Medicine and Hamburg Center for Kidney Health, University Medical Center Hamburg-Eppendorf, Hamburg, Germany, [3]Scripps Research, Center for Metabolomics, San Diego, California, United States, [4]Aarhus Institute of Advanced Studies, Aarhus University, Aarhus, Denmark

Introduction

More than 64 million people suffered from heart failure worldwide in 2017, and this number is expected to be growing (1). Originally, sodium-glucose cotransporter-2 (SGLT2) inhibitors were used to treat type 2 diabetes, but several clinical studies have demonstrated their significant beneficial effects in patients with heart failure independent of their diabetic status (2). The underlying mechanisms are unknown, but intensively investigated. A recent study proposes that a part of the cardioprotective mechanism is a result of SGLT2 inhibition-related improvements in metabolic communication reflecting in the kidney (3). However, heart morphology and function were not investigated. Nevertheless, changes in cardiac metabolism are suggested to promote heart failure development, including left ventricular hypertrophy (4).

We hypothesized that SGLT2 inhibitors may reduce severity of heart failure by preventing cardiac remodeling due to an improved cardiometabolic state.

Methods

33 Bl57c6j male mice were randomly divided into the following 5 subgroups; I) mice on a normal diet, II) vehicle-treated mice on High Fat Diet (HFD); III) vehicle treated mice on HFD receiving N-nitro-1-arginine methyl ester (L-NAME, 600 mg/kg/day) in drinking water; IV) SGLT2 inhibitor-treated (dapagliflozin; 10 mg/kg diet (DAPA)) mice on HFD; and V) SGLT2 inhibitor-treated mice on HFD and L-NAME with all interventions lasting for 6-8 weeks. This combination of HFD and L-NAME was used to induce heart failure with preserved ejection fraction (5).

Blood pressure measurements and echocardiography were conducted before intervention and every 2nd week during the intervention period.

The protocol was conducted in accordance with the animal experiment permissions from the Danish Ministry of Food, Agriculture and Fisheries.

Data were analyzed using mixed-effects model followed by Tukey post-test for multiple comparison (GraphPad Prism 10.2.1). Data are presented as means ± standard errors of the means, $P<0.05$ is considered statistically significant.

Results

L-NAME increased mean arterial pressure in both groups receiving HFD and HFD+DAPA. Six weeks after intervention, mean arterial pressure was 91±4, 118±6, 89±2 and 122±6 mmHg (n=4-5, *P*=0.0004) in HFD, HFD+L-NAME, HFD+DAPA and HFD+DAPA+L-NAME, respectively. An increased heart rate by L-NAME was also observed in the group receiving HFD (588±9 BPM), but the effect was absent in the HFD+DAPA-group (545±16 BPM).

No difference was observed between the groups in stroke volume, ejection fraction, fractional shortening and cardiac output. However, the left ventricular mass was increased in the groups receiving HFD and HFD+L-NAME but this was prevented in both groups receiving DAPA (Figure 1).

Conclusion

Our results suggest that one of the mechanisms underlying SGLT2-inhibitor-related cardiac protection is its ability to reduce the development of left ventricular hypertrophy, which is a known part in the pathogenesis of heart failure.

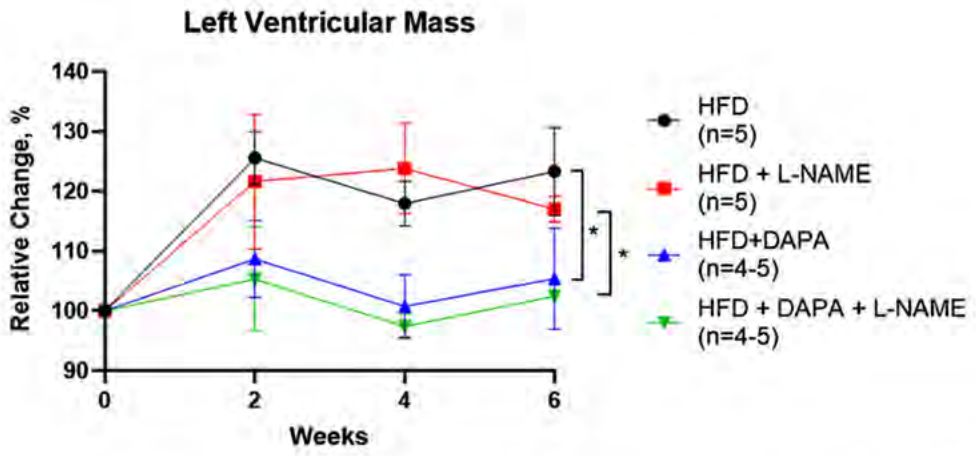

Figure 1: Left ventricular mass presented as relative changes over weeks of interventions (n=4-5). *, P <0.05

1. Savarese G, Becher PM, Lund LH, Seferovic P, Rosano GMC, Coats AJS. Global burden of heart failure: a comprehensive and updated review of epidemiology. Cardiovasc Res. 2023;118(17):3272-87. 2. Zou X, Shi Q, Vandvik PO, Guyatt G, Lang CC, Parpia S, et al. Sodium-Glucose Cotransporter-2 Inhibitors in Patients With Heart Failure : A Systematic Review and Meta-analysis. Ann Intern Med. 2022;175(6):851-61. 3. Billing AM, Kim YC, Gullaksen S, Schrage B, Raabe J, Hutzfeldt A, et al. Metabolic Communication by SGLT2 Inhibition. Circulation. 2024;149(11):860-84. 4. Nakamura M, Sadoshima J. Mechanisms of physiological and pathological cardiac hypertrophy. Nat Rev Cardiol. 2018;15(7):387-407. 5. Schiattarella GG, Altamirano F, Tong D, French KM, Villalobos E, Kim SY, et al. Nitrosative stress drives heart failure with preserved ejection fraction. Nature. 2019;568(7752):351-6.

PCB019

A Single Session of Combined 4-7-8, Box and Pursed Lip Breathing Patterns Reduces Blood pressure and Heart Rate at Rest and After Exercise

Basheer Waziri[1], Fatima Saleh Barau[2], Nafisa Y. Wali[3]

[1]Cardiovascular & Molecular Unit, Department of Human Physiology, Bayero University, Kano, Nigeria, [2]Department of Human Physiology, Bayero University, Kano, Nigeria, [3]Endocrine Physiology Unit, Department of Human Physiology, Bayero University, Kano, Nigeria

Introduction: Various breathing exercises promote relaxation, reduce blood pressure and heart rate. However, findings from existing literature indicated that some of these exercises have more effect on systolic blood pressure (SBP), some on diastolic blood pressure (DBP) and some lower blood pressure only but not heart rate (HR). Some studies reported no immediate effect on SBP, DBP and Heart rate following breathing exercise. It is unclear whether combining different breathing exercises at a time have an immediate positive effect on SBP, DBP, HR and peripheral oxygen saturation (SPO2) at rest and after exercise and whether the combination has more effect than individual techniques. **Aim**: The purpose of this study was to investigate immediate effect of combining 4-7-8, Box and Pursed lip breathing patterns at a time on SBP, DBP, HR and SPO2 at rest and after exercise. **Method**: Following ethical approval (**ref: SHREC/2024/4721**) by the Health Research Ethics Committee, Kano State Ministry of Health, Kano Nigeria, eighty healthy young adults (18 – 25 years) with normal BMI (Mean ± SE: 20.72 ± 0.19) were recruited into the study. HR, SBP, DBP and SPO2 of the participants were recorded at rest and after one session of combined 4-7-8, box and pursed lip breathing patterns. The participants were then divided into two groups, intervention and control groups, both performed five minutes of fast walking (using a treadmill speed of 4-mph). At the end of this exercise, the intervention group performed the same pattern of combined breathing exercise as described above. HR, SBP, DBP and SPO2 of the participants from the two groups were recorded at exactly one-minute after fast walking. IBM SPSS version 26 was used for data analysis, paired t-test was used to compare the baseline variables recorded before and after breathing exercise while independent t-test was used to compare variables between the two groups recorded after exercise. **Results**: A significant decrease in resting HR, SBP and DBP was recorded after one session of combined 4-7-8, box and pursed lip breathing patterns (Mean ± SE: HR 82.26 ± 1.33 – 79.05 ± 1.40, p=0.001; SBP 114.42 ±1.24 – 109.94 ± 1.14, p=0.001; DBP 80.44 ± 1.06 – 76.51 ±1.03, p=0.01). No significant change in SPO2 was observed (p=0.35). Independent t-test revealed significantly lower HR, SBP and DBP (82.04 ± 1.39, 117.18 ± 1.36 and 80.11 ±1.16) in the intervention group than in the control group (89.61 ±1.38, 124.21 ± 1.35 and 84.07 ± 1.28). The decline in HR was significantly higher with the combine pattern than with individual technique (Mean ± SE: Combine, 7.58 ± 1.08; individual, 4.90 ± 0.83; p=0.02). **Conclusion**: One session of combined 4-7-8, box and Pursed lip breathing caused immediate decrease in HR, SBP and DBP at rest and after exercise. Furthermore, the combine pattern was more effective in lowering heart rate after exercise than individual technique.

PCB020

Effect of short-term culture on t-tubule structure and L-type Ca current in adult cardiac ventricular myocytes.

Kester EJ Young[1], Stephen C Harmer[1], Cherrie HT Kong[1], Laura MK Pannell[1], Andrew F James[1]

[1]*University of Bristol, Bristol, United Kingdom*

Introduction:

T-tubules (TTs) are invaginations of sarcolemma in cardiomyocytes important in excitation-contraction coupling. Mechanisms underlying the genesis and maintenance of TTs are poorly understood, but their loss in disease states contributes to the pathogenesis of heart failure and arrhythmia. Short-term culture of cardiac myocytes may provide a model system to study mechanisms underlying the maintenance of TT function.

Aims:

To examine changes in TTs and L-type calcium current (ICa) in adult rabbit ventricular myocytes (ARVMs) in short-term culture.

Method:

ARVMs were isolated from hearts of adult male rabbits and cultured on laminin-treated borosilicate glass coverslips for up to four days. TTs were identified by confocal imaging using Alexa-680-conjugated wheat germ agglutinin (WGA) and quantified by fast Fourier transform analysis ('TT-power'). Junctophilin-2 (JPH2) staining was examined by immunofluorescence on the day of isolation (day 0) and following 4 days in culture (day 4). ICa was recorded from ARVMs at 37 ºC using the whole-cell patch clamp technique on days 0,1,2 and 4. Response to 100 nM of the β-adrenoceptor agonist, isoprenaline (ISO), was examined in currents activated by depolarisation to 0 mV. Current densities were calculated as currents normalised to whole-cell capacitance, as an index of cell surface area. Data are reported as mean ± standard error and sample sizes as n cells/N animals. ICa density-voltage relations were plotted and fitted with Equation 1:

$ICa = (Gmax(Vm - Vrev)/(1 + e^{(Vm-Vhalf)}/k))$,

where *Gmax* = maximal conductance density for ICa, *Vm* = command potential, *Vrev* = effective reversal potential for the current, *Vhalf* = voltage of half-maximal activation and *k* = slope factor. Fits to ICa density-voltage relations on days in culture were compared by extra sum-of-squares F test (GraphPad Prism 10.2). Responses to ISO were quantified as percentage increases relative to control and compared across days in culture by Welch's one-way ANOVA).

Results:

Cultured ARVMs became more rounded and whole-cell capacitance decreased exponentially with a time constant of 1.68 days (n/N = 16/3, 11/3, 18/5, 6/2 for days 0,1,2 and 4). TT-power showed a threefold-reduction from day 0 to day 4 ($p = 0.001$, unpaired t-test, n/N = 6/1 and 4/1). JPH2 staining intensity (AU) was significantly less at day 4 (25.5 ± 2.29; n/N = 5/1) compared to day 0 (36.1 ± 1.74; n/N = 6/1) of culture ($p = 0.0045$). At culture day 1, *Gmax* fell from 0.36 ± 0.03 nS/pF to 0.21 ± 0.02 nS/pF, but then recovered to 0.25 ± 0.02 nS/pF at day 2 and by day 4 had recovered to 0.33 ± 0.05 nS/pF ($p < 0.0001$, n/N = 11/3, 10/3, 13/5, 6/2 for days 0,1,2 and 4). The response to 100 nM ISO was preserved across days in culture ($p = 0.91$, n/N = 8/3, 6/3, 6/4, 3/2 for days 0,1,2 and 4).

Conclusions:

Short-term culture of ARVMs was associated with loss of membrane surface area, loss of TT-power, reduced ICa density and reduced JPH2 staining, although responses to β-adrenoceptor stimulation were preserved. In future studies, we will use this experimental model to investigate mechanisms underlying loss of TTs and ICa.

PCB021

Diversifying laboratory assessment modes broadens engagement with practical competencies in life science students

Bernard Drumm[1], Ronan Bree[1], Caoimhin Griffin[1], Niall O'Leary[2]

[1]Dundalk Institute of Technology, Dundalk, Ireland, [2]University College Cork, Cork, Ireland

Laboratory practicals in life science subjects at many undergraduate institutions are traditionally assessed by written reports which reflect disciplinary norms of documenting experimental activities. Over the last 20 years, assessment of scientific laboratory classes has continued to diversify, with the sole use of report or research paper writing style assessments becoming increasingly less ubiquitous. Such alternative assessments include but are not limited to student reflections on skills obtained, poster presentation sessions on laboratory experiments and skills, drafting of grant proposals based on data obtained in laboratory practicals and various survey instruments designed to evaluate experimental design capability. However, over-reliance on reports can potentially promote rote learning and evaluate a narrow set of competencies. A commonly reported drawback of report writing is students struggle with placing experimental data in a wider context and find writing introductions and discussions tedious and challenging, to the point that students often revert to copy and paste exercises to fill out their reports. In this study, we explored how multiple modes of laboratory assessments (a group presentation, an online quiz and a written report) might affect student perceptions of learned skills in a life science module at Dundalk Institute of Technology, Ireland.

For this study, we aimed to address the following specific research questions:

1. In an undergraduate life science module that uses 3 different assessments (reports, online quizzes, group presentations), on average across a class, do students score higher in any of these assessment modes over another?
2. Do students perceive that different assessments (reports, online quizzes, group presentations) promote awareness of, and engagement with, a broad range of practical competencies?

This was informed by universal design for learning (UDL) and teaching for understanding (TfU) frameworks. Anonymous surveys collected over 3 consecutive years (2020-2022) with 66 total students, evaluated whether this expanded portfolio of assessments promoted awareness of, and engagement with, a broader range of practical competencies. Interestingly, when student scores were compared across the assessments, there was no significant difference between any comparisons in any year ($P>0.05$, unpaired one-way ANOVA, Tukey test, n=29 for 2020, n=13 for 2021, n=24 for 2022). Survey data showed that aspects that influenced student preferences in assessment mode included time limitations, time investment, ability to practice new skills, links with lecture material and experience of assessment anxiety. In particular, presentations were highlighted as promoting collaboration and communication and the quiz as an effective means of diversifying assessment schedules. A key takeaway from students was that while reports were important, an over reliance on them was detrimental, as exemplified by one student *"I think that the three of these modes work well together. They provide different ways of learning that is not just*

the usual lab report", also summarized in Figure 1. This study suggests that undergraduate life science students can benefit significantly from a holistic assessment strategy that complements reports with performance-based approaches that incorporate broader competencies and allow for greater student engagement and expression in undergraduate modules.

Effect of Diversifying Laboratory Assessment on Student Performance And Skills

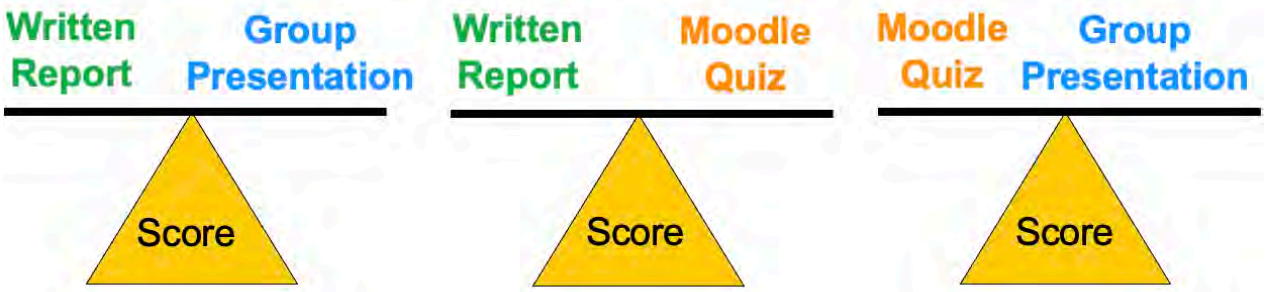

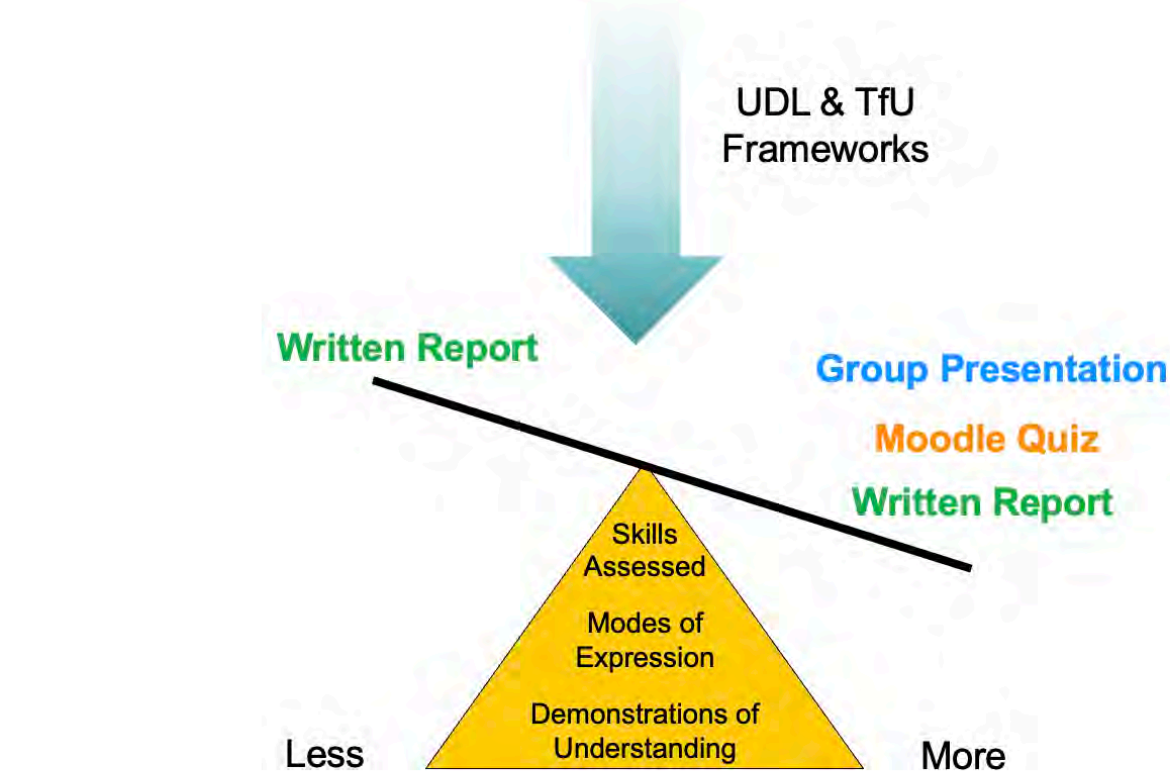

"I think that the three of these modes work well together. They provide different ways of learning that is not just the usual lab report."

"The assessments worked well together, makes student take different approaches to learning."

"This module had great engagement out of all the other modules of third year. I found it kept me on my toes and I had to work hard but it was completely worth the effort. The different methods of assessment were good as they varied and were not boring. "

Student Voice

PCB022

Neurodiversity and the Physical Environment of the University - An undergraduate research project

Dawn Davies[1]

[1]*University of Bristol, Bristol, United Kingdom*

Neurodiversity can manifest in many different ways. One issue that many neurodivergent individuals face is hypersensitivity to sensory stimuli, for example auditory stimuli where decreased sound tolerance can lead to disabling features, including inability to concentrate. There is an increasing interest in designing spaces for a neurodiverse population with the understanding that a good environment for the neurodivergent will be good for all. Within the University, teaching spaces are often being refurbished. However, how much does the sensory environment and its effect on members of our community impact on the design criteria of these spaces? In this undergraduate project, third year life sciences students ran focus groups to understand the student experience of University spaces, with a particular focus on the sensory environment. This information was incorporated into a presentation to members of staff who are involved in decision making regarding building design. The aim was to increase awareness of criteria that should be included in those decisions. Data, gathered through pre- and post-presentation questionnaires, showed that the participants had gained knowledge of the issues and, importantly, that they would be interested in finding out more. In their dissertations, students combined this research with a review of the current understanding of the neural pathways involved in sensory hypersensitivity, appropriate to their degree programme. Student agency was key to the development of this project as they decided who to consult with to gather information. The resulting presentation highlighted the importance of design for inclusion, addressing a key challenge for higher education.

PCB024

Microscopy for Teaching Physiology: An Online Perspective

Katja Rietdorf[1], Mark Hintze[1], Francesco Crea[1], Martin Bootman[1]

[1]*The Open University, Milton Keynes, United Kingdom*

The Open University (OU) is a distance learning university that offering several STEM subjects as part of its curriculum. Within those courses, various aspects of physiology are taught through explanation and interactive content via the OU's virtual learning environment. This includes presenting numerous techniques as interactive screen experiments (ISEs) to around 400-500 students per course, allowing our students to gain experience of these techniques and explore the underlying theoretical concepts. The ISEs are primed with images and data that enable students to collect individualised data and generate independent reports and interpretations. Here, we present examples how we teach microscopy online at the OU.

In both Biology and Health Sciences modules, we use three digital microscopes: a digital light microscope for presenting micrographs after histological staining, a digital fluorescence microscope for immunofluorescence staining micrographs, and a digital transmission electron microscope to showcase ultrastructure images. These microscopes aid student learning by featuring a unified interface. Storing images within a database allows easy interchange of images, facilitating the use of the digital microscopes across different levels or subject areas.

The digital light microscope serves, for example, to teach cancer biology concepts by counting Ki67-positive cells and grading prostate cancers in patient-derived tissue samples. These examples highlight the impact of cancer on cell and tissue physiology and enhance the students' ability to visualise and understand core concepts around tissue structure-function relationships and gain an understanding in diagnostics. Similarly, the digital fluorescence microscope provides insights into the structure of organelles and alterations induced by diseases. Students can visualise, for instance, the changes in the Golgi apparatus due to spinal muscular atrophy or the variances in CFTR expression in cells with *CFTR* mutations. This interactive approach significantly enhances students' understanding of tissue structure-function relationships and diagnostic skills.

In another ISE students learn how to collect and analyse data from imaging experiments using the fluorescent mitochondrial membrane potential indicator TMRE. The images used within this ISE were obtained from fibroblasts of healthy individuals and patients with a lysosomal storage disorder. Students quantitate fluorescence intensity from mitochondria in regions of interest they choose and students learn about experimental design, application of statistics, as well as the broad changes in cell physiology caused by lysosomal dysfunction.

Using ISE means that our students can study asynchronously and remotely. In one such remote experiment, students measure cell proliferation or cell migration after pharmacological treatments they decide on. The experiment is running live at the OU campus in Milton Keynes, and students access the instrument remotely for their data collection.

Presentation of work carried out using these ISEs is integral to assessment in teaching modules, allowing for authentic assessment. The individualised data enables the re-use of assessment in successive presentations of a module with reduced concerns about plagiarism.

Although online microscopy does not replace the hands-on experience of using a microscope, our students appreciate that the ISEs are based on real data and allow them to participate as researchers in a laboratory through designing experiments, collecting information and producing reports.

PCB025

Remote STEM outreach improves STEM engagement.

Jamie Young[1], Sharon Parkinson[1], Etain Tansey[1]

[1]Centre for Biomedical Sciences Education, Queen's University Belfast, Belfast, United Kingdom

Background

STEM outreach initiatives aim to address the consistent decline of student interest in STEM which becomes increasingly apparent as students transition from primary to secondary school (1). Typically, outreach programmes are delivered in-person and require volunteers to travel to schools or students to travel to outreach sites. This takes time out of an already busy curriculum and can place students in less accessible locations at a disadvantage, e.g., rural students are already underperforming within STEM education when compared to their metropolitan counterparts (2). Remote/on-line delivery presents a possible alternative for STEM outreach programmes. The main advantage is greater accessibility and flexibility, enabling its use for a greater number of audiences. The aim of this study was to determine if remote delivery of STEM activities is a viable outreach alternative to in-person events.

Methods

As part of the STEM Ambassador Programme (https://www.stem.org.uk) and during the COVID-19 pandemic, secondary schools in Northern Ireland were approached to participate in an on-line STEM outreach activity suitable for students in Years 10-12 (ages 14-17). The activity consisted of an interactive presentation (40 minutes) covering the importance of a STEM education and then specifically the topics of genetics and inheritance. Pre-and post-presentation questionnaires were sent in advance to teachers. The anonymous questionnaires assessed students' understanding of STEM, knowledge of genetics and inheritance and opinions on remote delivery. A Likert scale was used to quantitatively analyse data related to student perceptions and aspirations (5 - strongly agree to 1 - strongly disagree). Data are presented as means ± SEM. A Student's unpaired *t*-test assessed statistical significance ($p<0.05$). Ethical approval was obtained through the Queen's University Belfast Research Ethics Committee.

Results

Four student groups completed the outreach activity from three different schools, completing both a pre-presentation questionnaire (n=126) and a post-questionnaire (n=95). Results from the pre- and post-questionnaires highlight that the STEM event produced a significant increase in student 1) knowledge of genetics and inheritance ($p\leq0.0001$), 2) STEM awareness ($p\leq0.001$) and 3) positive association with on-line learning ($p=0.01$). In one school with 2 separate cohorts, significant differences between year 10 and year 12 post-presentation responses were found with the older cohort more positively affected by the outreach than the younger cohort. This was evident in the categories of STEM awareness (4.3±0.2 year 10 vs. 4.8±0.2 year 12, $p=0.02$), perception of online learning (3.7±0.2 year 10 vs. 4.1±0.2 year 12, $p=0.03$) and student acquisition of knowledge (4.3±0.5 year 10 vs. 5.3±0.5 year 12, average correct answers, $p=0.03$).

Discussion

One of the ultimate goals of STEM outreach is to drive student aspirations towards STEM fields. Remote delivery of STEM outreach increased student knowledge of a STEM-related subject, raised STEM awareness and increased students' positive perceptions of on-line learning. The increase was greater for year 12 students than year 10 which may relate to prior learning experiences. Overall, the results suggest that remote delivery of STEM outreach activities is a viable alternative to in-person events and may assist with encouraging STEM awareness particularly in otherwise difficult to access students.

(1) Fadzil HM, Saat RM. (2014). Enhancing STEM education during school transition: Bridging the gap in science manipulative skills. Eurasia J Math Sci Technol Educ; 10: 209–21 (2) Morris J, Slater E, Fitzgerald MT, et al. (2019). Using Local Rural Knowledge to Enhance STEM Learning for Gifted and Talented Students in Australia. Research in Science Education; 1–19.

PCB026

Enhancing Physiology Learning Through Gamification

Marta Woloszynowska-Fraser[1], Jenny Moran[1]

[1]Keele Univeristy, Newcastle-under-Lyme, United Kingdom

Mastering physiology requires not only knowledge of individual organ systems, but also appreciation for their intricate interconnectedness. This work explores two novel game-based activities designed to enhance student understanding of complex physiological concepts.

The first activity, a collaborative card game, was inspired by the human body as a complex ecosystem. Students were involved in co-design of the game where players are tasked with creating functioning human body by strategically selecting and passing cards representing anatomical structures and physiological processes. Points are awarded for correctly placing cards, reinforcing connections between components like red blood cells and veins or gas exchange in the lungs. This adaptable game can target specific systems like the heart, liver, or brain, ensuring knowledge acquisition while highlighting interdependencies and core functions.

The second activity utilises a family quiz format. Divided into teams, students research and develop questions related to a provided prompt, varying in difficulty and point value. A designated quiz master then poses these questions to other groups, awarding points based on answer complexity. This approach fosters teamwork, research skills, and reinforces understanding of key physiological concepts. Additionally, its quick implementation maintains high student engagement.

By implementing these interactive and collaborative games, lecturers can create dynamic learning experiences that not only solidify physiological knowledge, but also cultivate a sense of ownership and relevance among students. Gamification and teamwork provide lecturers with powerful tools to enhance learning efficacy without sacrificing student engagement or instructional efficiency.

PCB027

Investigating Toll-like receptor expression in the adrenal gland of a male and female rat pup model of physiological stress.

Maria L. Dias Casacao[1], Anna O'Connell[1], Ken D. O'Halloran[1,3], Fiona B McDonald[1,3]

[1]Department of Physiology, School of Medicine, College of Medicine and Health, University College Cork, Cork, Ireland, [2]University College Cork, Cork, Ireland, [3]INFANT Research Centre, Cork, Ireland

Introduction: Newborn neonatal infants that require intensive care often exhibit unstable patterns of breathing and require oxygen support for several weeks. These infants are at risk of late onset, nosocomial, infection. Toll-like receptors (TLR) and their down downstream signalling pathways are important mediators of the innate immune system and upon activation by, damage associated molecular patterns or pathogen associated molecular patterns, promote inflammation. TLRs have a critical role in facilitating immune-adrenal crosstalk during inflammation and may modulate adrenal physiology under common clinical conditions of oxygen dysregulation and infection.

Objective: To quantify TLR expression in the adrenal gland of male and female rat pups which have been exposed to chronic oxygen dysregulation and acute gram-positive protein challenge.

Methods: Ethical approval was obtained locally by University College Cork and project authorisation was issued by Health Products Regulatory Authority Ireland AE19130/P100,/P163 and experiments performed under authorisation in accordance with Irish and European directive 2010/63/EU. Sprague Dawley rat pups and their dam were exposed either to room air or intermittent hypoxia (FiO_2 8%)-hyperoxia (FiO_2 30%)—normoxia (FiO_2 21%)- (IHH) 24-hour protocol from postnatal day (PND) 3-12 and acutely challenged the animals with either sterile saline i.p. or mixture of 3mg/kg of lipoteichoic acid and 5mg/kg peptidoglycan i.p. on PND 13. Adrenal glands were dissected following rapid decapitation and either snap frozen in dry ice and stored at -80C and later used for TLR mRNA analysis of TLR-1, -2, -4, -9, MYD88, NOD2 and NFκB or cryoprotected and frozen in cooled isopentane and later used for histological assessment.

Results: TLR-4, TLR-9, MYD88, NOD2 and NFκB mRNA expression were increased in IHH exposed animals compared to Sham animals ($P \leq 0.02$; n=8 per group). IHH exposure interacted with LTA&PGN administration to reveal a higher expression of TLR-2 mRNA (gas x drug, P=0.01) and NFκB mRNA (gas x drug, P=0.05), (n=8 per group). GAPDH mRNA was utilised as the housekeeper for the mRNA analysis performed on the adrenal gland.

Discussion and Conclusions: We have previously reported that in PND13 rat pups LTA&PGN administration increased plasma cytokine and cortisol concentrations. Interestingly, Ilβ, IL-10, Leptin and Gro/KC were increased many fold when animals were pre-exposed to oxygen dysregulation. In this further analysis we sought to investigate the expression of TLR expression and some of its downstream signalling molecules. We found that TLR-2 was robustly increased with gram- positive bacterial proteins only when the animals were pre-exposed to oxygen dysregulation. This indicates that in early life pre-exposure to oxygen dysregulation may act to prime the body to generate a heightened inflammatory response upon infection.

PCB028

Preadipocytes as drivers of inflammation in white adipose tissue – A pilot study

Adrian O'Hara[1], Paul Trayhurn[2]

[1]School of Pharmacy and Biomolecular Sciences, Liverpool John Moores University, Liverpool, United Kingdom, [2]Institute of Ageing and Chronic Disease, University of Liverpool, Liverpool, United Kingdom

Obesity can be characterised as a mild chronic inflammatory condition. Observed inflammation can be driven by different factors, including infiltration of macrophages into adipose tissue and by hypoxia. As white adipose tissue is heterogenous at the cellular level, it provides an ideal environment for cell-to-cell communication, and in particular for crosstalk between adipocytes, preadipocytes and macrophages. Over the past two decades there have been several studies that have examined the role of macrophage-driven inflammation in adipose tissue and how this impacts the inflammatory state of both adipocytes and preadipocytes. An area that has yet to be fully explored involves the crosstalk between adipocytes and preadipocytes, as well as their influence on macrophages. This pilot study seeks to investigate this area of crosstalk through a candidate gene approach.

SGBS (human) preadipocytes were cultured (20,000 cells/well) and maintained at 37°C in a humidified atmosphere of 5% CO2/ 95% air. Once confluent, the media was collected to be used as preadipocyte conditioned medium (PACM). The preadipocytes were then differentiated into adipocytes, and 10 days post differentiation media was collected to be used as adipocyte conditioned media (ACM). U937 monocytes were plated at 2 x 10^5 cells/ml at 37°C in a humidified atmosphere of 5% CO2/95% air, differentiation was induced by the addition of 30 nM phorbol myristic acid. Cells were treated with 150 µl of the relevant conditioned media for 24 h, after which mRNA was extracted and reverse transcribed. Expression of candidate genes was carried out using qPCR (n = 6) and fold-changes determined using the $2^{-\Delta\Delta CT}$ method, results expressed as ± standard error of the mean and a Student's t-test applied to the results to determine statistical significance ($p<0.05$).

Treating adipocytes with PACM led to changes in mRNA expression of key adipokines. A 16-fold increase in IL-6 mRNA was observed ($p<0.001$ compared to control), and an 8-fold increase was seen in MCP-1 mRNA level ($p<0.001$ compared to control). When it came to adiponectin expression, the treatment led to no significant changes in mRNA level. Macrophages treated with PACM demonstrated a 1.8-fold increase in IL-6 expression ($p<0.05$ compared to control), 2.1-fold increase in TNFα ($p<0.01$ compared to control), and a 3.2-fold increase in MCP-1 mRNA levels ($p<0.05$ compared to control). When treated with ACM, preadipocytes demonstrated no measurable changes in IL-6, MCP-1 and adiponectin mRNA levels. However, when U937 cells were treated with ACM, no significant change in TNFα expression was seen, but a statistically significant decrease in IL-6 (1.7-fold) and MCP-1 (2.5-fold) mRNA level ($p<0.05$ compared to control) was evident.

These experiments show that preadipocytes can exert an inflammatory response in adipocytes, and a very mild effect on macrophages. In contrast, adipocytes do not appear to induce a

significant change in inflammation-related genes in preadipocytes but a slight decrease in inflammation related genes in macrophages is apparent. These data suggest a possible pro-inflammatory role for preadipocytes in adipose tissue, with adipocytes possibly exerting an anti-inflammatory effect on macrophages.

PCB029

Outcomes of Variable Stress and Vitamin C Supplements on Ovarian Cycle in Wistar Rats

Odunayo Olumide[1], Aaron Alale-Yusuf[1], Olawale Aina[1], Ibiyemi Olatunji-Bello[1]

[1]Department of Physiology, Faculty of Basic Medical Sciences, Lagos State University College of Medicine, Ikeja, Lagos, Nigeria

The influence of stress on female fertility is multifaceted with intricate mechanisms that are not fully elucidated. Nonetheless, it is certain that free radicals play a role.

This study was therefore aimed at investigating the effects of vitamin C supplement and stress on the ovarian functions in Wistar rats.

Twenty female Wistar rats with regular estrus cycle of 4 to 5 days were divided into four groups (n=5). Group A (Control); 10ml/kg BW/day distilled water, group B (VitC); 10mg/kg BW/day vitamin C, group C (Stress); exposed to varying stress models alongside 10ml/kg distilled water, group D (stress/vitC); exposed to varying stress alongside 10ml/kg BW/day vitamin C, Animals were exposed to dark cycles stress models; overnight saturated beddings and strange objects. Light cycles: Multiple cage changes, immobilty and noise. The animals were exposed to varying stress every other day for 3 weeks. Vagina secretion was taken from each rat between 8 and 9am for daily monitoring of estrus cycle. After 3 weeks, each rat was placed in diethylether fume chamber, blood samples were taken from the heart after cervical dislocation. Blood samples were centrifuged to assay estradiol, progesterone, follicle stimulating hormone (FSH), luitenizing hormone (LH) and cortisol using enzyme linked immunosorbent assay (ELISA) (AccuBind, USA). The activities of superoxide dismutase (SOD), catalase (CAT), and malondialdehyde (MDA) were assayed in the ovaries with randox kit (Sigma Chemicals Ltd, USA). Histology of the ovaries were done. Procedures were done at estrus phase. Graphed pad prism 8.0 was used to analyze data, ANOVA was used to compare the means, Newman keuls was posthoctest and P values ≤ was considered significant.

Results showed a significant decrease ($P<0.05$) in the number of complete estrus cycle in stress (3.0±0.05 days) compared with vitC (4.87±0.03 days) and control (4.9±0.21 days). Stress (5.80±0.66 days), (3.40±0.40 days) significantly reduced ($P<0.05$) diestrus and estrus compared with VitC (8.40±0.40 days), (5.00±0.48 days) and control (6.40±0.51 days), (5.20±0.37 days). Occurrence of metestrus was significantly increased ($P<0.05$) in stress (8.00±0.63 days) compared with VitC (3.80±0.37 days) and control (4.80±0.37 days). Progesterone and estradiol were significantly higher ($P<0.05$) in Vitamin C (15.8±1.19 ng/dl), (22.24±1.31 ng/dl) than stress (11.58±0.80 ng/dl), (19.38±1.16 ng/dl) and control (13.70±0.66 ng/ml), (20.13±0.74 ng/dl). Progesterone was also higher ($P<0.05$) in stress/vitC (13.21±0.70 ng/dl) than in stress (11.58±0.80 ng/dl). Cortisol was significantly higher ($P<0.05$) in Stress (1.14±0.12 µg/dl) than stress/vitC (0.78±0.09 µg/dl), vitC (0.32±0.07 µg/dl) and control (0.34±0.24µg/dl). Serum MDA was higher ($P<0.01$) in stress (2.30±0.14 mol/ml) than in stress/vitC (1.64±0.25 mol/ml), vitC (1.0±0.24 mol/ml) and control (1.46±0.20 mol/ml). Activities of SOD and CAT were lower ($P<0.05$) in stress (4.38±0.27 mg/dl), (3.08±0.48 mg/dl) compared with stress/vitC (5.10±0.42 mg/dl), (3.70±0.25 mg/dl), vitC (7.36±0.43 mg/dl), (5.14±0.68 mg/dl) and control (6.48±0.40 mg/dl), (4.2±0.27 mg/dl). Histology of the ovary

showed reduced follicular development with degenerating corpus luteum in stress group compared with control and VitC

In conclusion, despite the disruption of the estrus cycle and ovarian follicle distortion induced by stress, the supplementation of vitamin C facilitated follicular development and regulated the cycle.

Casillas F, Flores-González A, Juárez-Rojas L, López A, Betancourt M, Casas E, Bahena I, Bonilla E, Retana-Márquez S. (2023). Chronic stress decreases fertility parameters in female rats. Syst Biol Reprod Med. 69(3):234-244. Vašková, J., Klepcová, Z., Špaková, I., Urdzík, P., Štofilová, J., Bertková, I., Kľoc, M., & Rabajdová, M. (2023). The Importance of Natural Antioxidants in Female Reproduction. Antioxidants (Basel, Switzerland), 12(4): 907.

PCB031

Male sex and age do not associate with higher kidney tissue protein abundance of ACE2 and TMPRSS2 while ACE2 is shedded into the urine in patients with COVID-19

Marie Lykke Bach[1], Sara Latif[1], Jesper Kingo Andresen[1], Rune Micha Pedersen[1,2], Lone W Madsen[2], Kirsten Madsen[1,2], Gitte Rye Hinrichs[1,2], Rikke Zachar[2], Per Svenningsen[1], Lars Lund[2], Isik Somuncu[2], Lennart Friis Hansen[3], Yaseelan Palarasah[1], Boye L. Jensen[1]

[1]University of Southern Denmark, Odense, Denmark, [2]Odense University Hospital, Odense, Denmark, [3]Hillerød Hospital, Hillerød, Denmark

Background: The SARS-CoV-2 virus infects cells in a TMPRSS2-dependent mechanism by engaging with ACE2. ACE2 display high levels in kidneys, and risk factors for severe disease are high age and male sex. We hypothesized that in human kidneys, ACE2 and TMPRSS2 are 1) more abundant in male and with increasing age; 2) co-localize; 3) more abundant in urine and extracellular vesicles (EVs) from male patients with acute SARS-CoV-2 and 4) SARS-CoV-2 antigen is present in urine and EVs.

Methods: Kidney cortex tissue from cancer nephrectomy patients (male >75y n=6, female >75y, male <50y n=6, female <50y n=6) was analyzed for ACE2 and TMPRSS2 protein level. Urine collected from hospitalized patients with SARS-CoV-2 (male=7, female n=11) was analyzed for ACE2 and albumin and compared with healthy control (n=3) and patients with albuminuria with COVID (n=12). Urine EVs from patients with COVID-19 were used to detect ACE2, TMPRSS2 and SARS-CoV-2 antigen. Studies were approved by the Ethics Committee of the Region of Southern Denmark and the Danish Data Protection Agency and carried out in accordance with the Declaration of Helsinki. Data were tested for normal distribution, and log transformed if this yielded normal distribution. The 2-variables dataset and 1-variable dataset were analyzed by two-way-ANOVA or Student's t-test, respectively. Correlation between parameters was assessed by linear regression with 95% confidence intervals. For all data, a p-value < 0.05 was considered significant. Normally distributed data are displayed as mean ± standard error of mean (SEM), and non-normally distributed as mean ±interquartile range. Analyses were carried out using GraphPad Prism 9.5.0

Results: Immunoblot analyses (n=6) of ACE2 and TMPRSS2 protein levels were not different with age. ACE2 was more abundant in female kidneys across ages. Immunohistochemistry (n=6) showed that ACE2 protein was associated with proximal tubule apical membranes in the cortex, while TMPRSS2 was observed predominantly in the medulla. ACE2 was elevated significantly in uEVs (immunoblot n=4) and urine from patients with severe SARS-CoV-2 with no sex difference compared with urine from controls w/wo albumin (ELISA). TMPRSS2 was elevated in EVs from male patients compared to female (immunoblot n=4). ACE2 and TMPRSS2 did not co-immunopreciptate in EVs/apical membranes (immunoblot n=6). SARS-CoV-2 antigen and mRNA were not detected in urine and EVs (PCR).

Conclusion: Higher kidney ACE2 protein abundance is unlikely to explain higher susceptibility to SARS-CoV-2 in male or elderly. Higher TMPRSS2 in male tissues could contribute. Loss of ACE2 into urine in COVID-19 could impact susceptibility and angiotensin metabolism with systemic consequences.

PCB032

Characterization of the cœlenteron pH in a reef coral with microsensors: spatial variability, effect of environmental parameters and relationship with calcification

Lucas Crovetto[1,2], Alexander Venn[1], Duygu Sevilgen[1], Sylvie Tambutté[1], Eric Tambutté[1]

[1]Marine Biology Department, Centre Scientifique de Monaco, Monaco, Monaco, [2]Sorbonne Université - ED 515 Complexité du Vivant, Paris, France

Coral reefs, the largest bioconstruction on Earth, are formed by calcium carbonate skeletons of corals through a process commonly referred to as calcification. As increasing anthropogenic carbon dioxide dissolves in the world's oceans, the pH of seawater decreases (a phenomenon known as ocean acidification), leading to a reduction in the rate of coral calcification. Calcification models often assume a direct relationship between the surrounding seawater and the extracellular calcifying medium (ECM), which is located between the aboral calcifying ectoderm and the skeleton. However, the ECM is separated from the seawater by several tissue layers and the cœlenteron, which contains the cœlenteric fluid. Symbiotic dinoflagellate-containing cells line the cœlenteron and their photosynthetic activity contributes to changes in the chemistry of the cœlenteric fluid, particularly with respect to pH. Therefore, to understand the pH gradients in the different compartments of corals (both cellular and extracellular), the pH values in all compartments, including the cœlenteron, need to be determined. The cœlenteron may indeed play an important role in mediating the transport of molecules/ions between the external environment and the compartment where calcification occurs (i.e. the ECM). The aim of our study was to determine whether dinoflagellate density (based on tissue coloration), light/dark conditions, and decreasing seawater pH could affect cœlenteron pH and potentially influence pH in the ECM in a single coral species, *Stylophora pistillata*. To accomplish this, we worked with liquid ion exchange (LIX) pH microsensors to measure pH in the cœlenteron under different environmental conditions. Seven samples of *S. pistillata* grown in long-term coral culture facilities on glass slides at the Centre Scientifique de Monaco were used for this study. For each sample, at least three replicate measurements were performed under all conditions to allow statistical analysis. Our results show that pH of the cœlenteron differs between tissues with high and low dinoflagellate density (HDD and LDD respectively). In HDD tissues, pH of the cœlenteron indeed exhibits light-dark fluctuations due to the photosynthetic activity of the symbiotic dinoflagellates. No such fluctuations are observed in LDD tissues, as the combined photosynthetic activity of the few dinoflagellates present in these tissues is not sufficient to increase the pH of the cœlenteron in the light. We interpret our results in terms of what light and dark exposure means for the proton gradients between the ECM and the cœlenteron and how this might affect calcification.

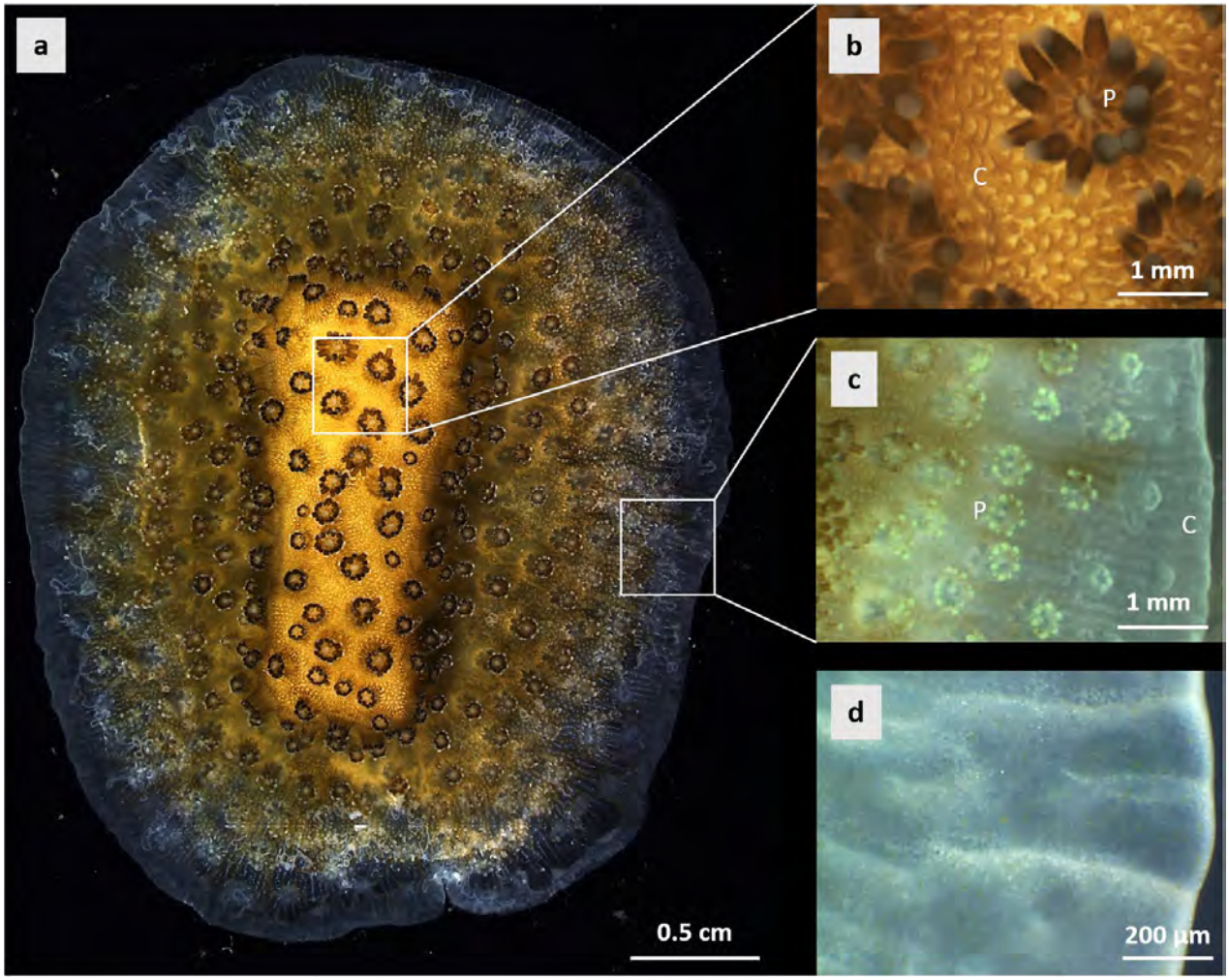
a
b
P
C
1 mm
c
P
C
1 mm
d
0.5 cm
200 µm

PCB033

Elevated blood pressure in aged male mice with hyperaldosteronism is associated with reduced blood vessel compliance.

Debra Fong[1], Robert Little[1], Mariavittoria D'acierno[1], Tina Myhre Pedersen[1], Michael Stowasser[2], Eric Delpire[3], Vladimir Matchkov[1], Robert Andrew Fenton[1]

[1]Aarhus University, Aarhus, Denmark, [2]The University of Queensland, Brisbane, Australia, [3]Vanderbilt University Medical Center, Tennessee, United States

Introduction
Primary aldosteronism (PA) is a common cause of secondary hypertension and is characterized by excessive production of aldosterone despite lower renin activity (1). Mutations in the chloride channel 2 (*Clcn2*) gene cause Familial Primary Aldosteronism Type II (FH-II), which is a milder form of hyperaldosteronism associated with high blood pressure (BP) (2). However, the mechanisms behind the association of high levels of aldosterone and the elevation in BP are poorly understood. Volume regulation by the kidney and vascular function are well established regulators of BP (3). Thus, in this study we aimed to examine BP, renal function, and vessel compliance in a novel mouse model of FH-II due to a R180Q *Clcn2* mutation.

Methods
The mouse model with a R180Q *Clcn2* mutation was generated using CRISPR/Cas9 gene editing. Young and aged male wildtype (WT), heterozygote (Hz) and homozygote mutant (Mut) mice were characterized for BP, vessel compliance (wire myography), and kidney function (metabolic cage studies). BP in 8-11-week-old mice (WT, n=5; Mut, n=5; Hz, n=5) were measured via tail cuff plethysmography, whereas BP in older 16-20-week-old mice (WT, n=3; Mut, n=3; Hz, n=5) were measured via gold standard radio-telemetry. 24-hour urine samples were collected via metabolic cage studies, and blood samples were collected via submandibular vein for plasma. Mesentery arteries were collected from a separate cohort of similarly aged mice and vessel compliance studies were performed *ex vivo* using wire myography. Data are presented as mean ± standard error mean (SEM) and were analyzed using 2-way ANOVA with Tukey's multiple comparisons test. P-value of ≤0.05 is considered statistically significant.

Results
In the older cohort of animals, systolic BP was found to be significantly higher in the Mut and Hz groups compared to their age-matched WT controls ($P<0.05$). Furthermore, this increase in BP was associated with a decrease in vessel compliance ($P<0.05$). However, in the younger animals, there was no significant difference in BP and/or vessel compliance between the genotypes, suggesting that there could be a time-dependent increase in BP due to increase in aldosterone, which could be a potential driving factor for the development of disease in this model. The urine and plasma analyses for this study are still to be determined.

Conclusion
We have shown that BP increases with age in the Mut in our model of hyperaldosteronism, and that this elevation in BP with age is associated with reductions in vessel compliance. This suggests that the increase in aldosterone levels could be a potential driving factor behind the development of

higher blood pressure with age in this model. Further studies are still required to determine whether the development of disease in this model is also associated with any changes in renal function. This would help to determine potential developmental origins and further our understanding of the physiological mechanisms behind the development of this disease.

References 1. Funder JW, Carey RM, Mantero F, Murad MH, Reincke M, Shibata H, et al. The Management of Primary Aldosteronism: Case Detection, Diagnosis, and Treatment: An Endocrine Society Clinical Practice Guideline. J Clin Endocrinol Metab. 2016;101(5):1889-916. 2. Schewe J, Seidel E, Forslund S, Marko L, Peters J, Muller DN, et al. Elevated aldosterone and blood pressure in a mouse model of familial hyperaldosteronism with ClC-2 mutation. Nat Commun. 2019;10(1):5155. 3. Guyton AC. Roles of the kidneys and fluid volumes in arterial pressure regulation and hypertension. Chin J Physiol. 1989;32(2):49-57.

PCB034

Assessing the role of glucocorticoid signalling in the development/maintenance of resistive, transporting epithelia in the renal collecting duct.

Taksaporn Tangwanchai[1], Struan Loughlin[1], Etang Collins Etang[1], Morag Milne[1], Morag Mansley[1]

[1]*University of St Andrews, St Andrews, United Kingdom*

Background: Tight junctions (TJs) are the most apical intercellular junctional complexes in epithelia. These demark apical and basolateral aspects of the plasma membrane, enabling vectoral transport of molecules. Within the epithelial monolayer lining the collecting duct (CD) of the kidney, the tightly regulated transcellular transport of Na^+ and H_2O critically maintains both the volume and osmolality of our circulating volume. Here, corticosteroid hormones modulate Na^+ transport, signalling *via* mineralocorticoid (MR) and glucocorticoid (GR) receptors. In a model of CD epithelia with deletion of the GR, preliminary electrophysiological measurements demonstrated attenuated transepithelial voltage (V_t) and resistance (R_t). This suggests a role of glucocorticoid signalling in the development and/or maintenance of TJs in the CD, though the specific TJ proteins involved remains unclear.

Aim: To assess the role of glucocorticoid signalling in the development of polarised and electrically resistive CD epithelia and determine which TJ proteins are involved.

Methods: Two experimental models were employed. Firstly, comparison of $mCCD_{cl1}$ murine CD cells [1] with *Nr3c1* deletion (GR knockout, GR-KO) with non-targeting controls (SHAM). Secondly, parental $mCCD_{cl1}$ cells grown in culture media with (DEX) or without (NO-DEX) the glucocorticoid dexamethasone. All cells were cultured on permeable supports for 9-11d, V_t and R_t were measured by epithelial volt-ohm-meter. RNA was extracted and expression of genes encoding TJ protein families: Zona occludens, Occludin, Claudins, Tricellulin and Angulins were quantified by qRT-PCR. SHAM and GR-KO cells on filters were labelled with antibodies against: GR, ZO-1, Claudin7 and Claudin8, and imaged using a Zeiss AxioScanZ1 slidescanner. Data are shown as mean±SD and statistical significance determined by Mann-Whitney or unpaired t-test, where appropriate.

Results: In GR-KO cells, R_t was negligible compared to SHAM cells after 9d, measuring 0.3±0.1 kΩ·cm^2 and 5.6±0.4 kΩ·cm^2, respectively (n=8, p<0.001). Similarly, V_t was greatly reduced compared to SHAM cells at 9d, measuring -0.9±0.6 mV and -28.0±11.1 mV, respectively (n=8, p<0.001). Interestingly, R_t remained unaltered in NO-DEX cells compared to DEX cells after 9d, measuring 2.5±0.5 kΩ·cm^2 and 2.3±0.3 kΩ·cm^2, respectively (n=6). V_t, however, was greatly reduced in NO-DEX cells compared to DEX cells after 9d, measuring -14.9±3.4 mV and -50.3±7.2 mV, respectively (n=6, p<0.01).

Across the panel of genes assessed, GR-KO cells had decreased *Tjp3*, *Cldn3*, *Cldn7*, *Cldn8* and *Ildr1* (n=8, p<0.05), but increased *Cldn1*, *Cldn2* and *Cldnd1* (n=8, p<0.01). NO-DEX cells exhibited decreased expression of *Tjp1*, *Tjp2*, *Tjp3*, *Cldn8*, *Cldn12* and *Ildr1* (n=8, p<0.05), but increased expression of *Ocln*, *Cldn2* and *Cldnd1* (n=8, p<0.01), compared to DEX cells.

Qualitative assessment of immunolabelled cells confirmed loss of nuclear GR but no change to lateral ZO-1 labelling in GR-KO cells (*n*=6). Furthermore, initial studies revealed lateral labelling of Claudin7 and 8 in SHAM cells was greatly reduced in GR-KO cells (*n*=2).

Conclusions: Together these data provide evidence that glucocorticoid signalling plays an important role in the development of polarised, transporting CD epithelia. Whilst a number of TJ genes were modified by loss of receptor or removal of ligand, Claudin7 and Claudin8 protein expression was modified, indicating their possible role in development/maintenance of V_t and R_t.

[1] Gaeggeler, H.P., et al. (2005) JASN 16: 878-891.

PCB035

Investigating novel transport mechanisms for aldosterone and the identification of putative corticosteroid transporters in the collecting duct of the kidney.

Morag Milne[1], Morag Mansley[1], Natalie Homer[2]

[1]University of St Andrews, St Andrews, United Kingdom, [2]The University of Edinburgh, Edinburgh, United Kingdom

Background: The kidney is responsible for the long-term control of blood pressure (BP) and this is achieved by maintaining total body Na^+ balance. The kidneys match Na^+ excretion with Na^+ intake with fine-tuning of Na^+ balance occurring in the collecting duct (CD). In response to decreased BP, the key volume-regulating corticosteroid aldosterone (ALDO) increases Na^+ reabsorption *via* the epithelial sodium channel (ENaC) by upregulating its expression and activity, driving fluid reabsorption and thus normalising BP. ALDO exerts its effects specifically in principal cells (PC) of the CD due to expression of the enzyme 11βHSD2 which inactivates the related hormone cortisol (CORT). Corticosteroids are typically thought to passively diffuse into target cells owing to their lipophilicity. However, preliminary studies in the lab have provided the first evidence that CORT may be actively transported in the CD. This study aimed to determine if ALDO is also actively transported in PCs and to identify which transporters may be responsible.

Methods: Murine cortical collecting duct cells ($mCCD_{cl1}$) were cultured on permeable supports for 9 days [1]. Cells were treated with ALDO (3nM, 3h) in the basolateral bath. Amiloride-sensitive ENaC-mediated Na^+ transport was assessed by measuring the equivalent short-circuit current. Samples of media were collected from the apical and basolateral baths and the monolayer lysed in 0.1% SDS. ALDO concentration was determined by solid-liquid phase (SLE) extraction and targeted LC-MS/MS analysis using an assay optimised to detect physiological concentrations of ALDO. The apical membrane was isolated from polarised $mCCD_{cl1}$ cells by biotin labelling and streptavidin pulldown. Isolation was validated by western blot using antibodies against streptavidin and α-ENaC. Unbiased proteomic analysis of the apical fraction was carried out by LC-MS/MS enabling assessment of changes in protein expression in response to ALDO.

Results:

The stimulatory effect of ALDO on ENaC activity was confirmed where ALDO increased I_{eq} by -3.0±1.3 $\mu A \cdot cm^{-2}$ after 3h compared to control, where the change in I_{eq} was 0.1±0.2 $\mu A \cdot cm^{-2}$. Interestingly, after 3h, ALDO was unevenly distributed across the monolayer of cells. 16.5±2.8% was detected in the apical bath, 72.3±10.2% detected in the basolateral bath, and a small proportion 2.7±1.1% in cell lysates (n=6-9).

Following separation of the apical membrane from the remaining protein lysate (supernatant) in vehicle or ALDO-treated cells, streptavidin was detected in the apical fraction but not the

supernatant, confirming successful isolation (*n*=2). α-ENaC was also detected in both fractions, the presence in the apical fraction correlating with functional channel activity. Subsequent proteomic analysis of the apical membrane detected a total of 3188 proteins. Changes in expression of 9 members of the ABC and SLC transporter superfamilies was seen in response to ALDO treatment; 6 up-regulated and 3 down-regulated.

Conclusions: Together these data suggest an active mechanism contributes to ALDO transport into and/or out of PCs of the CD. This has important implications for the control of ALDO bioavailability within target PCs, and may present a possible therapeutic target. Ongoing work is being carried out to interrogate which transporter(s) are responsible.

PCB036

TRPV4 and chloride channels: Ion movement in relation cerebrospinal fluid production

Verayna Newland[1], Bonnie Blazer-Yost[1], Cameryn Davis[1]

[1]*Indiana University Indianapolis, Indianapolis, United States*

Introduction: Hydrocephalus is a disease caused by an overproduction of cerebrospinal fluid (CSF), blockage of flow, or decreased reabsorption. When CSF accumulates in the brain it causes ventriculomegaly, increased intracranial pressure, inflammation, and cell damage. The choroid plexus within the brain's ventricles consists of a fenestrated capillary network surrounded by an epithelial monolayer. This tissue produces CSF. Choroid plexus epithelial cells (CPe) are polarized, meaning that the ion channels are located apically (CSF-facing) or basolaterally (blood-facing) and regulation of these channels is responsible for the composition and production of CSF. Some notable channels include transient receptor potential vanilloid 4 (TRPV4), calcium-activated chloride channel (TMEM16A), cystic fibrosis transmembrane conductance regulator (CFTR), and Na+/Cl- co-transporter (NCC). Activation of TRPV4, a nonselective cation channel that is osmo-, shear-, temperature-, and pressure-sensitive, allows Ca2+ and Na+ influx into the CPe which, secondarily, causes transepithelial electrolyte flux that involves multiple electrolyte transporters. In Tmem67-/- rats, a genetic form of hydrocephalus was reversed with TRPV4 antagonist treatment [1]. TMEM16A and CFTR are located basolaterally on the CPe while NCC is apical. Interestingly, patients with posthemorrhagic hydrocephalus (PHH) have elevated Cl- levels in their CSF [2]. This could be caused by an interaction of blood components with chloride channels. We investigated hemoglobin, a major protein found in red blood cells.

Aims: The goal of this study was to determine if there was intercellular signaling between activated TRPV4, TMEM16A, CFTR, and NCC. By investigating the role of these channels in the CPe, we aim to understand the regulation of CSF production in normal and pathophysiological states. Additionally, we investigated the role of hemoglobulin as a potential pathological factor in hydrocephalus development.

Methods: Human choroid plexus papilloma (HIBCPP) cells were grown in Dulbecco's modified eagle media (DMEM) with sodium bicarbonate, 10% fetal bovine serum, 1% penicillin/streptomycin, and 5 ng/L insulin. Ussing-style electrophysiology was used to measure net transepithelial electrolyte flux and transepithelial permeability in the cultures. To determine the relationship between the ion channels, cells were pre-treated with the following compounds and concentrations: Ani9 10 uM (TMEM16A inhibitor), FeCl3 10 nM (TMEM16A activator), CFTR Inhibitor 172 5 μM, metolazone 0.2 mM (NCC inhibitor), and bovine hemoglobulin 140 mg/mL . Compounds were added apically, basolaterally, or bilaterally to determine polarity. 10 minutes after effector treatments, TRPV4 agonist GSK1016790A (GSK) was used to stimulate the influx of Ca2+ and Na+ into the cells. Each drug treatment group (n=6) was analyzed for statistical significance with a multiple T-test.

Results: TMEM16A activation or inhibition substantially altered the complex, multiphase transepithelial ion flux that is activated in response to TRPV4 agonist stimulation. When CFTR was inhibited basolaterally, the membrane permeability increased. NCC inhibition had no significant

effect. Hemoglobulin treatment potentiated the agonist-stimulated transepithelial ion flux and increased conductance.

Conclusion: There is a relationship between TRPV4 and chloride channels. By investigating these interactions, we hope to understand PHH pathophysiology and identify drug targets for non-invasive hydrocephalus treatments.

1. Hochstetler, A.E. et al. (2020). Jci Insight 5, 1-14. 2. Otun A. et al (2021). Fluids and Barriers of the CNS 18, 1-14.

PCB037

Functional analysis of gene-edited CF variant G542X.

Isabelle Rose[1], Lucia Nicosia[2], Miriam Greenwood[3], Kader Doran-Cavusoglu[2], Mathew Biggart[4], Patrick Harrison[2], Stephen Hart[3], Robert Tarran[4], Deborah Baines[1]

[1]St George's University of London, London, United Kingdom, [2]University College Cork, Cork, Ireland, [3]UCL Great Ormond Street Institute of Child Health, London, United Kingdom, [4]Kansas City University Medical Centre, Kansas City, United States

The Cystic Fibrosis (CF) causing variant G542X (**G**GA>**T**GA) results in premature termination of translation of the cystic fibrosis transmembrane regulator (CFTR) protein, and nonsense-mediated decay of the CFTR mRNA resulting in almost complete loss of functional CFTR protein expression. This leads to defective anion transport and the development of CF disease pathology. Currently available CF modulator therapies cannot be used to treat this variant, but an Adenine Base Editor (ABE) and guide RNA combination can convert the G542X stop codon to G542R, a variant which retains about 30% of WT activity[1] and is amenable to CFTR triple modulator therapy (Elexacaftor-Tezacaftor-Ivacaftor ETI).

Plasmid DNA encoding this ABE and guide RNA with GFP were encapsulated in lipid-based nanocomplexes, which have reduced immunogenicity and high cellular uptake, and were delivered to human airway epithelial cells (HAECs) harboring the G542X CFTR variant. Transfected cells were identified by analysing GFP fluorescence. Ion transport was measured as short circuit current (Isc) across resistive epithelial monolayers. Cultures were equilibrated using standard physiological salt solution before addition of pharmacological drugs, forskolin, 10 μM (bilateral) to activate CFTR; CFTRInh-172, 10 μM (apical) to inhibit CFTR; and ouabain, 100 μM (basolateral) to inhibit Na^+K^+ATPase activity. Airway Surface Liquid (ASL) height was visualised using Texas-red dextran as a soluble fluorescent label of volume, and perfluorocarbon-77 to prevent fluid evaporation. CFTR was activated using vasoactive intestinal peptide (VIP)(100 nM, basolateral), and changes were calculated from *XZ* scans taken at regular intervals. ASL pH was measured using pHrodo-dextran pH-sensitive fluorescent labelling normalised to a pH-insensitive (pHins) *in situ* control.

48 hours post transfection, next-generation sequencing showed 17% of alleles had been edited from G542X to G542R. Isc measurements showed that even as little as 17% of editing restored CFTR activity to ~ 60 % that of normal levels when in combination with modulators. CFTRInh-172 inhibitable current was ~ four-fold greater in ETI treated G542R compared to G542X samples (Table 1; p=0.015, n = 6). Transfected cells were sorted using fluorescence-activated cell sorting (FACS) to concentrate the population of edited cells (henceforth called edited and sorted). CFTRInh-172 inhibitable Isc was not significantly different to that of wild-type samples (p = 0.97; n = 6, N = 2). VIP stimulated changes in ASL height indicated that edited and sorted cell monolayers displayed wild-type like airway hydration (Table 1). Additionally, VIP stimulated changes in ASL pH were positively correlated to the proportion of G542R cells, suggesting that bicarbonate transport was also being restored by correction of G542X to G542R CFTR protein.

This data provides proof-of-concept for restoration of anion transport by gene editing of G542X.

[1] Xue, X. et al. Hum Molec Gen. 2017; 26 (16), 3116–3129.

PCB038

Altered voltage-gated ion channel expression around drusen accumulations in induced pluripotent stem cell model of age-related macular degeneration.

Molly Rowland[2], Majlinda Lako[1], Marzena Kurzawa-Akanbi[1], Gerrit Hilgen[1,2]

[1]Biosciences Institute, Faculty of Medical Sciences, Newcastle University, Newcastle, United Kingdom, [2]Applied Sciences, Faculty of Health and Life Sciences, Northumbria University, Newcastle, United Kingdom

Age-related macular degeneration (AMD) is one of the leading causes of irreversible blindness globally and is associated with increasing prevalence and socioeconomic burden. As a result, additional treatment avenues are under constant investigation. AMD can be characterised into a wet or dry form; wet AMD involves the formation of a pathological neovascular membrane that results in the accumulation of subretinal fluid and/or haemorrhaging and dry AMD is characterised by the presence of protein and lipid deposits, known as drusen, that form beneath the retinal pigment epithelium (RPE). Although wet AMD results in a sudden, severe loss of vision, treatment options are available. Dry AMD is slow progressing and has a high conversion rate into wet AMD before reaching end stage disease. The exact cause of AMD is unknown, although it is thought to originate within the RPE and is multi-factorial with both genetic and environmental factors playing a role. An overlooked potential contributing mechanism to AMD is the dysfunction of ion channels, or channelopathies, with their involvement in AMD pathophysiology being poorly understood.

Induced pluripotent stem cell (iPSC) derived RPE can be used to model AMD, both low (control) and high-risk lines were stained for pan markers of voltage-gated sodium channels (Nav) alongside key RPE cell markers such as CRALBP and ZO1. Early experiments show that Nav is expressed in the cell membrane of iPSC RPE, aligned with Z0-1, a tight junction protein (data obtained from three 24-well inserts). Additionally, drusen were identified using antibodies against complement proteins C3b and C5b-9. Initial data has shown altered Nav localisation relative to drusen formations, with less homogenous and more numerous Nav staining in the high-risk lines (data obtained from six low-risk and six high-risk 12-well inserts). Further experiments will confirm and quantify these fundings, including a physiological characterisation of these ion channels in AMD.
Funding for this project has been received from the Academy of Medical Sciences (GH) and the ECR support Northumbria University. Acknowledgement goes to Northumbria Microscopy Lab for their exceptional service and support during the project.

PCB039

Exploring the metabolic fate of adenine in adenine-induced chronic kidney disease in mice

Jasmine Atay[1], Søren Elsborg[1], Johan Palmfeldt[1], Rikke Nørregaard[1]

[1]*Department of Clinical Medicine, Aarhus University, Aarhus, Denmark*

Animal models of chronic kidney disease (CKD) are crucial for understanding the disease, its pathogenesis, and for developing new treatments. The adenine-induced CKD model offers a non-surgical approach to studying CKD pathogenesis. At physiological concentrations, adenine is metabolised to AMP through adenine phosphoribosyl transferase, serving as a precursor for several adenine derivatives, and is ultimately metabolised to uric acid and excreted by the kidneys. However, at supraphysiological doses, adenine follows an alternative pathway, resulting in the formation of 2,8-dihydroxyadenine (2,8-DHA). Due to its limited solubility in urine, 2,8-DHA precipitates as crystals and deposits within the renal tubules, leading to tubulointerstitial injury. This study investigates kidney injury and fibrosis at 2 and 4 weeks of adenine-feeding, while also measuring plasma and urine levels of adenine metabolites to investigate the molecular fate of adenine.

To induce CKD, 8-week-old C57BL/6J mice were fed a diet enriched with 0.2% adenine. Mice were grouped randomly into three categories: control (n=11), 2-week adenine diet (n=8) and 4-week adenine diet (n=8). At sacrifice, anaesthesia was induced with 5% sevoflurane and maintained at 3–4%. Blood was collected and immediately after both kidneys were excised and cortical tissue was isolated for subsequent RNA analysis. Mice were euthanised by cervical dislocation. Plasma and urinary metabolites were analysed by LC-MS and compound identification was performed using the mzLogic Data Analysis Algorithm (Compound Discoverer Software, Thermo Scientific). Statistical analyses were performed using a one-way ANOVA, followed by Tukey's multiple comparisons test. $p<0.05$ was considered significant.

Following 2 weeks of adenine feeding, kidney injury, as measured by plasma creatinine, blood urea nitrogen and cortical hepatitis A virus cellular receptor 1 (*Havcr1*) mRNA expression, was significantly increased compared with the control group. Additionally, fibrosis markers, fibronectin (*Fn1*), collagen type 1 (*Col1a1*) and transforming growth factor-β (*Tgfb1*) mRNA expressions were significantly increased compared with control. Unexpectedly, extending adenine feeding to 4 weeks resulted in significant reduction of both kidney injury and fibrosis markers compared to 2 weeks. These markers remained significantly elevated compared to control, except for Havcr1 expression, which had returned to control levels at 4 weeks.

Following 2 weeks of adenine feeding, plasma levels of adenine and 2,8-DHA were elevated compared to the control group, but at 4 weeks, these levels had returned to control levels. Interestingly, plasma concentrations of other adenine metabolites, such as inosine, hypoxanthine, guanine, and uric acid, were higher at 4 weeks compared to 2 weeks. In contrast, urinary levels of adenine and 2,8-DHA increased following 2 weeks of adenine feeding and remained elevated at 4 weeks compared to control levels.

The adenine-enriched diet resulted in significant increase in markers of renal injury and fibrosis within 2 weeks, which showed a noteworthy decrease at 4 weeks. Analysis of plasma metabolites revealed that adenine and 2,8-DHA levels were reduced at 4 weeks, suggesting an adaptive response in adenine metabolism over time, which could explain the less severe kidney injury and fibrosis observed at 4 weeks. We are currently further exploring these mechanisms by investigating the expression levels of enzymes involved in adenine metabolism.

PCB040

Physiological network mapping predicts survival in critically ill patients with sepsis

Emily Ito[1], Tope Oyelade[1], Alireza Mani[1]

[1]Network Physiology Lab, Division of Medicine, University College London (UCL), London, United Kingdom

Introduction: Sepsis is a life-threatening condition in which dysregulated host response to infection leads to multiorgan failure. Early detection of deterioration in sepsis is key to improving overall patient outcomes. Studies investigating complex disorders using a network physiology approach have shown a distinct pattern of organ system connectivity between different patient populations with positive and negative disease outcomes. Physiological network mapping is not currently used in intensive care units. This study used a parenclitic network approach to compute organ connectivity for individual patients with sepsis using records of routine laboratory test results.

Aims/objectives: The goal of this study was to investigate whether analysing organ connectivity in individual patients with sepsis using a parenclitic network could predict the deterioration and mortality of sepsis patients.

Method: Electronic patient records from 162 patients with sepsis were obtained from the MIMIC-III database (Ethics IRB protocol nos. 2001P001699). Patients were studied retrospectively, and clinical data on 48-hour deterioration and 30-day survival were obtained. Fifteen physiological variables (serum phosphate, arterial pH, urea, haemoglobin, lactate, white blood cell count, serum sodium, international normalized ratio, platelets, total bilirubin, blood glucose, serum creatinine, alanine transaminase, bicarbonate, and serum potassium) representing different organ systems were extracted from the laboratory data. Correlation analysis of physiological variables was performed to study the pattern of interaction between patient groups with different outcomes (i.e., survivors versus non-survivors). The parenclitic network investigated organ connectivity in individual patients by examining how individual patient data deviated from the characteristics of organ relationships established in a reference population (survivors). Parenclitic deviations were computed for everyone, and Cox regression was used to investigate if parenclitic deviations could predict 48-hour deterioration and 24-hour survival in sepsis patients.

Results: Correlation analysis identified 7 and 9 pairs of unique correlations in physiological variables that were significantly different between survivors and non-survivors for 30-day survival and between deteriorated and non-deteriorated patients for 48-hour deterioration, respectively. Parenclitic deviations for the pH-bicarbonate axis (hazard ratio = 2.081, $p < 0.001$) and pH-lactate axis (hazard ratio = 2.773, $p = 0.024$) were able to significantly predict 30-day mortality in sepsis patients independent of the measures of organ dysfunction severity, SOFA, and ventilation status. None of the parenclitic deviations were able to predict 48-hour deterioration.

Conclusions: Investigating organ connectivity in individual patients using parenclitic network analysis significantly predicted 30-day mortality in sepsis population. Parenclitic deviation may

potentially offer useful insight into pathophysiology of sepsis and give useful insight into different physiological response towards sepsis between survivors and non-survivors.

PCB042

Comparative study of systemic and local delivery of mesenchymal stromal cells for the treatment of chronic kidney disease

Jean-Claude Kresse[1], Emil Gregersen[1], Anders Toftegaard Boysen[1], Peter Nejsum[1], Rikke Nørregaard[1]

[1]*Department of Clinical Medicine, Aarhus University, Aarhus, Denmark*

Introduction:
Renal fibrosis is a hallmark of chronic kidney disease (CKD), characterized by excessive inflammation and fibrosis, and contributes significantly to progressive renal dysfunction. There is a pressing need for effective anti-fibrotic interventions, an area where options are lacking. One such promising treatment method is the employment of cell therapy with mesenchymal stromal cells (MSCs). MSCs have shown promise as anti-inflammatory and immunomodulatory agents, making them a promising opportunity for intervention. This study investigates two critical factors influencing treatment specificity 1) delivery methods as well as 2) preconditioning of adipose tissue derived MSCs, for the treatment of CKD-associated renal fibrosis.

Methods:
We investigated the effects of proinflammatory preconditioning on MSCs and their derived secretome using an *in vitro* fibrosis model. To this end, conditioned medium (CM) was collected from either preconditioned MSCs (Pr-MSCs) treated with TNF-α and IFN-γ or vehicle, or naïve MSCs. Furthermore, CM was processed using size exclusion chromatography, a soluble protein (SP) fraction and an extracellular vesicle (EV) fraction collected and employed in TGF-β stimulated HKC-8 cells. Analysis of gene expression of inflammatory and fibrotic markers was carried out using qPCR.

Additionally, *in vivo* experiments were conducted using a murine unilateral ureteral obstruction (UUO) model of CKD to evaluate the therapeutic efficacy of systemic versus local administration of preconditioned MSCs and their EVs. For this, C57BL/6j mice were anesthetized with isoflurane by inhalation and the left kidneys surgically obstructed with silk ligature or SHAM operated. Mice were concurrently treated with either local (subcapsular) or systemic (tail vein) delivered Pr-MSCs. Mice were sacrificed by collecting blood through the heart under anesthesia after five days. Analysis on gene expression levels with qPCR as well as immunohistochemical analyses and cytokine multiplex (V-PLEX Mouse Cytokine 19-plex, Meso Scale Diagnostics) screening of inflammatory cytokines were carried out.

Results:
Pr-MSC derived CM and SP demonstrated significant antifibrotic effects *in vitro*, reducing expression of fibrotic markers fibronectin ($n=6$, $p<0.05$) and collagen type 1α1 in TGF-β-stimulated HKC-8 cells ($n=6$, $p<0.05$) compared to vehicle-treated cells. EVs did not replicate these effects when compared to vehicle-treated cells ($n=6$, $p>0.05$), suggesting that SPs secreted by Pr-MSCs may be the primary mediators of antifibrotic effects. In vivo, both systemic and local delivery of Pr-MSCs were explored in a murine UUO model. Local administration of0020 showed a more pronounced impact on the cytokine profile of UUO compared to systemic administration.

Particularly, local administration resulted in the upregulation of the mRNA of the inflammatory cytokine IL-10 ($n=6$, $p<0.05$) indicating anti-inflammatory properties of locally delivered Pr-MSCs *in vivo*. Additionally, local delivery, but not systemic delivery, showed a reduction in the number of myofibroblasts, as shown by decreased staining of the myofibroblast marker α-smooth muscle actin, compared to vehicle-treated UUO mice ($n=5$, $p=0.059$).

Conclusion:
This study provides critical insights into the therapeutic efficacy of MSCs and emphasizes the importance of delivery methods and preconditioning strategies in enhancing MSC-based therapies for renal fibrosis. Further optimization of MSC delivery strategies and mechanistic elucidation is warranted to fully exploit their potential in treating CKD.

PCB043

Physiologic responses during exertional heat strain following 34-39h complete caloric restriction.

Toby Mundel[1], Huixin Zheng[2], Chung-Yu Chen[3], Claire Badenhorst[4]

[1]Brock University, St. Catharines, Canada, [2]University of Otago, Wellington, New Zealand, [3]University of Taipei, Taipei, Taiwan, Province of China, [4]Massey University, Auckland, New Zealand

Complete caloric restriction is common to most humans. Whether characterised by regular religious practise, a surgical patient's perioperative period or the trend of intermittent fasting for health (e.g., periodic fasting, time-restricted feeding) a large proportion of the global population experiences caloric restriction. These examples often accompany physical activity for sport, exercise, or occupation. Whilst the separate and combined effects of caloric restriction and exercise have been studied for several physiological consequences, few investigations have investigated the thermoregulatory outcomes. Previous research demonstrated that 48h of caloric restriction in both men and women increased metabolic rate and peripheral blood flow such that core temperature was reduced when subjected to cold stress. To our knowledge, no study has determined this for heat stress, the purpose of the current study.

Eight healthy and recreationally active adults (4 female, age: 31±8 y, weight: 69±15 kg, body fat: 15±8%, VO_2max: 3.8±1.1 L·min^{-1}) performed two treadmill trials in a heat chamber (30°C, 40% RH) that consisted of consecutive 20 min bouts at 40% (5.7±0.6 km·h^{-1}) and 70% (10.0±1.0 km·h^{-1}) of their individually-determined ventilatory threshold. Both trials were scheduled at ~10am and followed either 34-39h of complete caloric restriction or their usual diet. Measures of gastro-intestinal temperature (T_{gi}), heart rate (HR), blood pressure (MAP), skin blood flow (SkBF, laser Doppler flowmetry), fluid loss (body weight change) and sweat rate (technical absorbent), expired gases, urine specific gravity (USG) and blood biochemical markers were taken. Descriptive data are provided as mean±SD, with all analyses conducted using SPSS software for Windows and significance accepted at $p<0.05$. Data were analysed using either a paired samples *t*-test or ANOVA for repeated measures.

Baseline resting data for T_{gi}, HR, MAP, SkBF, USG and body weight were not different between trials ($p\geq0.22$), whilst caloric restriction decreased blood glucose (4.7±0.3 vs. 5.4±0.3 mmol·L^{-1}, $p<0.01$) and insulin (28±15 vs. 89±53 pmol·L^{-1}, $p<0.01$) and increased free fatty acids (0.6±0.2 vs. 0.3±0.2 mEq·L^{-1}, $p<0.01$). Participants were exercising at 34±4 and 78±10 VO_2max respectively, with no difference between trials ($p=0.60$); although caloric restriction reduced the respiratory exchange ratio (0.77±0.04 vs. 0.81±0.03 a.u., $p=0.02$). Exercise increased T_{gi} (Δ1.2±0.3 °C, $p<0.01$) reaching 38.5±0.4 °C with no difference between trials ($p=0.56$). Water consumed (0.35±0.43 L·h^{-1}, $p=0.62$), whole-body sweat loss (0.66±0.35 kg·h^{-1}, $p=0.32$) and local sweat rate (0.60±0.28 mg·min^{-1}·cm^{-1}, $p=0.16$) were not different between trials. Exercise increased SkBF and decreased MAP (both $p<0.01$) with no difference between trials (both $p>0.60$). Exercising HR continued to increase ($p<0.01$) and was higher with caloric restriction (Δ3±3 beats·min^{-1}), reaching 90±8% VO_2max.

Complete caloric restriction lasting 34-39h had minimal physiologic impact during 40 min of exertional heat strain, with only heart rate mildly increased.

PCB044

Application of physiological network mapping in the prediction of survival in critically ill patients with acute liver failure

Tope Oyelade[1,4], Kevin Moore[2], Ali R. Mani[3,4]

[1]Institute for Liver and Digestive Health, Division of Medicine, UCL, London, United Kingdom,
[2]Institute for Liver and Digestive Health, Division of Medicine, UCL, London, United Kingdom,
[3]Institute for Liver and Digestive Health, Division of Medicine, UCL, London, United Kingdom,
[4]Network Physiology Laboratory, UCL Division of Medicine, London, United Kingdom

Background: Reduced functional connectivity of physiological systems is associated with poor prognosis in critically ill patients. However, physiological network analysis is not commonly used in clinical practice and needs further validation. Acute liver failure (ALF) is associated with multiorgan failure and mortality. Prognostication in ALF is highly important for clinical management but is currently dependent on models that do not consider the interaction between organ systems. This study aims to examine the impact of physiological network analysis in prognostication of patients with ALF.

Methods: Data from 640 adult patients admitted to the intensive care unit (ICU) for paracetamol-induced ALF between 2001 and 2012 were extracted from the MIMIC-III database. Parenclitic network analysis was performed on patients' routine biomarkers and network clusters were identified using the k-clique percolation method. Statistical analysis was performed to predict the 28-day survival of patients independent of their sequential organ failure assessment (SOFA) score and King's College Criteria.

Results: There is higher organ system disconnection in non-survivals compared with survivals with a shift toward acidosis. pH regulation was respectively directed toward renal function and respiratory functions in survivors and nonsurvivors (Figure 1). Parenclitic deviation along the blood pH and serum creatinine (HR(hazard ratio) = 187.08, $p = 0.001$), blood pH and bicarbonate (HR = 78.94, $p < 0.001$), lactate and glucose level (HR = 1.10, $p < 0.001$), lactate and heart rate (HR = 1.09, $p < 0.001$), as well as oxygen saturation (SpO2) and respiratory rate (HR = 1.13, $p = 0.018$) axes, predicted ICU mortality independent of SOFA. The addition of the parenclitic network indices significantly improved the prognostic value of SOFA.

Conclusion: These results demonstrate that network analysis can provide pathophysiologic insight and predict survival in critically ill patients with paracetamol-induced ALF

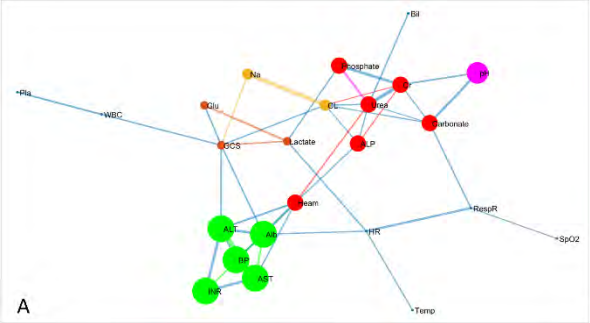
Bil
Na
Phosphate
Cr
pH
Plq
WBC
Glu
Cl
Urea
Carbonate
GCS
Lactate
ALP
Haem
RespR
ALT
Alb
HR
SpO2
BP
AST
INR
Temp
A

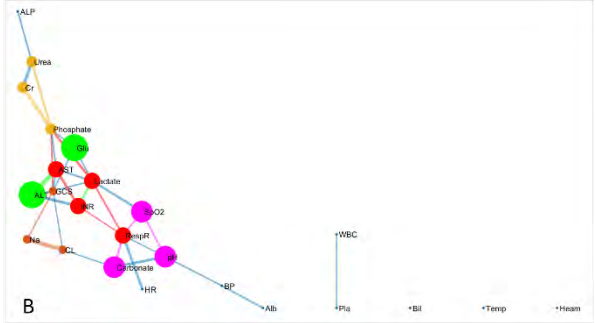
ALP
Urea
Cr
Phosphate
Glu
AST
Lactate
Alb
GCS
Haem
SpO2
RespR
Na
Cl
pH
Carbonate
HR
BP
Alb
WBC
Plq
Bil
Temp
Haem
B

PCB045

Intra- and inter-session reliability and repeatability of proton magnetic resonance spectroscopy for quantifying total creatine levels in multiple human brain regions

Jedd Pratt[1], James McStravick[1], Aneurin Kennerley[1], Craig Sale[1]

[1]*Department of Sport and Exercise Sciences, Manchester Metropolitan University Institute of Sport, Manchester, United Kingdom*

Introduction: Creatine (Cr) dynamics within the human brain is a research area with promising clinical value, particularly for cohorts exposed to metabolically demanding periods (*e.g.,* ageing, neurological diseases, sleep deprivation). Consequently, increasing reliance will be placed upon proton magnetic resonance spectroscopy (^{1}H-MRS) for determining total creatine (tCr) concentrations in the brain. Importantly, however, before data from experimental studies can be accurately interpreted, more consideration should be given to the inherent sources of error in ^{1}H-MRS, and their effect on the reliability of repeated measurements. This need is underscored by weaknesses in the design of existing studies, and ultimately, by large margins of error in repeated ^{1}H-MRS reported to date. Herein, we examined the intra- and inter-session reliability and repeatability of ^{1}H-MRS for quantifying tCr concentrations in multiple brain regions (midbrain: MB; visual cortex: VC; frontal cortex FC).

Methods: Eighteen healthy adults aged between 20-32 years were recruited for this study [mean age=25.8±3.0years; 50% female; n=14 intra-session analysis; n=15 inter-session analysis (n=11 both)]. MR imaging and ^{1}H-MRS (PRESS) were performed on a 3T Siemens scanner using a 20-channel head coil. Intra-session analyses involved repeated measurements of the MB, VC and FC without removing the participant from the scanner, while inter-session analyses involved repeated measurements from the same regions, but with a brief break between measurements (involving repositioning of the participant and voxels). TARQUIN was used to analyse ^{1}H-MRS data, and water unsuppressed data were used to determine absolute tCr concentrations. Paired t-tests, minimum detectable change (MDC), Pearson's correlation coefficient (r), coefficient of variation (CV), intra-class correlation coefficient (ICC) were calculated. Bland-Altman plots were generated to visually assess the data.

Results: A total of 174 spectra were acquired, including 84 for intra-session analyses and 90 for inter-session analyses. No significant differences in absolute tCr concentrations between repeated intra- or inter-session measurements were shown in any region (mean differences=0.1-1.2%). Intra- and inter-session r values were between 0.909-0.985 and 0.836-0.858 (all $p<0.001$), depending upon region, and no trends in measurement bias were found. For the MB, VC and FC, intra-session CVs were 1.7%, 0.8% and 2.1%, ICCs were 0.903 (95%CI=0.727-0.968), 0.979 (95%CI=0.935-0.993) and 0.921 (95%CI=0.772-0.974) (all $p<0.001$), and MDCs were 1.2%, 0.6% and 1.5%, while inter-session CVs were 2.7%, 1.7% and 2.7%, ICCs were 0.835 (95%CI=0.578-0.941), 0.854 (95%CI=0.619-0.948) and 0.847 (95%CI=0.603–0.946) (all $p<0.001$), and MDCs were 1.9%, 1.2% and 1.9%. Inter-region differences in tCr concentration of up to 20.7% were shown.

Conclusions: Our findings indicate that ^{1}H-MRS at 3T can reliably and repeatably quantify absolute tCr concentrations in multiple human brain regions, when appropriate consideration is given to

potential sources of error. Changes in tCr concentration as small as 2% may be discernible from measurement error, however, centre-specific margins of error should be established prior to experimental investigation. More studies are required to determine whether similar findings are shown in other populations of interest, such as people suffering from neurological diseases or movement disorders.

Ethical statement: Manchester Metropolitan University's research ethics committee granted ethical approval and all participants provided written informed consent.

PCB046

Verification of the effectiveness and safety of serpentine-containing arm supports

Yoshinori Sato[1], Jun Hirayama[4], Naotoshi Sugimoto[3]

[1]Komatsu University, Komatsu, Japan, [2]Kanazawa University, Kanazawa, Japan, [3]Kanazawa Universty, Kanazawa, Japan, [4]Komatsu University,, Komatsu, Japan

Research Background and Objectives

In ancient Japan, warm stones ("*onjaku*") were used to warm the body during cold weather. *Onjaku* retains heat well and is considered the prototype of modern portable heat pads. Talc, pagodite, serpentinite, and hornblende were suitable for this purpose. We created arm supporters from serpentine-containing fibers and examined their effectiveness and safety.

Participants and Methods

Participants were young, healthy Japanese adults who were asked to enter a 25 °C room and stay there for approximately 30 min. The arm support was worn for 30 min, and we measured forearm temperature and the median venous vessel diameter of the forearm before and after wearing the arm support. Data are presented as means ± standard errors. A $p < 0.05$ indicated statistical significance. All research experiments were approved by the Ethics Committee of Komatsu University (approval number IRIN2219-2).

Results

We recruited ten Japanese female undergraduate students (age: 20.3 ± 0.2 years, body mass index: 20.4 ± 0.6 kg/m^2). No adverse events, such as burning, redness, and swelling, or complaints of discomfort occurred during or after the 30-min period where the arm support was worn. We observed significant increases in forearm temperature (32.47 ± 0.29 °C to 34.59 ± 0.32 °C) and in median venous vessel diameter (2.65 ± 0.2 mm to 3.56 ± 0.14 mm) while the arm supporter was worn.

Discussion

Warming devices, such as modern disposable heat pads, often lead to burns and dermatitis. In this study, we used non-self-heating arm supports, which are considered extremely safe. Wearing the serpentine-containing arm supports for 30 min did not cause any adverse events, thus demonstrating their safety.

Moreover, we observed an increase in skin temperature and dilation of the median vein owing to the use of arm supports. Because the median vein is usually targeted during blood collection and infusion, increasing venous dilation might be beneficial for collecting blood or placing an intravenous line. Our novel, serpentine-containing arm supports have the potential for implementation in clinical practice.

Conclusion

Our results confirm the heat retention properties and safety of serpentine-containing arm supports.

Sato Y, Hirayama J, Sugimoto N (2023): Safety and heat retention of arm warmers made of serpentine-containing fibers. J Well Health Care 47, 9-14.

PCB047

Exploring skin blood flow signals with the wavelet transform

Henrique Silva[1,2,3], Carlota Rezendes[2]

[1]Research Institute for Medicines (iMed.ULisboa), Faculdade de Farmácia, Universidade de Lisboa, Av. Prof. Gama Pinto, 1649-003, Lisbon, Portugal, [2]Department of Pharmacy, Pharmacology and Health Technologies, Faculdade de Farmácia, Universidade de Lisboa, Av. Prof. Gama Pinto, 1649-003, Lisbon, Portugal, [3]Biophysics and Biomedical Engineering Institute (IBEB), Faculdade de Ciências, Universidade de Lisboa, Campo Grande, 1749-016, Lisbon, Portugal

The wavelet transform (WT) is an analytical tool that allows the decomposition of complex physiological signals into their respective spectral components, showing better performance than the fast Fourier transform. WT has been extensively applied to many physiological time series, including perfusion signals, where it has contributed to a deeper understanding of the underlying mechanisms of flowmotion regulation. However, there is a considerable heterogeneity in terms of application of the WT among different authors, which often leads to highly different conclusions regarding the same physiological mechanism. Our objective was to test different approaches regarding the application of WT to skin blood flow signals during a classic maneuver to evoke the venoarteriolar reflex (VAR). In particular, we aimed to clarify whether the characteristics of the original signal influenced the WT output and its interpretation. Fifteen healthy subjects (22.4 ± 5.2 y.o.) participated in this study after giving informed consent. After acclimatization, subjects performed a protocol to evoke VAR on the upper limb while sitting upright – 7 min resting with both arms at heart level (phase I), 5 min with one random arm (i.e., test limb) placed 40 cm below heart level (VAR, phase II) and 7 min recovery in the initial position (phase III). Skin blood flow was assessed in the index finger of the test limb with photoplethysmography (PPG). From the raw PPG signals (PPGr), two new time series were created – (1) PPG amplitude over time (PPGa) and (2) pulse over time (PPGp). All three signals were then processed with the wavelet transform (WT) and decomposed into their respective spectral components. For all WT spectra the dominant frequency and amplitude ratio of each major component were assessed. Both parameters were statistically compared between phases and between signals with the Wilcoxon test for related samples ($p<0.05$). The PPGr and PPGa spectra showed the same components (cardiac, respiratory, myogenic, endothelial NO-dependent and endothelial NO-independent) in regions with similar dominant frequencies. In contrast, the PPGp spectra only showed components in regions consistent with the cardiac, respiratory and sympathetic activity. The amplitude ratios of the low frequency components (myogenic, sympathetic, endothelial) were significantly different between the PPGr and PPGa spectra during all phases of the protocol. Our results show that although highly valuable as an analytical tool, the WT shows considerable different outputs to different signals, especially in the low frequency components. This suggest that different WT analytical approaches could be considered to extract different information from the same physiological signal.

PCB048

Assessing superficial vein topography with a near-infrared vein finder – a pilot study

Henrique Silva[1,2,3], Carlota Rezendes[2]

[1]Research Institute for Medicines (iMed.ULisboa), Faculdade de Farmácia, Universidade de Lisboa, Av. Prof. Gama Pinto, 1649-003, Lisbon, Portugal, [2]Department of Pharmacy, Pharmacology and Health Technologies, Faculdade de Farmácia, Universidade de Lisboa, Av. Prof. Gama Pinto, 1649-003, Lisbon, Portugal, [3]Biophysics and Biomedical Engineering Institute (IBEB), Faculdade de Ciências, Universidade de Lisboa, Campo Grande, 1749-016, Lisbon, Portugal

The study of vessel topography is highly relevant in vascular physiology since it can have a considerable effect in hemodynamics. Furthermore, vascular abnormalities or dysmorphic features are present in several cardiovascular disorders. Branching regions of vascular trees are common sites for dysfunctional blood flow patterns due to well-known biophysical factors. Several imaging technologies are useful to assess vascular topography, although their high cost limits their use in experimental physiology. In the last decade the so-called portable “vein finders” were introduced and their popularity has been considerably increasing. These devices use near-infrared or visible light to improve the contrast of superficial veins and facilitate their detection for venipuncture. However, their potential has been underexplored in vascular physiology. This pilot study aimed at quantitatively describing the branching topography of the superficial veins of the hand dorsum using a low-cost near-infrared vein finder. Five healthy subjects (25.5 ± 5.2 y.o.) participated in this study after giving informed consent. While sitting upright and with both hands at heart level, an image of each hand dorsum was obtained from each subject. From these images 30 bifurcating superficial veins were assessed using ImageJ®, which allowed the calculation of several branching parameters (branching angle, branching coefficient, angular asymmetry, area ratio, optimality ratios, length-to-diameter ratio, junctional exponent deviation). Linear correlations between these parameters were tested with the Spearman coefficient ($p<0.05$). Significant positive correlations were detected between the branching coefficient and area ratio, branching coefficient and optimality ratios and between the branching vessel diameter and the junctional exponent deviation. These results suggest that portable vein finders are useful tools for characterizing venous superficial vein topography. Further studies are needed to test their usefulness to assess venous perfusion in vivo.

Francisco MD, Chen W-F, Pan C-T, Lin M-C, Wen Z-H, Liao C-F, Shiue Y-L. Competitive Real-Time Near Infrared (NIR) Vein Finder Imaging Device to Improve Peripheral Subcutaneous Vein Selection in Venipuncture for Clinical Laboratory Testing. Micromachines. 2021; 12(4):373. https://doi.org/10.3390/mi12040373 Ikram MK, Cheung CY, Lorenzi M, Klein R, Jones TL, Wong TY. Retinal vascular caliber as a biomarker for diabetes microvascular complications. Diabetes care 2013, 36(3), 750.

PCB049

Investigating the acute effect of transcutaneous vagal stimulation on respiration and heart rate variability in healthy subjects

Heba Mohamed[2], Jenifer Gunaseelan[1], Sereene Ghariani[1], Richard Struthers[3], Mirza Subhan[1]

[1]School of Biomedical Sciences, University of Plymouth, Plymouth, United Kingdom, [2]School of Biomedical Sciences, University of Plymouth, Plymouth, United Kingdom, [3]Anaesthetic Department, University Hospitals Plymouth NHS Trust, Plymouth, United Kingdom

Previous work has suggested that transcutaneous vagus nerve stimulation (tVNS) of the auricular branch of the vagus nerves might be associated with symptom relief pre-operatively and fewer complications after surgery. Recent studies have also shown improvements in heart rate variability (HRV) after tVNS in healthy subjects, but there is limited published data. The aim of this study was to compare the acute effects of tVNS with sham stimulation on respiration and HRV.

Thirty healthy subjects were recruited and gave written informed consent. The study was approved by the Science and Engineering Ethical Committee and was in accordance with the Declaration of Helsinki. Inclusion criteria was 18-65 year old healthy adults. Exclusion criteria was previous history of neuromuscular, autonomic, cardiorespiratory or ear skin conditions. Subjects completed a questionnaire, anthropometry and resting blood pressure, heart rate, and oxygen saturation measurements. Each participant completed three randomized interventions, each having a rest (10 minutes), stimulation (15 minutes), and recovery period (10 minutes), therefore, they completed nine consecutive experiments supine.

Electrical stimulation was delivered by placing an electrode clip to the auricular branch of the vagus nerve on the tragus of the external ear, earlobe, or thenar web space (the space between the thumb and index finger), using a commercial non-invasive transcutaneous electrical nerve stimulation (TENS) device. Electrodes were applied bilaterally, with the amplitude gradually adjusted until just below participants' level of sensory perception. The earlobe and the web space simulated sham stimulation, occurring at two different anatomical locations, relative to the tragus. During the stimulation, the electrocardiogram, heart rate variability, breathing rate (BR) and skin temperature were measured with Equivital wireless physiological monitoring equipment using LabChart software. HRV was assessed using time domain (heart rate - HR, standard deviation of the RR interval – SDRR) and frequency domain (low and high frequency - LF and HF). Data were statistically analysed for the complete time, the first and last five minutes, by repeated measures ANOVA, using SPSS. $P<0.05$ was considered as significant.

Results were analyzed over all nine experiments. SDRR showed a significant increase ($P<0.05$) for the first five minutes. Over the complete time, skin temperature ($P<0.0001$) significantly increased. HR, LF, HF, LF/HF ratio, BR ($P>0.05$) were not significantly different.

The primary findings of our investigation showed that tVNS & other sham site stimulation largely did not have a significant effect on the HRV, HR or BR, demonstrating that tVNS is not effective in modifying these aspects of autonomic function in our subjects. One reason our subjects did not show a marked vagal cardiorespiratory effect of tVNS could be due to their younger age (mean SD = 27.8 (12.1) years), relative to previous work. A steady increase in temperature across the interventions could have been due to a cold couch the subjects were lying on. This investigation includes limitations such as the small population size and a varied TENS neuro-sensitivity threshold. In conclusion, these findings provide a potential foundation for further research into the effects of tVNS and possible clinical applications.

PCB050

HAEMATOLOGICAL EFFECTS OF MELATONIN ADMINISTRATION ON OBESE WISTAR RATS: A COMPARATIVE ANALYSIS

Tahir Abdussalam[2], Luqman Olayaki[1]

[1]University of Ilorin, Ilorin, Nigeria, [2]University of Ilorin, Ilorin, Nigeria

The prevalence of obesity, characterized as a metabolic disorder, has escalated to epidemic levels, posing significant public health challenges. Studies have demonstrated a direct correlation between increased body weight, altered haematological indices and elevated mortality rates. Despite concerted efforts, the persistent struggle against these conditions has prompted the exploration for innovative therapeutic interventions. For the treatment of obesity, the gastrointestinal lipase inhibitor orlistat has been suggested. Nonetheless, the majority of patients have been dissuaded from continuing to use it due to the gastrointestinal adverse effects. Therefore, a stronger medication with fewer adverse effects is required. It has been observed that melatonin, a commonly used alternative medication, effectively lowers body weight with very little negative effects. Therefore, the present study investigated the haematological effects of melatonin administration in obesity model of male Wistar rats weighing between 120 – 140 g. It was hypothesized that combined administration of melatonin and orlistat are not anti-obesitogenic therapy on obese rat model. Sixty (60) rats of ten (10) animals per group were divided into the following: control (untreated); high fat diet (HFD); high fat diet recovery (hfd); HFD + melatonin (4 mg/kg); hfd + orlistat (30 mg/kg); and HFD + melatonin (4 mg/kg) + orlistat (30 mg/kg). Obesity was induced by exposing the rats to high fat diet for 16 weeks and confirmation was done using Lee index, which was determined by the formula: $4\sqrt{}$body weight (g) / nose-anal length (cm) (Adeyemi et al., 2020). Rats with an index higher than 0.30 were considered obese and were used for the study. Diagnostic kits for the determination of the biomarkers were obtained from Abcam PLC, Cambridge, UK and the assays were performed according to the manufacturer's instruction. Data were analyzed using analysis of variance and LSD *post hoc* test at 0.05 level of significance. The results showed that the induced obesity was accompanied with significant increases in plasma glucose, plasma insulin, packed cell volume (PCV), haemoglobin (HB), red blood cells (RBC) and white blood cells (WBC). Relative to the obese control, treatments with melatonin, orlistat and combined administration of both agents caused significant decrease in those parameters with the combined administration having a more potent effect. Hence, it was concluded that combined administration of melatonin and orlistat could be a better candidate in the management of haematological parameters in obese conditions.

Figure 5: Effects of combined administration of melatonin and orlistat on white blood cells

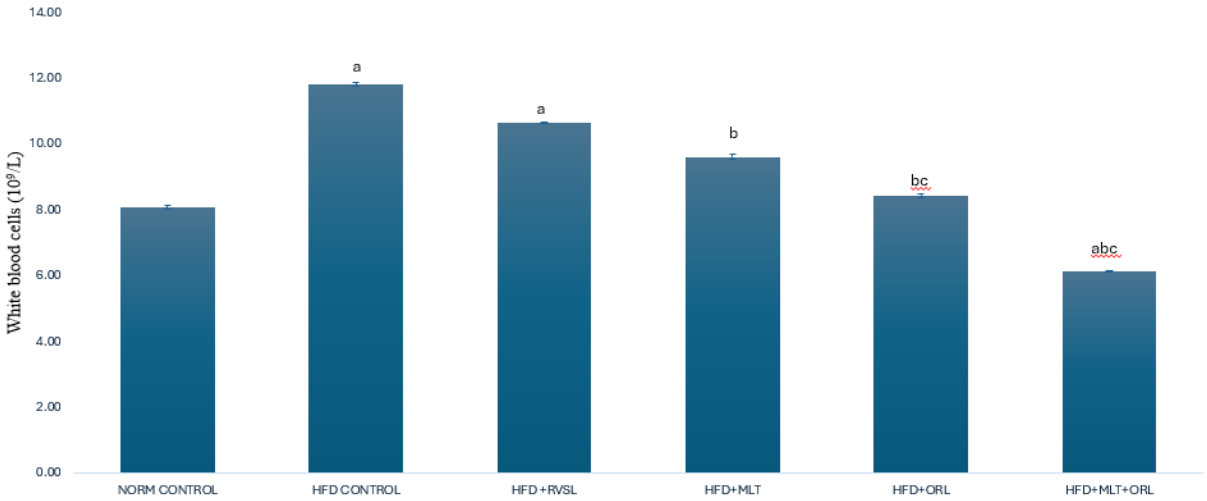

Values are expressed as MEAN±SEM. [a]p< 0.05 vs control, [b]p< 0.05 vs high fat diet (HFD) control, [c]p< 0.05 vs HFD reversal group.

Figure 4: Effects of combined administration of melatonin and orlistat on red blood cells

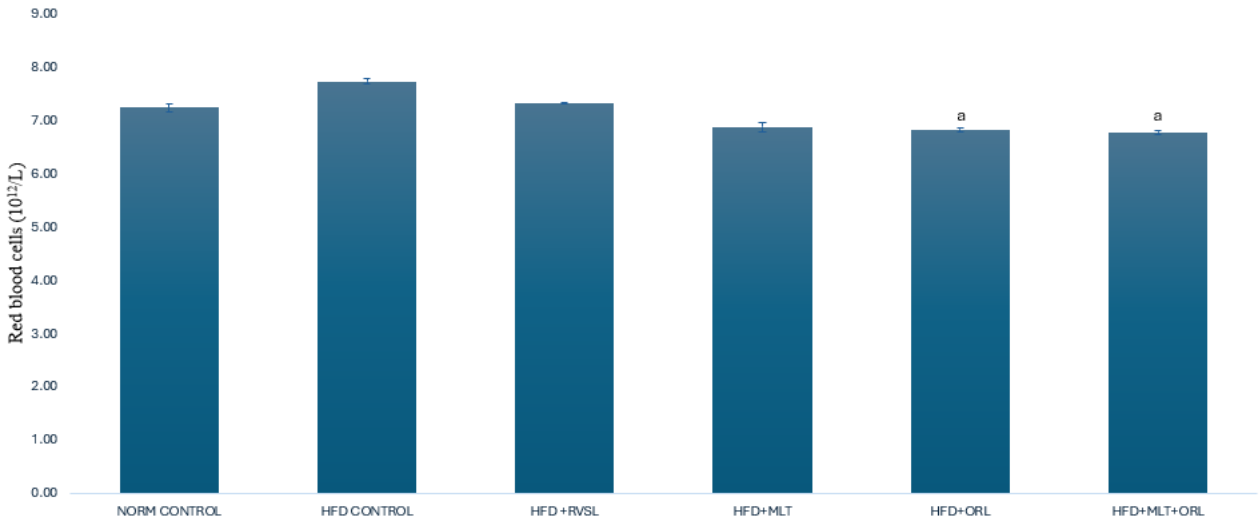

Values are expressed as MEAN±SEM. [a]p< 0.05 vs high fat diet (HFD) control.

Figure 1: Effects of combined administration of melatonin and orlistat on plasma glucose

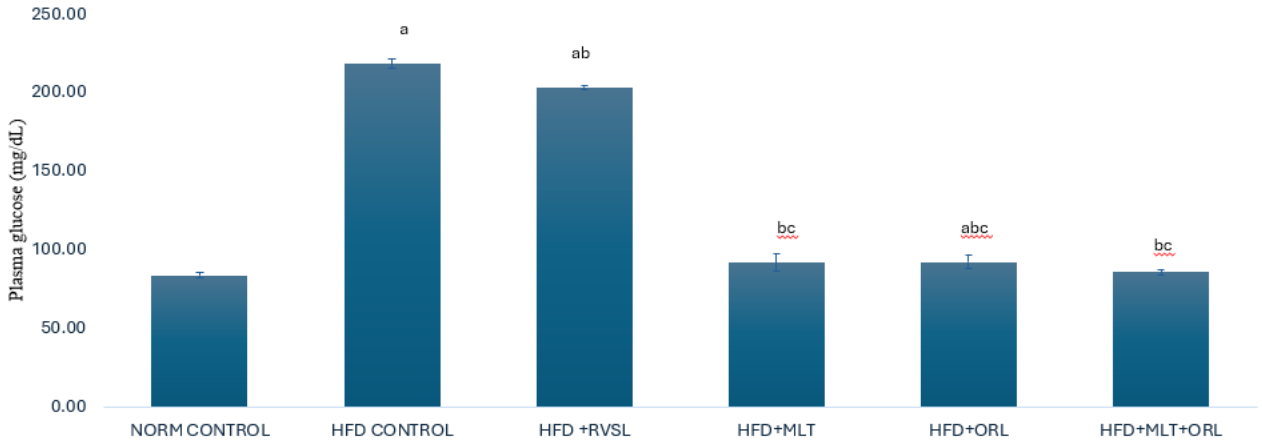

Values are expressed as MEAN±SEM. [a]p< 0.05 vs control, [b]p< 0.05 vs high fat diet (HFD) control, [c]p< 0.05 vs reversal group.

Figure 3: Effects of combined administration of melatonin and orlistat on packed cell volume

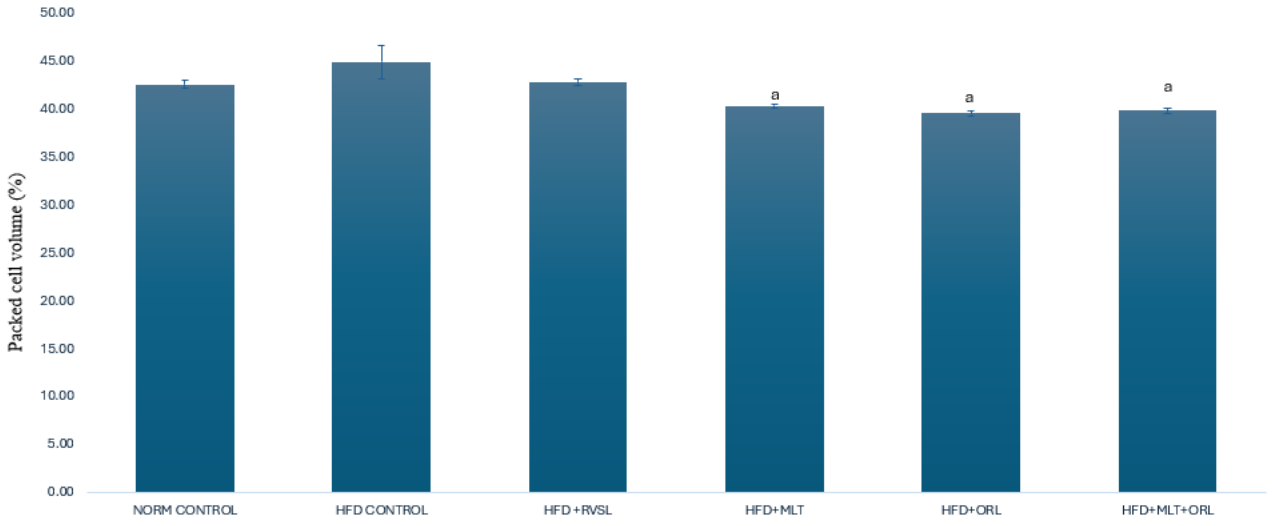

Values are expressed as MEAN±SEM. [a]p< 0.05 vs high fat diet (HFD) control.

Figure 2: Effects of combined administration of melatonin and orlistat on plasma insulin

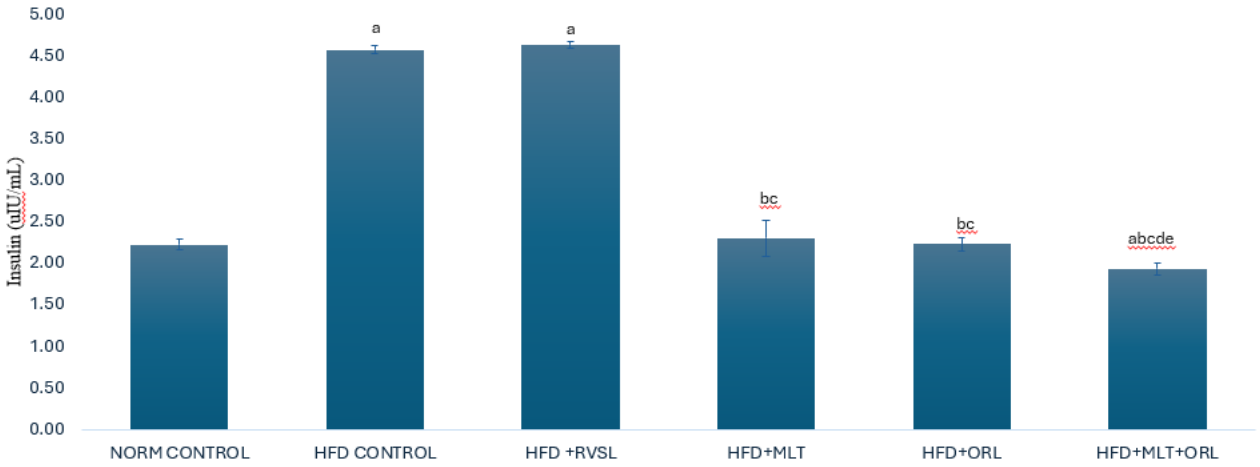

Values are expressed as MEAN±SEM. [a]p< 0.05 vs control, [b]p< 0.05 vs high fat diet (HFD) control, [c]p< 0.05 vs reversal group, [d]p< 0.05 vs HFD+MLT group, [e]p< 0.05 vs HFD+ORL group.

Adeyemi et al. (2020). PharmaNutrition 13, 100192.

PCB051

Mechanistic insights into plasma glucose lowering action of whey protein: role of glucoregulatory hormones on glucose flux

Giang Dao[1,2], Chris Shaw[2], Andrew Betik[2], Vicky Kuriel[2], Clinton Bruce[2], Greg Kowalski[1,2]

[1]Metabolic Research Unit, School of Medicine, Deakin University, Geelong, Australia, [2]Institute for Physical Activity and Nutrition, School of Exercise and Nutrition Sciences, Deakin University, Geelong, Australia

Introduction: It is generally regarded that insulin and glucagon exert opposing actions on plasma glucose: insulin lowers glucose by suppressing endogenous glucose production (EGP) and stimulating glucose uptake, while glucagon increases glucose by stimulating EGP. Protein and glucose co-ingestion stimulates both insulin and glucagon secretion, however glucose excursions are typically reduced compared to ingestion of a matched amount of glucose alone. Despite stimulating glucagon secretion, it is unclear how protein lowers glucose excursions. Therefore, this study addressed this by measuring postprandial glucose fluxes via the triple stable isotope glucose tracer technique following ingestion of either glucose (alone), or glucose and whey protein combined.

Methods: The study was approved by Deakin University Human Research Ethics Committee (2022-181). Eleven adults (5M/6F, 27±1.5 years, BMI: 23.4±0.6 kg/m^2) underwent three trials in random order, ingesting either 25g glucose (25G;~100 kcal), 50g glucose (50G;~200kcal) or 25g glucose plus 25g whey protein (WG;~200kcal). This allowed group comparisons where both glucose (WG vs 25G) and calories (WG vs 50G) were matched. Each trial utilised three stable isotope glucose tracers: [6,6-^{2}H] and [U-^{13}C] for variable infusions, and [1-^{2}H] for ingestion. Arterialised blood samples were obtained for 4h post-meal, to determine tracer enrichments (gas chromatography-mass spectrometry), insulin, glucagon, GLP-1, GIP, and C-peptide (ELISA). Glucose fluxes (EGP and rates of exogenous glucose appearance (meal Ra) and glucose disappearance (Rd)) were calculated using Steele's non-steady-state model. Data were reported as mean±SEM. One-way or two-way ANOVA were used for analyses where appropriate, followed by a Holm-Sidak's post hoc test (Graphpad Prism), with statistical significance set at $p<0.05$.

Results: The integrated postprandial glucose response (incremental area under the curve; iAUC) was markedly lower for WG (78±13 mmol.240min/L) compared to both 25G (182±27 mmol.240min/L, $p<0.001$) and 50G (310±45 mmol.240min/L, $p<0.001$). As expected, WG increased glucagon concentrations (~3-fold basal), while both 25G and 50G reduced glucagon levels. Insulin total iAUC was higher for WG vs 25G ($p=0.01$). Comparing WG vs 50G (calories matched), WG produced higher peak insulin concentrations (630±131 pmol/L vs 442±82 pmol/L, $p=0.04$) and tended to produce a higher insulin response over the initial 30min postprandial period ($iAUC_{0\text{-}30min}$, $p=0.07$). Despite the enhanced early insulin response, WG and 50G produced comparable GIP and GLP-1 responses ($p>0.05$). EGP suppression was less pronounced for WG (~48% suppressed) compared to 25G (~70% suppressed) or 50G (79% suppressed), $p<0.001$. WG vs 25G resulted in comparable Rd $iAUC_{0\text{-}60min}$ ($p>0.05$) but tended to lower meal Ra $iAUC_{0\text{-}60min}$ (254±35 mg.60min/kg vs 294±36 mg.60min/kg, $p=0.07$).

Conclusion: The findings confirm that whey/glucose co-ingestion, compared to the same glucose dose alone, reduces postprandial glucose excursions, enhances the insulin response, and induces a robust glucagon response. Additionally, we show that for the same caloric content but half glucose amount, whey/glucose co-ingestion enhances the early insulin response compared to glucose alone, which could be driven by amino acids and/or glucagon but not GLP-1 or GIP. We also provide novel mechanistic data, revealing that the addition of whey protein lowers glycaemic excursions despite less EGP suppression, with the net glycaemic benefit coming from reduced glucose absorption rates, not enhanced Rd.

PCB052

Effect of Vitamin B12 on leucine-induced anabolic signaling in C2C12 myotubes

Naoki Fukao[1], Mito Watanabe[1], Satoshi Fujita[2]

[1]Graduate School of Sport and Health Science, Ritsumeikan University, Kusatsu, Shiga, Japan,
[2]Faculty of Sport and Health Science, Ritsumeikan University, Kusatsu,Shiga, Japan

Introduction

Skeletal muscle mass is regulated by the balance between protein synthesis and degradation. Leucine, an essential amino acid, is known to activate mechanistic/mammalian target of complex1 (mTORC1) activity and enhance muscle anabolic response (Atherton et al. 2010). Recently, lower serum level of vitamin B12 (VB12) (<350pg/ml) has been reported to be associated with the incidence of sarcopenia (Choi et al. 2023). One of the factors contributing to sarcopenia is believed to be blunted skeletal muscle anabolic response to protein and amino acids intake (Cuthbertson et al. 2005, Aragon et al. 2023). However, effect of VB12 on leucine-induced anabolic signaling has not been investigated. Therefore, this study aimed to investigate the effect of VB12 on leucine-induced responses on anabolic signaling pathways.

Methods

Mouse C2C12 cells were seeded at 0.5×10^5 cells/ml in 12-well plates and cultured in DMEM containing 2% horse serum for 6 days to form myotubes. After differentiation, myotubes were cultured in serum-free medium for 1 hour, followed by incubation in amino acids and serum-free medium for 1 hour. Cells were then cultured in (1) Control (Con), (2) Leucine 1.5mM (Leu), (3) Leucine 1.5mM + VB12 10μM (Leu + Low-VB12), (4) Leucine1.5mM + VB12 100μM (Leu + High-VB12) for 30 minutes and collected (n=4/group). Western blotting was performed to evaluate the expression levels of proteins involved in muscle protein synthesis. For statistical analysis, SPSS Statistics ver.28 was used. One-way ANOVA was performed, and multiple comparisons were conducted by Tukey only when significant differences were found. Significance level was set at $p < 0.05$.

Results

There was a significant difference in phosphorylation / total-p70S6K expression, a downstream factor of mTORC1, between groups ($p < 0.001$). Multiple comparisons showed that Leu + Low-VB12 group showed significantly lower phosphorylation / total-p70S6K expression than Leu group (Leu + Low-VB12: 1.02 ± 0.08 *vs* Leu: 1.46 ± 0.10, $p = 0.016$) and there is no significant difference between Leu + Low-VB12 group and Con group (Leu + Low-VB12: 1.02 ± 0.08 *vs* Con: 1.00 ± 0.06, $p = 0.998$). On the other hand, Leu + High-VB12 group showed significantly higher phosphorylation / total-p70S6K expression compared to Con and Leu group (Leu + High-VB12: 2.02 ± 0.10 *vs*Con: 1.00 ±

0.06 / Leu: 1.46 ± 0.10, $p < 0.001$, $p = 0.003$, respectively). Moreover, there was a significant difference in t-4E-BP1 γ form ratio between groups ($p = 0.002$). Multiple comparisons showed that Leu and Leu + High-VB12 group showed significantly higher t-4E-BP1 γ form ratio than Con group (Leu: 1.20 ± 0.02 / Leu + High-VB12 1.18 ± 0.03 *vs* Con: 1.00 ± 0.02, $p = 0.002$, $p = 0.006$, respectively).

Conclusion

These results suggest that low-level VB12 blunt anabolic signaling but high-level VB12 enhanced leucine-induced anabolic signaling in C2C12 cells.

Atherton et al. (2010). Amino Acids, 38(5). Choi et al. (2023). Nutrients, 15(4). Aragon et al. (2023). Nutrition Reviews, 81(4). Cuthbertson et al. (2005). FASEB J, 19(3)

PCB053

Identifying microbial protein metabolites that regulate Glut4 translocation in skeletal muscle

Sati Gurel[1], Rashmi Sivasengh[2], Madalina Neacsu[2], Brendan M. Gabriel[2]

[1]Department of Nutrition and Dietetics, Faculty of Health Sciences, Trakya University, Edirne, Turkey, [2]University of Aberdeen, Aberdeen, United Kingdom

The intake of plant-based foods has been shown to lead to a reduction in plasma levels of branched-chain amino acids, phenylalanine, and tyrosine, which are amino acids linked to insulin resistance (Neacsu et al., 2022). Hemp is a high protein crop and stands out due to its quality nutritional profile among gluten-free plant species that provide valuable industrial outputs with less impact on the environment (Yano & Fu ,2023). After consuming isoproteic meals rich in hemp or meat, certain plasma microbial metabolites were significantly elevated following the hemp meal and linked to lower levels of insulin and ghrelin. It is important to investigate the impact of plant-based foods on altering plasma amino acid profiles and gut hormone levels, given that diets rich in high-protein crops have been shown to be inversely related to the risk of metabolic syndrome and Type 2 Diabetes (T2D) (Neacsu et al., 2022). Several metabolomics studies have explored the relationship between systemic and microbial metabolites and metabolic diseases, underscoring the importance of comprehending their diverse roles in insulin resistance development for identifying novel therapeutic targets against metabolic disorders.

Skeletal muscle, which is considered a central organ in T2D pathology, has an important role in glucose homeostasis in the body. In insulin resistant skeletal muscle, proximal insulin signalling events are impaired and this blocks the insulin-dependent GLUT4 translocation to the plasma membrane. Thus, impaired glucose uptake in skeletal muscle is often considered a primary defect in T2D and is therefore targeted as a therapeutic strategy against insulin resistance (Abdelmoez et al., 2020). In this study we have conducted a scoping review of human studies that investigated protein microbial metabolites and insulin sensitivity. For our scoping review, Pubmed, Scopus, ScienceDirect databases were searched to determine studies examining the effects of protein microbial metabolites on glucose metabolism. From a total 203 articles initially identified, 17 were included in this review. 11 were epidemiological studies, 6 were clinical studies (including dietary intervention studies). The majority of the identified studies (14 articles) report an inverse relationship of indole-3-propionic acid with T2D development and/or its effect on glucose metabolism. Furthermore, the hippuric acid, benzoic acid and phenylalanine were reported to have a beneficial effect on glucose metabolism (fasting glucose, fasting insulin, HOMA-IR, insulin sensitivity) (Neacsu et al. 2022; Koistinen et al. 2024; Vangipurapu et al. 2020). In summary, our scoping review has identified several promising protein microbial metabolites that may affect peripheral tissue insulin sensitivity and could be used as nutritional therapies for T2D.

Abdelmoez, A. M., Sardón Puig, L., Smith, J. A., Gabriel, B. M., Savikj, M., Dollet, L., ... & Pillon, N. J. (2020). Comparative profiling of skeletal muscle models reveals heterogeneity of transcriptome and metabolism. American Journal of Physiology-Cell Physiology, 318(3), C615-C626. Koistinen, V. M., Haldar, S., Tuomainen, M., Lehtonen, M., Klåvus, A., Draper, J., ... & Hanhineva, K. (2024). Metabolic changes in response to varying whole-grain wheat and rye intake. npj Science of Food, 8(1), 8. Neacsu, M., Vaughan, N. J., Multari, S., Haljas, E., Scobbie, L., Duncan, G. J., ... & Russell,

W. R. (2022). Hemp and buckwheat are valuable sources of dietary amino acids, beneficially modulating gastrointestinal hormones and promoting satiety in healthy volunteers. European journal of nutrition, 1-16. Vangipurapu, J., Fernandes Silva, L., Kuulasmaa, T., Smith, U., & Laakso, M. (2020). Microbiota-related metabolites and the risk of type 2 diabetes. Diabetes care, 43(6), 1319-1325. Yano, H., & Fu, W. (2023). Hemp: A sustainable plant with high industrial value in food processing. Foods, 12(3), 651.

PCB054

Investigating the inter-organ crosstalk between liver and heart in a model of metabolic disease

Joanna Konieczny[1], John Martin Fredriksen[1], Cecilie Ness[1], Julija Lazarevic[1], Manar Kalaaji[1], Trine Lund[1], Kirsti Ytrehus[1], Neoma Boardman[1]

[1]University of Tromsø-The Arctic University of Norway, Tromsø, Norway

Fatty liver is a silent manifestation of the metabolic syndrome that affects millions worldwide leading to metabolic-associated fatty liver disease (MAFLD) with both a lean and overweight phenotype. There is a high risk of cardiovascular complications and mortality associated with the disease, that is more prevalent than liver pathology-related deaths. To study changes occurring in early stages of the disease can shed a light on the extend of those associations related to inter-organ crosstalk.

We hypothesized that chronic fructose intake leads to liver steatosis and can induce liver mitochondrial stress and an alarm response in the heart. In this project, we have investigated the consequences of fructose intake in the liver and heart, with a focus on mitochondrial stress and its drivers in liver-heart crosstalk under these conditions.

Methods

Animal experiments were designed according to European guidelines (FELASA; EU animal research directive 86/609/EEC and 2010/63/ EU) and approved by the local authority of the National Animal Research Authority in Norway. Male rats (Sprague-Dawley, 250 g) were given normal chow and tap water ad libitum (CON, n=12) or a 15% fructose drink (FRU, n=12) for 16 weeks. Body composition was measured throughout the intervention (EchoMRI) as well as tail-cuff measurement of blood pressure (CODA) and tail-vein blood samples. Serum cytokines (Bioplex) were analyzed. Tissue from liver and heart was obtained postmortem following 16-weeks fructose intake. Liver triglycerides (TG) were assessed by a colorimetric assay. Cardiac and liver mitochondrial respiratory capacity was determined in tissue homogenate (O2K, Oroboros) and mitochondrial H2O2 production was determined in the heart. Histology and Reverse Transcription quantitative PCR were used to assess changes in liver and heart, including hematoxylin and eosin (H&E), PicroSirius Red (PSR), Oil Red O (ORO) and dihydroethidium (DHE) stainings.

Results

16-week fructose intake increased body weight, percentage of fat mass and induced liver steatosis. Histological analysis determined increased ORO staining of lipid droplets in liver and TG in tissue homogenate was increased. H&E staining did not reveal macrovesicular steatosis, nor was increased liver collagen deposition observed with PSR. Mean arterial pressure as well as serum levels of interleukin-6 and tumour necrosis factor-alpha were elevated in fructose (FRU) rats. The heart weights were elevated in FRU however histological analysis did not reveal changes in cardiomyocyte size by H&E staining, collagen deposition, lipid droplet and reactive oxygen species formation in the nuclei measured by DHE. Complex I-linked mitochondrial oxidative

phosphorylation (CI-OXPHOS) and mitochondrial respiratory capacity was lower in liver homogenate from FRU and mRNA expression indicated metabolic changes, mitochondrial stress and elevated Fibroblast Growth Factor 21 (FGF21). CI-OXPHOS was also lower in heart homogenates from FRU along with altered mitochondrial H2O2 production.

Conclusion

Liver steatosis is associated with cardiac adaptations that may contribute to the development of heart failure. Increased FGF21 expression levels in the liver indicate potential driver of detrimental liver-heart crosstalk, a role that is of interest for further investigation.

PCB055

The effects of cysteamine on visceral adipose tissue remodelling in an LDL receptor knockout model after a high-fat diet

Chiemelum Okagbue[1], Feroz Ahmed[2], David Leake[1], Sam Boateng[1], Dyan Selleyah[1]

[1]University of Reading, Reading, United Kingdom, [2]Race Oncology, Sydney, Australia

Obesity contributes to the pathological remodelling of adipose tissue due to accommodating the caloric imbalance. Obesity can lead to several associated risk factors such as elevated cholesterol (specifically low-density lipoproteins (LDLs)) which can result in an increased risk of cardiovascular disease. However, the administration of anti-oxidizing agents and switching to a balanced diet have been shown to ameliorate the pathological effects of obesity on adipose tissue. For example, cysteamine has been previously shown to reduce the size of atherosclerotic lesions in the aorta in an LDL receptor knockout ($Ldlr^{-/-}$) model fed a high-fat diet (HFD) as well as inhibit the oxidation of LDLs by iron at optimal lysosomal pH (4.5). (Wen et al., 2019).

Therefore, this study explored whether cysteamine can enhance the benefits of switching from a high-fat diet (HFD) to a balanced chow diet. This was done by investigating the extent of the remodelling of visceral adipose tissue (VAT) in an LDL receptor knockout model fed an HFD.

Nine-week-old female $Ldlr^{-/-}$ mice were separated into an HFD group, a regular chow diet-only (RCD) group, and a regular chow diet + cysteamine (RCD/C) group. The VAT cellularity was studied using haematoxylin and eosin staining. The extent of VAT fibrosis and VAT oxidative stress were measured using picro sirius red and dihydroethidium staining respectively. Lastly, the gene expression in the VAT was studied using RNA-Seq Analysis. All procedures complied with the Animals (Scientific Procedures) Act 1986 and were approved by the Ethical Review Process Committee of the University of Reading.

The VAT cellularity analysis showed that switching to a balanced chow diet alone resulted in a significant decrease in the adipocyte diameter of the VAT (960.36 ± 62.45μm; n=5) in comparison to the RCD/C group (1889.49 ± 298.20μm; n=5). This implies the possible inhibition of lipolysis by cysteamine because the VAT larger adipocytes were a similar size to the HFD control group (1363.19 ± 179.40μm; n=5). Markers of both fibrosis and oxidative stress showed no marked difference in any of the treatment groups suggesting cysteamine did not affect the VAT phenotype in terms of fibrosis and oxidative stress.

The gene ontology (GO) enrichment analysis highlighted GO terms associated with glucose homeostasis and the negative regulation of cell growth/signalling in the sole downregulated gene between the RCD group and the RCD/C group (Bmal1). The GO enrichment analysis for the differentially spliced genes also revealed GO terms associated with cell growth/signalling such as “anatomical structure morphogenesis” between the RCD group and the RCD/C group. Additionally, the GO term “regulation of cold-induced thermogenesis” was also enriched during the analysis that is specific to adipose tissue function. This possibly corroborates the inhibition of the reduction in the VAT adipocyte diameter with cysteamine treatment due to the role of thermogenesis in the lipolysis of white adipose tissue.

Overall, this suggests that cysteamine can influence adipocyte remodelling during the switch from an HFD to an RCD by preventing the lipolysis of the VAT lipid stores required for lipid homeostasis under normal conditions and obesity.

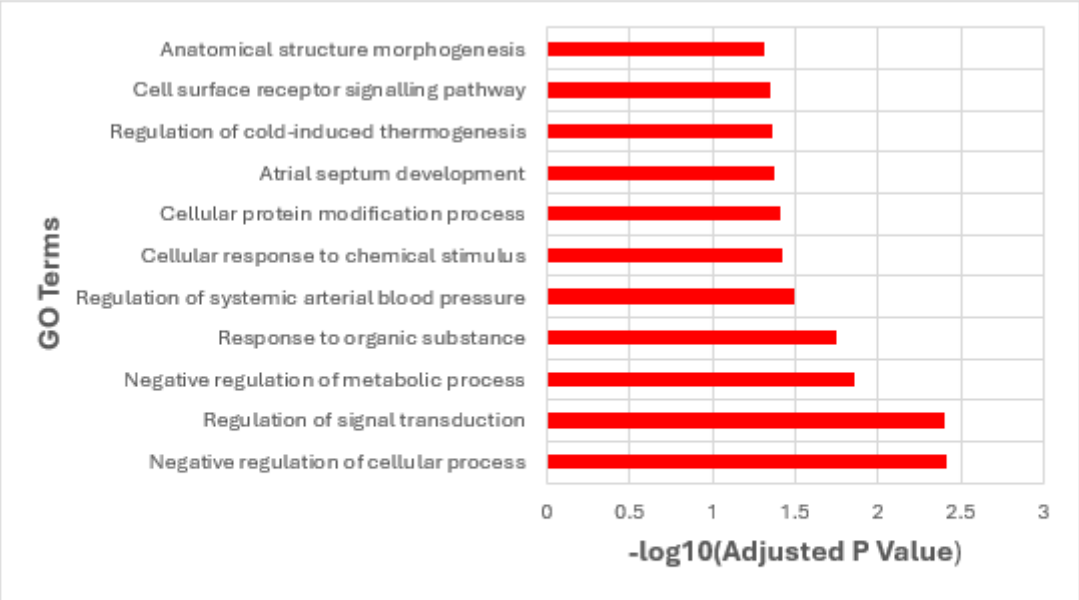

Figure 4: The gene ontology of the genes that were differentially spliced between the RCD/C and RCD groups showing the biological processes that spliced variants are involved in determined by the Fisher exact test with n=4 from the RNA-Seq Analysis by Genewiz ($p<=0.05$).

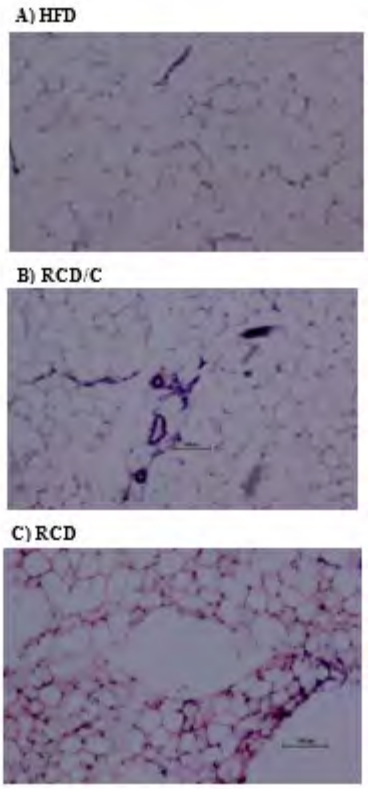

Figure 1: H&E staining showing the adipocyte morphology of VAT at a magnification of 100x in (A) The HFD control, (B) The cysteamine treatment group and (C) The regression diet only group after 8 weeks of a HFD and a further 8 weeks of a normal chow diet and cysteamine treatment (B and C); bar = 100µm.

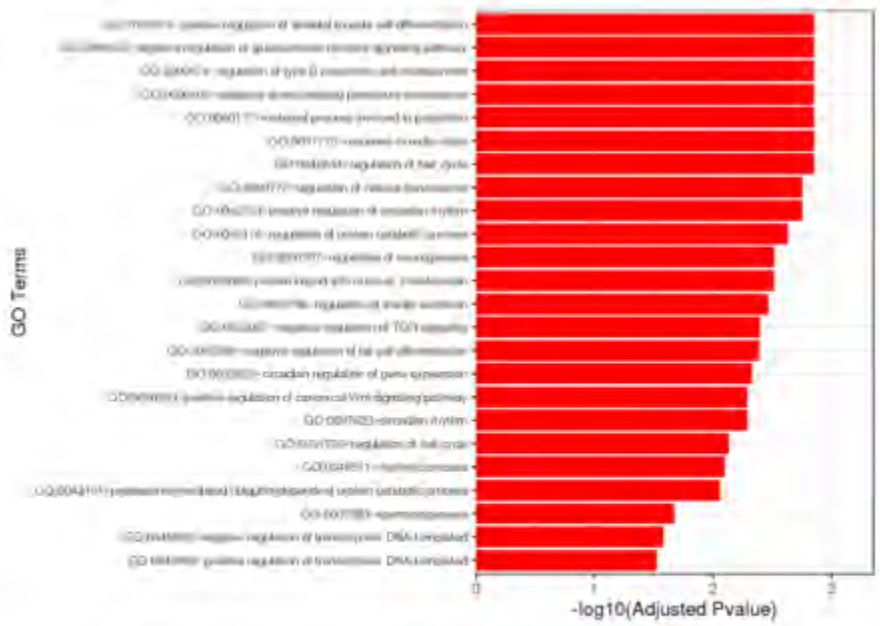

Figure 3: The gene ontology of the genes that were differentially expressed between the RCD/C and RCD groups showing the biological processes that the genes are involved in determined by the Fisher exact test with n=4 from the RNA-Seq Analysis by Genewiz ($p<=0.05$).

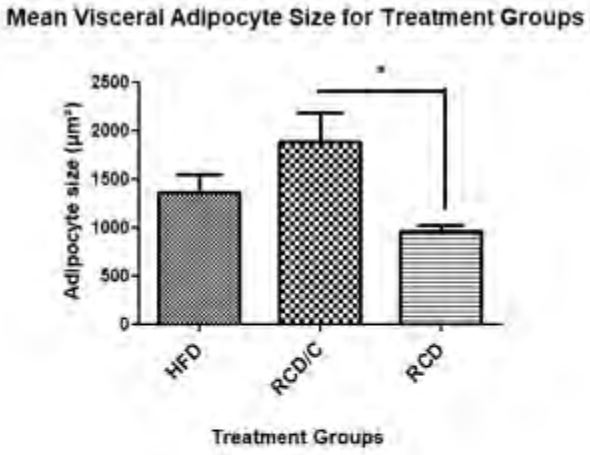

Figure 2: A regression diet alone can reduce the diameter of visceral adipocytes after the administration of an HFD. The addition of cysteamine has no marked effect on the diameter of visceral adipocytes. All values represent the mean ± the standard error of the mean with n= 5. In comparison across the experimental groups, the statistical significance is denoted as *= $p<0.05$ using the Kruskal-Wallis test and post hoc Dunn's correction.

WEN, Y., ET AL. (2019). "Cysteamine inhibits lysosomal oxidation of low-density lipoprotein in human macrophages and reduces atherosclerosis in mice." Atherosclerosis 291: 9-18.

PCB056

The impact of acute exercise before and after a simulated nightshift on metabolic health markers in healthy adults: an interim analysis of a randomised controlled trial

Cian Sweeney[1], David Clayton[1], Fran Pilkington-Cheney[1], Angus Hunter[1], Emma Sweeney[1]

[1]Nottingham Trent University, Nottingham, United Kingdom

Introduction

Shift work is associated with an increased risk of developing cardiometabolic diseases (Ho et al., 2022). Experimental research has demonstrated decreased insulin sensitivity after simulated nightshifts (Morris et al., 2016). Despite these well-documented consequences of shift work, feasible mitigation strategies are lacking. Exercise is beneficial for cardiometabolic health, with moderate-intensity exercise improving insulin sensitivity (Bird and Hawley, 2016). Therefore, exercise may alleviate the effect of shift work on cardiometabolic health. Hence, this study aimed to investigate the impact of exercise before or after a simulated nightshift on metabolic health in adults.

Methods

Seven healthy participants completed a familiarisation and three experimental trials in a randomised, counterbalanced, crossover design, separated by at least seven days. The experimental protocol involved a simulated 12-hour nightshift, with exercise (30 minutes cycling at 60% of VO_{2max} peak power) either immediately before (PRE) or immediately after (POST) the shift, or no exercise (CON). Each trial started at 07:00, with a nap opportunity from 15:00-17:00. The simulated nightshift then started at 20:00. During the shift, participants completed cognitive assessments, appetite and fatigue questionnaires, light physical activity, and consumed a standardised diet. Participants were then in bed from 10:00-16:00. Wrist actigraphy was used to ensure compliance. At 17:00, an oral glucose tolerance test (OGTT) was conducted, with blood samples collected for measurement of insulin and glucose, followed by an ad-libitum evening meal to assess energy intake. Linear mixed models were used to compare outcomes between trials. Data are presented as mean ± SD, with significance set at $p<0.05$.

Results

No significant differences were present between the PRE, POST and CON trials for glucose AUC (675.3 ±131.1 AU, 700.1 ± 134.7 AU and 726.3 ± 140.8 AU, respectively; p= 0.761), insulin AUC (2862.1 ± 1307.3 AU, 3376.0 ± 1350.3 AU, and 3054.1 ± 617.2 AU, respectively; p= 0.470), Matsuda index (13.20 ± 3.44, 11.08 ± 2.34 and 11.72 ± 2.81 respectively; p= 0.381) and HOMA-IR (0.66 ± 0.06, 0.80 ± 0.25, and 0.77 ± 0.67, respectively; p= 0.151). No significant differences were observed for substrate utilisation (CHO oxidation PRE: 106.4 ± 25.8g vs POST: 105.4 ± 20.0g; p= 0.516 and fat oxidation PRE; -1.1 ± 3.4g vs POST: -2.3 ± 3.0g; p= 0.263), rate of perceived exertion (p= 0.216) or heart rate (p= 0.106) during exercise before compared to after the simulated nightshift. Ad-libitum energy intake was not significantly different between trials (1021 ± 500 Kcal, 1137 ± 454 Kcal, and 1108 ± 677 Kcal for PRE, POST and CON, respectively; p= 0.106).

Discussion

This interim analysis demonstrated no significant impact of exercise before or after a simulated nightshift on metabolic health markers during an OGTT, or changes in physiological variables during exercise before compared to after a shift. The findings suggest that acute exercise is not sufficient to induce meaningful improvements in metabolic markers. However, due to the sample size in the current interim analysis, further research is warranted to fully understand the efficacy of exercise in mitigating the consequences of shift work on metabolic health.

1. Bird, S.R., & Hawley, J.A. (2017). Update on the effects of physical activity on insulin sensitivity in humans. BMJ Open Sport & Exercise Medicine, 2(1), e000143. 2. Ho, F.K., Celis-Morales, C., Gray, S.R., Demou, E., Mackay, D., Welsh, P., Katikireddi, S.V., Sattar, N., & Pell, J.P. (2022). Association and pathways between shift work and cardiovascular disease: a prospective cohort study of 238,661 participants from UK Biobank. International Journal of Epidemiology, 51(2), 579–590. https://doi.org/10.1093/ije/dyab144 3. Morris, C.J., Purvis, T.E., Mistretta, J., & Scheer, F.A.J.L. (2016). Effects of the Internal Circadian System and Circadian Misalignment on Glucose Tolerance in Chronic Shift Workers. The Journal of Clinical Endocrinology & Metabolism, 101(3), 1066–1074. https://doi.org/10.1210/jc.2015-3924

PCB057

Effects of β-hydroxybutyrate on muscle protein synthesis and anabolic signaling in C2C12 myotubes

Mito Watanabe[1], Fukao Naoki[1], Ryo Takagi[3], Jonathan Little[4], Satoshi Fujita[5]

[1]Graduate School of sports and health science, Ritsumeikan University, kusatsu, Japan, [2]Graduate School Sports and Health Science, Ritsumeikan University, Kusatsu, Japan, [3]Ritsumeikan Global Innovation Research Organization, Ritsumeikan University, Kusatsu, Japan, [4]School of Health and Exercise Sciences, University of British Columbia Okanagan, Kelowna, Canada, [5]Faculty of Sport and Health Science, Ritsumeikan University, Kusatsu, Japan

Introduction:

Ketone bodies are small molecules consisting of β-hydroxybutyrate, acetoacetate, and acetone that serve as an alternative energy source when carbohydrates are depleted [1)]. In particular, β-hydroxybutyrate, which accounts for approximately 80% of ketone bodies in the blood, has been shown to have potent physiological effects. It has been reported that β-hydroxybutyrate improves mitochondrial function and may suppress muscle catabolism caused by inflammation in skeletal muscle [2)3)]. However, the effect on skeletal muscle protein synthesis response is not clear. Therefore, the purpose of this study was to examine the direct effects of β-hydroxybutyrate on muscle protein synthesis and anabolic signaling in C2C12 myotubes.

Methods:

C2C12 myoblasts were cultured in DMEM containing 2% horse serum for 5 days to induce differentiation into myotubes. After differentiation, the myotubes were incubated with DMEM containing different concentrations of β-hydroxybutyrate (0, 0.25, 0.5, 1, 2, 5mM) for 30 minutes. For assessment of protein synthesis, myotubes were treated with 1 μM puromycin 30 min prior to cell collection. Protein synthesis and mTORC1 related proteins were quantified using Western blotting. Data were analyzed using one-way ANOVA.

Results:

A significant increase in puromycin-labeled protein expression was observed after stimulation with 1mM β-hydroxybutyrate (1.20±0.06 arbitrary units) compared to 0mM (1.00±0.05, $p<0.05$). However, phosphorylation of mTORC1 related proteins (p70S6K^{Thr389}, rpS6$^{Ser240/244}$, 4E-BP1$^{Thr37/46}$) was not changed by any concentrations of β-hydroxybutyrate.

Conclusion:

These results suggest that β-hydroxybutyrate might enhance muscle protein synthesis in C2C12 myotubes. In contrast, mTORC1-related signaling did not change with short-term exposure to β-hydroxybutyrate. It appears that β-hydroxybutyrate may activate muscle protein synthesis through mTORC1-independent pathways.

1) Evans M et al., J Physiol, 2017 2) Thomsen HH et al., Am J Clin Nutr, 2018 3) Parker BA et al., Int J Mol Sci, 2018

PCB058

Exploring the Link Between Microglial Morphology and Beta-Amyloid Accumulation in an Alzheimer's Disease Mouse Model

AlBeshr AlMasri[1], Harry Trewhitt[1], Kira Shaw[1], Catherine Hall[1]

[1]*University of Sussex, Brighton, United Kingdom*

Introduction: Microglia, central nervous system resident immune cells, play a pivotal role in the neuroinflammatory response associated with Alzheimer's disease (AD). Their dysregulation and morphological changes contribute to AD pathogenesis, activating in response to beta amyloid plaques (Doens and Fernández, 2014). However, the timing of microglial activation in relation to early Alzheimer's pathology remains unclear. This study aims to elucidate whether microglial morphological changes occur in the early stages of amyloid-beta (Aβ) accumulation, using a mouse model to selectively induce amyloid precursor protein expression (thus Aβ-production).

Methods: We bred transgenic mice with human APOE3/APOE4 alleles, using a Tet-off system and dietary doxycycline to modulate APP expression and control Aβ production. The study assessed the impact of APOE genotypes, entorhinal cortex and hippocampus regions, and Aβ production on Alzheimer's pathology. Microglia visualization was through IBA1 immunohistochemistry, Aβ quantification via the MSD 6E10 Aβ panel (protein-normalized), and amyloid aggregation detected with MethoxyX04 staining. We assessed microglial morphology in 150 cells from 28 animals using ImageJ's Moti-Q plugin, following Hansen et al., 2022. Statistical analysis involved principal component analysis (PCA) for morphological data dimensionality reduction and a targeted approach focusing on neuroinflammation-related metrics, as per Olabiyi et al., 2023.

Results: Without doxycycline for 18 weeks, APPSwe/Ind mice exhibited increased Aβ levels (38, 40, 42 isoforms; $p = 0.012$) without amyloid aggregation. Neither Aβ levels nor microglial morphology were affected by APOE genotype. Unbiased PCA revealed nine principal components, explaining 80% of the variance in microglial morphology, with the primary component explaining 46%, largely reflecting cell size and branching complexity. However, multi-way ANOVA found no significant morphological differences between control mice and those accumulating Aβ.

Targeted analysis on key microglial activation markers—Iba1 intensity, tree length, branching, and ramification — did however reveal significant inflammation-linked changes in Aβ-producing mice: heightened intensity (100.52 ± 5.69 vs. 68.48 ± 2.90; $p < 0.0001$), fewer branches (98.27 ± 9.23 vs. 162.72 ± 13.67; $p = 0.0038$), lower ramification index (7.05 ± 0.26 vs. 10.37 ± 0.36; $p < 0.00001$), and reduced tree lengths (615.08 ± 47.89 µm vs. 935.32 ± 65.32 µm; $p = 0.00282$). However, cell volume remained unchanged (4304.56 ± 312.92 µm^3 vs. 4699.72 ± 290.89 µm^3; $p = 0.424$), despite its previous association with microglial activation (Olabiyi et al., 2023). Post-hoc analysis revealed marked intensity and ramification differences in Aβ mice in the assessed regions (intensity: cortex $p=0.00086$, hippocampus $p=0.00218$; ramification: cortex $p=0.00005$, hippocampus $p=0.007$) and significant cross-regional variations (intensity: cortex vs. control hippocampus $p<0.00001$; ramification: hippocampus vs. control cortex $p=0.0081$, cortex vs. control hippocampus $p=0.00006$). These results indicate early, albeit incomplete, microglial activation in early Alzheimer's disease pathology, prior to beta amyloid plaque formation.

Conclusion: Our results demonstrated elevated neuroinflammation and Aβ levels in early AD mouse model, irrespective of APOE genotype. Initial PCA and multi-way ANOVA showed no significant microglial morphology changes due to Aβ. Yet, targeted analysis of microglial activation markers—like increased intensity, reduced branches, shorter tree length, and lower ramification index—indicates early microglial activation signs during initial Aβ accumulation, before plaque formation.

Doens, D. and Fernández, P.L., 2014. Microglia receptors and their implications in the response to amyloid β for Alzheimer's disease pathogenesis. Journal of Neuroinflammation, 11(1), p.48. Available at: https://doi.org/10.1186/1742-2094-11-48. Hansen, J.N., et al., 2022. MotiQ: an open-source toolbox to quantify the cell motility and morphology of microglia. Molecular Biology of the Cell, 33(11), ar99. doi: 10.1091/mbc.E21-11-0585. Olabiyi, B.F., et al., 2023. Pharmacological blockade of cannabinoid receptor 2 signaling does not affect LPS/IFN-γ-induced microglial activation. Scientific Reports, 13(1), 11105. doi: 10.1038/s41598-023-37702-z.

PCB059

Central and peripheral serotonin levels and its ovarian mRNA receptors interplay at diestrus in perimenopausal rats following exercise

Adesina Arikawe[1], Adetoke Adekitan[2], Okikiade Oghene[3], Adedunni Olusanya[4], Abimbola Ogunsola[5], Naomi Ojedokun[1], Daniel Adebayo[1], Valentine Nwachukwu[1], Folashade Ofere[1]

[1]Department of Physiology, Faculty of Basic Medical Sciences, College of Medicine, University of Lagos, Idi-Araba, Lagos, Nigeria, [2]Department of Physiology, Faculty of Basic Medical Sciences, College of Medicine, University of Lagos, Idi-Araba, Lagos, Nigeria, [3]Department of Physiology, Faculty of Basic Medical Sciences, College of Medicine, University of Lagos, Idi-Araba, Lagos, Nigeria, [4]Department of Pharmacology, Therapeutics & Toxicology, Faculty of Basic Medical Sciences, College of Medicine, University of Lagos, Idi-Araba, Lagos, Nigeria, [5]Department of Physiology, Babcock University, Ilishan-Remo, Ilishan, Nigeria

Reproductive aging in females is characterized by a progressive decline in fertility that begins at birth and extends through the perimenopausal transition. A decline in estrogen concentrations during this transitory period lowers the activity of serotonin; a known neurotransmitter which has been well established to ultimately improve mental health status. Thus, this study aimed to assess ovarian serotonin mRNA receptors; its central and peripheral levels interplay at diestrus phase of the estrous cycle in perimenopausal rats subjected to standard exercise regimen.

Female immature Wistar rats (postnatal day [PND] 21) were housed in groups of seven per cage (n = 7) and randomly divided into three major groups (Control, VCD, and Aging). At PND 28, Control rats were injected with Corn oil (2.5uL/kg BW) for 15 days; VCD rats were injected with 4-Vinylcyclohexene diepoxide (160mg/kg BW) diluted in Corn oil (2.5uL/kg BW) for 15 days; naturally Aging rats 180 days old (no injection of VCD or Corn oil) were used as aged rats. Fifty (50) days after corn oil/VCD injection and 230 days in Aging rats, animals were further sub-divided into 2 groups; exercise (subjected to exercise regimen of 1 hour duration 3 times weekly on a treadmill for 3 weeks) and non-exercise group. On diestrus morning after the exercise regimen, animals were humanely sacrificed, prefrontal cortex (PFC) and hippocampus (HIPPO) were removed on ice and homogenized; and cardiac puncture was carried out to collect blood (serum) for measurement of peripheral serotonin levels using specialized ELISA kits. Both ovaries were quickly removed and placed in RNA later fluid for storage until serotonin mRNA analysis using standard mRNA extraction and RT-qPCR techniques. Data was analyzed using One-way ANOVA followed by a Bonferroni post hoc test using GraphPad Prism 7 software.

Serum serotonin (ng/ml) was significantly higher ($p<0.05$) in Aging rats (45.61±6.72) compared to Control (19.45±2.80) and VCD (20.90±2.30). Exercise significantly reduced ($p<0.05$) serum serotonin in VCD (14.62±1.13ng/ml) and Aging rats (26.72±5.71) compared to Control (23.52±1.83). In PFC, serotonin (ng/ml) in Aging rats (3.41±0.31) was significantly lower ($p<0.05$) compared to Control (5.91±0.60) and VCD (6.90±0.90) rats. Exercise significantly increased ($p<0.05$) serotonin in Aging rats (6.99±1.04) compared to Control (5.79±0.83) and VCD (8.01±0.71). In HIPPO, there were no significant changes observed across the groups. In the ovaries, 5-HT_1 receptors were significantly reduced ($p<0.05$) in Aging rats (4.33±0.43) compared to VCD (9.63±0.82) rats only [Control was (4.60±1.58)]. Exercise significantly reduced ($p<0.05$) 5-HT_1 receptors (6.41±0.95) in

VCD rats; while significantly increasing it ($p<0.05$) in Aging rats (8.04±1.69), and no significant difference in Control rats (5.97±1.33). The 5-HT_2 receptors in ovaries, were significantly lowered ($p<0.05$) in VCD (2.27±0.49) and Aging (2.81±0.56) compared to Control (5.20±1.23). Exercise significantly increased ($p<0.05$) 5-HT_2 receptors in Aging (5.91±1.57), Control (8.32±1.37) and VCD (4.23±1.41) rats.

Exercise seems beneficial in improving mental health during perimenopausal transitory period by enhancing central, peripheral and ovarian serotonin interplay.

PCB060

Investigating the luminance-response function of human retinal cone-driven responses to 30 Hz flickering stimuli presented on different backgrounds

Charlie Bosshard[1,2], Harry Arbuthnott[1,2], Isabelle Chow[3,4], Shaun Leo[2,5], Xiaofan Jiang[2,4], Omar Mahroo[1,2,3,4,5]

[1]Physiology, Development and Neuroscience, University of Cambridge, Cambridge, United Kingdom, [2]Institute of Ophthalmology, University College London, London, United Kingdom, [3]Department of Ophthalmology, St Thomas' Hospital, London, United Kingdom, [4]Section of Ophthalmology, King's College London, St Thomas' Hospital Campus, London, United Kingdom, [5]NIHR Biomedical Research Centre at Moorfields Eye Hospital and the UCL Institute of Ophthalmology, London, United Kingdom

Purpose

The electroretinogram (ERG) reflects changes in electrical activity across the entire retina, in response to light stimulation, and can be recorded non-invasively from the human eye. The amplitude of cone-driven ERG responses to flashes increases with flash luminance up to a maximum and then declines with further increases in flash luminance, termed the “photopic hill”. In this study we investigated the cone-driven response to 30 Hz flickering stimuli of increasing luminance as well as the effect of changes in background luminance on the response.

Methods

Extended recordings were conducted in 2 healthy adults, both male, aged 20-21. The study had Research Ethics Committee approval and conformed to the tenets of the Declaration of Helsinki. Subjects’ pupils were dilated pharmacologically with 1% tropicamide, and conductive fibre electrodes were placed into the lower conjunctival fornix of only one eye for recording, whilst the other eye was patched. Participants were exposed to a standard white light-adapting, rod-saturating background (30 photopic cd.m^{-2}; 86 scotopic cd.m^{-2}) and ERGs were recorded in response to white 30 Hz flicker stimuli of increasing luminance (ranging from 0.5 to 50 cd.s.m^{-2}). The same flicker stimuli were also delivered on other background luminances (50 and 100 photopic cd.m^{-2}; approximate scotopic luminances, 143 and 287 cd.m^{-2} respectively) following initial adaptation to each background for one minute.

Results

Each participant underwent five repetitions of the same experiment over several days, with recordings made from right and left eyes (yielding a total of 20 experiments for analysis). Findings were broadly consistent for both subjects. For the 30 cd.m^{-2} background, a photopic hill effect was observed with maximal amplitudes to a stimulus c.5-10 cd.s.m^{-2}. With increasing background

luminance, the hill effect was also observed, such that response amplitudes to the strongest stimuli for each background were lower than responses to weaker stimuli; the response elicited by the 50 cd.s.m^{-2} stimulus was smaller than that elicited by the 10 cd.s.m^{-2} stimulus on each background ($p<0.0002$, paired t test). Also, as background strength increased, a rightward shift was seen in the luminance-response relation. For the 1 cd.s.m^{-2} stimulus (consistently on the ascending limb of the photopic hill in each background), the response-amplitude was significantly smaller on backgrounds of greater luminance ($p<0.01$ for all pair-wise comparisons between backgrounds, paired t test).

Conclusion

Our findings show a photopic hill effect can be observed in responses to 30 Hz flicker stimuli. The decline in response amplitudes to a fixed stimulus strength delivered on brighter backgrounds is consistent with a reduction in sensitivity with greater background luminance, reflecting retinal light adaptation. The flicker ERG arises largely from signals in cone-driven ON and OFF bipolar cells, and concurrent changes in amplitude and response kinetics of the two pathways are likely to underlie the trends observed.

PCB061

Alcohol triggers the accumulation of oxidatively damaged proteins in neuronal cells and tissues.

Anusha Mudyanselage[1], Wayne Carter[2]

[1]Clinical Toxicology Research Group, School of Medicine, University of Nottingham, Royal Derby Hospital Centre, Derby, United Kingdom, [2]Clinical Toxicology Research Group, School of Medicine, University of Nottingham, Royal Derby Hospital Centre,, Derby, United Kingdom

Alcohol is toxic to neurons and can trigger alcohol-related brain damage, neuronal loss, and cognitive decline. Neuronal cells may be vulnerable to alcohol toxicity and damage from oxidative stress after differentiation. To consider this further, the toxicity of alcohol to undifferentiated SH-SY5Y cells was compared with that of cells that had been acutely differentiated. Cells were exposed to alcohol over a concentration range of 0-200 mM for up to 24 hours and alcohol effects on cell viability were evaluated by MTT and LDH assays. Effects on mitochondrial morphology were examined via transmission electron microscopy, and mitochondrial functionality was examined using measurements of ATP and the production of reactive oxygen species (ROS). Alcohol reduced cell viability and depleted ATP levels in a concentration and exposure duration-dependent manner, with undifferentiated cells more vulnerable to toxicity (viability threshold concentration of ≥20 mM for 6 h, $p < 0.001$ for undifferentiated cells and $p < 0.0001$ for differentiated cells). Alcohol exposure resulted in significant neurite retraction (from ≥50 mM for 6 h, $p < 0.001$), altered mitochondrial morphology, and increased the levels of ROS in proportion to alcohol concentration from 10 mM ($p < 0.0001$); these peaked after 3 and 6 h exposures and were significantly higher in differentiated cells. Protein carbonyl content (PCC) lagged ROS production and peaked after 12 and 24 h, increasing in proportion to alcohol concentration (from 10 mM, $p < 0.0001$), with higher levels in differentiated cells. Carbonylated proteins were characterised by their denatured molecular weights and overlapped with those from adult post-mortem brain tissue, with levels of PCC higher in alcoholic subjects than matched controls ($p < 0.01$). Hence, alcohol can potentially trigger cell and tissue damage from oxidative stress and the accumulation of oxidatively damaged proteins.

PCB062

Folate binding protein-1 localisation in the plexiform layers of the mouse retina

Emily Flood[1], Bernadett Gnotek[1], Gerrit Hilgen[1]

[1]Northumbria University, Newcastle Upon Tyne, United Kingdom

Folate (vitamin B9) is the naturally occurring form of folic acid. Folate cannot be synthesised by the human body so must be acquired through diet/supplementation. Folate carries one-carbon groups for methylation reactions and nucleotide base synthesis making it fundamental for DNA replication, repair, and RNA synthesis. Folate deficiency has been implicated in retinal diseases, including nutritional amblyopia, diabetic retinopathy, exfoliation glaucoma and age-related macular degeneration. In most cases, the exact mechanism of how this contributes to disease is still unknown. There are 3 cellular mechanisms for folate transport: folate receptors, reduced folate carrier and the proton-coupled folate transporter. Folate receptors are attached to the surface of the cell plasma membrane via glycosylphosphatidylinositol. In mice, there are 3 isoforms referred to as the folate binding protein which are analogous to the -a, -b, and -d human forms. RT-PCR, immunohistochemistry and confocal imaging have been used to identify folate binding protein-1 expression in mouse RPE cells, retinal Müller cells and in several layers of retinal tissues, with particularly prominent staining in the outer plexiform layer (Bozard et al. 2010; Smith et al. 1999). To the best of our knowledge, no study has tried to localise any of these folate receptors at the subcellular level in the retina. Such cellular knowledge of folate receptor expression in the retina is critical for understanding their involvement in retinal physiology in health, disease onset and ageing, as well as cell-type specific drug development. Our research will reveal not only whether and which folate receptors are expressed in the retina, but also where they are expressed. Immunohistochemistry analysis (methods previously stated by (Hilgen 2023)) of adult mouse retinal tissue was used to establish localisation of folate binding protein-1 on key retinal cell types, particularly those with dendritic structures extending into the inner plexiform layer (bipolar, amacrine and ganglion cells). Preliminary data shows colocalization of folate binding protein-1 with SMI-32 (alpha retinal ganglion cells), PKCα (bipolar cells) and Calretinin (retinal ganglion cells) at the inner nuclear at plexiform layers of the retina. Experimental procedures were granted ethical approval by Northumbria University and all procedures accorded with current UK legislation.

Bozard, B. R., P. S. Ganapathy, J. Duplantier, B. Mysona, Y. Ha, P. Roon, R. Smith, I. D. Goldman, P. Prasad, P. M. Martin, V. Ganapathy, and S. B. Smith. 2010. 'Molecular and biochemical characterization of folate transport proteins in retinal Müller cells', Invest Ophthalmol Vis Sci, 51: 3226-35. Hilgen, G. 2023. 'Connexin45 colocalization patterns in the plexiform layers of the developing mouse retina', J Anat, 243: 258-64. Smith, S B, R Kekuda, X Gu, C Chancy, S J Conway, and V Ganapathy. 1999. 'Expression of folate receptor alpha in the mammalian retinol pigmented epithelium and retina', Investigative Ophthalmology & Visual Science, 40: 840-48.

PCB063

Homocysteine and Post-Stroke Cognitive Decline: Unravelling the Neurovascular nexus

Rahul Kumar[1]

[1]Assistant Professor, Department of Biotechnology, GITAM School of Sciences, GITAM (Deemed to be) University, Visakhapatnam, Visakhapatnam, India

Introduction: A significant proportion of stroke patients exhibits impaired reperfusion (1), which manifests in different clinical outcomes including cognitive impairment. Although effective treatments to reverse cognitive decline following stroke are still not available, interventions to control risk factors implicated in the disease onset may help to reduce the burden of dementia (2). One such modifiable risk factor is hyperhomocysteinemia (HHcy) or elevation in plasma total homocysteine (tHcy), which has been extensively studied for its cerebrovascular effects (3). HHcy is independently associated with increased incidence of stroke as well as dementia (4-7).

Objective: We wanted to determine if Hcy exacerbates post-stroke memory impairment through a NMDAr dependent mechanism.

Methods: From 4 weeks of age, mice were fed either a control diet or a high methionine/low folate (HM/LF) diet that increases the blood plasma level of Hcy leading to HHcy. Inhibition of NMDAr was achieved using memantine. The stroke was modelled using middle cerebral artery occlusion, followed by the assessment of learning and memory impairment using a battery of behavioral tests. Blood brain barrier (BBB) leakage was assessed using Evans Blue extravasation. We performed repeated measures for time dependent assays and the analysis of variance (ANOVA) with Tukey's post-hoc analysis for multiple comparisons within several groups. For unpaired comparisons, with a standard deviation of 30% and a minimum expected difference between groups of 40%, 10 mice were included in each group to achieve 80% likelihood of detecting significance at the 0.05% level. Values presented as Mean

Results: In fear conditioning, I observed that overall freezing time was significantly less ($p<0.05$) in mice after stroke (84.75±5.99) compared to naive mice (111.75±11). Next, I observed significantly less freezing in HHcy (Control (84.75±5.99; HHcy 61.75±5.69, $p<0.05$), suggesting that it can exacerbates loss of memory post-stroke. Next, we assessed if HHcy can promote learning and memory impairment in novel object recognition. Mice acquired a memory of the familiar object by exploring two identical objects. 24 hours after acquisition, we assessed NOR by replacing one of the familiar objects with a novel object and assessing the amount of time that mice spent interacting with the novel and familiar objects. Surprisingly, when NOR was assessed 24 h later, we found that mice with HHcy failed to discriminate between the novel and familiar objects lower discrimination index s compared to controls (Control 71.35±3.63; HHcy 54.25±6.27; $p<0.05$). We further made an interesting observation that HHcy leads to BBB leakage that was reversed by the administration of memantine (Control; 2.65±0.36 µg/g; HHcy 4.2±0.38; HHcy with memantine 2.57±0.53; p value for HHcy vs Control<0.05; p value for HHcy vs HHcy with memantine<0.05).

Conclusion: Altogether, the findings from the project suggests that HHcy exacerbates cognitive and BBB leakage following stroke. The findings from the project will allow us to initiate clinical

trials to determine if stroke patients with higher level of Hcy are more vulnerable to the development of cognitive dysfunction and need a memantine or Vitamin B12 supplementation as prophylactic treatment.

PCB064

The Use and Effectiveness of Traditional Turmeric-Based Preparations and Vitamin Products as Antioxidants in Combating Oxidative Stress in Various Neuropathologies

Krishma Parwana[1], Marta Wołoszynowska-Fraser[1], Jenny Moran[1]

[1]Keele University, Keele, United Kingdom

Turmeric has been a key player in Ayurvedic medicine for thousands of years, mentioning its antioxidant and anti-inflammatory properties which have gained increasing popularity in modern medicine (Hewlings and Kalman, 2017). As of present, the use of turmeric or its main polyphenol compound curcumin has been investigated as a therapy in conditions such as Alzheimer's Disease, Osteoarthritis and Schizophrenia to either improve symptoms or the condition itself (Hewlings and Kalman, 2017). Although the antioxidant properties of turmeric have been studied to combat oxidative stress within these conditions, there is a lack of studies which implement traditional turmeric-based products as a treatment and little supporting evidence of how effective turmeric-based vitamin products are as antioxidants. This study aimed to investigate the antioxidant properties of various traditional fresh (FT) and powdered (PT) turmeric-based preparations with or without black pepper (BP) which were boiled in either milk or water and three different turmeric-based vitamin products. Their antioxidant properties were tested using a superoxide scavenging assay in a Nicotinamide Adenine Dinucleotide + Hydrogen-Phenazine Methosulfate system, where the percentage inhibition of Nitro Blue Tetrazolium Chloride was calculated using absorbance values from a spectrophotometer to determine the amount of superoxide scavenging from the assay. ANOVA results showed a significant difference between all milk-based assays ($F_{(5, 18)}$=10.99, $p<0.0001$) (Figure 1) and water-based assays ($F_{(5,18)}$=384.1, $p<0.0001$) (Figure 2). Within milk, powdered turmeric showed the highest percentage inhibition (44.19%) (Figure 1) and powdered turmeric and black pepper showed the highest percentage inhibition in water (49.65%) (Figure 2). Within our data, all assays showed percentage inhibition besides water as a control and fresh turmeric in water, which was deemed an unexpected result. All three vitamin products exhibited antioxidant properties ($F_{(3, 12)}$ = 218.7, $p<0.0001$) (Figure 3), with Holland & Barratt (H&B) having a significantly higher percentage inhibition compared to the other two products ($p<0.0001$) (Figure 3), suggesting it displays the highest efficacy. These findings quantify the antioxidant properties of both traditional turmeric-based preparations and turmeric-based vitamin products and reveal the efficacy of their free radical scavenging properties. Evidence from these results suggests that traditional turmeric-based assays are effective as antioxidants in certain combinations, particularly when extracted in milk overall. Furthermore, Holland & Barrett displayed the highest percentage inhibition, which suggests that it may be the most effective therapy and that not all turmeric-based vitamin products display high free radical scavenging properties despite their claims. These results provide preliminary data which suggests that using turmeric-based preparations or vitamin products could be as an antioxidant to combat oxidative stress which has been suggested to be present in multiple neuropathologies. Findings from this study could be translated into further studies, such as *in vitro* cell work to test the efficacy of turmeric-based preparations and vitamin products to determine their effectiveness in combatting oxidative stress or potentially long-term *in vivo* studies to observe how they may improve various neuropathologies and their symptoms which may be induced or worsen by oxidative stress.

Hewlings, S. and Kalman, D. (2017). Curcumin: A Review of Its' Effects on Human Health. Foods, [online] 6(10), p.92. doi:https://doi.org/10.3390/foods6100092.

PCB065

Late Maternal Separation provides resilience to stress-induced behavioral disorder

Padmasana Singh, Rajesh Kumar Ojha, Shweta Dongre, Raj Kamal Srivastava

undefined

Introduction: Maternal separation (MS) is a widely recognized paradigm that can be employed to investigate the physiological effects of stress experienced during early life. During the first two weeks of life, daily maternal separation plays a crucial role in the development of the hypothalamic–pituitary–adrenocortical (HPA) axis, a significant neuroendocrine system that responds to environmental stressors. Prior research has indicated that MS has demonstrated that the plasticity of the central nervous system in childhood renders it vulnerable to stress in adulthood. Early maternal separation in adult mice leads to increased stress responsiveness, resulting in elevated glucocorticoid levels after acute or chronic stress. However, the effects of late MS (LMS) on HPA axis during adolescence have not been studied. Hence, aim of the current investigation was to examine the effects of late maternal separation (LMS) on neurobehavioral changes and stress responsiveness during adolescence.

Methodology: Swiss Albino male and female pups from LMS group were daily removed from their home cage for 3 hours from PND 10 to PND 21 between 14:00 h - 17:00 h. After 3 hours of maternal separation, the pups were returned to their home cage. At PND 22, both non-maternal separation group (NMS) and LMS mice were separated and housed together with littermates of the same sex. At PND 56, each mouse from NMS and LMS group were subjected to one chronic variable stress (CVS) randomly for 21 days - (a) overnight fasting; (b) 30 min of restraint stress; (c) shaking for 30 min at 80-100 rpm; (d) placed in ice cold water for 15 min (only paws); (e) placed on a hot surface for 30 min at 400C; (f) isolated and kept in a separate cage; (g) swimming for 5 min. After this period, each mouse was subjected to a series of behavioural tests for five consecutive days that comprised of sucrose preference test, open field test, light-dark box test, elevated plus maze test, and tail suspension test (TST).

Results: Behavioral tests suggested that male LMS mice are more resilient to chronic variable stress (CVS)-induced anxiety and depressive-like behavior, as confirmed by the open field, light dark field, elevated plus maze, sucrose preference, and tail suspension tests. In contrast, female LMS mice were equally resilient as mice without maternal separation. We found an increased expression of Npy, Npy1r, Npy2r, Npffr1, and Npffr2 in the hypothalamus of male LMS mice, whereas the opposite effect was observed in the hippocampus. LMS in male and female mice did not affect circulating corticosterone levels in response to psychological or physiological stressors. Thus, LMS makes male mice resilient to CVS-induced neurobehavioral disorders in adulthood.

Conclusion: LMS from PND10-PND21 provides resilience to anxiety and depression in male mice, while there were no significant changes in female mice. Our study indicated the role of two neuropeptides, Npy and Npvf, and their receptors in stress resilience to CVS-induced anxiety- and depression-like behavior in male LMS mice.

PCB066

Using a mouse model of Alzheimer's disease to unravel early pathological neurovascular changes preceding cognitive decline.

Harry Trewhitt, Kira Shaw, Silvia Anderle, Letitia McMullan, Catherine N. Hall

undefined

Accumulating evidence suggests at a link between amyloid beta (Aβ) accumulation and neurovascular dysfunction in early stages of Alzheimer's disease (AD) (Iadecola, 2004). The 'two-hit' vascular model proposes that age and cardiovascular risk-factor related neurovascular deterioration, such as a reduction in neurovascular coupling and the breakdown of the blood brain barrier, may act synergistically with initial Aβ deposition creating a feedforward cycle of progressive change, ultimately promoting neuronal dysfunction and loss (Zlokovic, 2011). However, the factors that first establish such a vicious cycle have not yet been determined. We hypothesised that early Aβ-induced hyperactivity of excitatory neurons (Busche et al., 2012), combined with a reduced capacity of the neurovasculature to support this (Korte et al., 2020), emerge early in disease, which could subsequently create repeated transient hypoxic areas throughout the brain, promoting further Aβ deposition (Chen & Hassan, 2021).

To interrogate this we have used a novel mouse model combining humanised APOE and doxycycline-inducible APPSwe/Ind transgenes as well as the CaMKII driven GCaMP6f neuronal calcium reporter. *In vivo* 2Photon imaging and combined haemoglobin spectrometry/ laser doppler flowmetry allowed us to investigate neuron and vessel function over a time-course of Aβ accumulation. A surgically implanted cranial window placed over the visual cortex allowed us to record baseline measurements before APP expression is 'switched on' and at subsequent timepoints up to four months after.

A behavioural testing regime, on the same mice we imaged *in vivo,* indicates that four-months of Aβ accumulation represents an early AD model, with mild cognitive symptoms starting to appear. After four months of APP expression (and Aβ accumulation) mice performed around 35% worse than non-APP expressing controls during the acquisition trials of a simple, non-appetitive Barnes Maze paradigm (LMM interaction between APP expression and time, **p = 0.005**). Although these mice are still able to learn, this indicates a mild deficit in spatial working memory. Preliminary *in vivo* data from the visual cortex reveals an increase in neuronal calcium peak size (LMM interaction between APP expression and time, **p = 0.04**) and duration (LMM main effect of APP expression, **p = 0.002**) after four months of Aβ accumulation. Such an increase in neuronal activity should be met by a requisite increase in oxygen supply via neurovascular coupling, however oxygen saturation measurements from the same cortical region indicate a significant drop in tissue oxygenation from baseline in APP expressing mice (one-sided T-Test, **p = 0.01**).

Further data is being collected and analysed which will hopefully help inform our understanding of how neuronal and neurovascular changes induced by Aβ accumulation contribute to early AD pathological changes, preceding significant cognitive decline.

References Iadecola, C. (2004) ‘Neurovascular regulation in the normal brain and in alzheimer’s disease’, Nature Reviews Neuroscience, 5(5), pp. 347–360. doi:10.1038/nrn1387. Zlokovic, B.V. (2011) ‘Neurovascular Pathways to neurodegeneration in alzheimer’s disease and other disorders’, Nature Reviews Neuroscience, 12(12), pp. 723–738. doi:10.1038/nrn3114. Busche, M.A. et al. (2012) ‘Critical role of soluble amyloid-β for early hippocampal hyperactivity in a mouse model of alzheimer’s disease’, Proceedings of the National Academy of Sciences, 109(22), pp. 8740–8745. doi:10.1073/pnas.1206171109. Korte, N., Nortley, R. and Attwell, D. (2020) ‘Cerebral blood flow decrease as an early pathological mechanism in alzheimer’s disease’, Acta Neuropathologica, 140(6), pp. 793–810. doi:10.1007/s00401-020-02215-w. Chen, R. and Hassan, H. (2021) ‘Hypoxia in alzheimer’s disease: Effects of hypoxia inducible factors’, Neural Regeneration Research, 16(2), p. 310. doi:10.4103/1673-5374.290898.

PCB067

Differences in Thoracic Fluid Content and Cardiac contractility in Individuals with Myasthenia Gravis are Associated with the Severity of Autonomic Dysfunction

Monika Zawadka-Kunikowska[1], Mirosława Cieślicka[1], Wieńczysława Adamczyk[1], Monika Bejtka[1], Joanna Fanslau[1], Wojciech Kaźmierczak[1,3], Łukasz Rzepiński[4,5]

[1]Department of Human Physiology, Nicolaus Copernicus University Ludwik Rydygier Collegium Medicum in Bydgoszcz, Bydgoszcz, Poland, [2]Department of Human Physiology, Nicolaus Copernicus University Ludwik Rydygier Collegium Medicum in Bydgoszcz, Bydgoszcz, Poland, [3]The Institute of Physiology and Pathology of Hearing, Warszawa, Poland, [4]Sanitas - Neurology Outpatient Clinic, Bydgoszcz, Poland, [5]Department of Neurology, 10th Military Research Hospital and Polyclinic, Bydgoszcz, Poland

Introduction: Myasthenia gravis (MG), a rare autoimmune disorder, poses diagnostic and management challenges, with significant impacts on patients' quality of life. Cardiac autonomic dysfunction has been identified in patients with MG, often with limited comprehensive assessments integrating impedance cardiography (ICG).

Aims: We assessed cardiac function, including thoracic fluid content and myocardial contractility, in both MG patients and healthy controls (HCs), and its correlation with the severity of autonomic impairment using cardiovascular autonomic function tests (AFTs).

Methods: Fifty-three patients with MG (median age 41, interquartile range 36-45) and 30 HCs (median age 38, interquartile range 25-42) underwent standardized AFTs. Patients were categorized into Non-CAN (n=33) and CAN (n=20) groups based on their Cardiovascular Autonomic Neuropathy (CAN) status, as evaluated using the Composite Autonomic Scoring Scale (CASS). We continuously measured cardiovascular parameters using ICG, including thoracic fluid content (TFC), stroke volume (SV), cardiac output (CO), and myocardial contractility indices such as left ventricle ejection time (LVET), left ventricular work index (LVWI), index of contractility (IC), Heather Index (HI), and mean systolic ejection rate (MSER). Preload was assessed as end-diastolic index (EDI), and afterload as total peripheral vascular resistance (TPR). Heart rate and blood pressure (BP) were calculated from electrocardiography and plethysmography.

Results: At baseline before VM, the CAN-MG group exhibited significantly higher HR, diastolic BP, TPR, and lower values of EDI ($p < 0.001$), IC ($p < 0.001$), ACI ($p = 0.005$), LVET ($p = 0.003$), MSER ($p < 0.001$) than the HCs. Both MG groups (CAN, Non-CAN) had significantly lower values of SV, TFC than HCs ($p < 0.001$). In contrast, the CAN MG group showed significantly lower cardiac inotropy (HI) compared to the Non-CAN MG and HCs groups. Total CASS score correlated with lower resting thoracic fluid content ($R = -0.36$, $p=0.009$) and myocardial contractility parameters: IC ($R=-0.36$, $p=0.007$), HI ($R = -0.40$, $p=0.003$), EDI ($R = -0.36$, $p=0.009$), MSER ($R = -0.33$, $p=0.016$), LVWI ($R=-0.32$, $p=0.019$), ACI ($R = -0.31$, $p=0.024$), At baseline, decreased preload (EDV), TFC, myocardial contractility (MSER, LVWI, ACI), and cardiac inotropy (HI) parameters were associated with higher TPR at rest.

Conclusions: These findings underscore the significance of subclinical cardiac impairment associated with decreased thoracic fluid content and myocardial contractility in MG patients, as well as their relationship with the severity of autonomic abnormalities.